Hunting for Hidden Explosions: Exploring the Transient Infrared Sky with the *Spitzer Space Telescope*

Thesis by
Jacob Edmund Jencson

In Partial Fulfillment of the Requirements for the
Degree of
Doctor of Philosophy

CALIFORNIA INSTITUTE OF TECHNOLOGY
Pasadena, California

2020
Defended 2019 September 24

Jacob Edmund Jencson
ORCID: 0000-0001-5754-4007

For Mom, Dad, Gena, Anna, and Emma.

ACKNOWLEDGEMENTS

The completion of this thesis would never have been possible were it not for the help, guidance, and support provided to me by the following incredible people to whom I owe innumerable thanks:

First and foremost, to my advisor, Mansi Kasliwal. Your unwavering support and belief in me, especially in moments of self-doubt and uncertainty, were invaluable throughout my years in grad school. I learned a great deal from you, perhaps most importantly, the value of maintaining enthusiastic curiosity and excitement for discovery.

To my first research mentors at Ohio State, Kris Stanek and Ben Shappee, who gave me a chance and taught me so many things. To Jose Prieto, Chris Kochanek, Rick Pogge, who supported my in me first research project, and to Matthew Penny, who took me on my first observing run and showed me Andromeda in the night sky. To my mentors at NRAO and Wisconsin, Miller Goss, Snez Stanimirović, and Claire Murray, who taught me radio astronomy, and have been a major source of encouragement.

To the fantastic members of my research group at Caltech, Kishalay, Kaew, Anna, Viraj, Shreya, Yuhan, Scott, Ryan, Nadia, Dave, Matt, Igor, Ragnhild, Christoffer, Lin, and in particular Yi, who provided invaluable help in my first few years, as well as the incomparable SPIRITS team, in particular Howard Bond, Joel Johansson, Dan Perley, Schuyler Van Dyk, Ann Marie Cody, Frank Masci, Andy Monson, John Bally, George Helou, Lee Armus, Bob Gehrz, Bob Williams, Ori Fox, Nathan Smith, Eric Hsiao, and Patricia Whitelock, with all of whom it has been an absolute joy to work. Also to Stuart Ryder, Assaf Horesh, and Kunal Mooley, who provided substantial help and guidance throughout my grad school years.

To the members of my thesis committee, Chuck Steidel, Sterl Phinney, Tom Soifer, and Gregg Hallinan, whose guidance and advice have improved the work in this thesis manyfold.

To the staff and support teams of Palomar and Keck Observatories, especially Carolyn, Kevin, Carlos, and Percy, whose knowledge, patience, assistance, and good spirits made the many nights of observing that went into this thesis not only productive, but also enjoyable. Also to the observers of Las Campanas, especially

Nidia Morell, Carlos Contreras, and Sergio Castellón, who provided substantial help in completing this work.

To the staff and support teams of the *Spitzer Space Telescope* and *Spitzer* Science Center whose dedicated efforts enabled the observations that have provided the foundation of this thesis.

To the administrative staff of Cahill, especially Judy, Gita, and Althea, who have helped me countless times, and whose presence always made Caltech Astronomy a more positive place to work.

To my friends in Pasadena, inside and outside of Caltech Astronomy, who made this a wonderful place to spend five years:

- To Denise and Rachel, the other members of my cohort and forever the cutest class of astronomy grads, I never would have made it through without the both of you. Your constant support and unwavering friendship, even as we all faced our own struggles, have meant more to me than you know.

- To Matt, for endless games of *Smash Bros.*, bro-night dinners, dumb nicknames, early morning *Pajama Game* sing-alongs, and altogether five unbelievably fun years living together. I don't think I could have asked for a better roommate and friend.

- To Peter, for all the games of tennis (even though you always win), afternoons of Buckeye football and "Yinkies Biesbol", and most importantly for being someone I could talk to about anything.

- To Marin, for always being down for trips to the opera and the Wendy's drive-through, the most formidable tennis partner, giver of the best advice, and all-around someone to look up to.

- To Gillian, for taking me under your wing in so many ways: on the tennis court, the yoga mats, and for literally giving me a place to live my last few months in Pasadena.

- To Allison and Gina, for both the most fun nights out dancing and nights in playing cards and *Mario Party*. But also for being such positive forces in the astronomy and broader graduate student communities at Caltech.

- To Scott, for keeping the department fun and friendly, and always having a pun ready.

- To Sebastian, for showing me the ropes around Cahill, helping me stay active on the tennis courts, and always being an ear to listen.

- To these amazing astrograds at Caltech, with whom I've had the wonderful privilege of becoming friends: Abhilash, Alicia, Anna, Antonija, Becky, Donal, Dillon, Io, Ivanna, Jackie, Kaew, Kishalay, Marta, Matt O., Melodie, Michael E., Mislav, Nicha, Pavan, Ryan M., Swarnima, Yi, Yuguang, and a special shoutout to all those regular passengers on the lunch train, especially Chris, Kathryn, Lee, Michael Z., Mia, Nikita, Nitika, Ryan, and Sarah.

- To the other steadfast friends I've made here: Alistair, Ellen A., Ellen L., Mark, Ricky, Tatiana, and Teddy.

- And to Serg, whose companionship, support, and love kept me going over the final stretch. I'm so unbelievably happy my last year at Caltech brought us together.

To the friends, though many miles away, who are always there and for whom I'm a better person having known, especially Rochelle, Scott, Stef, Brittany, Andrea, Cassie, Becky, and Dan.

Finally to my family, the constant source of love and support in my life, and who have made possible everything I've ever done. To my amazing parents, who've been behind me from the beginning, have provided me every opportunity, and who continue to be a source of encouragement when I need it most. To my incredible sisters, Gena, Anna and Emma, who are some of the funniest, most creative, and simply the best people I know. To Aunt Beth, my biggest cheerleader and who always reminds me why I love getting to do astronomy. To my Grandma Jo, who taught me the importance of always questioning and to always keep a sense of humor. To my Grandpa Dave, who taught me to work hard and always measure things twice. And to my Grandma Jeanne, who inspired a sense of creativity and imagination that I'll always carry with me.

ABSTRACT

The study of time-variable astronomical phenomena is undergoing an explosive renaissance ushered in by recent advancements in capabilities to monitor the sky from radio to gamma rays. The infrared region of the electromagnetic spectrum provides a unique window to uncover a vast array of stellar eruptions and explosions that are otherwise obscured; however, the dynamic infrared sky has remained largely unexplored.

To uncover these hidden cosmic explosions, I undertook a systematic search in the infrared with the *Spitzer Space Telescope* called SPIRITS—the SPitzer InfraRed Intensive Transients Survey. Targeting a specially chosen sample of nearby galaxies, the search revealed a bounty of exceptionally red events, and may have discovered entirely new and diverse populations, including deeply embedded supernovae, catastrophic stellar mergers, and giant eruptions of massive, violently unstable stars. Providing a first census of stellar infrared transients, SPIRITS has paved the way for new and upcoming surveys to further expand our exploration of the dynamic infrared sky.

PUBLISHED CONTENT AND CONTRIBUTIONS

Jencson, Jacob E., et al. 2019a. "Discovery of an Intermediate-luminosity Red Transient in M51 and Its Likely Dust-obscured, Infrared-variable Progenitor". *ApJ* 880 (2): L20–40.
J.E.J. contributed to data acquisition and analysis, and wrote the manuscript. doi:10.3847/2041-8213/ab2c05. arXiv: 1904.07857 [astro-ph.SR].

Jencson, Jacob E., et al. 2019b. "The SPIRITS Sample of Luminous Infrared Transients: Uncovering Hidden Supernovae and Dusty Stellar Outbursts in Nearby Galaxies". *ApJ* 886 (1): 40.
J.E.J. served as Project Scientist for the SPIRITS survey, led dedicated observing campaigns for this project, contributed to data acquisition and analysis, and wrote the manuscript. doi:10.3847/1538-4357/ab4a01. arXiv: 1901.00871 [astro-ph.HE].

Jencson, Jacob E., et al. 2018. "SPIRITS 16tn in NGC 3556: A Heavily Obscured and Low-luminosity Supernova at 8.8 Mpc". *ApJ* 863 (1): 20–44.
J.E.J. led dedicated observing campaigns for this project, contributed to data acquisition and analysis, and wrote the manuscript. doi:10.3847/1538-4357/aacf8b. arXiv: 1803.00574 [astro-ph.HE].

Jencson, Jacob E., et al. 2017. "SPIRITS 15c and SPIRITS 14buu: Two Obscured Supernovae in the Nearby Star-forming Galaxy IC 2163". *ApJ* 837 (2): 167–185.
J.E.J. contributed to data acquisition and analysis and wrote the manuscript. doi:10.3847/1538-4357/aa618f. arXiv: 1609.04444 [astro-ph.HE].

TABLE OF CONTENTS

LIST OF ILLUSTRATIONS

LIST OF TABLES

Chapter 1

INTRODUCTION

The sudden appearance of new, ephemeral sources of light in the cosmos have long puzzled and intrigued observers of the night sky. Over 1700 years, ago in the year 185, ancient Chinese astronomers noted a "guest star" in today's constellation Centaurus, now believed to be the first recorded supernova. These early astronomers had only their eyes as observational instruments, limited to the visible range (about 4000–7000 Å) of the electromagnetic spectrum. The development of the telescope, and later, photographic astronomy led to Baade and Zwicky's division between the Galactic novae and the much more luminous, extragalactic supernovae, and furthermore, their remarkable insight in connecting supernovae to the deaths of massive stars and the formation of their neutron star remnants in 1934. In the past few decades, time-domain astrophysics has been revolutionized by the development of wide-field, primarily optical, digital imaging surveys now finding, for example, thousands of supernovae every year, with broad implications for our understanding of the stellar evolution, the formation of galaxies, and the expansion history of the Universe itself. Moreover, technological advancements have moved the field well beyond the optical, with several high-energy space-based missions (e.g., Swift and Fermi) dedicated to transient detection and follow-up. Excitingly, the exploration of the dynamic infrared sky (here, referring to the region between $\approx$ 1 and 700 μm) is just beginning, opening new avenues for the discovery and characterization of previously hidden phenomena.

1.1 The landscape of infrared transients in 2014

I begin simply with a look back at the types of astrophysical transients that were known to be strong producers of IR emission when I started my thesis work. These events may first be broadly characterized by the time-evolution of their IR luminosity. In Figure 1.1, I show the 4.5 μm light curves of the varied classes of events that were known in 2014. While the number of individual, well-characterized events was small, the diagram spans more than seven orders of magnitude in peak IR luminosity, from $\nu L_\nu \gtrsim 10^2\ L_\odot$ to $\nu L_\nu \lesssim 10^9\ L_\odot$, and already indicates striking diversity in the time evolution of the types of events shown.

At the faint end are the classical novae, explosions arising from a thermonuclear

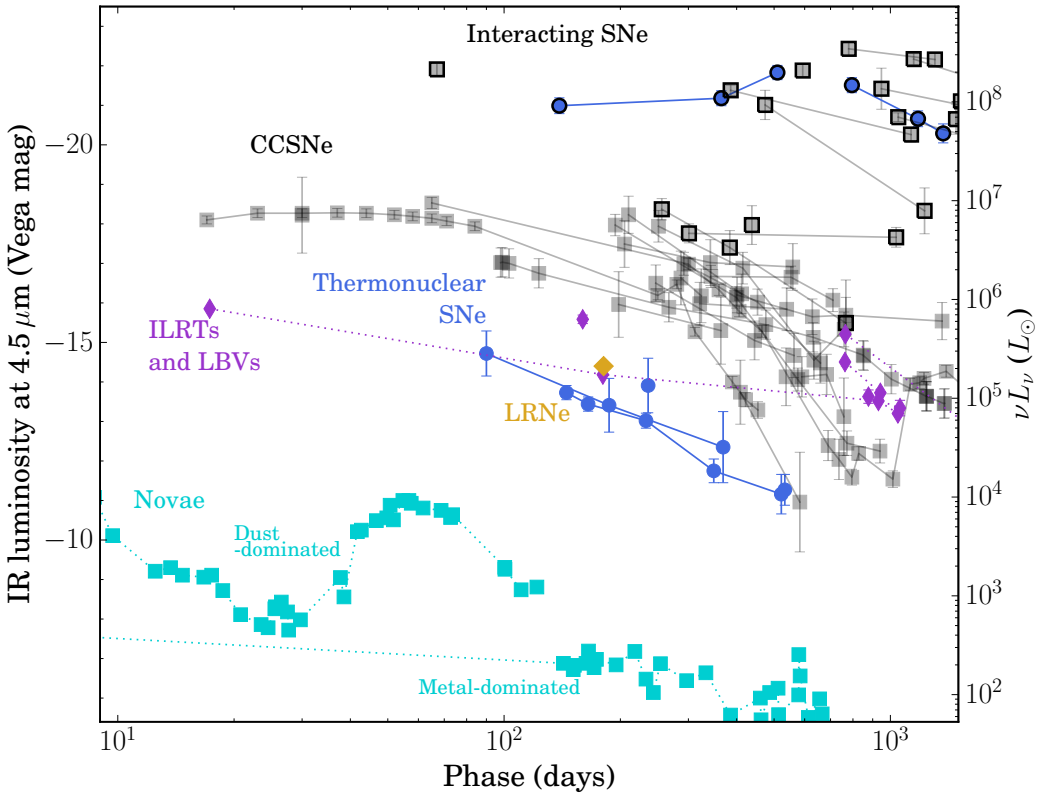

Figure 1.1: The mid-IR 4.5 μm light curves of transients of various classes as of 2014. We include all CCSNe (gray squares) and thermonuclear SNe Ia (blue circles) with *Spitzer*/IRAC published by 2014 from Meikle et al. (2005), Meikle et al. (2006), Meikle et al. (2007), Mattila et al. (2008), Kotak et al. (2009), Andrews et al. (2010), Fox et al. (2010), Andrews et al. (2011), Fabbri et al. (2011), Fox et al. (2011), Meikle et al. (2011), Kochanek, Szczygiel, and Stanek (2011), Szalai et al. (2011), Gallagher et al. (2012), Prieto et al. (2012), Stritzinger et al. (2012), Fox and Filippenko (2013), Fox et al. (2013), Gandhi et al. (2013), Helou et al. (2013), Szalai and Vinkó (2013), and Van Dyk (2013). Strongly interacting SNe, including Types IIn, Ibn, and Ia-CSM, are indicated by the thick-outlined points. Measurements for ILRTs SN 2008S, NGC 300 OT2008-1, and SN 2010dn, and the LBV transient SN 2002bu from *Spitzer*/IRAC (Wesson et al. 2010; Szczygieł, Kochanek, and Dai 2012; Szczygieł et al. 2012) and WISE (Hoffman et al. 2011) are shown as thin purple diamonds. Observations of the LRN M85 OT2006-1 from *Spitzer*/IRAC are shown as the thick yellow diamond. Finally, the light curves of classical novae with dust-dominated (V1668 Cyg; Gehrz et al. 1980) and metal-dominated (QU Vul; Gehrz et al. 1995) ejecta are shown as the cyan squares.

runaway on a white dwarf accreting material from a non-degenerate companion in a close binary system. The brightest novae in the IR had been observed to peak near $\nu L_\nu \approx 3 \times 10^4\ L_\odot$ at 4.5 μm (absolute Vega magnitude $M \approx -12.5$ mag) on a timescale of $\approx$ 50–80 days due to the condensation of dust grains in circumburst shells. Novae with metal-dominated ejecta, in contrast, do not develop strong IR emission (Gehrz et al. 1980; Gehrz et al. 1995). While novae play an important role in chemical enrichment and dust budget of galaxies (e.g., Gehrz 1988), no IR census of their relative rates in the nearby universe had been conducted.

Typically at least 100 times brighter than novae at peak in the IR are the supernovae (SNe) with $\nu L_\nu \gtrsim 10^6\ L_\odot$ ($M \lesssim -16$ mag). Core-collapse SN (CCSN) arise from the explosive death of a star more massive than about $\approx 8\ M_\odot$ following the collapse of its iron core. CCSNe were known to produce luminous and long-lived IR light curves, sensitive probes of circumstellar dust formed in their ejecta or the pre-explosion winds of their progenitors (e.g., Fox et al. 2010, and references therein), declining on timescales typically exceeding $\approx$ 100 days. Furthermore, claims of a discrepancy between the CCSN rate measured by optical searches and the rate of massive star formation (e.g., Horiuchi et al. 2011), may be resolved if a significant fraction of CCSNe are obscured by dusty environments (e.g., Grossan et al. 1999; Maiolino et al. 2002; Mattila et al. 2012).

Thermonuclear Type Ia SNe—arising from runaway nuclear fusion inside a white dwarf triggered by a companion that completely disrupts the star—while similarly luminous to CCSNe at peak, were observed to fade more rapidly at IR wavelengths. Despite suggestions that circumstellar dust could explain the unusual color evolution of some Type Ia SNe (Goobar et al. 2014; Amanullah et al. 2014), no direct evidence for dust emission had been seen in the few events observed with the *Spitzer Space Telescope*.

In between the novae and SNe are classes of stellar transients for which the observed emission may even be predominately IR. The luminous red novae (LRNe) are believed to be associated with the ejection of a common-envelope driven by close binary interactions or stellar merger, a scenario spectacularly confirmed in the case of the compact binary merger V1309 Sco (Tylenda et al. 2011). This class also includes the Galactic events V4332 Sgr (Martini et al. 1999) and the more massive V838 Mon (Bond et al. 2003; Sparks et al. 2008), and the extra-galactic transients M31 RV (Rich et al. 1989; Bond and Siegel 2006; Bond 2011) and M85 OT2006-1 (Kulkarni et al. 2007). A separate class, the intermediate-luminosity red transients

(ILRTs), are of debated origins, but have been proposed to result from the electron-capture-induced collapse of an extreme asymptotic giant branch (AGB) star (e.g., Botticella et al. 2009; Thompson et al. 2009), or alternatively, as suggested by Smith et al. (e.g., 2011), may be akin to the non-terminal "giant eruptions" of the much more massive luminous blue variable stars (e.g., the Great Eruption of η Car and other SN "impostors"; Humphreys, Davidson, and Smith 1999; Van Dyk and Matheson 2012; Smith et al. 2010). LRNe, ILRTs, and LBV-related transients have shown slow-declining IR light curves lasting several hundred days, but as of 2014, only a handful of these intermediate-luminosity events had been well-observed in the IR.

To interpret their light curve evolution and gain physical insight on the diverse classes of transient phenomena that populate the IR sky, it is necessary to discuss the physical processes and conditions that give rise to their IR-dominated spectral energy distributions (SEDs). It is to this point that we now turn our attention, below.

1.2 The physics of infrared transients

The light radiated during an astrophysical transient carries abundant information about the physical processes and conditions of the system driving the outburst. There are several scenarios in which the bulk of the emission produced will be observable in the IR. The SED of intrinsically cool transients, for example, will peak in the IR at wavelengths $\gtrsim 1\,\mu$m for temperatures $\lesssim 3000\,$K. Transients that drive cool, opaque winds or outflows will thus naturally produce IR-dominated spectra. Even for transients with higher intrinsic temperatures, external extinction from dust in the host galaxy or the immediate inter- or circumstellar environment of the progenitor can obscure the event in the visible and ultraviolet (UV). Given suitable conditions, newly formed dust in the aftermath of a stellar explosion can provide additional opacity (e.g., Kochanek, Adams, and Belczynski 2014), further shifting the observed SED of a transient into the IR[1]. Warm dust in the vicinity of a transient, possibly newly formed, will also radiate thermal emission in the IR, producing a so-called "IR excess". Alternatively, pre-existing circumburst dust,

[1]Though not of primary relevance to this thesis, we also note for completeness that line opacity from atomic bound-bound transitions can also lead to the redistribution of higher energy photons to longer wavelengths. The effects of higher optical opacity from the numerous bound-bound transitions of heavy elements (e.g., Neodymium and other Lanthanides), for example, were predicted to shift the spectra of r-process powered transients into the IR (e.g., Barnes and Kasen 2013; Kasen, Badnell, and Barnes 2013). While not appearing in this thesis, the author contributed to the spectral analysis that confirmed this effect in the kilonova associated with the neutron star merger GW170817 (Kasliwal et al. 2017a).

which may have formed in the pre-outburst stellar wind or prior eruptive mass-loss event of the progenitor star, can be heated by the transient peak or ongoing shock-interaction, producing an "IR echo" owing to light-travel time effects (e.g., Bode and Evans 1980; Dwek 1983; Mattila et al. 2008).

These considerations now lead to the open questions and topics in astrophysics that have provided the major motivation behind the work presented in this thesis.

Finding the missing CCSNe

CCSNe, as the final event in the life of a massive star, are important probes of star formation (e.g., Mannucci, Della Valle, and Panagia 2007), stellar evolution and mass loss (Smith 2014), and the circum- and interstellar environments of massive stars in galaxies. Measurements of the CCSN rate have largely been made using optical searches, but it has long been recognized that these rate estimates will only be lower limits if a significant fraction of CCSNe are obscured by dust (e.g., Grossan et al. 1999; Cresci et al. 2007). Horiuchi et al. (2011), in fact, claimed that half of all CCSN were missing from rate estimates in comparison to the rate of massive star formation both locally and across cosmic time from redshifts $z = 0$ to 1; however, other more recent studies have found better agreement (Cappellaro et al. 2015), and some estimates have even suggested that CCSNe may be overproduced compared to Hα and ultraviolet- (UV-) inferred star-formation rates in the local Universe (Botticella et al. 2012; Horiuchi et al. 2013; Xiao and Eldridge 2015). Properly accounting for obscured or otherwise optically dim CCSNe is necessary to resolve lingering discrepancies (Mannucci, Della Valle, and Panagia 2007; Mattila et al. 2012).

A great deal of work, for example, has been dedicated to uncovering heavily extinguished CCSNe in the dense, highly star-forming nuclear regions of (ultra-) luminous infrared galaxies (U/LIRGS) employing seeing-limited imaging (e.g., Mannucci et al. 2003; Miluzio et al. 2013) or high resolution imaging from space or with ground-based adaptive optics (e.g., Cresci et al. 2007; Mattila et al. 2007; Kankare et al. 2008; Kankare et al. 2012; Kool et al. 2018) in the near-IR, and radio imaging (Lonsdale et al. 2006; Pérez-Torres et al. 2009; Romero-Cañizales et al. 2011; Romero-Cañizales et al. 2014; Bondi et al. 2012; Varenius et al. 2017). As of 2014, no direct search for obscured CCSNe in the less extreme environments of normal galaxies in the nearby Universe had been conducted. Beyond the question of simply accounting for missing CCSNe, it is even possible that new populations

of CCSNe that originate preferentially in regions of extreme local environments may be systematically missed by the myriad optical searches currently operating. For example, supernovae occurring directly in the molecular clouds in which their progenitors were born have long been thought to occur (Chevalier 1999), but have never been directly observed. A systematic search for transients in the IR with unbiased sampling of environments within nearby galaxies would directly probe these questions.

Unveiling self-obscuring stellar outbursts

The classes of hydrogen-rich transients living in the "gap" between novae and SNe, known variously as LRNe, ILRTs, and those events associated with LBVs, develop IR dominated SEDs due to the presence of copious dust surrounding the star at the time of the explosion, or due to the formation of dust in the ejecta of the explosions themselves. While LRNe may only be accompanied by short/faint optical transients, their cool, dense outflows are favorable to dust formation that can power long-lived, IR excess emission (Rau et al. 2007). More recent studies have even suggested the formation of dust for certain binary system may completely obscure the optical peak, leading to events observable only in the IR (Metzger and Pejcha 2017). ILRTs arise from massive ($\approx$10–15$M_{\odot}$) progenitors, self-obscured by an opaque, dusty wind (Prieto 2008; Prieto et al. 2008). While briefly observed as optically luminous transients, the explosions are later obscured once again by dust (re)-formed in the aftermath (Kochanek 2011a; Szczygieł et al. 2012). Dust formation is known to occur around hot LBVs (see reviews by Humphreys and Davidson 1994; Vink 2012), but is only possible during eruptive states due to enhanced mass-loss rates, and importantly, the formation of a cool "pseudo"-photosphere (Kochanek 2011b).

It is notable that, despite the bulk of the emission of these classes of transients emerging in the IR, the majority of events studied thus far have been identified via their optical emission. The question naturally arises again whether optical searches are sensitive to the full populations and range of progenitor systems of IR-dominated transients. A dedicated IR search for transients could address a number of important astrophysical questions, specifically: What is the distribution of binary systems that lead to common-envelope ejections and catastrophic mergers? What are the origins of ILRTs, and what is their connection to the giant eruptions of the more massive LBVs? What is the full landscape of LBV-like transients, and what kinds of LBV activity are inaccessible in the optical?

Motivated thus, I set out to perform a systematic search for IR transients in nearby galaxies. In this endevour, I joined a pioneering survey with *Spitzer* called SPIRITS—the SPitzer Infrared Intensive Transients Survey. In the following section, I describe the survey, including the initial experiment design and subsequent extensions, and our strategy to identify and verify astrophysical transients.

1.3 Discovery engine: SPitzer Infrared Intensive Transients Survey

SPIRITS (PIDs 11063, 13053, 14089; PI M. Kasliwal) is a six-year, large program totalling 1,690 hours to monitor nearby galaxies with the Infrared Array Camera (IRAC; Fazio et al. 2004) on board the warm *Spitzer Space Telescope* (Werner et al. 2004; Gehrz et al. 2007) in the 3.6 and 4.5 μm imaging bands ([3.6] and [4.5]). The original survey design is described in Kasliwal et al. (2017b), but I provide a overview of the full survey and technical details relevant to this thesis here.

For the first three years (2014–2016), SPIRITS observed a sample of 190 nearby galaxies with the 5×5 arcmin IRAC field of view. The sample was selected to cover a large range of galaxy types, sizes, and star-formation rates, and included: 1) the 37 galaxies within 5 Mpc including both early and late-type galaxies, dwarf galaxies and giant galaxies, 2) the 116 most luminous galaxies between 5 and 15 Mpc, including 83% of the B-band starlight within 15 Mpc, and 3) the 37 most luminous and massive galaxies in the Virgo Cluster at $\approx$ 17 Mpc. In the final three years (2017-2019), as described in Jencson et al. (2019d), the survey was extended to continue to monitor a subset of the 105 galaxies of the original sample most likely to host new transients. These included the 58 galaxies that had previously hosted at least one IR transient candidate, and the 47 remaining most luminous and highly star-forming galaxies ($L_B > 2 \times 10^{10}\ L_\odot$). In Figure 1.2, we show the distribution of SPIRITS galaxy distances[2] and B-band luminosities for the original full sample of 190 galaxies and the reduced 105 galaxy sub-sample. The bulk of the full (92%) and extension galaxy samples (89%) are within 20 Mpc, and we note the distribution of galaxy distances, particularly for the extension subsample, is relatively flat for $D \lesssim 20$ Mpc. In B-band luminosity, the sample spans $4 \times 10^6 \lesssim L_B \lesssim 9 \times 10^{10}\ L_\odot$, and 61% of the original sample of galaxies have $L > 10^{10}\ L_\odot$. This fraction increases to 77% for the extension sub-sample.

Each galaxy of the original sample was observed three times in 2014 at approximately one- and six-month intervals, and in 2015–2016, additional time baselines

[2]With the inclusion of updated distance measurements made since 2014, a handful of galaxies included in the SPIRITS sample lie outside the original distance limit for the survey of $\approx$ 20 Mpc.

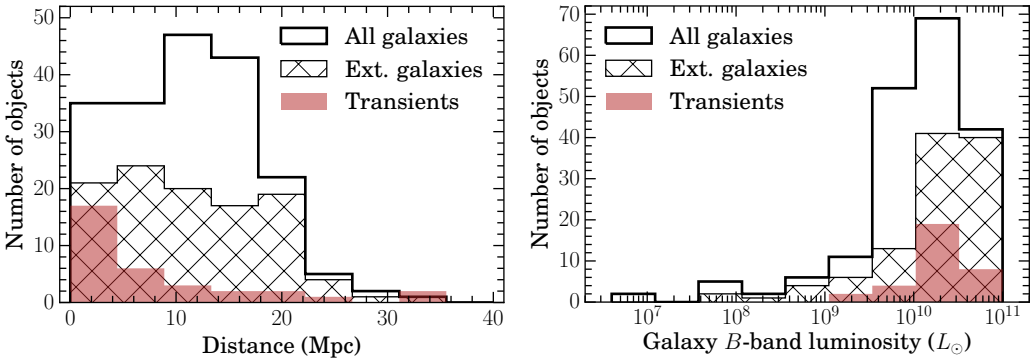

Figure 1.2: Distances (left panel) and host B-band luminosities (right panel) of SPIRITS galaxies (black-lined histograms), and the SPIRITS sample of transients (red histogram). The original, full sample of SPIRITS galaxies is shown as the thick-lined, unfilled histograms, and the extension, sub-sample of galaxies is shown as the thin-lined, cross-hatched histograms.

at one- and three-week intervals were added. In 2017–2018, the observing cadence was reduced to $\sim$ 6 month intervals for the extension sample, typically with one observation per galaxy per visibility window. In the final phase of the survey continuing throughout 2019 until January 2020, we will obtain four additional observations of each galaxy in the extension sample, with two visits per visibility window. To demonstrate the timescales probed by the survey, in Figure 1.3, we show histograms of time baselines for every image pair, and the survey cadence (time between consecutive observations) for each galaxy in the SPIRITS sample obtained through 2019 July 15. The longest baselines accessible from only SPIRITS data of $\approx$ 2000 days are set by the duration of the survey, but with the inclusion of archival imaging, we are sensitive in some cases to timescales up to $\approx$ 5700 days ($\approx$ 15 yr). The dominant peak in the cadence distribution at $\approx$ 180 days corresponds to the typical time separation between observations of a galaxy set by the available visibility windows for *Spitzer* to observe a given patch in the sky from its location in its orbit. The peaks at time separations corresponding to approximately one, two, and three week cadence are also evident from the higher cadence observations obtained within an individual visibility window during the 2015–2016 observing cycles.

Our imaging strategy throughout the survey for each SPIRITS observation consists of 7 dithered, 100 s exposures in both IRAC channels. We achieve nominal 5σ point source limiting depths of 20.0 and 19.1 mag (Vega) at [3.6] and [4.5], respectively,

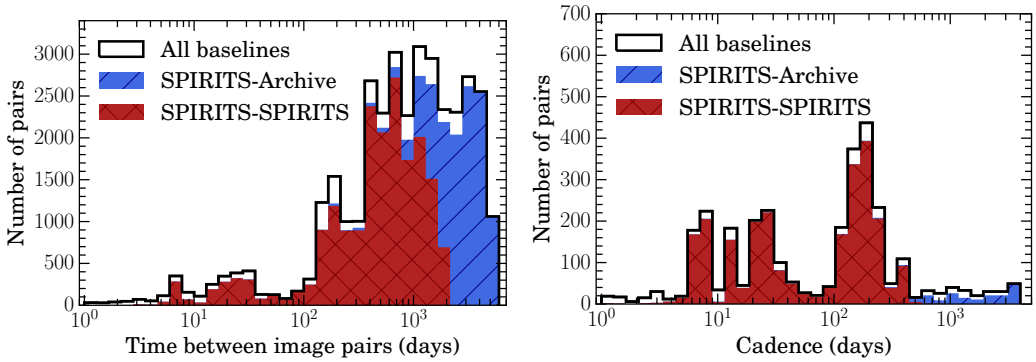

Figure 1.3: Histograms of time baselines for all image pairs (left panel) and consecutive observations (right panel) in *Spitzer*/IRAC [4.5] imaging for the SPIRITS sample of galaxies. In each panel, we show all baselines, including both archival imaging and SPIRITS data, as the black-outlined, unfilled histograms, the subset including at least one SPIRITS image as the blue, diagonal-hatched histograms, and the subset of SPIRITS–SPIRITS baselines as the red, cross-hatched histograms.

using the zero magnitude fluxes given in the IRAC instrument handbook[3] of F_{ν_0} = 280.9 Jy for [3.6] and F_{ν_0} = 179.7 Jy for [4.5].

Image subtraction pipeline and transient candidate identification

The details of our image subtraction and automated candidate identification pipeline are described in Kasliwal et al. (2017b). We use archival *Spitzer* frames, including Super Mosaics[4] or S4G (*Spitzer* Survey of Stellar Structure in Galaxies; PID 61065; PI K. Sheth; Sheth et al. 2010; Muñoz-Mateos et al. 2013; Querejeta et al. 2015), or stacks of archival "bcd" images (where Super Mosaics or S4G images were not available) as template reference images for subtraction. Candidates automatically identified by pipeline in the reference-subtracted images are vetted by human scanners, and sources passing human vetting are saved to our database and assigned a SPIRITS name. Transient candidates and strong variables discovered by SPIRITS were regularly reported via the Astronomer's Telegram (Kasliwal et al. 2014; Jencson et al. 2015; Jencson et al. 2016a; Jencson et al. 2016b; Jencson et al. 2016c; Jencson et al. 2017a, 2017b; Jencson et al. 2017d; Jencson et al. 2017c, 2018c; Jencson et al. 2018d; Jencson et al. 2019a; Jencson et al. 2019b).

Initial automated photometry is performed at the location of all newly saved SPIR-

[3] `http://irsa.ipac.caltech.edu/data/SPITZER/docs/irac/iracinstrumenthandbook/`

[4] Super Mosaics are available as Spitzer Enhanced Imaging Products through the NASA/IPAC Infrared Science Archive: `https://irsa.ipac.caltech.edu/data/SPITZER/Enhanced/SEIP/overview.html`

ITS candidates in the reference-subtracted images using a 4 mosaicked-pixel (2.″4) aperture and background annulus from 4–12 pixels (2.″4–7.″2). The extracted flux is multiplied by the aperture corrections of 1.215 for [3.6] and 1.233 for [4.5] as described in the IRAC instrument handbook, and converted to Vega system magnitudes using the handbook-defined zero magnitude fluxes for each IRAC channel. Our difference images are subject to a number of detector and processing artifacts. To mitigate these issues, we subsequently employ conservative error estimation for our photometry on all available difference images of convincing, "by eye"-vetted candidates. A description of the most significant types of difference image artifacts and our method to obtain reliable photometry and uncertainty estimates is provided in Appendix A. We then employ a strict 5σ threshold based on our robust error estimates for all transient candidates.

Transient verification and selection

From the sample of SPIRITS transient candidates saved to our database, I defined a set of rigorous selection criteria to identify bona fide transients:

1. At least two detections, either at both [3.6] and [4.5] or two detections in one channel.
2. An isolated outburst of individual, or consecutive detections, and sufficient upper limits from nondetections consisting of either:
    a) constraining (deeper than the transient's peak) limits from SPIRITS data both before and after the event of combined duration exceeding that of the detections, or,
    b) constraining limits either before or after the event, of duration exceeding one year or that of the detections, whichever is longer.
3. Absolute magnitude at the assumed distance to the host brighter than -11 mag, to which our observations are sensitive for the bulk of the sample out to ≈ 15 Mpc.

Criterion (1) allows us to reject false positives and moving solar system objects. Criterion (2) allows us to rule out (quasi)-periodic or otherwise episodic variables, like those presented by Karambelkar et al. (2019). Criterion (3) limits the biasing of the sample to abundant low-luminosity events from only the nearest galaxies, e.g., IR counterparts to classical novae.

I thus identify a total of 33 IR transients discovered by SPIRITS, listed in full in Table 1.1. The sample of SPIRITS transients arise from 22 host galaxies of the original 190 SPIRITS galaxies (2014-2016) and reduced sample of 105 galaxies (2017–2019). We provide some properties of this subset of galaxies in Table 1.2. All SPIRITS transient host galaxies, with the exception of the late-type lenticular galaxy NGC 4461 and the irregular galaxy NGC 3077, are star-forming, spiral galaxies. Four of these events discovered in 2014 were previously reported and discussed in our work describing the first year results of the SPIRITS survey (Kasliwal et al. 2017b), as noted in Table 1.1. Additionally, seven of these events were previously presented in (Jencson et al. 2019d), which describes the sample of luminous ($M \lesssim -14$ mag) SPIRITS events discovered in 2014–2018. Three additional events passed human vetting, but were not detected at $> 5\sigma$ significance in our photometry in at least two difference images, thus not passing criterion (1). These events, SPIRITS 17lk in IC 342 (originally announced in Jencson et al. 2017d), SPIRITS 19jk in NGC 3621, and SPIRITS 19jv in Centaurus A, are not included in the remaining analyses and discussion in this thesis.

1.4 Outline of this thesis

In what follows, I begin with detailed case studies of four luminous infrared transients, three of them newly discovered by SPIRITS. In Chapter 2, I present the discovery of SPIRITs 15c and SPIRITS 14buu, two obscured SNe in the nearby galaxy IC 2163, which provided the first confirmation that SPIRITS was uncovering CCSNe missed by optical searches owing to dust extinction. In Chapter 3, I examine the puzzle of SPIRITS 16tn, the most heavily reddened and one of the nearest luminous events in the SPIRITS sample at only 9 Mpc. I find that this event may be explained by a low-energy, deeply embedded CCSN, boasting a strong IR excess driven by a luminous dust echo. In Chapter 4, I turn to the case of M51 OT2019-1, the nearest ILRT discovered in over a decade, for which we can directly identify its luminous, dust-enshrouded progenitor in *Spitzer* imaging and track its history of IR variability over the last 12 years. Next, in Chapter 5, I undertake a systematic, in-depth study of the sample of all of the most luminous transients discovered by SPIRITS between 2014–2018. The sample includes 5 candidate obscured CCSNe, from which I derive robust estimates of the missing fraction in nearby galaxies, and four IR-dominated events possibly associated with an LRN, ILRT, and the dust-forming outbursts of massive LBVs. Finally in Chapter 6, I return to our landscape of IR transients (cf., Figure 1.1), highlighting the substantial progress that has been

made since 2014. In particular, I discuss the full ensemble of diverse transient phenomena uncovered by SPIRITS during our nearly 6 year run. To conclude, I turn an eye toward the future and discuss some exciting prospects for continued progress as *Spitzer* prepares to pass the torch.

Table 1.1: Sample of SPIRITS transients

Num.	Name	Host (J2000)	R.A. (J2000)	Decl.	UT discovery	Host offset ($''$)	Host offset (kpc)
1	SPIRITS 14aei[a]	M63	$13^h15^m52.''25$	$+42°02'29.''6$	2014 Mar 25.8	54.9	2.4
2	SPIRITS 14aje[a,b]	M101	$14^h02^m55.''51$	$+54°23'18.''5$	2014 Apr 24.8	206.0	6.8
3	SPIRITS 14axa[b]	M81	$09^h56^m01.''52$	$+69°03'12.''4$	2014 Jun 13.9	158.6	2.8
4	SPIRITS 14axb[b]	NGC 2403	$07^h36^m34.''70$	$+65°39'22.''3$	2014 Jun 19.4	216.7	3.3
5	SPIRITS 14azy[c]	NGC 2997	$09^h45^m40.''92$	$-31°12'07.''8$	2014 Jul 26.0	47.9	3.0
6	SPIRITS 14bay[b]	M64	$12^h56^m43.''25$	$+21°42'25.''7$	2014 Aug 20.8	86.1	2.2
7	SPIRITS 14bmc	NGC 300	$00^h54^m49.''68$	$-37°39'51.''2$	2014 Sep 5.2	87.3	0.8
8	SPIRITS 14bug	NGC 1385	$03^h37^m29.''43$	$-24°30'05.''6$	2014 Oct 18.5	15.3	0.6
9	SPIRITS 15c[c]	IC 2163	$06^h16^m28.''49$	$-21°22'42.''2$	2015 Feb 4.4	14.7	2.5
10	SPIRITS 15bb	M81	$09^h55^m32.''21$	$+69°02'49.''1$	2015 Feb 7.6	67.2	1.2
11	SPIRITS 15bh	M81	$09^h55^m33.''95$	$+69°02'46.''0$	2015 Feb 7.6	70.3	1.2
12	SPIRITS 15bk	M81	$09^h55^m57.''82$	$+69°02'12.''6$	2015 Feb 7.6	168.3	2.9
13	SPIRITS 15lq	NGC 4945	$13^h05^m39.''06$	$-49°28'18.''1$	2015 May 1.9	113.6	2.0
14	SPIRITS 15ud[c]	M100	$12^h22^m55.''29$	$+15°49'22.''0$	2015 Sep 6.7	6.2	0.4
15	SPIRITS 15ade[c]	NGC 5921	$15^h22^m05.''55$	$+05°03'15.''9$	2015 Nov 11.9	148.6	16.9
16	SPIRITS 15aht	M81	$09^h55^m18.''54$	$+69°04'22.''8$	2016 Jan 10.5	82.4	1.4
17	SPIRITS 16az	NGC 4490	$12^h30^m27.''78$	$+41°39'41.''3$	2016 Mar 5.2	115.6	5.7
18	SPIRITS 16ix[c]	NGC 4461	$12^h29^m03.''16$	$+13°11'30.''7$	2016 Mar 30.9	29.0	2.8
19	SPIRITS 16rs	NGC 4945	$13^h05^m07.''36$	$-49°32'40.''0$	2016 May 27.6	337.1	5.9
20	SPIRITS 16tn[c]	NGC 3556	$11^h11^m20.''40$	$+55°40'17.''3$	2016 Aug 15.0	89.9	3.8
21	SPIRITS 17ar	NGC 4945	$13^h05^m36.''89$	$-49°23'38.''2$	2016 Oct 12.8	282.7	4.9
22	SPIRITS 17fe	NGC 7793	$23^h57^m44.''77$	$-32°34'58.''4$	2017 Feb 16.7	69.1	1.2
23	SPIRITS 17lb[c]	IC 2163	$06^h16^m27.''78$	$-21°22'51.''7$	2017 May 28.7	20.2	3.5
24	SPIRITS 17mj	M81	$09^h55^m36.''20$	$+69°06'21.''0$	2017 Jun 23.7	145.7	2.6
25	SPIRITS 18q	NGC 3077	$10^h03^m12.''67$	$+68°43'31.''2$	2018 Feb 10.2	50.0	0.9
26	SPIRITS 18dz	NGC 2903	$09^h32^m04.''41$	$+21°32'50.''5$	2018 Aug 1.8	182.7	8.2
27	SPIRITS 18nu	IC 342	$03^h46^m45.''62$	$+68°03'26.''8$	2018 Dec 18.0	142.4	2.4
28	SPIRITS 18ny	IC 342	$03^h46^m32.''35$	$+68°05'17.''0$	2018 Dec 18.0	98.9	1.7
29	SPIRITS 19bh	NGC 1365	$03^h33^m49.''12$	$-36°04'26.''7$	2019 Apr 1.2	284.6	25.0
30	SPIRITS 19bj	M81	$09^h55^m25.''40$	$+69°03'45.''6$	2019 Apr 1.4	42.6	0.7
31	SPIRITS 19bl	M81	$09^h56^m02.''78$	$+69°05'18.''9$	2019 Apr 1.4	179.1	3.1
32	SPIRITS 19fi	NGC 4535	$12^h34^m16.''73$	$+08°10'00.''3$	2019 Apr 25.2	123.7	9.7
33	SPIRITS 19hb	M83	$13^h36^m57.''94$	$-29°52'38.''0$	2019 May 18.3	56.3	1.3

[a] These events were detected in the first epoch of SPIRITS imaging in 2014, and thus we have only weak constraints on their explosion times and peak magnitudes.
[b] Transient previously presented in Kasliwal et al. (2017b).
[c] Transient previously presented Jencson et al. (2017e), Jencson et al. (2018e), and/or Jencson et al. (2019d).

Table 1.2: SPIRITS transient host galaxies

Name	Num.	R.A. (J2000)	Decl. (J2000)	Type	$m - M$ (mag)	D (Mpc)	$E(B-V)_{\rm MW}$ (mag)	L_B ($L_\odot$)
NGC 300	1	$00^{\rm h}54^{\rm m}53\overset{\prime\prime}{.}53$	$-37°41'05\overset{\prime\prime}{.}5$	SAd	26.48 (0.06)	2.0	0.01	2.6×10^9
NGC 2403	1	$07^{\rm h}36^{\rm m}50\overset{\prime\prime}{.}65$	$+65°36'09\overset{\prime\prime}{.}4$	SABcd	27.51 (0.06)	3.2	0.03	8.8×10^9
IC 342	2	$03^{\rm h}46^{\rm m}49\overset{\prime\prime}{.}15$	$+68°05'47\overset{\prime\prime}{.}8$	SABcd	27.69 (0.08)	3.5	0.48	5.9×10^{10}
NGC 4945	3	$13^{\rm h}05^{\rm m}27\overset{\prime\prime}{.}48$	$-49°28'05\overset{\prime\prime}{.}6$	SBcd	27.77 (0.05)	3.6	0.15	2.9×10^{10}
NGC 7793	1	$23^{\rm h}57^{\rm m}49\overset{\prime\prime}{.}72$	$-32°35'27\overset{\prime\prime}{.}6$	SAd	27.77 (0.07)	3.6	0.02	4.6×10^9
M81	8	$09^{\rm h}55^{\rm m}33\overset{\prime\prime}{.}10$	$+69°03'56\overset{\prime\prime}{.}2$	SAab	27.79 (0.06)	3.6	0.07	3.1×10^{10}
NGC 3077	1	$10^{\rm h}03^{\rm m}20\overset{\prime\prime}{.}02$	$+68°44'01\overset{\prime\prime}{.}3$	I0 pec	27.90 (0.07)	3.8	0.06	1.8×10^9
M83	1	$13^{\rm h}37^{\rm m}00\overset{\prime\prime}{.}80$	$-29°51'55\overset{\prime\prime}{.}8$	SABc	28.34 (0.07)	4.7	0.06	3.6×10^{10}
M64	1	$12^{\rm h}56^{\rm m}43\overset{\prime\prime}{.}80$	$+21°41'00\overset{\prime\prime}{.}0$	SAab	28.60 (0.08)	5.2	0.04	2.8×10^{10}
M101	1	$14^{\rm h}03^{\rm m}12\overset{\prime\prime}{.}60$	$+54°20'56\overset{\prime\prime}{.}6$	SABcd	29.17 (0.13)	6.8	0.01	4.1×10^{10}
NGC 1385	1	$03^{\rm h}37^{\rm m}28\overset{\prime\prime}{.}31$	$-24°30'04\overset{\prime\prime}{.}6$	SBcd	29.48 (0.43)	7.9	0.02	1.0×10^{10}
NGC 3556	1	$11^{\rm h}11^{\rm m}30\overset{\prime\prime}{.}98$	$+55°40'26\overset{\prime\prime}{.}4$	SBcd	29.72 (0.43)	8.8	0.01	1.6×10^{10}
M63	1	$13^{\rm h}15^{\rm m}49\overset{\prime\prime}{.}32$	$+42°01'45\overset{\prime\prime}{.}4$	SAbc	29.74 (0.02)	8.9	0.02	4.6×10^{10}
NGC 2903	1	$09^{\rm h}32^{\rm m}10\overset{\prime\prime}{.}10$	$+21°30'06\overset{\prime\prime}{.}0$	SABbc	29.83 (0.43)	9.2	0.03	5.0×10^{10}
NGC 4490	1	$12^{\rm h}30^{\rm m}36\overset{\prime\prime}{.}36$	$+41°38'37\overset{\prime\prime}{.}0$	SBd pec	30.02 (0.40)	10.1	0.02	1.9×10^{10}
NGC 2997	1	$09^{\rm h}45^{\rm m}38\overset{\prime\prime}{.}81$	$-31°11'28\overset{\prime\prime}{.}3$	SABc	30.59 (0.39)	13.1	0.09	5.0×10^{10}
M100	1	$12^{\rm h}22^{\rm m}54\overset{\prime\prime}{.}90$	$+15°49'24\overset{\prime\prime}{.}8$	SABc	30.72 (0.06)	13.9	0.02	5.8×10^{10}
NGC 4535	1	$12^{\rm h}34^{\rm m}20\overset{\prime\prime}{.}10$	$+08°11'53\overset{\prime\prime}{.}5$	SABc	31.04 (0.09)	16.1	0.02	3.1×10^{10}
NGC 1365	1	$03^{\rm h}33^{\rm m}36\overset{\prime\prime}{.}43$	$-36°08'26\overset{\prime\prime}{.}1$	SBb	31.29 (0.04)	18.1	0.02	3.0×10^{10}
NGC 4461	1	$12^{\rm h}29^{\rm m}03\overset{\prime\prime}{.}01$	$+13°11'01\overset{\prime\prime}{.}8$	$SB0^+$	31.48 (0.25)	19.8	0.02	2.6×10^{10}
NGC 5921	1	$15^{\rm h}21^{\rm m}56\overset{\prime\prime}{.}41$	$+05°04'14\overset{\prime\prime}{.}2$	SBbc	31.85 (0.22)	23.4	0.03	7.2×10^9
IC 2163	2	$06^{\rm h}16^{\rm m}27\overset{\prime\prime}{.}77$	$-21°22'31\overset{\prime\prime}{.}5$	SBc pec	32.75 (0.40)	35.5	0.07	2.1×10^{10}

Chapter 2

CASE STUDY OF SPIRITS 15c AND SPIRITS 14buu: TWO OBSCURED SUPERNOVAE IN THE NEARBY STAR-FORMING GALAXY IC 2163

Jencson, Jacob E., et al. 2017. "SPIRITS 15c and SPIRITS 14buu: Two Obscured Supernovae in the Nearby Star-forming Galaxy IC 2163". *ApJ* 837 (2): 167–185. doi:10.3847/1538-4357/aa618f. arXiv: 1609.04444 [astro-ph.HE].

Jacob E. Jencson[1], Mansi M. Kasliwal[1], Joel Johansson[2], Carlos Contreras[3], Sergio Castellón[3], Howard E. Bond[4,5], Andrew J. Monson[4], Frank J. Masci[6], Ann Marie Cody[7], Jennifer E. Andrews[8], John Bally[9], Yi Cao[1], Ori D. Fox[5], Timothy Gburek[10], Robert D. Gehrz[10], Wayne Green[9], George Helou[6], Eric Hsiao[11], Nidia Morrell[3], Mark Phillips[3], Thomas A. Prince[1], Robert A. Simcoe[12], Nathan Smith[8], Samaporn Tinyanont[1], and Robert Williams[5]

[1]Division of Physics, Mathematics, and Astronomy, California Institute of Technology, Pasadena, CA 91125, USA
[2]Benoziyo Center for Astrophysics, Weizmann Institute of Science, 76100 Rehovot, Israel
[3]Las Campanas Observatory, Carnegie Observatories, Casilla 601, La Serena, Chile
[4]Dept. of Astronomy & Astrophysics, Pennsylvania State University, University Park, PA 16802, USA
[5]Space Telescope Science Institute, 3700 San Martin Dr., Baltimore, MD 21218 USA
[6]Infrared Processing and Analysis Center, California Institute of Technology, Pasadena, CA 91125, USA
[7]NASA Ames Research Center, Moffett Field, CA 94035, USA
[8]Steward Observatory, University of Arizona, 933 North Cherry Avenue, Tucson, AZ 85721, USA
[9]Center for Astrophysics and Space Astronomy, University of Colorado, 389 UCB, Boulder, CO 80309, USA
[10]Minnesota Institute for Astrophysics, School of Physics and Astronomy, 116 Church Street, S. E., University of Minnesota, Minneapolis, MN 55455, USA
[11]Department of Physics, Florida State University, 77 Chieftain Way, Tallahassee, FL, 32306, USA
[12]MIT-Kavli Institute for Astrophysics and Space Research, 70 Vassar Street., Cambridge, MA 02139, USA

Abstract

SPitzer InfraRed Intensive Transients Survey—SPIRITS–is an ongoing survey of nearby galaxies searching for infrared (IR) transients with *Spitzer*/IRAC. We present the discovery and follow-up observations of one of our most luminous ($M_{[4.5]} = -17.1 \pm 0.4$ mag, Vega) and reddest ([3.6]−[4.5] $= 3.0 \pm 0.2$ mag) transients, SPIRITS 15c. The transient was detected in a dusty spiral arm of IC 2163 ($D \approx 35.5$ Mpc). Pre-discovery ground-based imaging revealed an associated, shorter-duration transient in the optical and near-IR (NIR). NIR spectroscopy showed a

broad ($\approx$ 8400 km s^{-1}), double-peaked emission line of He I at 1.083 μm, indicating an explosive origin. The NIR spectrum of SPIRITS 15c is similar to that of the Type IIb SN 2011dh at a phase of $\approx$ 200 days. Assuming an $A_V = 2.2$ mag of extinction in SPIRITS 15c provides a good match between their optical light curves. The NIR light curves, however, show some minor discrepancies when compared with SN 2011dh, and the extreme [3.6]−[4.5] color has not been previously observed for any SN IIb. Another luminous ($M_{4.5} = -16.1 \pm 0.4$ mag) event, SPIRITS 14buu, was serendipitously discovered in the same galaxy. The source displays an optical plateau lasting $\gtrsim$ 80 days, and we suggest a scenario similar to the low-luminosity Type IIP SN 2005cs obscured by $A_V \approx 1.5$ mag. Other classes of IR-luminous transients can likely be ruled out in both cases. If both events are indeed supernovae (SNe), this may suggest that $\gtrsim$ 18% of nearby core-collapse SNe are missed by currently operating optical surveys.

2.1 Introduction

In the last few decades, the study of astrophysical transients has been revolutionized by the introduction of all-sky, high-cadence surveys dedicated to their discovery. The largest advances have been made in the optical, where the majority of time-domain surveys operate; the dynamic infrared (IR) sky is only now beginning to be explored. IR follow-up of optically discovered transients has revealed new classes of events that can be dominated by IR emission, especially at late times. At least two known classes of transients, with peak luminosities between those typical of novae and supernovae (SNe), can develop IR-dominated spectral energy distributions (SEDs) as they evolve: (1) stellar mergers, or luminous red novae, e.g., M31-RV (Bond 2011, and references therein), V1309 Sco (Tylenda et al. 2011), V838 Mon (Bond et al. 2003; Sparks et al. 2008), the 2011 transient in NGC 4490 (hereafter NGC 4490-OT, Smith et al. 2016) and M101 OT2015-1 (M101-OT, Blagorodnova et al. 2017), and (2) SN 2008S-like events, or intermediate luminosity red transients (Prieto et al. 2008; Thompson et al. 2009; Kochanek 2011a), also including NGC 300 OT2008-1 (hereafter NGC 300-OT, Bond et al. 2009; Humphreys et al. 2011) and PTF 10fqs (Kasliwal et al. 2011). Furthermore, otherwise luminous optical sources such as SNe may suffer extinction from obscuring dust, lending themselves to discovery and follow-up at IR wavebands where the effect of dust extinction is significantly reduced.

Previous searches for obscured SNe have thus been motivated by the notion that, if a significant fraction of SNe are heavily obscured, measurements of the SN rate

from optical searches will only be lower limits (e.g. Grossan et al. 1999; Mattila and Meikle 2001; Maiolino et al. 2002; Cresci et al. 2007). Searches at near-IR (NIR) wavelengths have focused on the dense, highly star-forming, nuclear regions of starburst galaxies, luminous IR galaxies (LIRGS) and ultra-luminous IR galaxies (e.g. van Buren et al. 1994; Grossan et al. 1999; Maiolino et al. 2002; Mattila et al. 2002; Mannucci et al. 2003; Mattila, Meikle, and Greimel 2004; Mattila, Monard, and Li 2005; Mattila et al. 2005; Miluzio et al. 2013; Fox and Casper 2015). Multi-wavelength studies of two obscured SNe, SN 2010O and SN 2010P, in LIRG Arp 299, for example, suggested its two merging components may have different extinction laws (Kankare et al. 2014; Romero-Cañizales et al. 2014). These searches have uncovered a handful of additional obscured SNe, but have been limited by insufficient angular resolution to probe the densest regions of starburst galaxies.

High angular resolution studies using space-based telescopes or adaptive optics have found several candidates, and confirmed four obscured SNe (Cresci et al. 2007; Mattila et al. 2007; Kankare et al. 2008; Kankare et al. 2012). The SN rate estimates from such searches are still a factor of 3–10 lower than is expected from the high star-formation rates inferred from the far-IR luminosities of the surveyed galaxies (e.g. Cresci et al. 2007). Radio very long baseline interferometry studies of the innermost regions of LIRGs have, in fact, revealed scores of radio SNe and SN remnants that have remained hidden at other wavelengths (Lonsdale et al. 2006; Pérez-Torres et al. 2009; Ulvestad 2009; Bondi et al. 2012; Herrero-Illana, Pérez-Torres, and Alberdi 2012; Romero-Cañizales et al. 2012). A few bona fide radio transients have also been identified as obscured SNe II, e.g., an SN in the starburst galaxy Mrk 297 (Yin and Heeschen 1991), VLA 121550.2+130654 (Gal-Yam et al. 2006), and SN 2008iz in M82 ($A_V > 10$ mag; Brunthaler et al. 2009; Brunthaler et al. 2010; Mattila et al. 2013).

Even in "normal" star-forming galaxies in the nearby Universe, where extinction is much less extreme, it has been suggested that the measured rates of core-collapse SNe (CCSNe) are still low compared to those expected from star-formation rates (Horiuchi et al. 2011). This indicates that optical surveys may be missing populations of nearby SNe that are either intrinsically faint or hidden by dust. By comparing the observed distribution of host extinctions for 13 SNe discovered within 12 Mpc between 2000 and 2011 to that predicted for smooth dust distributions in local galaxies, Mattila et al. (2012) estimate that locally 19^{+19}_{-10}% of CCSNe are missed by rest-frame optical surveys in normal galaxies. Moderate levels of visual extinction

($A_V \sim$ few mag) in the less extreme star-forming environments of nearby galaxies are sufficient to dim some SNe beyond the detection limits of current optical surveys, further motivating IR transient searches of such hosts.

Since 2013 December, we have been conducting a systematic search for transients in the IR with the SPitzer InfraRed Intensive Transients Survey (SPIRITS; PID11063; PI M. Kasliwal). This is an ongoing, three-year targeted survey of 194 galaxies within 20 Mpc using the InfraRed Array Camera (IRAC; Fazio et al. 2004) aboard the *Spitzer Space Telescope* (*Spitzer*; Werner et al. 2004; Gehrz et al. 2007) at 3.6 and 4.5 μm ([3.6] and [4.5], respectively). Every galaxy in our sample has archival *Spitzer*/IRAC imaging, such that our observing cadence covers time baselines from one week to several years. In our first year, SPIRITS discovered over 1958 IR variable stars, and 43 transients. Four of these transients were in the luminosity range consistent with classical novae, and 21 were known SNe (for details, see Fox et al. 2016, Tinyanont et al. 2016, and Johansson et al. 2017). Fourteen were in the IR luminosity gap between novae and supernovae and had no optical counterparts, possibly constituting a newly discovered class of IR-dominated transients (Kasliwal et al. 2017b).

Here, we report the discovery of two transients discovered in dusty spiral arms of the galaxy IC 2163, SPIRITS 15c and SPIRITS 14buu. The IR luminosity of SPIRITS 15c was brighter than -17 mag, one of the most luminous transients discovered by SPIRITS to date and more luminous than the new classes of IR-dominated transients described above. Additionally, the spectrum of SPIRITS 15c is dominated by a broad emission line of He I, suggesting that this is an explosive event, such as an SN, but with significant dust extinction that obscured the transient in the optical. In Section 2.2, we describe the discovery and optical/IR follow-up observations of SPIRITS 15c, and the subsequent post-outburst, serendipitous discovery of SPIRITS 14buu. In Section 2.3, we describe the analysis of our photometric and spectroscopic data. In Section 2.4, we explore the possibility that SPIRITS 15c is an obscured SN based on the similarity of its NIR spectrum to that of the well-studied Type IIb SN 2011dh. Using a similar analysis, we consider that SPIRITS 14buu is yet another obscured SN, likely of Type IIP. We also consider non-supernova IR transient scenarios in Section 2.4, including stellar mergers, SN 2008S-like events, and the proposed helium nova V445 Pup. Finally, in Section 2.5, we summarize the observational characteristics of SPIRITS 15c and SPIRITS 14buu and present our conclusions.

2.2 SPIRITS discovery and follow-up observations

We present the discoveries of SPIRITS 15c and SPIRITS 14buu, and describe observations of this event from our concomitant ground-based survey of SPIRITS galaxies.

Spitzer/IRAC Discovery in IC 2163

As part of the regular SPIRITS observing program, the interacting pair of late-type galaxies IC 2163 and NGC 2207 were observed at 10 epochs between 2014 January 13.9 and 2016 January 12.1. Image subtraction was performed using archival *Spitzer*/IRAC images from 2005 February 22.7 as references. For details on our image subtraction pipeline, see Kasliwal et al. (2017b). On 2015 February 19, a transient source, designated SPIRITS 15c, was identified by the SPIRITS team in an image at [4.5] taken on 2015 February 4.4.[1] The [4.5] discovery image is shown in Figure 2.1.

SPIRITS 15c was discovered at a R.A. and decl. of $06^{\rm h}16^{\rm m}28\farcs49$, $-21^\circ22'42\farcs2$ (J2000), coincident with a spiral arm of the galaxy IC 2163. We assume a distance modulus to IC 2163 of $\mu = 32.75 \pm 0.4$ mag from the mean of the JHK Tully–Fisher relation distance estimates (≈ 35.5 Mpc, Theureau et al. 2007 from NED[2]). IC 2163 has a redshift of $z = 0.00922$ ($v = 2765$ km s^{-1}, Elmegreen et al. 2000). We note that IC 2163 was originally selected as part of the SPIRITS sample based on an incorrect distance estimate that placed it within the 20 Mpc cutoff for SPIRITS galaxies. The foreground Galactic extinction toward IC 2163 is $A_V = 0.238$ mag from NED (Fitzpatrick 1999; Schlafly and Finkbeiner 2011). There is most likely additional extinction from the foreground spiral arm of NGC 2207.

Photometry was performed at the position of SPIRITS 15c on the reference subtracted images, using a 4-mosaicked-pixel aperture and a background annulus from 4–12 pixels. The extracted flux was multiplied by aperture corrections of 1.215 and 1.233 for [3.6] and [4.5], respectively, as outlined in the IRAC instrument handbook. The photometric measurements, given in Table 2.1, indicate a high luminosity of $M_{[4.5]} = -17.1 \pm 0.4$ mag at the distance of IC 2163 and an extremely red color of

[1] The lag between the observations and discovery of SPIRITS 15c was due to the time for *Spitzer*/IRAC observations to be made available on the *Spitzer* Heritage Archive. Since 2015 May, the SPIRITS team has made extensive use of the *Spitzer* Early Release Data Program, allowing us to discovery transients within a few days of observation.

[2] The NASA/IPAC Extragalactic Database (NED) is operated by the Jet Propulsion Laboratory, California Institute of Technology, under contract with the National Aeronautics and Space Administration.

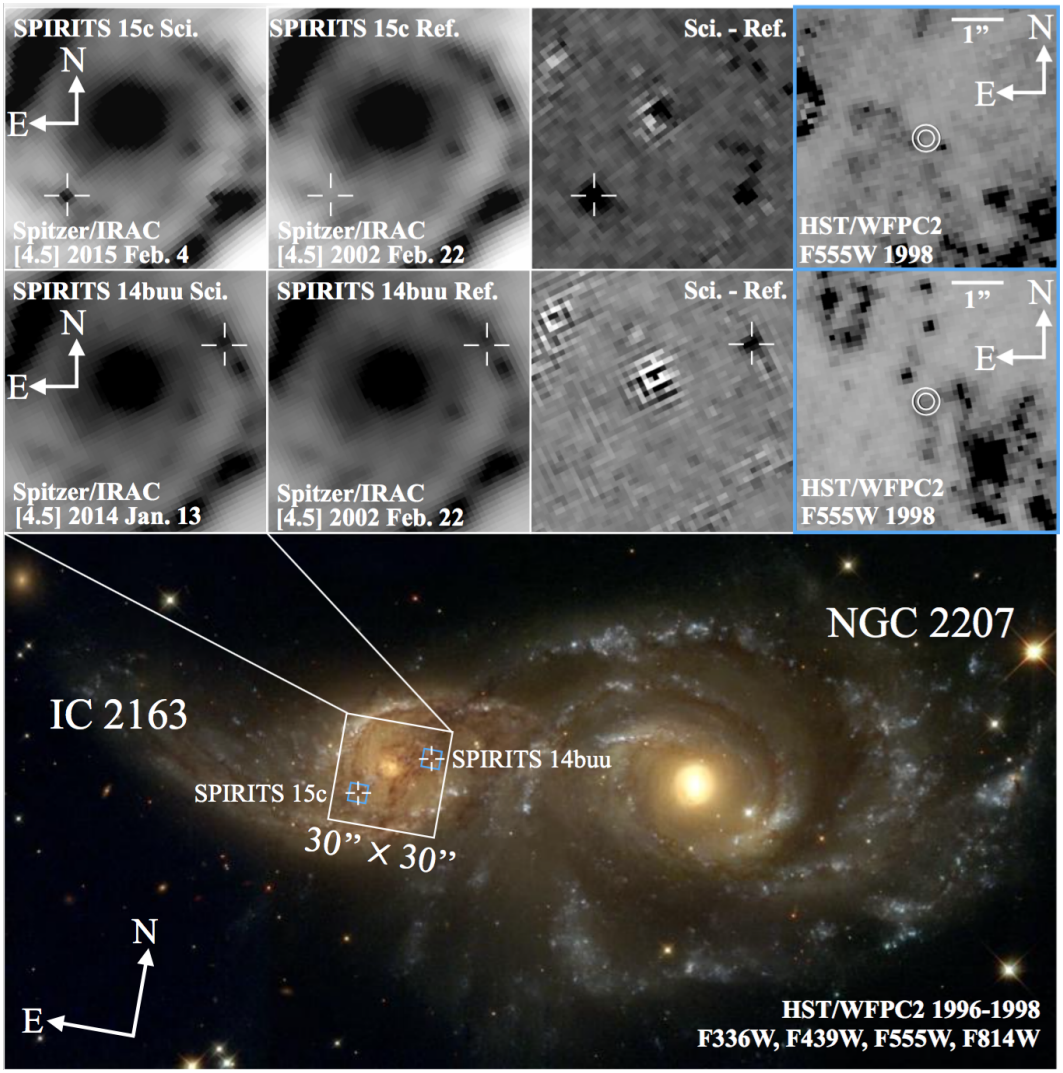

Figure 2.1: The bottom panel shows color-composite, archival *HST*/WFPC2 imaging of the interacting galaxy pair of IC 2163 and NGC 2207 from 1996-1998 in four filters (F336W and F439W in blue, F555W in green, and F814W in red). The image comes from the Hubble Heritage Project with credit to NASA and the Hubble Heritage Team (STScI/AURA). The approximate positions of SPIRITS 15c and SPIRITS 14buu in dusty spiral arms of IC 2163 are indicated with the crosshairs. The right panels of the top and middle rows show zoom-ins of the F555W image to the regions indicated by the blue squares for SPIRITS 15c and SPIRITS 14buu, respectively. The white circles show the 3σ and 5σ uncertainties on the precise positions of the transients. We are unable to identify an individual star as a candidate progenitor in either case. The left three panels in the top and middle rows show the $30'' \times 30''$ region indicated by the white zoom-in box. The first row of panels from the left are the *Spitzer*/IRAC discovery science frames at [4.5] from 2015 February 4.4 (top row; SPIRITS 15c) and 2014 January 13.9 (middle row; SPIRITS 14buu), the second row are the reference images from 2005 February 22.7 (PID3544; PI D. M. Elmegreen), and the third row are the science–reference subtraction images, clearly showing the new, transient sources. We note that, in the SPIRITS 15c discovery and subtraction images, the apparent variability of the galaxy nucleus is likely a subtraction artifact as both positive and negative flux appear in the subtracted frame. The apparent new source directly to the west of SPIRITS 15c, which is not present at [3.6] or at any other epoch, is also likely spurious, given its boxy and irregular shape.

[3.6]−[4.5] = 3.0±0.2 mag at the epoch of discovery. SPIRITS 15c was not detected in earlier images taken on 2014 June 8.7 to a limiting magnitude of $m \gtrsim 18.3$ mag at [4.5] (−14.5 mag absolute), providing an age constraint for SPIRITS 15c as an active mid-IR (MIR) source of 240.7 days. Additional detections were made at [4.5] in SPIRITS observations of IC 2163 on 2015 May 26.9, June 3.8, and June 24.1, fading by ≈ 2 mag in 140 days. On 2015 December 23.0, SPIRITS 15c was undetected at [4.5] and remained so in all subsequent SPIRITS observations through the most recent one on 2016 January 12.1. The source was undetected at [3.6] in all post-discovery epochs of *Spitzer*/IRAC observation. The 5σ depth in the reference images at the position of SPIRITS 15c is 14.9 mag (≈ −17.9 mag absolute) in both bands, and thus, we are unable to place meaningful constraints on the IR properties of the progenitor system. The full sequence of photometric measurements from *Spitzer*/IRAC for SPIRITS 15c is summarized in Table 2.1 and shown in Figure 2.2, along with the NIR and optical measurements described below in Section 2.2.

Table 2.1: Photometry of SPIRITS 15c

UT Date	MJD	Phase[a] (days)	Tel./Inst.	Band	App. Mag.[b,c] (mag)	Abs. Mag.[c,d] (mag)
2013 Dec 16.1	56642.1	-248	NOTCam	K_s	> 17.0	> −15.8
2013 Dec 24.3	56650.3	-240	P60	g	> 20.4	> −12.7
2014 Jan 13.9	56670.9	-220	*Spitzer*/IRAC	[3.6]	> 18.6	> −14.2
2014 Jan 13.9	56670.9	-220	*Spitzer*/IRAC	[4.5]	> 18.4	> −14.3
2014 Jan 10.2	56667.2	-223	du Pont/RetroCam	Y	> 19.7	> −13.2
2014 Jan 10.2	56667.2	-223	du Pont/RetroCam	J	> 19.2	> −13.6
2014 Jan 10.2	56667.2	-223	du Pont/RetroCam	H	> 18.8	> −14.0
2014 Feb 06.2	56694.2	-196	Baade/IMACS	WB6226–7171	> 22.0	> −10.9
2014 Feb 18.2	56706.2	-184	Swope/CCD	g	> 20.7	> −12.3
2014 Feb 18.2	56706.2	-184	Swope/CCD	r	> 20.7	> −12.2
2014 Feb 18.2	56706.2	-184	Swope/CCD	i	> 20.5	> −12.4
2014 Mar 07.1	56723.1	-167	Baade/FourStar	J	> 20.4	> −12.5
2014 Mar 15.1	56731.1	-159	du Pont/RetroCam	Y	> 20.7	> −12.2
2014 Mar 15.1	56731.1	-159	du Pont/RetroCam	J	> 20.4	> −12.4
2014 Mar 16.1	56732.1	-158	du Pont/RetroCam	H	> 19.0	> −13.8
2014 Apr 13.0	56760.0	-130	Swope/CCD	r	> 20.6	> −12.3
2014 Apr 13.0	56760.0	-130	Swope/CCD	i	> 20.5	> −12.4
2014 May 13.7	56790.7	-100	*Spitzer*/IRAC	[3.6]	> 18.8	> −14.0
2014 May 13.7	56790.7	-100	*Spitzer*/IRAC	[4.5]	> 18.6	> −14.2
2014 May 27.9	56804.9	-86	LCOGT-1m/CCD	i	> 18.7	> −14.2
2014 Jun 08.7	56816.7	-74	*Spitzer*/IRAC	[3.6]	> 18.7	> −14.0
2014 Jun 08.7	56816.7	-74	*Spitzer*/IRAC	[4.5]	> 18.3	> −14.4
2014 Jul 25.4	56863.4	-27	LCOGT-1m/CCD	i	> 19.0	> −13.9
2014 Aug 21.4	56890.4	0	LCOGT-1m/CCD	i	17.66 (0.06)	−15.2
2014 Sep 20.3	56920.3	30	LCOGT-1m/CCD	i	18.25 (0.06)	−14.6
2014 Sep 29.0	56929.0	39	Swope/CCD	g	20.9 (0.2)	−12.1

Table 2.1 – *Continued*

UT Date	MJD	Phase[a] (days)	Tel./Inst.	Band	App. Mag.[b,c] (mag)	Abs. Mag.[c,d] (mag)
2014 Sep 29.0	56929.0	39	Swope/CCD	r	19.2 (0.1)	−13.7
2014 Sep 29.0	56929.0	39	Swope/CCD	i	18.57 (0.09)	−14.3
2014 Oct 23.3	56953.3	63	LCOGT-1m/CCD	r	19.6 (0.3)	−13.3
2014 Oct 23.3	56953.3	63	LCOGT-1m/CCD	i	19.1 (0.3)	−13.8
2014 Nov 15.2	56976.2	86	LCOGT-1m/CCD	r	20.4 (0.3)	−12.6
2014 Nov 15.2	56976.2	86	LCOGT-1m/CCD	i	19.5 (0.3)	−13.4
2014 Nov 20.4	56981.4	91	Lemmon-1.5m/2MASSCam	J	> 14.3	> −18.5
2014 Nov 20.4	56981.4	91	Lemmon-1.5m/2MASSCam	H	> 13.5	> −19.3
2014 Nov 20.4	56981.4	91	Lemmon-1.5m/2MASSCam	K_s	> 13.1	> −19.7
2014 Dec 05.3	56996.3	106	du Pont/RetroCam	Y	18.8 (0.2)	−14.1
2014 Dec 05.3	56996.3	106	du Pont/RetroCam	H	17.79 (0.08)	−15.0
2014 Dec 14.3	57005.3	115	LCOGT-1m/CCD	r	> 19.6	> −13.3
2014 Dec 14.3	57005.3	115	LCOGT-1m/CCD	i	> 19.2	> −13.7
2014 Dec 20.2	57011.2	121	Swope/CCD	g	> 21.1	> −11.9
2014 Dec 20.2	57011.2	121	Swope/CCD	r	> 20.8	> −12.1
2014 Dec 20.2	57011.2	121	Swope/CCD	i	> 20.4	> −12.5
2015 Jan 13.2	57035.2	145	LCOGT-1m/CCD	r	> 19.6	> −13.3
2015 Jan 13.2	57035.2	145	LCOGT-1m/CCD	i	> 19.2	> −13.7
2015 Jan 16.3	57038.3	148	Lemmon-1.5m/2MASSCam	J	> 13.5	> −19.3
2015 Jan 16.3	57038.3	148	Lemmon-1.5m/2MASSCam	H	> 12.7	> −20.1
2015 Jan 16.3	57038.3	148	Lemmon-1.5m/2MASSCam	K_s	> 12.6	> −20.2
2015 Jan 20.0	57042.0	152	Baade/IMACS	WB6226–7171	21.4 (0.1)	−11.5
2015 Jan 29.1	57051.1	161	du Pont/RetroCam	Y	19.9 (0.2)	−12.9
2015 Jan 29.1	57051.1	161	du Pont/RetroCam	J	19.8 (0.1)	−13.0
2015 Jan 29.1	57051.1	161	du Pont/RetroCam	H	18.8 (0.1)	−14.0
2015 Feb 02.2	57055.2	165	Swope/CCD	g	> 20.2	> −12.8
2015 Feb 02.2	57055.2	165	Swope/CCD	r	> 20.1	> −12.8
2015 Feb 02.2	57055.2	165	Swope/CCD	i	> 20.1	> −12.8
2015 Feb 04.4	57057.4	167	*Spitzer*/IRAC	[3.6]	18.7 (0.2)	−14.1
2015 Feb 04.4	57057.4	167	*Spitzer*/IRAC	[4.5]	15.68 (0.02)	−17.1
2015 Feb 13.0	57066.0	176	LCOGT-1m/CCD	r	> 19.0	> −13.9
2015 Feb 13.0	57066.0	176	LCOGT-1m/CCD	i	> 18.9	> −14.0
2015 Feb 18.0	57071.0	181	Baade/FourStar	K_s	19.17 (0.08)	−13.6
2015 Feb 20.2	57073.2	183	Lemmon-1.5m/2MASSCam	J	> 14.3	> −18.5
2015 Feb 20.2	57073.2	183	Lemmon-1.5m/2MASSCam	H	> 13.5	> −19.3
2015 Feb 20.2	57073.2	183	Lemmon-1.5m/2MASSCam	K_s	> 13.2	> −19.6
2015 Mar 09.1	57090.1	200	du Pont/RetroCam	Y	> 20.3	> −12.6
2015 Mar 09.1	57090.1	200	du Pont/RetroCam	J	> 19.6	> −13.2
2015 Mar 09.1	57090.1	200	du Pont/RetroCam	H	> 18.8	> −14.0
2015 Mar 13.1	57094.1	204	Swope/CCD	g	> 20.6	> −12.4
2015 Mar 13.1	57094.1	204	Swope/CCD	r	> 19.9	> −13.0
2015 Mar 13.1	57094.1	204	Swope/CCD	i	> 19.5	> −13.4
2015 Mar 14.0	57095.0	205	du Pont/RetroCam	Y	> 20.2	> −12.6
2015 Mar 14.0	57095.0	205	du Pont/RetroCam	J	> 20.3	> −12.5
2015 Mar 14.0	57095.0	205	du Pont/RetroCam	H	> 19.4	> −13.4
2015 Mar 15.0	57096.0	206	LCOGT-1m/CCD	r	> 19.2	> −13.7
2015 Mar 15.0	57096.0	206	LCOGT-1m/CCD	i	> 18.8	> −14.1
2015 Mar 15.0	57096.0	206	Kuiper/Mont4k	R	> 20.5	> −12.4

Table 2.1 – *Continued*

UT Date	MJD	Phase[a] (days)	Tel./Inst.	Band	App. Mag.[b,c] (mag)	Abs. Mag.[c,d] (mag)
2015 Apr 05.1	57117.1	227	du Pont/RetroCam	Y	> 20.2	> −12.7
2015 Apr 05.1	57117.1	227	du Pont/RetroCam	J	> 19.3	> −13.5
2015 Apr 05.1	57117.1	227	du Pont/RetroCam	H	> 18.5	> −14.3
2015 Apr 16.4	57128.4	238	LCOGT-1m/CCD	r	> 20.1	> −12.8
2015 Apr 16.4	57128.4	238	LCOGT-1m/CCD	i	> 19.5	> −13.4
2015 Apr 30.0	57142.0	252	du Pont/RetroCam	Y	> 20.6	> −12.3
2015 Apr 30.0	57142.0	252	du Pont/RetroCam	J	> 20.1	> −12.7
2015 Apr 30.0	57142.0	252	du Pont/RetroCam	H	> 18.9	> −13.8
2015 May 26.9	57168.9	278	*Spitzer*/IRAC	[3.6]	> 18.8	> −14.0
2015 May 26.9	57168.9	278	*Spitzer*/IRAC	[4.5]	17.01 (0.06)	−15.7
2015 Jun 03.8	57176.8	286	*Spitzer*/IRAC	[3.6]	> 18.9	> −13.9
2015 Jun 03.8	57176.8	286	*Spitzer*/IRAC	[4.5]	17.05 (0.07)	−15.7
2015 Jun 24.1	57197.1	307	*Spitzer*/IRAC	[3.6]	> 18.7	> −14.1
2015 Jun 24.1	57197.1	307	*Spitzer*/IRAC	[4.5]	17.32 (0.08)	−15.4
2015 Sep 05.4	57270.4	380	Baade/FourStar	J	> 20.2	> −12.6
2015 Sep 05.4	57270.4	380	Baade/FourStar	H	> 19.9	> −12.9
2015 Sep 05.4	57270.4	380	Baade/FourStar	K_s	> 19.5	> −13.3
2015 Nov 19.3	57345.3	455	du Pont/RetroCam	Y	> 20.9	> −11.9
2015 Nov 19.3	57345.3	455	du Pont/RetroCam	J	> 20.7	> −12.1
2015 Nov 19.3	57345.3	455	du Pont/RetroCam	H	> 19.8	> −13.0
2015 Nov 22.3	57348.3	458	du Pont/RetroCam	Y	> 20.7	> −12.2
2015 Nov 22.3	57348.3	458	du Pont/RetroCam	J	> 20.1	> −12.7
2015 Nov 22.3	57348.3	458	du Pont/RetroCam	H	> 19.5	> −13.3
2015 Dec 23.0	57379.0	489	*Spitzer*/IRAC	[3.6]	> 18.8	> −14.0
2015 Dec 23.0	57379.0	489	*Spitzer*/IRAC	[4.5]	> 18.5	> −14.3
2015 Dec 30.1	57386.1	496	*Spitzer*/IRAC	[3.6]	> 18.7	> −14.0
2015 Dec 30.1	57386.1	496	*Spitzer*/IRAC	[4.5]	> 18.4	> −14.3
2016 Jan 12.1	57399.1	509	*Spitzer*/IRAC	[3.6]	> 18.8	> −14.0
2016 Jan 12.1	57399.1	509	*Spitzer*/IRAC	[4.5]	> 18.3	> −14.4

[a] Phase is number of days since the earliest detection of this event on 2014 August 21.4 (MJD = 56890.4).

[b] 1σ uncertainties are given in parentheses.

[c] 5σ limiting magnitudes are given for non-detections.

[d] Absolute magnitudes corrected for Galactic extinction for IC 2163 from NED.

Host Galaxy Properties

Elmegreen et al. (2016) report global values of the 24 μm flux density from a *Spitzer*/MIPS 2013 archival image of $S_\nu(24\ \mu\mathrm{m}) = 5.9 \times 10^2$ mJy for IC 2136, and 2.06×10^4 mJy for the galaxy pair as a whole. They also give global Hα fluxes, derived from narrowband Hα and broadband R images from Elmegreen et al. (2001), of $S(\mathrm{H}\alpha) = 5.9 \times 10^{-13}$ and 3.49×10^{-12} erg s^{-1} cm^{-2} for IC 2163 and the pair as a whole, respectively. Combining these, and following Kennicutt et al. (2009), gives global star-formation rates of 1.9 $M_\odot$ yr^{-1} for IC 2163 and 6.8 $M_\odot$ yr^{-1} for both galaxies combined. The rate of SNe associated with this galaxy pair is also

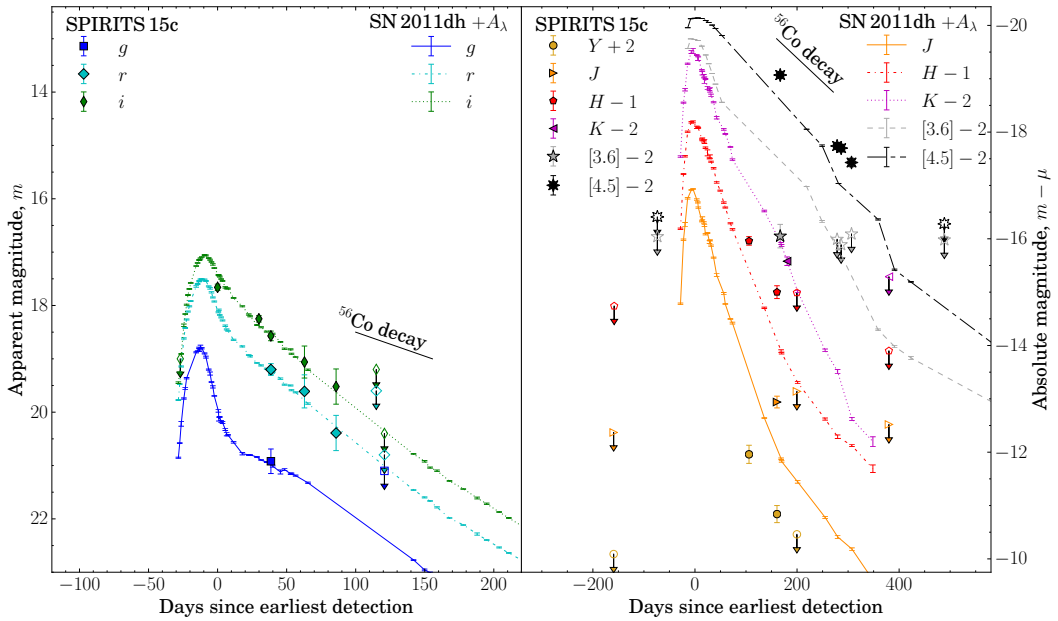

Figure 2.2: The optical (gri; AB magnitudes; left panel), and IR ($YJHK_s$, [3.6], and [4.5]; Vega magnitudes; right panel) light curves of SPIRITS 15c (points) and the Type IIb SN 2011dh (lines). Unfilled points with downward arrows indicate upper limits. Error bars are shown, but are sometimes smaller than the points. Time on the x-axis is given as the number of days since the earliest detection of SPIRITS 15c on 2014 August 21.4 (MJD = 56890.4). The light curves of SN 2011dh are shifted in apparent magnitude to the distance of SPIRITS 15c, with applied total reddening characterized by $E(B-V)_{\rm MW}+E(B-V)_{host} = 0.72$ mag, or $A_V \approx 2.2$ magnitudes of extinction assuming a standard $R_V = 3.1$ extinction law (Fitzpatrick 1999; Chapman et al. 2009; Schlafly and Finkbeiner 2011). The phase of the SN 2011dh light curves is set so that the earliest detection of SN 2011dh coincides with the most constraining non-detection preceding the outburst of SPIRITS 15c. For comparison, we also show the expected decay rate for a light curve powered by the radioactive decay of ^{56}Co (see Gehrz 1988; Gehrz and Ney 1990).

high, with five known SNe hosted in IC 2163 and NGC 2207 since 1975. These include four CCSNe (SN 1999ec, Jha et al. 1999; Modjaz and Li 1999; SN 2003H, Filippenko et al. 2003; SN 2013ai, Conseil et al. 2013; SN 2010jp, Smith et al. 2012) and one thermonuclear SN (SN 1975A, Kirshner, Arp, and Dunlap 1976). The most recent SN associated with the galaxy pair, SN 2010jp, is a peculiar SN IIn with evidence for strong interaction with a dense circumstellar medium (CSM) and a bipolar, jet-driven explosion (Smith et al. 2012).

In a 3.6 arcsec aperture centered on the location of SPIRITS 15c, $S_\nu(24\ \mu{\rm m}) = 8.38$ mJy, as measured in the HiRes devconvolution image from Velusamy et al. (2008) (1.9 arcsec resolution). In the same aperture, $S({\rm H}\alpha) = 1.25{\times}10^{-14}$ erg s^{-1} cm^{-2}.

Additionally, the ^{12}CO(1-0) (115.27 GHz, 2.6 mm) line flux in this region, measured with ALMA, implies a mean line-of-sight H_2 surface density of $\Sigma_{H_2} = 13.7\ M_\odot\ \mathrm{pc}^{-2}$ (Elmegreen et al. 2016; Kaufman et al. 2016, private communication). Estimates of the star-formation rate using Hα as tracer in such a small aperture, will include stochastic effects related to including too few O stars, but these measurements suggest ongoing star formation in the vicinity of SPIRITS 15c and that the transient may be associated with a young stellar population. The heliocentric radial velocity in the ALMA CO velocity image at the nearest non-blanked pixel to SPIRITS 15c is $v_{\mathrm{CO,helio}} = 2827\ \mathrm{km\ s}^{-1}$ (2″ separation; Elmegreen et al. 2016; Kaufman et al. 2016, private communication). We adopt this value as the velocity of SPIRITS 15c with respect to the observer frame throughout this paper.

Ground-based Imaging

To supplement our *Spitzer*/IRAC observations, the SPIRITS team is undertaking a concomitant, ground-based survey of SPIRITS galaxies in the optical and NIR, using a number of telescopes and instruments.

IC 2163 was imaged at several epochs in gri with the CCD camera on the Swope Telescope at Las Campanas Observatory (LCO). NIR YJH imaging of SPIRITS 15c was also obtained at several epochs with the RetroCam IR camera on the du Pont Telescope, and J, H, and K_s-band images were obtained with the FourStar IR camera on the Magellan Baade Telescope at LCO (Persson et al. 2013). Photometry was extracted using simple aperture photometry, with the aperture size defined by the seeing in each image, and calibrated against SDSS field stars for the optical images and 2MASS stars for the NIR images. For Y-band images, we adopt the conversion from 2MASS used for the Wide Field Camera on the United Kingdom Infrared Telescope from Hodgkin et al. (2009). Image subtraction was performed for the Swope/CCD and du Pont/Retrocam images using template images taken on 2015 March 13.2 (after SPIRITS 15c had faded) and 2014 January 10.2, respectively, to obtain more accurate photometry and deeper limits from non-detection images.

We also obtained optical imaging with the Las Cumbres Observatory Global Telescope (LCOGT; Brown et al. 2013) Network 1-m telescopes in the r- and i-bands. Photometry was performed by simultaneously fitting the point spread function (PSF) of the transient, measured using SDSS field stars, and background, modeled using low-order polynomials. The photometric measurements were also calibrated against SDSS field stars.

Additional imaging of IC 2163 was obtained on 2014 February 6.2 and 2015 January 20.0 with the Inamori Magellan Areal Camera and Spectrograph (IMACS) on the Magellan Baade Telescope, using a wide-band, red filter (WB6226–7171 calibrated to SDSS r'); on 2015 March 16, using the Mont4k on the Kuiper 61" Telescope in R-band; on 2013 December 24.3 with the optical camera on the 60-in telescope at Palomar observatory (P60) in g, r, and i; and on 2013 December 16.1 in K_s-band, with the Nordic Optical Telescope near-infrared Camera and spectrograph (NOTCam), at the Observatorio del Roque de los Muchachos.

The earliest detection of SPIRITS 15c on 2014 August 21.4 (MJD = 56890.4) was also the observed optical peak at $i = 17.66 \pm 0.06$ mag. Correcting for Galactic extinction gives a peak absolute magnitude $M_i \leq -15.1 \pm 0.4$ mag, where any additional foreground or host extinction would imply a higher intrinsic luminosity. Throughout the rest of this paper, we refer to days t since the earliest detection of SPIRITS 15c on this date. Our most stringent constraint on the age of SPIRITS 15c is the 28.4-day window between the earliest detection and the previous optical non-detection on 2014 July 24.0. The observed optical colors at $t = 38.6$ days were quite red with $g - r = 1.71 \pm 0.15$ mag and $g - i = 2.24 \pm 0.15$ mag. By $t = 120.8$ days, SPIRITS 15c had faded beyond detection with Swope/CCD, but was still detected in the Baade/IMACS image at 21.4 ± 0.1 mag.

At $t = 105.9$ days, SPIRITS 15c was detected in the NIR with $H = 17.84 \pm 0.06$ mag (-14.91 ± 0.4 mag absolute), and a red NIR color with $Y - H = 1.04 \pm 0.09$ mag. The transient then faded in the NIR by 1 mag at nearly constant color over the next 54.8 days. All of our photometric measurements for SPIRITS 15c are summarized in Table 2.1 and the light curves are shown in Figure 2.2.

Another transient discovery: SPIRITS 14buu

During the analysis of our imaging data, a second transient was serendipitously noticed in IC 2163 at a R.A. and decl. of $06^{\rm h}16^{\rm m}27\farcs2$, $-21°22'29\farcs2$ (J2000), located in a spiral arm directly on the other side of the galaxy from SPIRITS 15c. This transient was active in January 2014 SPIRITS *Spitzer*/IRAC data, before the implementation of our automated image subtraction and candidate identification pipeline. It was retroactively assigned the name SPIRITS 14buu. We show the [4.5] discovery image in Figure 2.1.

The earliest detection of this event is in the P60 r- and i-band images taken on 2013 December 24.3 (MJD = 56650.3). It was not detected in the K_s NOTCam image on

2013 December 16.1 to $K_s > 16.6$ mag (> -16.2 mag absolute), but this limit is not deep enough to constrain the age of SPIRITS 14buu. The optical and IR light curves of SPIRITS 14buu are given in Table 2.2 and shown in Figure 2.3. In the r- and i-bands, the source displays a plateau lasting at least 80 days at $i = 19.2 \pm 0.1$ mag ($M_i = -13.7$ mag absolute) and with $r - i = 0.7 \pm 0.2$ mag. The source is undetected in g-band indicating $g - i \gtrsim 1.7$ mag. Following the plateau, the optical light curves fall off steeply, dropping in i-band by $\gtrsim 1.1$ mag in $\lesssim 24$ days. A luminous NIR counterpart was detected during the optical plateau with $H = 17.44 \pm 0.07$ ($M_H = -15.3$ absolute). The source shows red NIR colors with $Y - H = 0.76 \pm 0.09$ and $J - H = 0.4 \pm 0.1$ mag, and a slow decline in the NIR of ≈ 0.2 mag over 65 days.

Table 2.2: Photometry of SPIRITS 14buu

UT Date	MJD	Phase[a] (days)	Tel./Inst.	Band	App. Mag.[b,c] (mag)	Abs. Mag.[c,d] (mag)
2013 Dec 16.1	56642.1	-8	NOTCam	K_s	> 16.6	> −16.2
2013 Dec 24.3	56650.3	0	P60	g	> 20.4	> −12.6
2013 Dec 24.3	56650.3	0	P60	r	20.0 (0.3)	−13.0
2013 Dec 24.3	56650.3	0	P60	i	19.4 (0.3)	−13.5
2014 Jan 10.2	56667.2	17	du Pont/RetroCam	Y	18.20 (0.06)	−14.6
2014 Jan 10.2	56667.2	17	du Pont/RetroCam	J	17.80 (0.08)	−15.0
2014 Jan 10.2	56667.2	17	du Pont/RetroCam	H	17.44 (0.07)	−15.3
2014 Jan 13.9	56670.9	21	*Spitzer*/IRAC	[3.6]	16.69 (0.08)	−16.1
2014 Jan 13.9	56670.9	21	*Spitzer*/IRAC	[4.5]	16.70 (0.05)	−16.1
2014 Feb 18.2	56706.2	56	Swope/CCD	g	> 20.9	> −12.2
2014 Feb 18.2	56706.2	56	Swope/CCD	r	20.0 (0.2)	−12.9
2014 Feb 18.2	56706.2	56	Swope/CCD	i	19.2 (0.1)	−13.7
2014 Mar 07.1	56723.1	73	Baade/FourStar	J	18.09 (0.02)	−14.7
2014 Mar 14.0	56730.0	80	Swope/CCD	g	> 20.8	> −12.2
2014 Mar 14.0	56730.0	80	Swope/CCD	r	20.0 (0.2)	−13.0
2014 Mar 14.0	56730.0	80	Swope/CCD	i	19.4 (0.1)	−13.5
2014 Mar 15.1	56731.1	81	du Pont/RetroCam	Y	18.43 (0.08)	−14.4
2014 Mar 15.1	56731.1	81	du Pont/RetroCam	J	18.11 (0.06)	−14.7
2014 Mar 16.1	56732.1	82	du Pont/RetroCam	H	17.6 (0.1)	−15.2
2014 Apr 13.0	56760.0	110	Swope/CCD	g	> 20.8	> −12.2
2014 Apr 13.0	56760.0	110	Swope/CCD	r	> 20.6	> −12.4
2014 Apr 13.0	56760.0	110	Swope/CCD	i	> 20.5	> −12.4
2014 May 13.7	56790.7	140	*Spitzer*/IRAC	[3.6]	18.0 (0.2)	−14.8
2014 May 13.7	56790.7	140	*Spitzer*/IRAC	[4.5]	17.13 (0.06)	−15.6
2014 Jun 08.7	56816.7	166	*Spitzer*/IRAC	[3.6]	18.4 (0.2)	−14.3
2014 Jun 08.7	56816.7	166	*Spitzer*/IRAC	[4.5]	17.28 (0.08)	−15.5
2014 Sep 29.4	56929.4	279	Swope/CCD	g	> 21.5	> −11.5
2014 Sep 29.4	56929.4	279	Swope/CCD	r	> 21.0	> −11.9
2014 Sep 29.4	56929.4	279	Swope/CCD	i	> 20.7	> −12.2
2014 Dec 05.3	56996.3	346	du Pont/RetroCam	Y	> 20.5	> −12.3
2014 Dec 05.3	56996.3	346	du Pont/RetroCam	H	> 20.1	> −12.7
2014 Dec 20.2	57011.2	361	Swope/CCD	g	> 21.4	> −11.6

Table 2.2 – *Continued*

UT Date	MJD	Phase[a] (days)	Tel./Inst.	Band	App. Mag.[b,c] (mag)	Abs. Mag.[c,d] (mag)
2014 Dec 20.2	57011.2	361	Swope/CCD	r	> 21.0	> -11.9
2014 Dec 20.2	57011.2	361	Swope/CCD	i	> 20.6	> -12.3
2015 Jan 29.1	57051.1	401	du Pont/RetroCam	Y	> 21.2	> -11.6
2015 Jan 29.1	57051.1	401	du Pont/RetroCam	J	> 20.6	> -12.2
2015 Jan 29.1	57051.1	401	du Pont/RetroCam	H	> 20.2	> -12.6
2015 Feb 02.2	57055.2	405	Swope/CCD	g	> 20.1	> -12.9
2015 Feb 02.2	57055.2	405	Swope/CCD	r	> 20.1	> -12.8
2015 Feb 02.2	57055.2	405	Swope/CCD	i	> 20.1	> -12.8
2015 Feb 04.4	57057.4	407	*Spitzer*/IRAC	[3.6]	> 18.6	> -14.2
2015 Feb 04.4	57057.4	407	*Spitzer*/IRAC	[4.5]	> 17.8	> -15.0
2015 Feb 18.0	57071.0	421	Baade/FourStar	K_s	> 19.1	> -13.6
2015 Mar 09.1	57090.1	440	du Pont/RetroCam	Y	> 20.2	> -12.6
2015 Mar 09.1	57090.1	440	du Pont/RetroCam	J	> 19.7	> -13.1
2015 Mar 09.1	57090.1	440	du Pont/RetroCam	H	> 19.2	> -13.6
2015 Mar 13.1	57094.1	444	Swope/CCD	g	> 21.5	> -11.5
2015 Mar 13.1	57094.1	444	Swope/CCD	r	> 21.0	> -12.0
2015 Mar 13.1	57094.1	444	Swope/CCD	i	> 20.4	> -12.5
2015 Mar 14.0	57095.0	445	du Pont/RetroCam	J	> 19.9	> -12.9
2015 Apr 05.1	57117.1	467	du Pont/RetroCam	Y	> 20.0	> -12.8
2015 Apr 05.1	57117.1	467	du Pont/RetroCam	J	> 19.4	> -13.5
2015 Apr 05.1	57117.1	467	du Pont/RetroCam	H	> 18.9	> -13.9
2015 Apr 30.0	57142.0	492	du Pont/RetroCam	Y	> 20.6	> -12.2
2015 Apr 30.0	57142.0	492	du Pont/RetroCam	J	> 20.1	> -12.7
2015 Apr 30.0	57142.0	492	du Pont/RetroCam	H	> 19.3	> -13.5
2015 May 26.9	57168.9	519	*Spitzer*/IRAC	[3.6]	> 18.8	> -14.0
2015 May 26.9	57168.9	519	*Spitzer*/IRAC	[4.5]	> 17.7	> -15.0
2015 Jun 03.8	57176.8	526	*Spitzer*/IRAC	[3.6]	> 18.7	> -14.1
2015 Jun 03.8	57176.8	526	*Spitzer*/IRAC	[4.5]	> 17.6	> -15.1
2015 Jun 24.1	57197.1	547	*Spitzer*/IRAC	[3.6]	> 18.4	> -14.3
2015 Jun 24.1	57197.1	547	*Spitzer*/IRAC	[4.5]	> 17.7	> -15.1
2015 Sep 05.4	57270.4	620	Baade/FourStar	J	> 19.6	> -13.2
2015 Sep 05.4	57270.4	620	Baade/FourStar	H	> 19.4	> -13.4
2015 Sep 05.4	57270.4	620	Baade/FourStar	K_s	> 19.0	> -13.8
2015 Nov 22.3	57348.3	698	du Pont/RetroCam	Y	> 20.8	> -12.0
2015 Nov 22.3	57348.3	698	du Pont/RetroCam	H	> 20.0	> -12.8
2015 Dec 23.0	57379.0	729	*Spitzer*/IRAC	[3.6]	> 18.5	> -14.3
2015 Dec 23.0	57379.0	729	*Spitzer*/IRAC	[4.5]	> 17.6	> -15.1
2015 Dec 30.1	57386.1	736	*Spitzer*/IRAC	[3.6]	> 18.4	> -14.4
2015 Dec 30.1	57386.1	736	*Spitzer*/IRAC	[4.5]	> 17.8	> -15.0
2016 Jan 12.1	57399.1	749	*Spitzer*/IRAC	[3.6]	> 18.3	> -14.5
2016 Jan 12.1	57399.1	749	*Spitzer*/IRAC	[4.5]	> 17.7	> -15.1
2016 Mar 02.1	57449.1	799	du Pont/RetroCam	Y	> 20.4	> -12.5
2016 Mar 02.1	57449.1	799	du Pont/RetroCam	H	> 18.5	> -14.2

[a] Phase is number of days since the earliest detection of this event on 2014 August 21.4 (MJD = 56650.3).

[b] 1σ uncertainties are given in parentheses.

[c] 5σ limiting magnitudes are given for non-detections.

[d] Absolute magnitudes corrected for Galactic extinction for IC 2163 from NED.

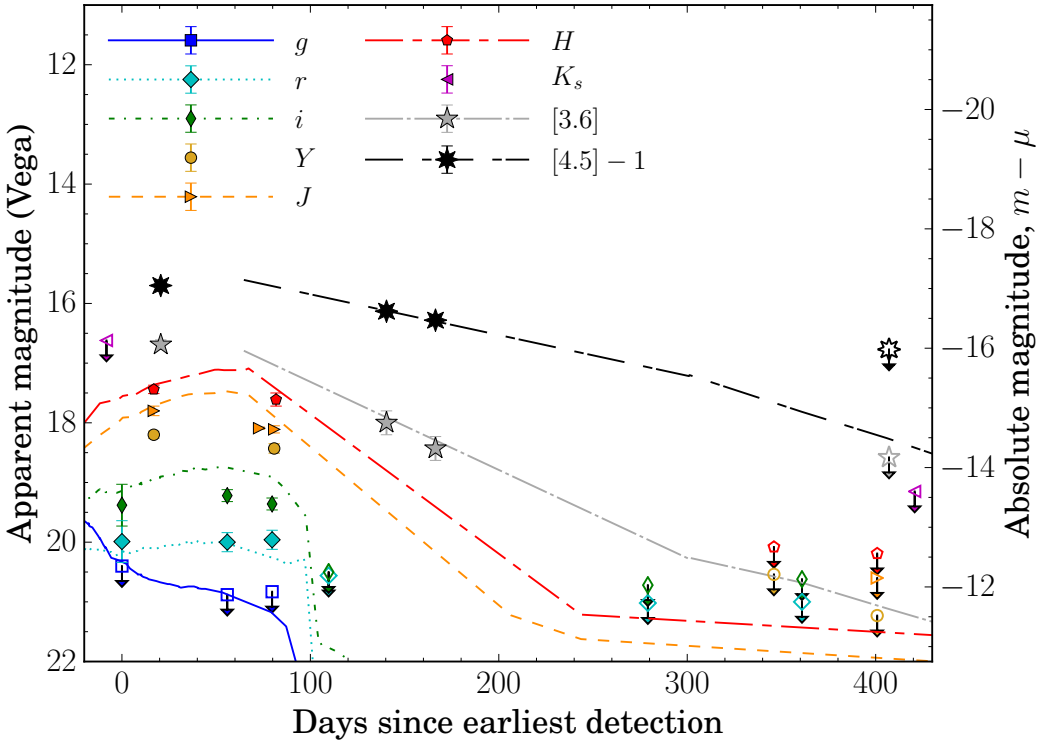

Figure 2.3: The optical (*gri*; AB magnitudes), and IR (*YJH*, [3.6], and [4.5]; Vega magnitudes) light curves of SPIRITS 14buu (points). Also shown are the *griJH* light curves of the Type IIP SN 2005cs and the [3.6] and [4.5] light curves of SN 2004et (lines). Unfilled points with downward arrows indicate upper limits. Error bars are shown, but are usually smaller than the points. Time on the x-axis is given as the number of days since the earliest detection of SPIRITS 14buu on MJD = 56650.3. The light curves of SN 2005cs are shifted in absolute magnitude by 0.1 mag, with applied total reddening characterized by $E(B-V) = 0.49$, or $A_V \approx 1.5$ mag assuming a standard R_V=3.1 extinction law (Fitzpatrick 1999; Chapman et al. 2009; Schlafly and Finkbeiner 2011). The light curves of SN 2004et are shifted fainter by 2.4 mag. The phase of the SN 2005cs light curves is set so that fall-off of the plateau lines up with that of SPIRITS 14buu. The phase of the SN 2004et light curves is time in days from the assumed explosion epoch (MJD = 53270.0; Li et al. 2005).

SPIRITS 14buu was also detected as a luminous MIR source with *Spitzer*/IRAC. The observed MIR peak occurred at 17 days after the earliest detection of this event at 16.7 ± 0.1 mag (-16.1 absolute) in both bands. At [4.5], the light curve declines slowly by 0.6 ± 0.1 mag over 145.8 days, extending well past the time of the plateau fall-off in the optical. At [3.6], the source fades more quickly developing a red [3.6]$-$[4.5] color of 1.2 ± 0.2 mag by 166.4 days after the earliest detection. The source faded beyond detection in both bands by 407.1 days.

We further describe the characteristics of this transient and discuss possible physical interpretations below in Section 2.4.

Archival *Hubble Space Telescope* (*HST*) Imaging

Images of the interacting galaxies IC 2163 and NGC 2207 were obtained with the *Hubble Space Telescope* (*HST*) on 1998 November 11 in program GO-6483 (PI: D. Elmegreen)[3]. These observations used the Wide Field Planetary Camera 2 (WFPC2), and fortuitously covered the site of SPIRITS 15c and SPIRITS 14buu, some 17 years before their outbursts. Images of this galaxy pair were also included in the Hubble Heritage collection. In the bottom panel of Figure 2.1, we show the color-composite Hubble Heritage Project[4] image of the field containing the transients made from imaging data in the F814W (red), F555W (green), F439W, and F336W (blue) filters. We note the locations of SPIRITS 15c and SPIRITS 14buu in dusty spiral arms of IC 2163.

In the *HST* images of IC 2163, the location of SPIRITS 15c unfortunately lies close to the edge of the PC chip, so we did not further analyze those frames. In the images of NGC 2207, the SPIRITS 15c site is well-placed in the WF2 field. We chose two sets of dithered frames taken with the F555W filter ($\sim V$; exposures of 3×160 s plus one of 180 s), and with F814W ($\sim I$; 4×180 s). We registered and combined these two sets of images, using standard tasks in IRAF[5].

To find the precise location of SPIRITS 15c in the WFPC2 frames, we employed the Baade/IMACS WB6226–7171 image from 2015 January 20.0. Using centroid measurements for 15 stars detected both in the Baade/IMACS frame and in the

[3]Based on observations made with the NASA/ESA Hubble Space Telescope, obtained from the data archive at the Space Telescope Science Institute. STScI is operated by the Association of Universities for Research in Astronomy, Inc. under NASA contract NAS 5-26555.

[4]Image Credit: NASA and The Hubble Heritage Team (STScI/AURA).

[5]IRAF is distributed by the National Optical Astronomy Observatory, which is operated by the Association of Universities for Research in Astronomy (AURA) under a cooperative agreement with the National Science Foundation.

two combined WFPC2 images, we determined the geometric transformation from Magellan to WFPC2 using the STSDAS[6] `geomap` task. By applying the `geotran` task to the Magellan frame, and blinking this transformed image against the WFPC2 frames, we verified the quality of the registration. The `geoxytran` task then yielded the x, y pixel location of SPIRITS 15c in the *HST* images. The standard deviations of the geometric fits for the reference stars were 0.50 and 0.48 pixels in each coordinate in F555W and F814W, respectively, corresponding to $0\farcs05$.

The precise location of SPIRITS 15c is shown in the upper right panel of Figure 2.1 with 3- and 5σ error circles overlaid on the F555W image. At the pre-eruption site in 1998, we detect no progenitor star in either F555W or F814W. The location is within a dark dust lane, with very few stars detected in its vicinity. The 5σ limiting magnitudes in the *HST* frames are $V > 25.1$ and $I > 24.0$ mag. These correspond to absolute magnitudes of $M_V > -7.9$ and $M_I > -8.9$ mag at the assumed distance of IC 2163, correcting only for Galactic extinction.

To analyze the location of the transient, we preformed the same analysis on the Baade/IMACS image from 2014 February 6.2 with a clear detection of SPIRITS 14buu. Again, we found the standard deviations of the geometric fits for the reference stars were ≈ 0.50 pixels ($\approx 0\farcs05$) in each coordinate in both the F555W and F814W frames. The precise location of SPIRITS 14buu is shown in the right panel of Figure 2.1. The transient is coincident with a poorly resolved stellar association or cluster in the center of a dusty spiral arm, but it is not possible to identify an individual star as a candidate progenitor given the distance to IC 2163.

NIR Spectroscopy

We obtained an epoch of NIR spectroscopy of SPIRITS 15c with the Folded-port InfraRed Echellette spectrograph (FIRE; Simcoe et al. 2008; Simcoe et al. 2013) on the Magellan Baade Telescope at LCO at $t = 205$ days on 2015 March 14, and a later epoch with the Multi-Object Spectrometer for Infra-Red Exploration (MOSFIRE; McLean et al. 2010; McLean et al. 2012) on the Keck I Telescope at W. M. Keck Observatory at $t = 222$ days on 2015 March 31. SPIRITS 14buu was also included in the MOSFIRE slit mask, but the source was not detected above the host galaxy light. This was 60 days after the du Pont/Retrocam non-detection of SPIRITS 14buu at $J > 20.6$ mag.

[6]STSDAS (Space Telescope Science Data Analysis System) is a product of STScI, which is operated by AURA for NASA.

The Baade/FIRE observations were obtained using the low-dispersion, high-throughput prism mode and a completed ABBA dither sequence. The data span 0.8–2.5 μm, at a resolution ranging from 300 to 500. Immediately afterward, we obtained a spectrum of the flux and telluric standard star HIP 32816. The data were reduced using the IDL pipeline FIREHOSE, which is specifically designed to reduce FIRE data (Simcoe et al. 2013). The pipeline performed steps of flat-fielding, wavelength calibration, sky subtraction, spectral tracing, and extraction. The sky flux was modeled using off-source pixels as described by Kelson (2003), and was subtracted from each frame. The spectral extraction was then performed using the optimal technique of Horne (1986) to deliver the maximum signal-to-noise ratio while preserving spectrophotometric accuracy. Individual spectra were then combined with sigma clipping to reject spurious pixels. Corrections for telluric absorption were performed using the IDL tool *xtellcor* developed by Vacca, Cushing, and Rayner (2003). To construct a telluric correction spectrum free of stellar absorption features, a model spectrum of Vega was used to match and remove the hydrogen lines of the Paschen and Brackett series from the A0V telluric standard, and the resulting telluric correction spectrum was also used for flux calibration.

The Keck/MOSFIRE observations were carried out using 180 s exposures in the Y- and K-bands and 120 s exposures in J and H. The target was nodded along the slit between exposures to allow for accurate subtraction of the sky background. Total integration times in each band were 1431.5 s in Y, 715.8 s in J, 1192.9 s in H, and 1079.6 s in K. Spectral reductions, including flat-fielding, the wavelength solution, background subtraction, and frame stacking, were performed using the MOSFIRE Data Reduction Pipeline. 1D spectra were extracted from the 2D frames using standard tasks in IRAF. The A0V telluric standard HIP 30090 was also observed immediately following the observations of SPIRITS 15c and telluric corrections and flux calibrations were performed using *xtellcor*. The 1D spectra are shown in Figure 2.4, shifted to the rest frame of the ^{12}CO ALMA velocity measurements at the position of SPIRITS 15c (discussed in Section 2.2).

2.3 Analysis

In this section, we provide our analysis of the observed spectral energy density (SED) evolution of SPIRITS 15c and of its NIR spectrum.

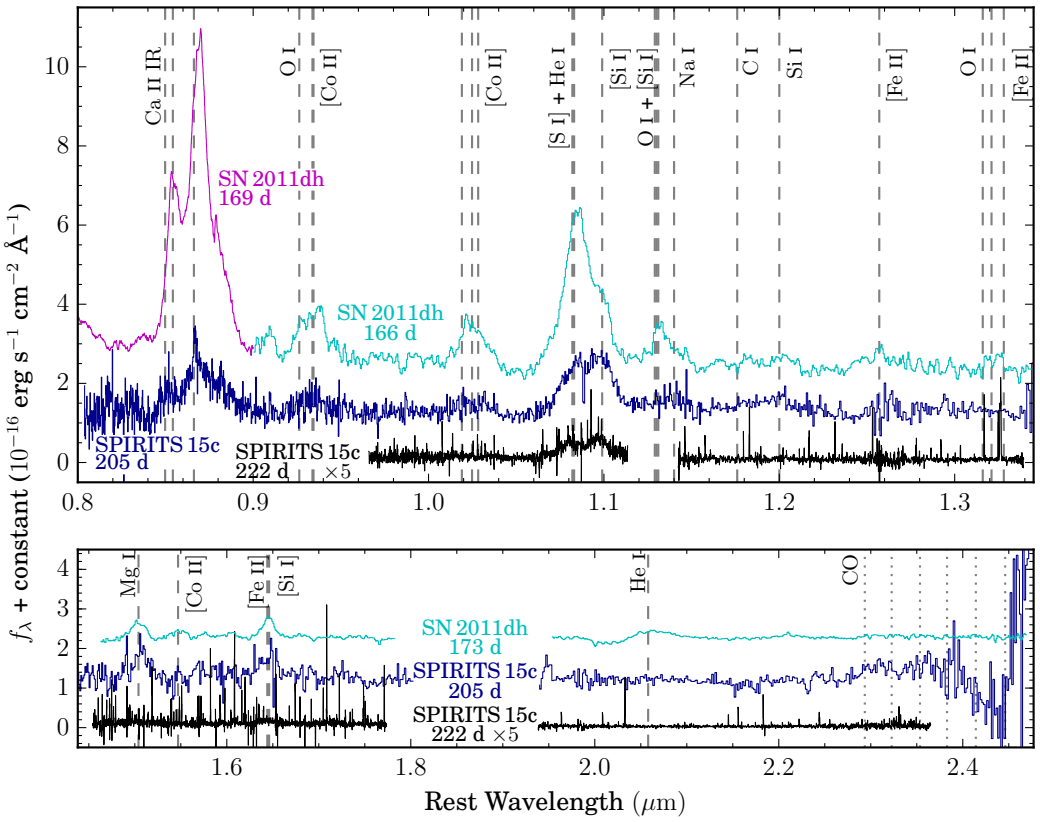

Figure 2.4: The NIR spectra of SPIRITS 15c taken with Baade/FIRE on $t = 205$ days (blue) and Keck/MOSFIRE on $t = 222$ days (black) shifted to the rest frame of the the location of SPIRITS 15c measured in an ALMA CO velocity map of IC 2163 ($v_{\mathrm{CO},helio} = 2827$ km s^{-1}, Elmegreen et al. 2016; Kaufman et al. 2016). The spectra are dereddened for Galactic extinction assuming a Fitzpatrick (1999) $R_V = 3.1$ extinction law. The Keck/MOSFIRE spectrum is multiplied by a factor of five and the Baade/FIRE spectrum is shifted up by 10^{-16} erg s^{-1} cm^{-2} Å^{-1} for clarity. We also show late-time spectra of SN 2011dh for comparison (cyan and magenta), shifted up by 2×10^{-16} erg s^{-1} cm^{-2} Å^{-1}, where the phases marked on the plot are set as in Figure 2.2. Dashed vertical lines show the locations of atomic transitions identified in the spectra of SN 2011dh by Ergon et al. (2014) and Ergon et al. (2015) and Jerkstrand et al. (2015). Dotted vertical lines mark the band heads of the $\Delta v = 2$ vibrational overtones of ^{12}C^{16}O, which may contribute to excess flux observed between 2.3 and 2.5 μm. The gaps in the spectra are due to the regions of low atmospheric transmission between the J, H, and K windows.

The Optical to IR SED

We constructed a spectral energy distribution (SED) of SPIRITS 15c at multiple epochs (t = 39, 63, 106, 161, and 167 days) during the evolution of the transient using the available optical and IR photometry. The photometric points, converted to band-luminosities (λL_λ) assuming a distance to the host galaxy of 35.5 Mpc and correcting for Galactic reddening, are shown in Figure 2.5 along with blackbody fits to the data at each epoch. To convert the gri optical points, we use AB flux zero points and broadband effective wavelengths for the SDSS filter system (Fukugita et al. 1996). For the Y-band, we adopt a Vega zero point of $f_\lambda = 5.71 \times 10^{-10}$ erg s^{-1} cm^{-2} Å^{-1} and an effective wavelength of $\lambda = 1.0305$ μm from Hewett et al. (2006). We adopt 2MASS system values from Cohen, Wheaton, and Megeath (2003) for our JHK_s photometry. For the *Spitzer* [3.6] and [4.5] points, we use the flux zero points and effective wavelengths listed in the IRAC instrument handbook for each channel.

At t = 39 days, the optical points are well-approximated by a blackbody with $T \approx 3300$ K and $R \approx 1.4 \times 10^{15}$ cm. Fits to the NIR points seem to indicate that the SED evolves in time to a higher effective temperature and smaller radius, with $T \approx 3500$ K and $R \approx 6.3 \times 10^{14}$ cm by t = 106 days. At t = 161–167 days, the SED shows at least two distinct components, with the NIR points approximated by a $T \approx 2700$ K, $R \approx 5.7 \times 10^{14}$ cm blackbody and a required cooler component to account for the [3.6] and [4.5] *Spitzer*/IRAC measurements, likely associated with dust emission. A blackbody fit to the measured band-luminosities at [3.6] and [4.5] gives a color temperature of $T \approx 270$ K. We note, however, that the sum of these two components significantly over-predicts the luminosity at [3.6].

Given that SPIRITS 15c coincides with an apparently dusty region of IC 2163, the observed SED is likely affected by significant extinction from host galaxy dust. Thus, it is difficult to infer intrinsic properties of the transient from our photometric data. In Table 2.3, we give the results of blackbody fits to the data assuming several different values for the total extinction.

The NIR spectrum

SPIRITS 15c was observed spectroscopically in the NIR at t = 205 and 222 days during the IR decline phase of the transient. As seen in Figure 2.4, a prominent feature in both spectra is the broad emission line near 1.083 μm, most likely due to He I. The full-width at half-maximum (FWHM) velocity of this line at t = 166 days is $\approx$ 8400 km s^{-1}. The line profile is shown in Figure 2.6, with a clear double-

Table 2.3: Parameters of SED component blackbody fits for SPIRITS 15c

Phase[a] (days)	Total Extinction[b], A_V (mag)	$T_{\rm eff}$ (K)	$R_{\rm BB}$ (cm)
39	0.238	3300	1.4×10^{15}
	1.0	3800	1.3×10^{15}
	2.0	4600	1.1×10^{15}
	2.2	4900	1.1×10^{15}
	3.0	5900	9.6×10^{14}
106	0.238	3500	6.3×10^{14}
	1.0	3700	6.2×10^{14}
	2.0	4000	6.1×10^{14}
	2.2	4100	6.1×10^{14}
	3.0	4400	5.9×10^{14}
161	0.238	2700	5.7×10^{14}
	1.0	2800	5.5×10^{14}
	2.0	3100	5.3×10^{14}
	2.2	3200	5.2×10^{14}
	3.0	3400	5.1×10^{14}
167	0.238	270	3.7×10^{17}
	1.0	270	3.7×10^{17}
	2.0	270	3.6×10^{17}
	2.24	270	3.6×10^{17}
	3.0	270	3.5×10^{17}

[a] Phase is number of days since the earliest detection of this event on 2014 August 21.4 (MJD = 56890.4).
[b] Assumed total extinction to SPIRITS 15c including both Galactic (A_V = 0.238), and any additional extinction, e.g., from the host environment.

peaked structure that may indicate a high-velocity, bipolar outflow, or a toroidal geometry. The blueward peak also appears relatively weaker compared to the red side in the second epoch, and the full profile has narrowed to a FWHM velocity of $\approx$ 7600 km s^{-1}. The lower S/N of the second spectrum, however, adds difficulty to evaluating the significance of the profile evolution between the two epochs. In the FIRE spectrum, the narrow (FWHM $\approx$ 300 km s^{-1}), redshifted dip in the profile is likely an artifact. This dip is only two pixels wide, and narrower than a resolution element ($R_{\rm FIRE}$ = 500). Moreover, it is not detected in the higher-resolution MOSFIRE spectrum ($R_{\rm MOSFIRE}$ = 3400).

The flux in this line appears to have faded by a factor of more than 10 during the 17 days between the first and second epochs. Extrapolating from the observed Y-band decay rate of 0.020 ± 0.005 mag day^{-1} between 106 and 161 days, however, we would only expect the flux to have faded by a factor of $\approx$ 1.4. We caution that the spectral flux calibrations using standard star observations are somewhat uncertain, and we do not have contemporaneous photometric data to verify the fading of this line. Slit losses due to a misalignment may also contribute to the apparent drop in

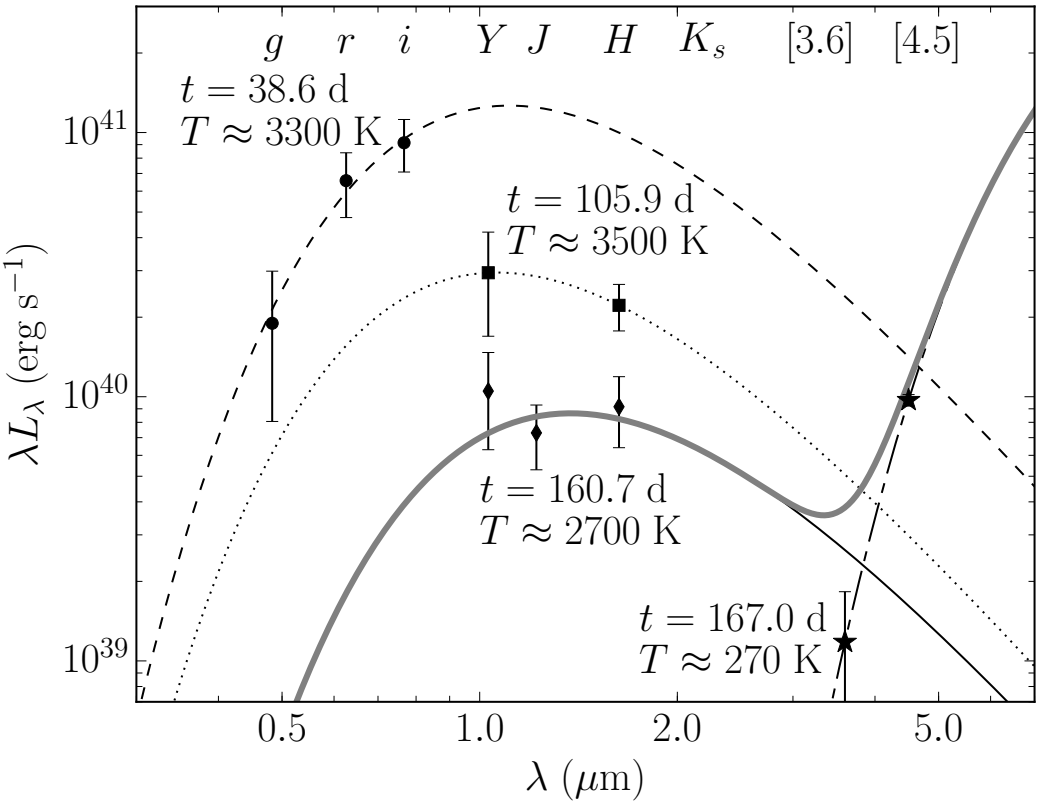

Figure 2.5: The optical-to-IR SED of SPIRITS 15c at multiple epochs during the evolution of the transient. Band-luminosities (λL_λ), calculated assuming a distance to IC 2163 of 35.5 Mpc and correcting for Galactic reddening characterized by $E(B-V) = 0.072$ mag, are shown at $t = 38.6$ (circles), 105.9 (squares), 160.7 (diamonds), and 167.0 days (stars). Best-fit, single-component blackbody curves are shown as black dashed, dotted, dashed–dotted, solid, and long-short dashed lines, respectively, with their corresponding temperatures labeled. Because the final two epochs are nearly contemporaneous ($\Delta t = 6.3$ days), we show the sum of these two blackbody components as the solid gray curve.

flux of the He I line, rather than true variability, in this feature. This could also explain the lack of detection of the continuum emission or any other features in the MOSFIRE spectrum.

The identification of the 1.083 μm line is somewhat uncertain because we do not detect the He I line at 2.058 μm in either spectrum. It is possible that there is a contribution to the red wing of the 1.083 μm feature from the Pa γ 1.094 μm line, but we do not detect Pa β or Pa δ (1.282 and 1.005 μm, respectively), indicating that H I is absent from the spectrum at this phase. Alternatively, it is possible that the two-component velocity profile is instead due to two distinct transitions: the [S I] 1.082 μm line for the blueward component, and the [Si I] 1.099 μm line for the

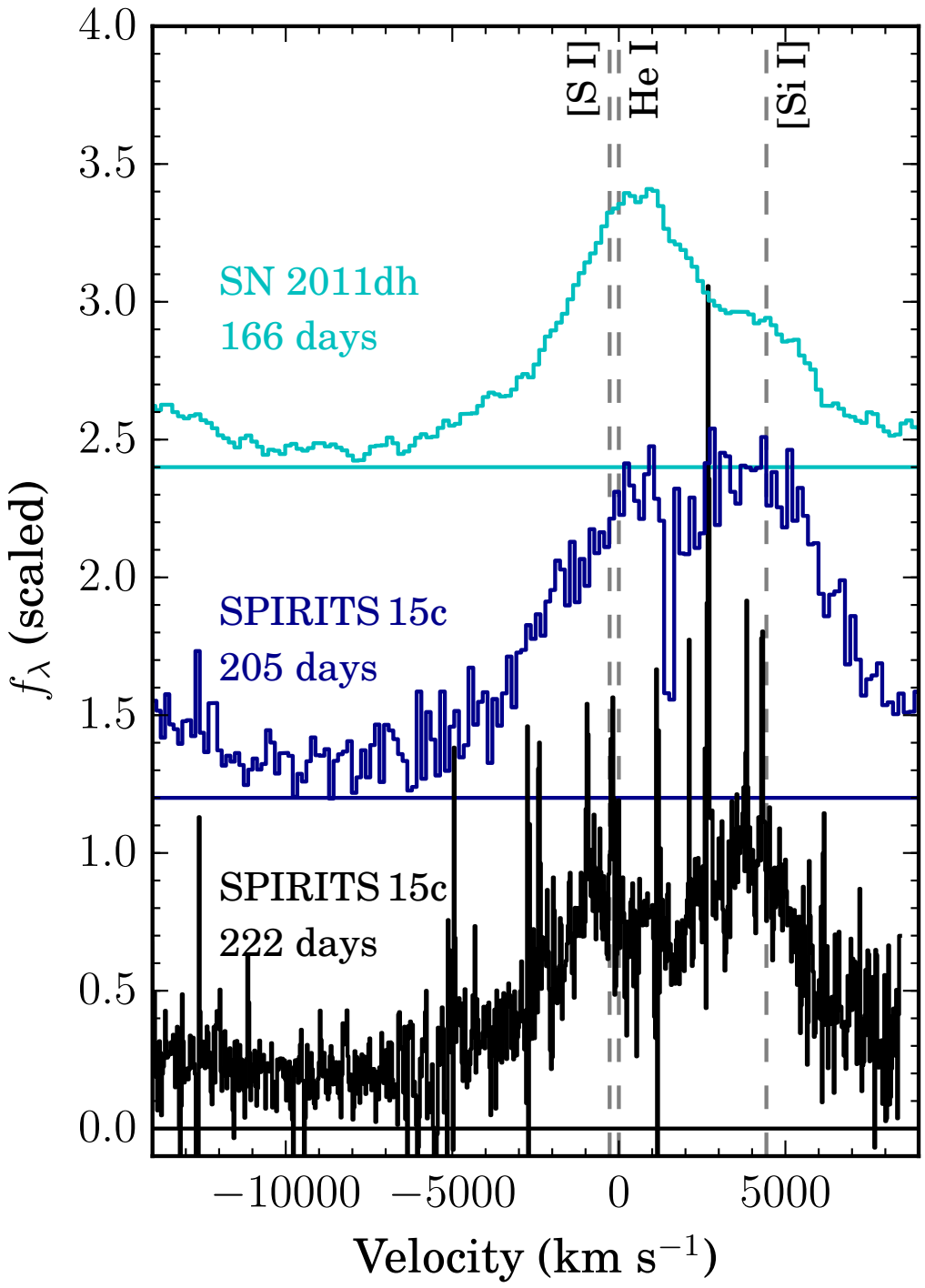

Figure 2.6: The observed velocity profile of the He I line at 1.0830 μm in the spectra of SN 2011dh at a phase of 166 days (top), and SPIRITS 15c at phases of 205 (middle) and 222 days (bottom). The phase of the SN 2011dh spectrum is set as in Figure 2.2. The profiles are scaled and shifted arbitrarily in flux for clarity.

redward component.

We also identify the blended 0.85 μm feature as the Ca II IR triplet (0.845, 0.854, and 0.866 μm). Without concurrent optical spectroscopy, we are unable to definitively identify any other features present in the $t = 205$ day spectrum of SPIRITS 15c. Also shown in Figure 2.4 are the NIR spectra of the Type IIb SN 2011dh at phases of ≈ 170 days, which show evident similarity to those of SPIRITS 15c. In addition to the broad, prominent He I line at 1.083 μm, we make tentative identifications of several other features in the spectra of SPIRITS 15c based on this comparison, including the blended O I and [Co II] feature near 0.93 μm, the [Co II] feature near 1.02 μm, the Mg I line at 1.504 μm, and the feature near 1.64 μm due to either [Fe II] or [Si I]. We list these identifications in Table 2.4, and discuss a detailed comparison between the NIR spectra of SPIRITS 15c and SN 2011dh below, in Section 2.4.

2.4 Discussion

Here, we discuss possible physical interpretations of SPIRITS 15c and SPIRITS 14buu and compare them to other classes of transients discovered in recent years.

SPIRITS 15c as an obscured SN: comparison to SN 2011dh

We examine the possibility that SPIRITS 15c is an SN explosion with significant obscuration by dust. We compare the properties of SPIRITS 15c to the well-studied Type IIb explosion in M51, SN 2011dh, based on the similarity of their NIR spectra at late phases (Section 2.4). Throughout this section, following Ergon et al. (2014), we adopt a median value from the literature for the distance to M51 of $7.8^{+1.1}_{-0.9}$ Mpc, and a reddening along the line of sight to SN 2011dh of $E(B-V) = 0.07$ mag assuming a standard $R_V = 3.1$ Milky Way extinction law as parametrized by Fitzpatrick (1999).

NIR spectrum comparison

The NIR spectrum of SPIRITS 15c at $t = 205$ d shows pronounced similarity to the NIR spectra of SN 2011dh at similar phases. We show a direct comparison between the spectra of these objects in Figure 2.4, where the phase of the SN 2011dh spectra is set so that the earliest detection of the SN coincides with the most constraining non-detection preceding the outburst of SPIRITS 15c. The SN 2011dh spectra, originally published in Ergon et al. (2015), were obtained from the Weizmann Interactive Supernova data REPository (WISeREP, Yaron and Gal-Yam 2012)[7]. To

[7]WISeREP spectra are available here:
`http://wiserep.weizmann.ac.il/`

Table 2.4: Spectral line identifications for SPIRITS 15c

Species[a]	Rest Wavelength[b] (air) (μm)
He I	1.083
	2.058
C I	1.175
O I	0.926
	1.129
	1.130
	1.317
Na I	1.140
Mg I	1.504
Si I	1.203
[Si I]	1.099
	1.129
	1.646
[S I]	1.082
Ca II	0.845
	0.854
	0.866
[Co II]	0.934
	0.934
	1.019
	1.025
	1.028
	1.547
[Fe II]	1.257
	1.321
	1.328
	1.644
$^{12}C^{16}O$	2.294
	2.323
	2.354
	2.383
	2.414
	2.446

[a] Line identifications come from Ergon et al. (2014), Ergon et al. (2015), and Jerkstrand et al. (2015).
[b] Wavelengths listed for $^{12}C^{16}O$ correspond to band heads of the $\Delta v = 2$ vibrational overtones of this molecule.

aid in the comparison, we mark the features identified in the spectra of SN 2011dh by Ergon et al. (2015) and Jerkstrand et al. (2015) in the figure.

A prominent feature in the spectra of both objects is the strong, broad ($\gtrsim 8000\,\mathrm{km\,s^{-1}}$) He I emission at 1.083 μm, shown in detail in Figure 2.6. This line is detected in both spectra of SPIRITS 15c at $t = 205$ and 222 days. Ergon et al. (2015) note a blueshifted P-Cygni absorption component of this line profile in the SN 2011dh spectrum, extending to a velocity of at least ≈ 10000 km s^{-1}, that may also be present in the line profile of SPIRITS 15c at $t = 202$ days. The He I line profile of SPIRITS 15c has a clear double-peaked structure that is not observed in SN 2011dh. This may suggest a bipolar outflow or toroidal geometry in SPIRITS 15c. We note that double-peaked [O I] lines present in many stripped-envelope CCSNe have been interpreted as evidence for a toroidal or disk-like geometry (e.g. Maeda et al. 2002; Mazzali et al. 2005; Maeda et al. 2008; Modjaz et al. 2008; Milisavljevic et al. 2010). The shoulder feature on the red side of the SN 2011dh line profile, likely due to contamination from the [Si I] feature at 1.099 μm, may contribute to the redshifted peak of the line profile in SPIRITS 15c.

The He I line at 2.058 μm, detected in the spectrum of SN 2011dh, is not detected in either spectrum of SPIRITS 15c. Assuming the same flux ratio between the 1.083 and 2.058 μm He I lines as is observed in SN 2011dh, and accounting for additional reddening as inferred for SPIRITS 15c (in Section 2.4), we would expect the 2.058 μm He I to peak at 0.09×10^{-16} erg s^{-1} cm^{-2} Å^{-1} above the continuum in the FIRE spectrum. This is below the RMS noise of 0.11 erg s^{-1} cm^{-2} Å^{-1} in this region of the spectrum, and thus, a non-detection of this feature is not surprising.

Other prominent emission features detected in the spectra of both objects include the Ca II IR triplet, the blended features due to O I and [Co II] near 0.93 μm, the [Co II] feature near 1.02 μm, the Mg I line at 1.504 μm, and the feature near 1.64 μm due to [Fe II] or [Si I]. We caution, however, that the NIR line identifications for SN 2011dh by Ergon et al. (2014) and Ergon et al. (2015) and Jerkstrand et al. (2015) relied on corroborating detections in the optical. We do not have optical spectroscopy of SPIRITS 15c to confirm the identifications of these features.

The excess emission beyond 2.3 μm, attributed to the $\Delta v = 2$ vibrational overtones of CO by Ergon et al. (2015) and Jerkstrand et al. (2015) in the spectrum of SN 2011dh, appears even stronger in SPIRITS 15c, but we note that the spectrum of SPIRITS 15c becomes increasingly noisy beyond ≈ 2.4 μm at the end of K-band. Some of the weaker spectral features, labeled in Figure 2.4 and present in

the spectrum of SN 2011dh, are not detected in SPIRITS 15c, but this can likely be accounted for by the relatively lower S/N of the SPIRITS 15c spectra, small intrinsic differences in the strength of these features between the two events, and the uncertainty of matching the evolutionary phase between the two events. Overall, we find that the late-time, NIR spectrum of SN 2011dh provides a good match to the spectra of SPIRITS 15c, and we evaluate the interpretation of SPIRITS 15c as a Type IIb SN similar to SN 2011dh, albeit subject to significant dust obscuration, below in Sections 2.4 and 2.4.

Progenitor comparison

As discussed above in Section 2.2, no progenitor star was detected at the position of SPIRITS 15c in pre-explosion *HST* imaging of IC 2163 and NGC 2207 to limiting magnitudes of $M_V > -7.9$ and $M_I > -8.9$ mag at the assumed distance to the host, correcting only for Galactic extinction. A candidate progenitor of SN 2011dh was identified as an intermediate-mass yellow supergiant star in pre-explosion *HST* images at the position of the SN (Maund et al. 2011; Van Dyk et al. 2011). The disappearance of this source in post-explosion imaging confirms that it was indeed the progenitor star (Van Dyk et al. 2013; Ergon et al. 2014). The observed magnitudes in the HST frames were $V \sim 21.8$ and $I \sim 21.2$, corresponding to absolute magnitudes of $M_V \sim -7.9$ and $M_I \sim -8.4$ at the assumed distance, and reddening to SN 2011dh (Maund et al. 2011; Van Dyk et al. 2011). These values are consistent with the non-detection of a progenitor star for SPIRITS 15c in the archival *HST* imaging of IC 2163, and furthermore, there may be significant, additional extinction from the foreground spiral arm of NGC 2207 and the local environment of the transient. Thus, we cannot rule out a progenitor system similar to that of SN 2011dh for SPIRITS 15c.

Light curve and SED comparison

The optical and IR light curves of SPIRITS 15c are shown in Figure 2.2. The peak observed brightness of the transient in the optical was in i-band at $i = 17.67 \pm 0.09$ mag ($M_i = -15.08$ mag absolute). The peak in i-band absolute magnitude of SN 2011dh was brighter by ≈ 2 mag, possibly indicating that SPIRITS 15c is subject to significant dust extinction. To examine this scenario, we compare the light curves of SN 2011dh from Helou et al. (2013), Ergon et al. (2014), and Ergon et al. (2015) to those of SPIRITS 15c in Figure 2.2. The light curves of

SN 2011dh have been shifted in apparent magnitude to the assumed distance of SPIRITS 15c, and are shifted in phase so that the earliest detection of SN 2011dh coincides with the last non-detection of SPIRITS 15c before its outburst. We then applied a Fitzpatrick (1999) extinction law with $R_V = 3.1$ and $E(B-V) = 0.72$ mag, corresponding to $A_V = 2.2$ mag, to the SN 2011dh light curves. As shown in the figure, this provides a good match to the observed magnitudes of SPIRITS 15c in gri at $t = 38.6$ days. We note a few small discrepancies with the optical light curves in this comparison. Namely, SPIRITS 15c is fainter than the adjusted brightness of SN 2011dh at $t = 0$ days in i-band by ≈ 0.3 mag and brighter by ≈ 0.1 mag at $t = 30$ days.

Although the reddened light curves of SN 2011dh provide a good match to the optical light curves of SPIRITS 15c, the IR light curves are more difficult to explain using only a standard extinction law. For the extinction and phase assumed for SN 2011dh in Figure 2.2, several discrepancies are apparent. At $t = 106$ days, the H-band magnitude is brighter than the corresponding value for SN 2011dh by 0.6 mag. Furthermore, the SN 2011dh H-band light curve decays faster, resulting in a larger discrepancy of 1.0 mag by $t = 161$ days. At the same phase, the adjusted magnitude of SN 2011dh is 0.9 mag fainter than that of SPIRITS 15c in J. The single K_s-band detection of SPIRITS 15c at 181 days matches the reddened light curve of SN 2011dh quite well.

The largest discrepancy occurs in the *Spitzer*/IRAC [3.6] and [4.5] bands. In [4.5], the SPIRITS 15c light curve is brighter the than that of SN 2011dh by ≈ 0.4 mag between $t = 167$ and 307 days, although they decay at similar rates. However, in [3.6] at $t = 167$ days, SPIRITS 15c is fainter than the reddened SN 2011dh by 1.5 mag. To explain the 1.9 mag excess in [3.6]−[4.5] color of SPIRITS 15c over SN 2011dh, using only a standard reddening law, would require $\gtrsim 100$ magnitudes of visual extinction.

We make a similar comparison between the SED of SPIRITS 15c and the reddened SED of SN 2011dh at several phases in Figure 2.7. As in the light curve comparison, we find that applying extinction with $E(B-V) = 0.72$ to the SED of SN 2011dh at $t = 39$ and 63 days does a good job reproducing the observed optical gri band-luminosities of SPIRITS 15c. The IR YJH, and [4.5] band-luminosities, however, are significantly over-luminous compared to the reddened SN 2011dh between $t = 106$ and 307 days. Again, the most apparent discrepancy in this comparison is the significant over-prediction of the luminosity of SPIRITS 15c at [3.6].

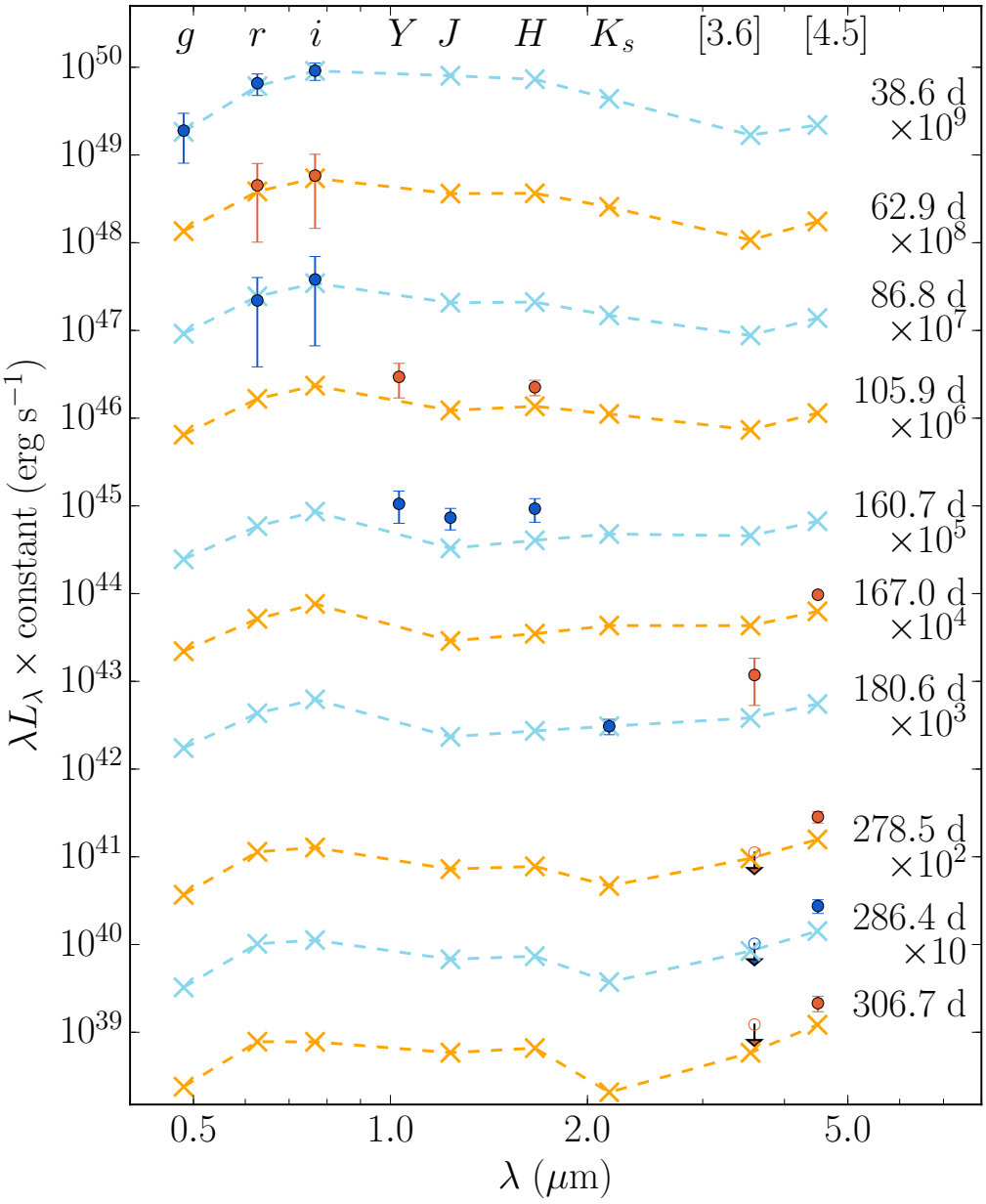

Figure 2.7: Comparison of the SED evolution of SPIRITS 15c (dark blue/orange circles) and SN 2011dh (light blue/orange 'X'-symbols). Unfilled points with downward arrows represent upper limits. The band luminosities for SPIRITS 15c are corrected for Galactic extinction to IC 2163 from NED (Fitzpatrick 1999; Chapman et al. 2009; Schlafly and Finkbeiner 2011). The points for are SN 2011dh drawn from a linear interpolation of the SN 2011dh light curves, and reddened by the assumed excess extinction in SPIRITS 15c characterized by $E(B-V)_{host} = 0.65$ with a standard $R_V = 3.1$ extinction law. Error bars for SPIRITS 15c are shown, but are sometimes smaller than the plotting symbols. The phase, set as in Figure 2.2, of each SED is listed along the right side. Each SED is shifted up by a factor of 10 from the one below, in alternating colors, so that they can be easily distinguished.

Because SPIRITS 15c appears over-luminous in some bands, and under-luminous in others, compared to the reddened light curves and SED of SN 2011dh, a phase shift in the light curves of SN 2011dh cannot account for the observed discrepancies. Furthermore, using a steeper or shallower extinction law to redden the observations of SN 2011dh would be unable to rectify all of the observed discrepancies at once.

SPIRITS 15c in the context of SNe IIb

The designation IIb indicates an SN that transitions spectroscopically from a hydrogen-rich SN II to a hydrogen-poor SN Ib. These events are believed to arise from the core collapse of massive stars that have been stripped of almost all of their hydrogen envelope. In addition to SN 2011dh, well-studied examples of SNe IIb include SN 1993J and SN 2008ax.

The progenitor of SN 1993J was shown to be a yellow supergiant star of 12–17 $M_{\odot}$, similar to that of SN 2011dh. It was proposed to have lost most of its hydrogen envelope to a blue, compact companion star (Podsiadlowski et al. 1993; Shigeyama et al. 1994; Woosley et al. 1994; Blinnikov et al. 1998; Maund et al. 2004; Stancliffe and Eldridge 2009). The progenitor observations of SN 2008ax by Crockett et al. (2008) were less conclusive, but Tsvetkov et al. (2009) proposed a 13 $M_{\odot}$ star with an extended, low-mass hydrogen envelope, based on hydrodynamical modeling of the SN optical light curves. As mentioned above in Section 2.4, we do not rule out a progenitor similar to those of other SNe IIb based on pre-explosion HST imaging.

Ergon et al. (2014) showed that these SNe had similar optical light curve and color evolution in the first 50 days. All three reached peak luminosity at $\approx$ 20 days post explosion, and evolved to redder colors with time. They noted some differences between the three events, such as a factor of three spread in peak luminosity, and a $\approx$ 0.4 mag spread in their optical colors, but these differences could be accounted for within the systematic uncertainties in the distance and extinction to each SN. The assumption of $E(B-V)_{host} = 0.65$ mag for SPIRITS 15c brings its optical light curves and color evolution into good agreement with the observed properties of well-studied SNe IIb.

The IR light curves of SPIRITS 15c are not as well-matched by a reddened version of SN 2011dh, but it is not as straightforward to draw a direct comparison between the two events at these wavelengths. SN 2011dh was shown to have a significant IR excess at [4.5] compared to the NIR and [3.6] measurements, possibly due to a thermal echo from heated CSM dust, dust formation in the ejecta, and/or

CO fundamental band emission (Helou et al. 2013; Ergon et al. 2014; Ergon et al. 2015). Similar confounding factors may be at play in SPIRITS 15c, given the observed excess at NIR wavelengths and at [4.5], and the possible CO $\Delta v = 2$ vibrational emission present in the K-band spectrum. The extreme [3.6]−[4.5] = 3.0 ± 0.2 mag color of SPIRITS 15c at a phase of 167 days has not been observed for another SN IIb, and provides the strongest challenge to the interpretation of SPIRITS 15c as a moderately obscured SN 2011dh-like event. SN 2011dh only reached a *Spitzer*/IRAC color of 1.6 mag at ≈ 400 days, and the Type IIb SN 2013df was observed to have a 1.3 mag color at ≈ 300 days (Tinyanont et al. 2016).

Although SPIRITS 15c and SN 2011dh show remarkable similarity in many respects, we note that we do not have sufficient data for this case to discriminate between an SN IIb or SN Ib. As is clearly demonstrated by Fremling et al. (2016), the light curves of PTF 12os (Type IIb SN 2012P) and PTF 13bvn (Type Ib SN) show only very minor differences to each other and to SN 2011dh. Spectroscopically, SNe Ib and IIb are only distinguished by the presence or absence of hydrogen in their early-time spectra. The absence of hydrogen in the spectrum of SPIRITS 15c after ≈ 200 days does not classify this event as a SN Ib, as hydrogen may very well have been present at earlier times.

SPIRITS 14buu: Yet another reddened SN?

The optical light plateau and subsequent fall-off observed for SPIRITS 14buu are similar to those characteristic of the SN IIP class of CCSNe. The duration of SNe IIP plateaus is typically ≈ 100 days (e.g Poznanski et al. 2009; Arcavi et al. 2012). Sanders et al. (2015) found, using a statistical sample of SN IIP light curves from Pan-STARRS1, a median r-band plateau duration of 92 days with a 1σ variation of 14 days, although the full distribution spanned a range of 42–126 days. The observed > 80 day plateau of SPIRITS 14buu in the r and i bands is thus consistent with the observed distribution for SNe IIP.

SNe IIP have been observed to exhibit a wide-ranging continuum in observed peak magnitude in the optical ($-14.5 \gtrsim M_r \gtrsim -20.0$, $-15.0 \gtrsim M_i \gtrsim -19.5$, Sanders et al. 2015), with higher-luminosity events exhibiting greater expansion velocities and producing larger amounts of nickel (e.g. Hamuy 2003). Correcting only for galactic extinction, SPIRITS 14buu is fainter than the faintest SN IIP in the Sanders et al. (2015) sample by ≈ 1.5 mag in both the r and i bands. It is possible that IC 2163 is an intrinsically low-luminosity SN IIP; however, the observed red colors

may also indicate additional dust extinction.

To examine this possibility, we compare SPIRITS 14buu to the low-luminosity Type IIP SN 2005cs in M51 in Figure 2.3. We obtained $BVRIJH$ light curves of SN 2005cs from Pastorello et al. (2009). For extinction, we assume their value of $E(B-V) = 0.05$ mag. For a direct comparison, the optical measurements were converted to SDSS system magnitudes using the conversions from (Jordi, Grebel, and Ammon 2006), and corrected for Galactic extinction to M51. Following a method similar to that used in Section 2.4, we then shifted the SN 2005cs light curves in apparent magnitude to the distance of IC 2163, and applied a total reddening characterized by $E(B-V) = 0.49$ mag with a standard $R_V = 3.1$ Fitzpatrick (1999) extinction law, corresponding to 1.5 mag of visual extinction. We also shifted SN 2005cs light curves by an additional 0.1 mag (smaller than the uncertainties in the distance moduli to the hosts) to achieve a better match to the r and H-band measurements for SPIRITS 14buu. The phase of SN 2005cs was set so that the fall-off of the optical plateau coincides with that of SPIRITS 14buu.

The reddened light curves of SN 2005cs provide a good match to the r, J, and H-band light curves of SPIRITS 14buu. The g-band upper limits for SPIRITS 14buu are also mostly consistent with the reddened g-band light curve of SN 2005cs. The largest discrepancy is in the i-band between 60 and 100 days, where SPIRITS 14buu is 0.5 mag fainter than the reddened SN 2005cs.

We also compare the [3.6] and [4.5] light curves of SPIRITS 14buu to those of the Type IIP SN 2004et from Kotak et al. (2009). in Figure 2.3. The SN 2004et light curves are shifted fainter in absolute magnitude by 2.4 mag, to match the level of SPIRITS 14buu. This also suggests that SPIRITS 14buu may be an intrinsically faint event like SN 2005cs, in addition to suffering from significant extinction. The decay rate of SN 2004et is somewhat faster than SPIRITS 14buu in both *Spitzer*/IRAC bands. Tinyanont et al. (2016) present a sample of SN light curves at [3.6] and [4.5], and find that SN II MIR light curves show a large degree of variety. Thus, we would not necessarily expect to find a good match to the MIR light curves of SPIRITS 14buu in the relatively small sample of SNe IIP that have been well studied at these wavelengths.

Without a spectrum, we cannot definitively determine the nature of this source. Overall, however, we find a low-luminosity SN IIP, similar to SN 2005cs with ≈ 1.5 mag of visual extinction, to be a reasonable explanation for the observed properties of SPIRITS 14buu.

Non-SN IR transient scenarios

We also consider the possibility that SPIRITS 15c and SPIRITS 14buu are not obscured SNe. Below, we find that scenarios involving a stellar merger and an SN 2008S-like transient can likely be ruled out for both events. We also consider a V445 Pup-like helium nova, which can likely be ruled out in the case of SPIRITS 15c due to its high luminosity.

Stellar merger

Known transients associated with stellar merger events include the low-mass (1 – 2 $M_{\odot}$) contact binary merger V1309 Sco (Tylenda et al. 2011), and the more massive merger of a B-type progenitor (5 – 10 $M_{\odot}$) V838 Mon (Bond et al. 2003; Sparks et al. 2008). Recently, the NGC 4490-OT has also been proposed to be a high-mass (20 – 30 $M_{\odot}$) analog of these events (Smith et al. 2016). The observed examples of stellar mergers are characterized by unobscured; optical progenitors, irregular, multi-peaked light curves; increasing red colors with time; and a significant IR excess at late times. The spectra during the decline phase show relatively narrow lines (O[10^2] km s^{-1}) of H I in emission and Ca II in absorption.

The light curve of SPIRITS 15c shows some similarities to the massive stellar merger NGC4490-OT although it is $\approx$ 1–2 mag brighter both during the optical peak, and in the IR *Spitzer*/IRAC bands at late times. The [3.6]−[4.5] color of SPIRITS 15c is significantly redder. The optical outburst of the NGC 4490-OT lasted longer than 200 days and the IR light curve extends in excess of 800 days. SPIRITS 15c, in contrast, faded beyond detection in the optical in $\lesssim$ 150 days and in the IR in $\lesssim$ 500 days. In the case of the NGC 4490-OT, the evidence for a massive stellar merger is corroborated by the detection of a massive progenitor at $M_{\rm F606W} \approx -6.4$, likely an $M \approx 30\ M_{\odot}$ LBV. This extends the observed correlation suggested by Kochanek, Adams, and Belczynski (2014) in peak luminosity and merger progenitor mass (Smith et al. 2016). Further extending this correlation to the luminosity of SPIRITS 15c would suggest an extremely massive progenitor ($M \gtrsim 60\ M_{\odot}$). The progenitor of SPIRITS 15c was undetected in the 1998 HST images to $M_V > -7.9$ mag. Furthermore, the velocities observed in SPIRITS 15c are $\gtrsim$ 10 times those seen in stellar mergers, indicating a significantly more explosive event. Finally, the lack of hydrogen observed for SPIRITS 15c would require a rare, very massive stripped-envelope system. Taken together, the evidence indicates that a massive stellar merger scenario is likely ruled out as an explanation for the

properties of SPIRITS 15c.

SPIRITS 14buu reached a similar peak luminosity in the i-band to the peak optical luminosity of the NGC 4490-OT, but SPIRITS 14buu is $\approx$ 1 mag brighter at [4.5]. As with SPIRITS 15c, the NGC 4490-OT evolved much more slowly than SPIRITS 14buu in both the optical and IR. Furthermore, the observed plateau of SPIRITS 14buu in the optical is inconsistent with the characteristic multi-peaked light curves of stellar merger events. We find that, despite the similarity in observed optical luminosity, SPIRITS 14buu is overall inconsistent with an NGC 4490-OT-like stellar merger.

SN 2008S-like transient

SN 2008S-like transients, including the 2008 luminous optical transient in NGC 300 (NGC 300 OT2008-1) and other similar events, are a class of so-called SN imposters. These events have highly obscured progenitors in the optical, but bright MIR detections ($M_{[4.5]} < -10$) suggest that the progenitors are likely extreme asymptotic giant branch stars (EAGB) of intermediate mass ($\approx$ 10 to 15 $M_{\odot}$), self-obscured by a dense wind of gas and dust (Prieto et al. 2008; Bond et al. 2009; Thompson et al. 2009). They are significantly less luminous than SNe in the optical, with peak absolute visual magnitude of only $M_V \approx -13$ for SN 2008S (Steele et al. 2008) and $M_V \approx -12$ to -13 for NGC 300 OT2008-1 (Bond et al. 2009). These events have peculiar spectral features, including narrow emission from [Ca II], Ca II, and weak Fe II (Steele et al. 2008; Bond et al. 2009; Humphreys et al. 2011). Moderate-resolution spectroscopy of NGC 300 OT2008-1 revealed that the emission lines showed a double-peaked structure, indicating a bipolar outflow with expansion velocities of $\approx 70 - 80$ km s^{-1} (Bond et al. 2009; Humphreys et al. 2011). A proposed physical picture of these events is that a stellar explosion or massive eruption, possibly an electron-capture SN, destroys most of the obscuring dust, allowing the transient to be optically luminous. In the aftermath, however, the dust reforms and re-obscures the optical transient, producing a significant IR-excess (Thompson et al. 2009; Kochanek 2011a). Both transients have now faded beyond their progenitor luminosities at [3.6] and [4.5], suggesting that the outbursts were terminal events (Adams et al. 2016).

The optical and late-time MIR luminosities of SPIRITS 15c are 1–2 mag brighter than is observed for SN 2008S-like events, and SPIRITS 15c is again significantly redder in the MIR (only $\approx$ 1 mag for SN 2008S-like events, Szczygieł et al. 2012).

As with SN 2008S and the NGC 300 OT2008-1, the progenitor of SPIRITS 15c was obscured in the optical. There was no detection of a MIR progenitor for SPIRITS 15c down to ≈ 14.9 mag (≈ -17.85 absolute), but this limit is not constraining due to the larger distance to IC 2163 and the bright background galaxy light in the vicinity of SPIRITS 15c. The observed velocities of SPIRITS 15c are much higher than those of SN 2008S or the NGC 300 OT2008-1, which show similar velocities to stellar mergers. The strongest evidence against SPIRITS 15c as a SN 2008S-like event is the lack of hydrogen in its spectrum. SN 2008S and the NGC 300 OT2008-1 both showed strong hydrogen emission features, and moreover, if the physical mechanism behind them is indeed an electron-capture SN, the lack of hydrogen in SPIRITS 15c would be inexplicable given the believed intermediate-mass progenitors of such events.

The i-band luminosity of SPIRITS 14buu is comparable to an SN 2008S-like event in the optical, and both SPIRITS 14buu and SN 2008S reached IR luminosities of $M_{[4.5]} \approx -16$. SN 2008S was also significantly redder in [3.6]−[4.5] color by ≈ 0.8 mag. Additionally, SN 2008S was fainter than SPIRITS 14buu in the NIR by ≈ 2 mag. The largest discrepancy is that the optical light curves of SN 2008S decayed steeply after only ≈ 30 days, in contrast with the $\gtrsim 80$ day plateau of SPIRITS 14buu. Thus, we find an SN 2008S-like event to be a poor match to the observed properties of SPIRITS 14buu.

V445 Pup-like transient or a helium nova

An intriguing possibility for an explanation of SPIRITS 15c is a helium nova, a rare and thus far largely theoretical class of events. Helium novae are due to thermonuclear runaway on the surface of a white dwarf accreting helium from a helium-rich donor (Kato, Saio, and Hachisu 1989). The most convincing and well-studied candidate for an observed helium nova is the 2000 outburst of the Galactic object V445 Pup. The optical outburst showed a similar decline to slow novae, but was smaller in amplitude with $\Delta m_V \approx 6$ mag. Its spectrum was also unusual for a classical nova, in that it was rich in He I and C I emission lines, but showed no evidence for hydrogen. Multi-epoch adaptive optics imaging and integral field unit spectroscopy revealed an expanding bipolar outflow from V445 Pup, with a velocity of ≈ 6700 km s^{-1} and some knots at even larger velocities of ≈ 8500 km s^{-1} (Woudt et al. 2009). Using their observations of the expanding shell, Woudt et al. (2009) derive an expansion parallax distance of 8.2 ± 0.5 kpc.

The broad, double-peaked He I line in the spectrum of SPIRITS 15c is in good agreement with the observed velocities of the bipolar helium outflow of V445 Pup. The largest problem with this scenario, however, is that the V445 Pup outburst was significantly less luminous than SPIRITS 15c in the optical, with a peak of only $M_V \approx -6$. The NIR of peak at $M_{K_s} \approx -10$ was more comparable to that of SPIRITS 15c, and both sources grew redder with time during the initial decline. Late-time observations of V445 Pup with *Spitzer*/IRAC in 2005 (P20100; PIs Banerjee & P. Dipankar) and 2010 (P61071; PI B. A. Whitney), approximately 5 and 10 yr after the outburst, respectively, revealed the source was slowing decaying at [3.6] from $m_{[3.6]} \approx 8.6$ to 9.5 (-6 to -5.1 absolute) over ≈ 5 yr. The source was saturated in the IRAC2, IRAC3, and IRAC4 channels, indicating very red lower limits on the MIR colors of $[3.6]-[4.5] \gtrsim 2.3$ mag, $[3.6]-[5.7] \gtrsim 3.4$ mag, and $[3.6]-[7.9] \gtrsim 4.2$ mag.

2.5 Conclusions

SPIRITS 15c is a luminous ($M_{[4.5]} = -17.1 \pm 0.4$), red ($[3.6]-[4.5] = 3.0 \pm 0.2$ mag), IR-dominated transient discovered by the SPIRITS team. The transient was accompanied by an optical precursor outburst with $M_i = -15.1 \pm 0.4$ mag that was quickly overtaken by IR emission within ≈ 100 days. The most prominent feature of the NIR spectrum is a broad (≈ 8000 km s^{-1}), double-peaked emission line at 1.083 μm, likely due to He I, and possibly indicating a He-rich, bipolar or toroidal outflow associated with the transient.

We explored several possible scenarios to explain the unusual observed properties of SPIRITS 15c. Both the stellar merger and SN 2008S-like scenarios can likely be ruled out by the high luminosity of SPIRITS 15c, as well as the explosive velocities and lack of hydrogen in its spectrum. In the case of a helium nova, the strong He I emission and high-velocity, bipolar outflow of SPIRITS 15c is similar to that observed in the candidate prototype helium nova V445 Pup, but again, the optical luminosity of SPIRITS 15c is too extreme.

We conclude that SPIRITS 15c is a stripped-envelope CCSN explosion similar to the well-studied Type IIb SN 2011dh, but extinguished by dust in the optical and NIR at a level of $A_V \approx 2.2$ mag. The spectrum of SPIRITS 15c is very similar to that of SN 2011dh at a phase of ≈ 200 days, but SPIRITS 15c shows a distinct double-peaked profile in the broad, strong He I emission line that is not observed in SN 2011dh. The assumption of $A_V = 2.2$ mag with a standard $R_V = 3.1$ extinc-

tion law in SPIRITS 15c provides a good match between the optical light curves and observed colors of SPIRITS 15c, and those of SN 2011dh. In the IR, however, SPIRITS 15c is more luminous than SN 2011dh, except at [3.6] where it is significantly under-luminous, illustrated by its extreme [3.6]−[4.5] color. Thus, we find that a shift in phase or simply a steeper extinction law cannot explain the observed differences between SPIRITS 15c and SN 2011dh.

SPIRITS 14buu, an earlier transient in IC 2163, was serendipitously discovered in the SPIRITS data during the analysis of SPIRITS 15c. The source was also luminous in the IR at $M_{[4.5]} = -16.1 \pm 0.4$ mag, and developed a fairly red [3.6]−[4.5] color of 1.2 ± 0.2 mag by 166 days after its first detection. The optical and NIR light curves showed a plateau lasting at least 80 days, similar to that observed in SNe IIP. Scenarios involving a stellar merger or SN 2008S-like transient can again likely be ruled out. A comparison to the low-luminosity Type IIP SN 2005cs, assuming ≈ 1.5 magnitudes of visual extinction, produced a reasonable match to the properties of SPIRITS 14buu. We find an obscured SN IIP to be the most likely interpretation for SPIRITS 14buu considered here.

The key to fully understanding the nature of these events is MIR spectroscopy, the likes of which will become available with the launch of the James Webb Space Telescope (JWST). A MIR spectrum would, for example, enable us to elucidate the origin of the extreme [3.6]−[4.5] color observed in SPIRITS 15c, and identify spectral features contributing to the flux at these wavelengths, e.g., the fundamental vibrational overtones of CO that may contribute to the high luminosity at [4.5]. Moreover, photometric coverage further into the MIR with JWST would allow us to detect the presence of a cooler dust component than is accessible with the warm *Spitzer*/IRAC bands.

The census of SNe in nearby galaxies from optical searches, even at only 35 Mpc, is incomplete. In less than three years of monitoring nearby galaxies at IR wavebands, SPIRITS has discovered at least one, and possibly two, moderately extinguished SNe that went unnoticed by optical surveys, SPIRITS 15c and SPIRITS 14buu. Since the start of the SPIRITS program, our galaxy sample has hosted nine optically discovered CCSNe. This may suggest a rate of CCSNe in nearby galaxies, missed by current optical surveys, of at least 10%. If SPIRITS 14buu is also indeed an SN, this estimate increases to 18%. In a future publication, we will present an analysis of the full SPIRITS sample of SN candidates to provide a more robust estimate of the fraction of SNe being missed by optical surveys. If this fraction is high, it

could have significant implications for our understanding of the CCSN rate and its connection to star-formation rates. Additionally, the discovery of IR transients such as SPIRITS 15c and SPIRITS 14buu in a galaxy-targeted survey indicates that the night sky is ripe for exploration by dedicated wide-field, synoptic surveys in the IR.

We thank the anonymous referee for their comments, which improved the manuscript. We thank M. Kaufman, B. Elmegreen, and the authors of Elmegreen et al. (2016) and Kaufman et al. (2016) for providing Hα, 24 μm, and CO measurements at the location of SPIRITS 15c. We also thank P. Groot, R. Lau, and S. Adams for valuable discussions.

This material is based upon work supported by the National Science Foundation Graduate Research Fellowship under Grant No. DGE-1144469. HEB acknowledges support for this work provided by NASA through grants GO-13935 and GO-14258 from the Space Telescope Science Institute, which is operated by AURA, Inc., under NASA contract NAS 5-26555. RDG was supported in part by the United States Air Force.

This work makes use of observations from the LCO network. This paper includes data gathered with the 6.5 meter Magellan Telescopes located at Las Campanas Observatory, Chile.

This work is based in part on observations made with the Spitzer Space Telescope, which is operated by the Jet Propulsion Laboratory, California Institute of Technology under a contract with NASA. The work is based, in part, on observations made with the Nordic Optical Telescope, operated by the Nordic Optical Telescope Scientific Association at the Observatorio del Roque de los Muchachos, La Palma, Spain, of the Instituto de Astrofisica de Canarias.

Funding for the Sloan Digital Sky Survey IV has been provided by the Alfred P. Sloan Foundation, the U.S. Department of Energy Office of Science, and the Participating Institutions. SDSS-IV acknowledges support and resources from the Center for High-Performance Computing at the University of Utah. The SDSS web site is www.sdss.org.

SDSS-IV is managed by the Astrophysical Research Consortium for the Participating Institutions of the SDSS Collaboration including the Brazilian Participation Group, the Carnegie Institution for Science, Carnegie Mellon University, the Chilean Participation Group, the French Participation Group, Harvard-Smithsonian Center for Astrophysics, Instituto de Astrofísica de Canarias, The Johns Hopkins University,

Kavli Institute for the Physics and Mathematics of the Universe (IPMU) / University of Tokyo, Lawrence Berkeley National Laboratory, Leibniz Institut für Astrophysik Potsdam (AIP), Max-Planck-Institut für Astronomie (MPIA Heidelberg), Max-Planck-Institut für Astrophysik (MPA Garching), Max-Planck-Institut für Extraterrestrische Physik (MPE), National Astronomical Observatories of China, New Mexico State University, New York University, University of Notre Dame, Observatário Nacional / MCTI, The Ohio State University, Pennsylvania State University, Shanghai Astronomical Observatory, United Kingdom Participation Group, Universidad Nacional Autónoma de México, University of Arizona, University of Colorado Boulder, University of Oxford, University of Portsmouth, University of Utah, University of Virginia, University of Washington, University of Wisconsin, Vanderbilt University, and Yale University.

Chapter 3

CASE STUDY OF SPIRITS 16tn: A HEAVILY OBSCURED AND LOW-LUMINOSITY SUPERNOVA AT 8.8 Mpc

Jencson, Jacob E., et al. 2018. "SPIRITS 16tn in NGC 3556: A Heavily Obscured and Low-luminosity Supernova at 8.8 Mpc". *ApJ* 863 (1): 20–44. doi:10.3847/1538-4357/aacf8b. arXiv: 1803.00574 [astro-ph.HE].

Jacob E. Jencson[1], Mansi M. Kasliwal[1], Scott M. Adams[1], Howard E. Bond[2,3], Ryan M. Lau[1,4], Joel Johansson[5], Assaf Horesh[6], Kunal P. Mooley[7], Robert Fender[7], Kishalay De[1], Dónal O'Sullivan[1], Frank J. Masci[8], Ann Marie Cody[9], Nadejda Blagorodnova[1], Ori D. Fox[3], Robert D. Gehrz[10], Peter A. Milne[11], Daniel A. Perley[12,13], Nathan Smith[11], and Schuyler D. van Dyk[8]

[1]Cahill Center for Astronomy and Astrophysics, California Institute of Technology, Pasadena, CA 91125, USA
[2]Department of Astronomy & Astrophysics, Pennsylvania State University, University Park, PA 16802, USA
[3]Space Telescope Science Institute, 3700 San Martin Dr., Baltimore, MD 21218, USA
[4]Jet Propulsion Laboratory, California Institute of Technology, 4800 Oak Grove Drive, Pasadena, CA 91109, USA
[5]Department of Physics and Astronomy, Division of Astronomy and Space Physics, Uppsala University, Box 516, SE-751 20 Uppsala, Sweden
[6]Racah Institute of Physics, The Hebrew University, Jerusalem 91904, Israel
[7]Department of Physics, Astrophysics, University of Oxford, Denys Wilkinson Building, Oxford OX1 3RH, UK
[8]Caltech/IPAC, Mailcode 100-22, Pasadena, CA 91125, USA
[9]NASA Ames Research Center, Moffet Field, CA 94035
[10]Minnesota Institute for Astrophysics, School of Physics and Astronomy, 116 Church Street SE, University of Minnesota, Minneapolis, MN 55455, USA
[11]University of Arizona, Steward Observatory, 933 N. Cherry Avenue, Tucson, AZ 85721, USA
[12]Dark Cosmology Centre, Niels Bohr Institute, University of Copenhagen, Juliane Maries Vej 30, DK-2100 Copenhagen Ø, Denmark
[13]Astrophysics Research Institute, Liverpool John Moores University, IC2, Liverpool Science Park, 146 Brownlow Hill, Liverpool L3 5RF, UK

Abstract

We present the discovery by the SPitzer InfraRed Intensive Transients Survey (SPIRITS) of a likely supernova (SN) in NGC 3556 (M108) at only 8.8 Mpc that was not detected by optical searches. A luminous infrared (IR) transient at $M_{[4.5]} = -16.7$ mag (Vega), SPIRITS 16tn is coincident with a dust lane in the inclined, star-forming disk of the host. Using observations in the IR, optical, and radio, we attempt to

determine the nature of this event. We estimate $A_V \approx 8$–9 mag of extinction, placing it among the three most highly obscured IR-discovered SNe. The [4.5] light curve declined at a rate of 0.013 mag day^{-1}, and the [3.6]−[4.5] color increased from 0.7 to $\gtrsim$ 1.0 mag by 184.7 days post discovery. Optical/IR spectroscopy shows a red continuum, but no clearly discernible features, preventing a definitive spectroscopic classification. Radio observations constrain the radio luminosity of SPIRITS 16tn to $L_\nu \lesssim 10^{24}$ erg s^{-1} Hz^{-1} between 3 and 15 GHz, excluding many varieties of core-collapse SNe. An SN Ia is ruled out by the observed IR color and lack of spectroscopic features from Fe-peak elements. SPIRITS 16tn was fainter at [4.5] than typical stripped-envelope SNe by $\approx$ 1 mag. Comparison of the spectral energy distribution to SNe II suggests that SPIRITS 16tn was both highly obscured and intrinsically dim, possibly akin to the low-luminosity SN 2005cs. We infer the presence of an IR dust echo powered by an initial peak luminosity of the transient of 5×10^{40} erg s^{-1} $\lesssim L_{\rm peak} \lesssim 4 \times 10^{43}$ erg s^{-1}, consistent with the observed range for SNe II. This discovery illustrates the power of IR surveys to overcome the compounding effects of visible extinction and optically subluminous events in completing the inventory of nearby SNe.

3.1 Introduction

The discovery and characterization of core-collapse supernovae (CCSNe), bursts of light heralding the explosive deaths of stars with initial mass $\gtrsim 8\ M_\odot$, have been largely driven in recent years by several large optical time-domain surveys, many specifically dedicated to the identification of transients. While such searches have been hugely successful, now discovering hundreds of SNe every year, a primary limitation is the susceptibility of visible photons to extinction by intervening dust. CCSNe in particular, often associated with the dense and dusty star-forming regions of late-type galaxies, may be subject to significant host extinction.

The measurement of the CCSN rate from optical surveys is an important probe of star formation and the fate of massive stars. However, these measurements only yield lower limits, as some SNe are missed owing to obscuration (e.g., Grossan et al. 1999; Maiolino et al. 2002; Cresci et al. 2007). In particular, Horiuchi et al. (2011) claim that half of all supernovae are missing across redshifts from $0 < z < 1$, termed the "supernova rate problem" and possibly indicating a large population of hidden or intrinsically dim SNe. Cappellaro et al. (2015) have challenged this claim, however, finding full agreement between CCSN rates and revised measurements of the cosmic star formation history. Still, Mannucci, Della Valle, and Panagia (2007) estimate

that 5–10% of CCSNe locally are inaccessible to optical searches, rising steeply to $> 30\%$ beyond $z = 1$. More recently, Mattila et al. (2012) find empirically that $\sim 20\%$ of SNe locally, growing to $\sim 40\%$ by $z = 1$, may be missed by optical searches owing only to obscuration by dust. The deep, galaxy-targeted $D < 40$ Mpc (DTL40) SN search recently reported, for example, the discovery of the obscured Type II SN DLT16am (SN 2016ija) in the nearby, edge-on galaxy NGC 1532 with $A_V \approx 6$ mag (Tartaglia et al. 2018). Further confounding the debate, recent studies suggest that CCSNe may even be overproduced in the local 11 Mpc volume (Botticella et al. 2012; Horiuchi et al. 2013; Xiao and Eldridge 2015) compared to Hα- and ultraviolet- (UV-) inferred star formation rates. Any CCSNe missed in the nearest galaxies only increase this tension.

Transient surveys at infrared (IR) wavelengths can overcome the limitations of optical searches introduced by the effects of extinction. A number of searches in the near-IR have focused specifically on the dense, highly star-forming, heavily extinguished environments of luminous and ultraluminous infrared galaxies (LIRGs and ULIRGs), where the SN rates are expected to be high, of order one per year (Mattila and Meikle 2001). Such surveys, using seeing-limited imaging (e.g., Mannucci et al. 2003; Miluzio et al. 2013) or high-resolution imaging from space or with ground-based adaptive optics to probe the densest nuclear regions of these galaxies (e.g., Cresci et al. 2007; Mattila et al. 2007; Kankare et al. 2008; Kankare et al. 2012; Kool et al. 2018) have now uncovered 16 CCSNe in (U)LIRGs.

The InfraRed Array Camera (IRAC; Fazio et al. 2004) aboard the *Spitzer Space Telescope* (Werner et al. 2004; Gehrz et al. 2007), in the 3.6 and 4.5 μm imaging bands (hereafter [3.6] and [4.5]), where the effects of extinction are minimal, is sensitive to even the most highly obscured events, up to $A_V \approx 100$ mag at 20 Mpc. Since 2014 December, the SPitzer InfraRed Intensive Transients Survey (SPIRITS; PIDs 11063, 13053; PI M. Kasliwal, Kasliwal et al. 2017b) has been conducting an ongoing monitoring campaign of nearby galaxies ($D \lesssim 20$ Mpc) for transients with *Spitzer*/IRAC at [3.6] and [4.5]. An example of the importance of IR surveys was demonstrated in Jencson et al. (2017e), where we reported the discovery of two obscured SNe in IC 2163, SPIRITS 14buu and SPIRITS 15c, missed by optical searches despite their proximity to Earth and only moderate amounts of extinction ($A_V \approx 1.5$–2.2 mag).

Beyond the ability to discover CCSNe hidden by dust, mid-IR observations offer important diagnostics of the explosions and their circumburst environments. Mid-

IR emission may be produced in SNe as thermal emission from the photosphere of the explosions, and it also traces the presence of warm dust in the system. This dust may be newly formed in the ejecta or in the rapidly cooling, post-shock material of the explosion. Alternatively, preexisting circumburst dust, possibly formed in the pre-SN stellar wind or an eruptive mass-loss event of the progenitor star, may be heated by the luminous SN peak, producing an "IR echo" owing to light-travel time effects (e.g., Bode and Evans 1980; Dwek 1983; Mattila et al. 2008). The multifaceted effects of dust, either newly formed or preexisting, on the mid-IR emission of SNe has been studied in numerous works (see, e.g., Kotak et al. 2009; Fox et al. 2010; Fox et al. 2011; Szalai and Vinkó 2013). Most recently, Tinyanont et al. (2016) and Szalai et al. (2019a) presented systematic studies of CCSNe observed in the mid-IR with *Spitzer*, finding remarkable diversity in the growing sample of well-characterized events at these wavelengths.

Here we report the discovery of SPIRITS 16tn, a likely highly obscured CCSN at only 8.8 Mpc in the nearby spiral galaxy NGC 3556 (M108). In Section 3.2, we describe the discovery and follow-up observations of this event using both space- and ground-based facilities in the optical, IR, and radio. In Section 3.3, we describe our analysis of the data, including constraints on the progenitor luminosity from archival, pre-explosion *Hubble Space Telescope* (*HST*) imaging (Section 3.3), analysis of the light curves and color evolution (Section 3.3), evolution of the spectral energy distribution (SED), and constraints on the extinction and dust emission (Section 3.3). In Section 3.4, we discuss of the overall properties of SPIRITS 16tn and our interpretation of the observations in the context of well-studied SNe and other types of luminous IR transients. We present our conclusions in Section 3.5.

3.2 SPIRITS discovery and follow-up observations

Spitzer/IRAC Discovery in NGC 3556

During the ongoing monitoring campaign of nearby galaxies with SPIRITS, we observed the star-forming galaxy NGC 3556 with *Spitzer*/IRAC at [3.6] and [4.5] at 10 epochs between UT 2014 January 18.4 and 2016 August 15.0. Image subtraction was performed using archival images from 2011 February 7.6 as references (observed as part of the *Spitzer* Survey of Stellar Structure in Galaxies, S^4; PID 61065; PI K. Sheth; Sheth et al. 2010). For details on our image subtraction pipeline see Kasliwal et al. (2017b). A new transient source, designated SPIRITS 16tn, was detected in both the [3.6] and [4.5] images on 2016 August 15.0 (MJD = 57,615.0; Jencson et al. 2016c). Throughout this paper, we refer to the phase as the number

of days since the earliest detection of SPIRITS 16tn on this date. We detect no significant variability at the location of SPIRITS 16tn in any of the prior *Spitzer*/IRAC images compared to the reference frame. We show the [4.5] discovery images in the middle row of Figure 3.1, along with mosaicked *gri* imaging of the field from the Sloan Digital Sky Survey Date Release 12 (SDSS-DR12; Eisenstein et al. 2011; Alam et al. 2015) in the top panel, showing the location of SPIRITS 16tn in a dust lane in the disk of NGC 3556. This galaxy was also the host of the probable Type II SN 1969B (Ciatti and Barbon 1971).

Host distance and Galactic extinction

SPIRITS 16tn was discovered at a R.A. and decl. of $11^{\rm h}11^{\rm m}20\farcs40$, $+55°40'17\farcs3$ (J2000). Located $89\farcs9$ from the center of the star-forming galaxy NGC 3556, the position of SPIRITS 16tn is coincident with a dust lane in the disk.

NED[1] lists 17 individual distance estimates to NGC 3556 with a median value of $\mu = 29.71$ mag and standard deviation of 0.67 mag. Throughout this work, we adopt the most recent value from Sorce et al. (2014) of $\mu = 29.72 \pm 0.41$ mag ($D \approx 8.8$ Mpc). This estimate is based on the mid-IR Tully–Fisher relation using the [3.6] micron flux with color and selection bias corrections. The redshift of NGC 3556 is $z = 0.002332$ ($v = 699$ km s^{-1}; Shostak 1975).

We assume Galactic extinction along the line of sight to NGC 3556 of $A_V = 0.046$ mag from the Schlafly and Finkbeiner (2011) recalibration of the Schlegel, Finkbeiner, and Davis (1998) IR-based dust map assuming a Fitzpatrick (1999) extinction law with $R_V = 3.1$. Furthermore, for all other considerations of the possible extinction to SPIRITS 16tn throughout this work, including any foreground host extinction, we assume the Fitzpatrick (1999) Milky Way extinction curve with $R_V = 3.1$ unless otherwise noted.

Follow-up Imaging

In this section, we describe our space- and ground-based imaging follow-up efforts to characterize SPIRITS 16tn.

[1]The NASA/IPAC Extragalactic Database (NED) is operated by the Jet Propulsion Laboratory, California Institute of Technology, under contract with the National Aeronautics and Space Administration.

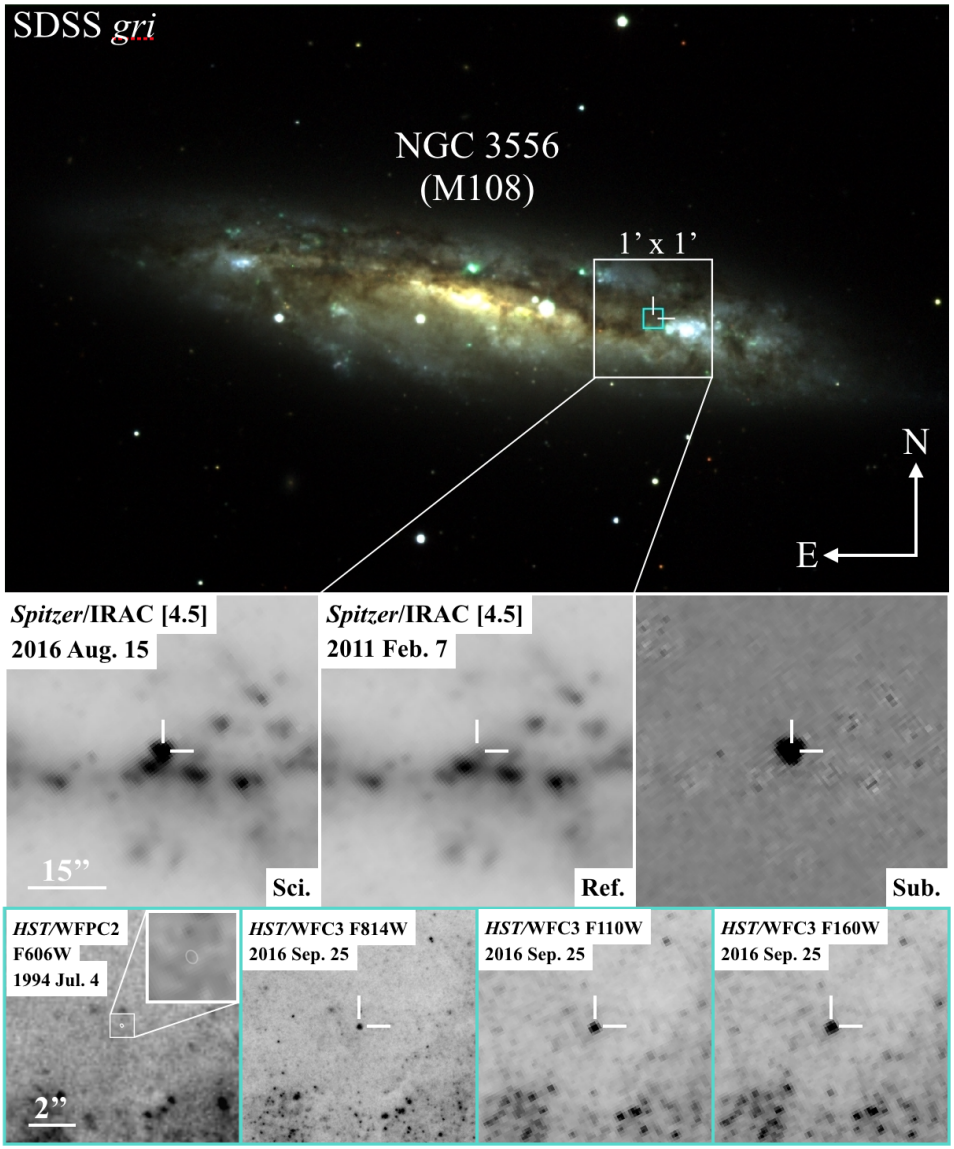

Figure 3.1: Top panel: color-composite SDSS imaging of NGC 3556 (M108) in three filters (g in blue, r in green, and i in red). The location of SPIRITS 16tn in a dust lane of NGC 3556 is indicated by the white crosshairs. The middle row shows the $1' \times 1'$ region indicated by the white zoom-in box in the top panel. From left to right, we show the *Spitzer*/IRAC [4.5] discovery science frame of SPIRITS 16tn from 2016 August 15, the archival reference image from 2011 February 7, and the science–reference subtraction image, clearly showing the new transient source. In the bottom row, we show the $10'' \times 10''$ region indicated by the cyan box in the top panel. In the leftmost panel, we show the archival *HST*/WFPC2 F606W image. The white ellipse (shown more clearly in the $1'' \times 1''$ zoom-in in the upper right corner of this panel) indicates the 10σ uncertainty on the position of SPIRITS 16tn. In the three rightmost panels of the bottom row, we show the post-discovery *HST*/WFC3 F814W, F110W, and F160W imaging of SPIRITS 16tn.

Space-based

Since its discovery, we continued to monitor SPIRITS 16tn with *Spitzer*/IRAC at [3.6] and [4.5] as part of the SPIRITS program. Image subtraction was performed on all subsequent epochs, as described in Section 3.2. Photometry was performed on the reference-subtracted images using a 4 mosaicked pixel (2.″4) aperture and a background annulus from 4–12 pixels (2.″4–7.″2). The extracted flux was multiplied by aperture corrections of 1.215 and 1.233 for [3.6] and [4.5], respectively, as described in the IRAC instrument handbook[2]. Fluxes then were converted to Vega system magnitudes using the handbook-defined zero-magnitude fluxes for each IRAC channel. At discovery, our photometry gives [4.5] = 13.04 ± 0.05 mag ($M_{[4.5]} = -16.7$ mag; $\lambda L_\lambda = 1.3 \times 10^7\ L_\odot$).

We triggered observations with the Ultra-violet/Optical Telescope (UVOT; Roming et al. 2005) on board the *Neil Gehrels Swift Observatory* (Gehrels et al. 2004; Nousek 2004) on 2016 August 29.1. No source was detected in the U, B, and V-band images with integration times of 540, 580, and 540 s, respectively (Adams, Jencson, and Kasliwal 2016). We derived 5σ limiting magnitudes of $V > 19.9$ mag, $B > 20.2$ mag, and $U > 19.9$ mag. The extreme $V - [4.5] \gtrsim 6.9$ mag color indicates that SPIRITS 16tn is likely highly obscured.

We observed SPIRITS 16tn on 2016 September 25, $t = 42$ days, with the Wide Field Camera 3 (WFC3) on the *Hubble Space Telescope* (*HST*) in the UVIS channel with the F814W filter and the IR channel with the F110W and F160W filters. These observations were part of our Cycle 23 Target of Opportunity program to observe SPIRITS transients (GO-14258; PI: H. Bond). All three images are shown in the bottom row of Figure 3.1. The photometry and limits from our space-based follow-up effort are listed in Table 3.1 and shown in Figure 3.2.

Table 3.1: Photometry of SPIRITS 16tn

UT Date	MJD	Phase[a] (days)	Tel./Inst.	Band	App. Mag.[b,c] (mag)	Abs. Mag.[c,d] (mag)
1999 Jul 04	51,363	-6252	*HST*/WFPC2	F606W	> 24.5	> −5.2
2016 Mar 03.6	57,450.6	-164.4	*Spitzer*/IRAC	[3.6]	> 17.8	> −11.9
2016 Mar 03.6	57,450.6	-164.4	*Spitzer*/IRAC	[4.5]	> 17.6	> −12.1
2016 May 25.0	57,533.0	-82.0	KPNO-4m	z	> 22.5	> −7.2
2016 Aug 15.0	57,615.0	0.0	*Spitzer*/IRAC	[3.6]	13.71 (0.05)	−16.0
2016 Aug 15.0	57,615.0	0.0	*Spitzer*/IRAC	[4.5]	13.04 (0.05)	−16.7

[2] http://irsa.ipac.caltech.edu/data/SPITZER/docs/irac/iracinstrumenthandbook/

Table 3.1 – *Continued*

UT Date	MJD	Phase[a] (days)	Tel./Inst.	Band	App. Mag.[b,c] (mag)	Abs. Mag.[c,d] (mag)
2016 Aug 29.0	57,629.0	14.0	*Swift*/UVOT	U	> 20.5	> -9.3
2016 Aug 29.0	57,629.0	14.0	*Swift*/UVOT	B	> 20.8	> -9.0
2016 Aug 29.0	57,629.0	14.0	*Swift*/UVOT	V	> 20.5	> -9.2
2016 Sep 25.9	57,656.9	41.9	*HST*/WFC3	F814W	21.68 (0.03)	-8.0
2016 Sep 25.9	57,656.9	41.9	*HST*/WFC3	F110W	19.76 (0.02)	-10.0
2016 Sep 25.9	57,656.9	41.9	*HST*/WFC3	F160W	18.64 (0.02)	-11.1
2016 Oct 11.5	57,672.5	57.5	P200/WIRC	K_s	16.9 (0.1)	-12.8
2016 Oct 13.5	57,674.5	59.5	P60/SEDM	i	> 19.4	> -10.3
2016 Oct 31.6	57,692.6	77.6	Keck/LRIS	g	> 22.4	> -7.4
2016 Oct 31.6	57,692.6	77.6	Keck/LRIS	I	> 21.9	> -7.8
2016 Nov 09.4	57,701.4	86.4	1.5m/RATIR	r	> 19.7	> -10.0
2016 Nov 09.4	57,701.4	86.4	1.5m/RATIR	i	> 19.6	> -10.1
2016 Nov 09.4	57,701.4	86.4	1.5m/RATIR	z	> 19.7	> -10.0
2016 Nov 09.4	57,701.4	86.4	1.5m/RATIR	Y	> 18.6	> -11.1
2016 Nov 09.4	57,701.4	86.4	1.5m/RATIR	J	> 18.0	> -11.7
2016 Nov 09.4	57,701.4	86.4	1.5m/RATIR	H	> 17.5	> -12.2
2016 Nov 10.4	57,702.4	87.4	1.5m/RATIR	r	> 19.9	> -9.8
2016 Nov 10.4	57,702.4	87.4	1.5m/RATIR	i	> 19.8	> -9.9
2016 Nov 10.4	57,702.4	87.4	1.5m/RATIR	z	> 19.7	> -10.0
2016 Nov 10.4	57,702.4	87.4	1.5m/RATIR	Y	> 18.8	> -10.9
2016 Nov 10.4	57,702.4	87.4	1.5m/RATIR	J	> 18.2	> -11.5
2016 Nov 10.4	57,702.4	87.4	1.5m/RATIR	H	> 17.6	> -12.1
2016 Dec 14.7	57,736.7	121.7	UKIRT	H	18.9 (0.3)	-10.8
2016 Dec 22.7	57,744.7	129.7	UKIRT	H	19.2 (0.1)	-10.5
2016 Dec 23.6	57,745.6	130.6	UKIRT	K	18.1 (0.2)	-11.6
2017 Jan 17.4	57,770.4	155.4	P200/WIRC	J	20.5 (0.3)	-9.2
2017 Jan 17.4	57,770.4	155.4	P200/WIRC	H	19.7 (0.5)	-10.0
2017 Jan 17.4	57,770.4	155.4	P200/WIRC	K_s	18.5 (0.3)	-11.2
2017 Feb 15.7	57,799.7	184.7	*Spitzer*/IRAC	[3.6]	> 17.4	> -12.3
2017 Feb 15.7	57,799.7	184.7	*Spitzer*/IRAC	[4.5]	16.41 (0.07)	-13.3
2017 Mar 07.4	57,819.4	204.4	P200/WIRC	K_s	19.0 (0.2)	-10.7
2017 Apr 09.8	57,852.8	237.8	*Spitzer*/IRAC	[3.6]	> 17.7	> -12.0
2017 Apr 09.8	57852.8	237.8	*Spitzer*/IRAC	[4.5]	17.2 (0.2)	-12.5
2017 May 03.3	57,876.3	261.3	P200/WIRC	J	> 20.0	> -9.7
2017 May 03.3	57,876.3	261.3	P200/WIRC	H	> 19.2	> -10.5
2017 May 03.3	57,876.3	261.3	P200/WIRC	K_s	> 18.5	> -11.2
2017 Jul 10.3	57,944.3	329.3	*Spitzer*/IRAC	[3.6]	> 17.6	> -12.1
2017 Jul 10.3	57,944.3	329.3	*Spitzer*/IRAC	[4.5]	> 17.5	> -12.2
2018 Feb 21.3	58,170.3	555.3	*Spitzer*/IRAC	[3.6]	> 17.9	> -11.8
2018 Feb 21.3	58,170.3	555.3	*Spitzer*/IRAC	[4.5]	> 17.9	> -11.8

[a] Phase is number of days since the earliest detection of this event on 2016 August 15.0 (MJD = 57, 615.0).

[b] Vega magnitudes, except for the $griz$ bands which are AB magnitudes on the SDSS system. 1σ uncertainties are given in parentheses.

[c] 5σ limiting magnitudes are given for nondetections.

[d] Absolute magnitudes corrected for Galactic extinction for NGC 3556 from NED.

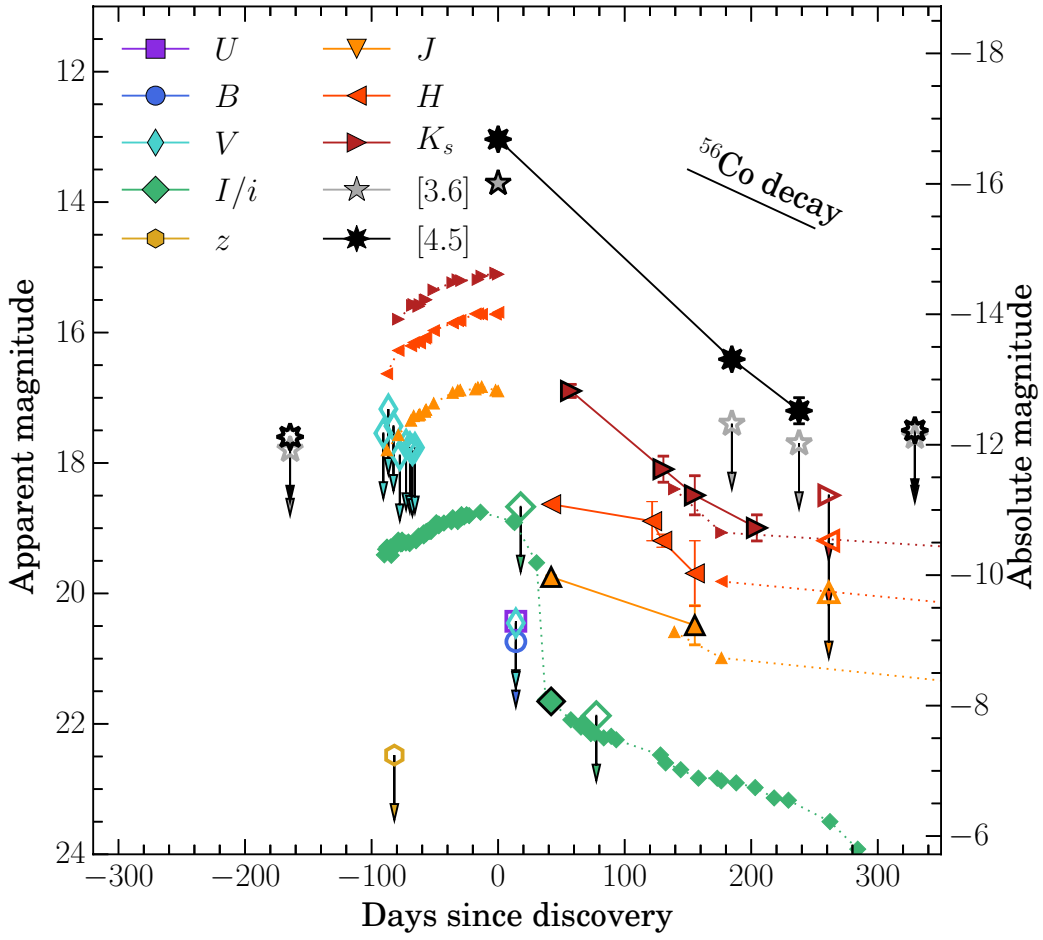

Figure 3.2: Multiband light curves of SPIRITS 16tn, corrected for Galactic extinction only, are shown as the large filled symbols, with 5σ upper limits from nondetections indicated by open symbols with downward-pointing arrows. We also show the ASAS-SN V-band limits (Shappee et al. 2016) and Sloan-i band limit (Vinko, Varga-Verebelyi, and Sarneczky 2016) as reported. Small symbols are the corresponding light curves of the low-luminosity SN 2005cs from Pastorello et al. (2006) and Pastorello et al. (2009), shifted to the distance of NGC 3556 plus an additional $\Delta m = 0.7$ mag, and reddened by $E(B-V) = 2.5$ mag. The black solid line indicates the expected decline rate for a light curve powered by the radioactive decay of ^{56}Co (see, e.g., Gehrz 1988; Gehrz and Ney 1990).

Ground-based

At the time of its discovery, SPIRITS 16tn was inaccessible for ground-based observing except at high latitudes. We began ground-based follow-up of SPIRITS 16tn from Palomar Observatory in 2016 October, approximately 2 months after discovery. We obtained near-IR images of SPIRITS 16tn in JHK_s with the Wide Field Infrared Camera (WIRC; Wilson et al. 2003) on the Palomar 200-inch Hale telescope (P200) at several epochs, employing large dithers approximately every minute to allow for accurate subtraction of the bright near-IR sky background. Flat-fielding, background subtraction, astrometric alignment, and final stacking of images in each filter were performed using a custom pipeline.

Additional near-IR H and K_s-band imaging was obtained with the Wide Field Camera (WFCAM; Casali et al. 2007) on the United Kingdom Infrared Telescope (UKIRT) at Mauna Kea Observatories. We obtained simultaneous optical/near-IR $rizYJH$ with the Reionization and Transients InfraRed camera (RATIR; Butler et al. 2012) on the 1.5 m Johnson Telescope at the Mexican Observatorio Astronomico Nacional on the Sierra San Pedro Martir in Baja California, Mexico (Watson et al. 2012).

We obtained one epoch of optical (i-band) imaging with the Spectral Energy Distribution Machine (SEDM; Blagorodnova et al. 2018) on the fully automated Palomar 60-inch Telescope (P60; Cenko et al. 2006) and an epoch of g- and I-band imaging with the Low-Resolution Imaging Spectrometer (LRIS; Oke et al. 1995) on the Keck I Telescope on Maunakea.

Photometry was performed by simultaneously fitting the point-spread function of the transient, measured using field stars, and background, modeled using low-order polynomials. The photometric zero-point in each image was obtained by performing photometry on stars of known magnitude in the field. For the near-IR JHK images we selected 10 bright, isolated Two Micron All Sky Suvery (2MASS) stars, and for Y band we adopt the conversion from 2MASS used for WFCAM/UKIRT from Hodgkin et al. (2009). For optical images, we used 12 SDSS stars, adopting the conversions of Jordi, Grebel, and Ammon (2006) to convert from the Sloan $ugriz$ system to $UBVRI$ magnitudes where necessary.

We examined the location of SPIRITS 16tn in a deep z-band image of NGC 3556 from 2017 May 25.0, taken with the CCD Mosaic imager on the 4 m Mayall Telescope at Kitt Peak National Observatory (KPNO) as part of the Mayall z-band Legacy

Survey (MzLS). We derive a limit on the flux from the transient of $z > 22.5$ mag, providing our most stringent constraint on the explosion date of SPIRITS 16tn at 82.0 days before the first detection.

We list all of our photometry of SPIRITS 16tn in Table 3.1. For nondetections we list 5σ upper limits, where we estimated σ as the standard deviation of the pixel values near the transient position to account for uncertain variations in the background flux from the host galaxy. Our light curves of SPIRITS 16tn are shown in Figure 3.2.

Additionally, Shappee et al. (2016) reported pre-discovery limits from nondetections of SPIRITS 16tn in the All-Sky Automated Survey for Supernovae (ASAS-SN) between UT 2016 May 16.3 and 2016 June 10.3, constraining optical emission from SPIRITS 16tn to $V > 17.81$ mag at $t = -65.7$ days. Vinko, Varga-Verebelyi, and Sarneczky (2016) also reported observations in the Sloan i filter of SPIRITS 16tn on 2016 September 1.8, placing a limit on the flux from the transient of $i > 18.7$ mag at $t = 17.8$ days. We show these limits along with our own photometry in Figure 3.2. As reported, these limits do not further constrain the extinction or explosion date beyond the data newly presented here.

Spectroscopy

We obtained optical spectroscopy of SPIRITS 16tn with Keck/LRIS on 2017 November 2 ($t = 79$ days post discovery). We used the D560 dichroic to split the light between the red and blue sides, and we used the 400/8500 grating on the red side and the 300/3400 grism on the blue side. We obtained one 1800 s integration on the blue side and two 860 s integrations on the red side. Spectroscopic reductions were performed using the analysis pipeline LPIPE[3]. A weak trace is visible at the position of the transient on the red-side camera. The low signal-to-noise ratio (S/N) 1D extracted spectrum was flux-calibrated using observations of the standard star Feige 34 from the same night. The Keck/LRIS optical spectrum is shown in Figure 3.3.

We observed SPIRITS 16tn with the Gemini Near-Infrared Spectrograph (GNIRS) on the 8.1 m Gemini North Telescope on the summit of Maunakea in Hawaii through Gemini Fast Turnaround program GN-2016B-FT-25. We obtained two epochs[4] of near-IR cross-dispersed (XD; multi-order) spectroscopy on 2016 December 29

[3]Software available at `http://www.astro.caltech.edu/~dperley/programs/lpipe.html`

[4]Our observations were submitted as a single observation to the Gemini queue, but the execution of our program was split between two separate dates instead, possibly due to deteriorated weather conditions.

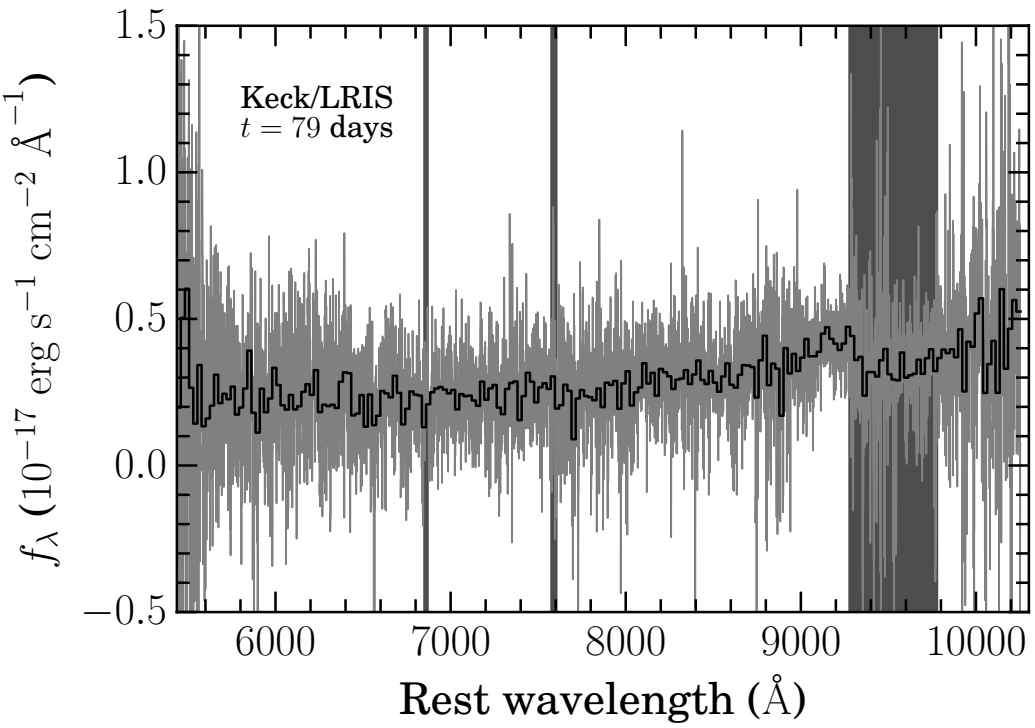

Figure 3.3: Optical spectrum of SPIRITS 16tn from Keck/LRIS taken on 2016 November 2 (t = 79 days) in the rest frame of the host galaxy, NGC 3556 (z = 0.002332). The data are shown in light gray, and the median-binned spectrum with a bin size of 20 pixels is overplotted in black. Regions affected by telluric absorption features are indicated by the dark-grey vertical bands.

(t = 136 days) and 2017 January 9 (t = 147 days) using a 0.″45 wide slit with the 32 line mm^{-1} grating and the short blue camera with its cross-dispersing prism for a spectra resolution of R = 1200. In this configuration, a spectrum of the entire near-IR region (0.85–2.5 μm) is obtained at once. The observations were carried out using 300 s exposures, with the target nodded along the slit between frames to allow for accurate subtraction of the sky background. We obtained a total of 70 minutes of integration during the first epoch and 50 minutes during the second. Baseline calibrations were also obtained, including observations of A0V stars at similar airmass immediately before/after the science observations as near-IR standards for flux calibration and telluric corrections.

Reductions, including detector pattern noise cleaning, radiation event removal, flat-fielding, background subtraction, spatial distortion corrections, wavelength calibration, and 1D extractions, were perform using standard tasks in the Gemini IRAF[5]

[5]IRAF is distributed by the National Optical Astronomy Observatory, which is operated by the

package following the procedures outlined on the Gemini webpage[6]. In the reduced 2D spectra, a faint trace was visible at the position of SPIRITS 16tn in spectral orders 3 and 4, corresponding to the K and H spectral regions, respectively.

Corrections for the strong near-IR telluric absorption features and flux calibrations were performed using the IDL tool *xtellcor* developed by Vacca, Cushing, and Rayner (2003). For the first epoch, a detector bias fault occurred during the science target observations, after which the target had to be reacquired. We reduced the two groups of data separately, using the star HIP 53735, observed immediately preceding SPIRITS 16tn, as the A0V flux standard for the first group and HIP 56147, observed immediately after, for the second. The two telluric-corrected, flux-calibrated spectra were then averaged. For the second epoch we again used HIP 53735. Our Gemini/GNIRS spectra of SPIRITS 16tn are shown in Figure 3.4.

We note that we did not attempt to subtract the contribution from the host-galaxy background from our optical/near-IR spectra, which may be significant for our late-time observations as the transient fades.

Host spectroscopy

The Palomar Cosmic Web Imager (PCWI; Matuszewski et al. 2010) is an integral field spectrograph mounted on the Cassegrain focus of the 200-inch Hale telescope at Palomar Observatory. The instrument has a field of view of $40'' \times 60''$ divided across 24 slices with dimensions of $40''times2.5''$ each. The spectrograph uses an $R \sim 5000$ volume phase holographic grating (in the red filter) to achieve an instantaneous bandwidth of $\approx$ 550 Å. A complete description of the instrument, observing approach, and data analysis methodology can be found in Martin et al. 2014.

We observed the host region of SPIRITS 16tn with PCWI (centered at the location of the transient) on 2017 October 18 in order to characterize the star formation rate in the transient environment. The instrument was configured to a central wavelength of 6630 Å, covering the wavelength range from approximately 6400 to 6900 Å. We obtained one 600 s exposure of the transient region with the instrument oriented to a position angle of 270° (slices oriented in the north-south direction) followed by one 600 s background sky exposure of a nearby field with no bright sources.

Association of Universities for Research in Astronomy (AURA) under a cooperative agreement with the National Science Foundation.

[6]Procedures for reducing GNIRS XD spectra are found at `http://www.gemini.edu/sciops/instruments/gnirs/data-format-and-reduction/reducing-xd-spectra`

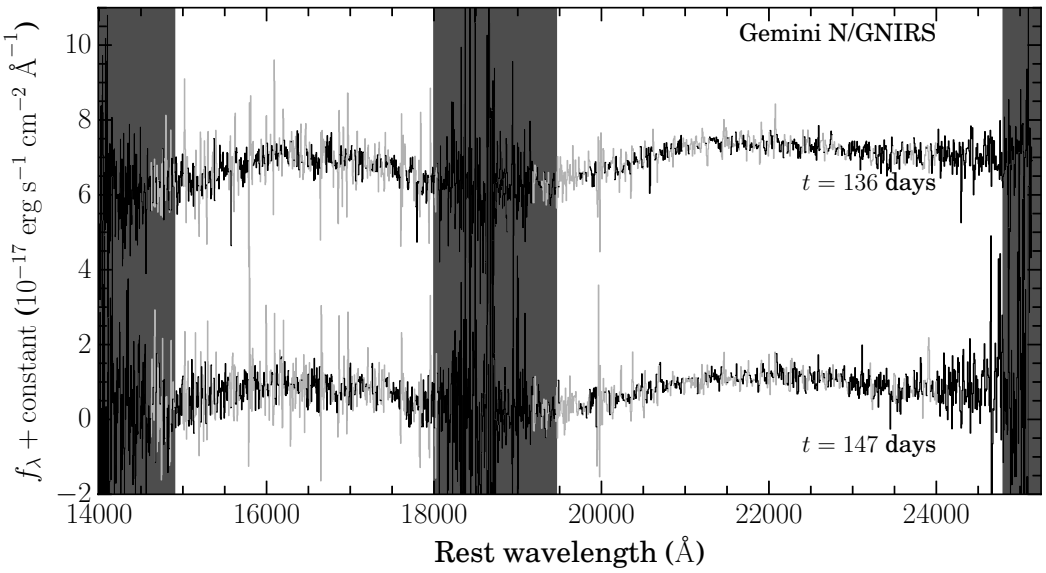

Figure 3.4: Near-IR spectra of SPIRITS 16tn from GNIRS on Gemini N. Spectral bins of lower S/N due to coincidence with an OH emission lines of the night sky are shown in light gray. Regions of low atmospheric transmission at the end of the *H* and *K* windows are indicated by the gray vertical bars. The spectra have been shifted in wavelength to the rest frame of the host galaxy, NGC 3556 ($z = 0.002332$). The spectrum from 2016 December 29 has been shifted up by the constant indicated on the figure for clarity.

We also obtained calibration images including arc lamp spectra, dome flats, and a standard-star spectrum. The 2D spectra were sliced, rectified, spatially aligned, and wavelength-calibrated using the calibration images to produce data cubes for each sky exposure, sampled at (R.A., decl., λ) intervals of (2.″6, 0.″6, 0.22 Å). The sky background cube was subtracted from the source cube to remove the sky emission lines, followed by flux calibration using the standard star Feige 15. This produces the final flux-calibrated spectral cube of the $40'' \times 60''$ region centered at the location of the transient.

Radio observations

We observed SPIRITS 16tn in the radio with the Karl G. Jansky Very Large Array (VLA) at two epochs on 2016 September 9.0 ($t = 19.0$ days) in the *S*, *C*, and *X* bands (3, 6, and 10 GHz, respectively) and 2017 January 12.4 ($t = 149.4$ days) in the *C* and *Ku* bands (10 and 15.5 GHz, respectively). The data were reduced using standard imaging techniques for the VLA in CASA. We also obtained radio imaging at 15 GHz with the Arcminute Microkelvin Imager Large Array (AMI-LA) on 2017 September 2–5 ($t = 17 - 20$ days). The AMI-LA data were processed

Table 3.2: Summary of radio observations of SPIRITS 16tn

UT Date	MJD	Phase[a] (days)	Inst.	Frequency (GHz)	Flux[b] (mJy)	Luminosity[b,c] (erg s^{-1} Hz^{-1})
2016 Sep 2–5	57,633 - 57,636	17–20	AMI-LA	15.0	< 0.3	$< 2.8 \times 10^{25}$
2016 Sep 4.0	57,635.0	19.0	VLA	10.0	< 0.047	$< 4.4 \times 10^{24}$
2016 Sep 4.0	57,635.0	19.0	VLA	6.0	< 0.075	$< 7.0 \times 10^{24}$
2016 Sep 4.0	57,635.0	19.0	VLA	3.0	< 0.10	$< 9.3 \times 10^{24}$
2017 Jan 12.4	57,765.4	149.4	VLA	15.5	< 0.029	$< 2.6 \times 10^{24}$
2017 Jan 12.4	57,765.4	149.4	VLA	6.0	< 0.029	$< 2.7 \times 10^{24}$

[a] Phase is number of days since the earliest detection of this event on 2016 August 15.0 (MJD = 57, 615.0).
[b] 5σ limiting magnitudes are given for nondetections.
[c] Luminosities calculated assuming a distance to NGC 3556 from NED of 8.8 Mpc.

(RFI excision and calibration) with a fully automated pipeline, AMI-REDUCE (e.g., Davies et al. 2009; Perrott et al. 2013), and later imported and imaged in CASA. SPIRITS 16tn was undetected at all epochs and frequencies in the radio, and we provide a summary of our limits on the observed fluxes and radio luminosities of the source in Table 3.2. The 5σ limits are calculated as 5 times the RMS noise at the position of the transient in the final radio images.

3.3 Analysis

Here we describe our analysis of both the archival imaging data at the position of the transient and our photometric and spectroscopic measurements of SPIRITS 16tn obtained as part of our follow-up effort.

Progenitor constraints and host environment

We examined the *Spitzer*/IRAC pre-explosion images of NGC 3556 from 2011 February 7, which we also used as references for image subtraction as described in Section 3.2, for the presence of a possible IR progenitor star. No clear point source is detected in either IRAC channel to 5σ limiting magnitudes of $[3.6] > 14.6$ mag and $[4.5] > 14.4$ mag, where the depth is primarily limited by bright, spatially varying background emission from the host. At the assumed distance to NGC 3556 and correcting only for Galactic extinction, the limits on the absolute magnitudes of the progenitor are $M_{[3.6]} > -15.1$ mag and $M_{[4.5]} > -15.3$ mag.

Images of NGC 3556 were obtained with the *HST* on 1994 July 4 in program SNAP-5446 (PI: G. Illingworth). These observations used the Wide Field Planetary Camera 2 (WFPC2) with the F606W filter and covered the site of SPIRITS 16tn, approximately 22 yr before its outburst. To determine the precise location of SPIR-

ITS 16tn in the archival WFPC2 F606W image, we registered this frame with the WFC3 F814W detection image of the active transient described above in Section 3.2. Using centroid measurements for 10 bright stars detected in both frames, we determined the geometric transformation from WFPC2 to WFC3 using the Space Telescope Science Data Analysis System (STSDAS)[7] `geomap` task. By applying the `geotran` task to the WFPC2 frame and blinking this transformed image against the WFC3 image, we verified the quality of the registration. The rms errors of the geometric fits for the reference stars were 0.15 and 0.20 pixels in the x and y coordinates, respectively, corresponding to 0.006 and 0.008 arcsec. We did not detect a source consistent with the position of SPIRITS 16tn to a 5σ limiting magnitude of $V \gtrsim 24.5$ mag in the archival WFPC2 F606W image. We show the location of SPIRITS 16tn in the WFPC2 F606W image in the bottom left panel of Figure 3.1.

At the distance to NGC 3556 and correcting for only Galactic extinction, this corresponds to an upper limit on the absolute magnitude of the progenitor star of $M_V \gtrsim -5.2$ mag. Assuming a bolometric correction for an intermediate red supergiant (RSG) spectral type M0 of -1.23 mag from Levesque et al. (2005), and adopting a solar bolometric magnitude of $M_{\odot,\mathrm{bol}} = +4.74$ mag, we obtain a limit on the luminosity of the progenitor of $L < 2.9 \times 10^4\ L_\odot$. However, if we assume $A_V \approx 7.8$ mag, as inferred for SPIRITS 16tn below in Section 3.3, our limit on the progenitor luminosity becomes far less constraining at $L \lesssim 3.9 \times 10^7\ L_\odot$.

We use our PCWI observations to constrain the environment of the progenitor of SPIRITS 16tn. For each pixel in the processed data cube, we fit a simple polynomial to remove the continuum emission from the galaxy. We then measured the Hα flux in each pixel by integrating over the Hα emission line at the known velocity of the galaxy (≈ 699 km s^{-1}), to produce a 2D map of Hα flux near the location of the transient (Figure 3.5). The fluxes were then transformed to an equivalent luminosity using the distance to the galaxy, followed by conversion to an estimated star formation rate using the relations in Kennicutt (1998). The star formation rates in each pixel were then converted to an equivalent star formation surface density using an angular scale of 0.043 kpc arcsec^{-1}. As shown, SPIRITS 16tn is coincident with a dense star forming environment with star formation rate densities of $\sim 10^{-2}\ M_\odot$ yr^{-1} kpc^{-2}.

[7] STSDAS is a product of STScI, which is operated by AURA for NASA.

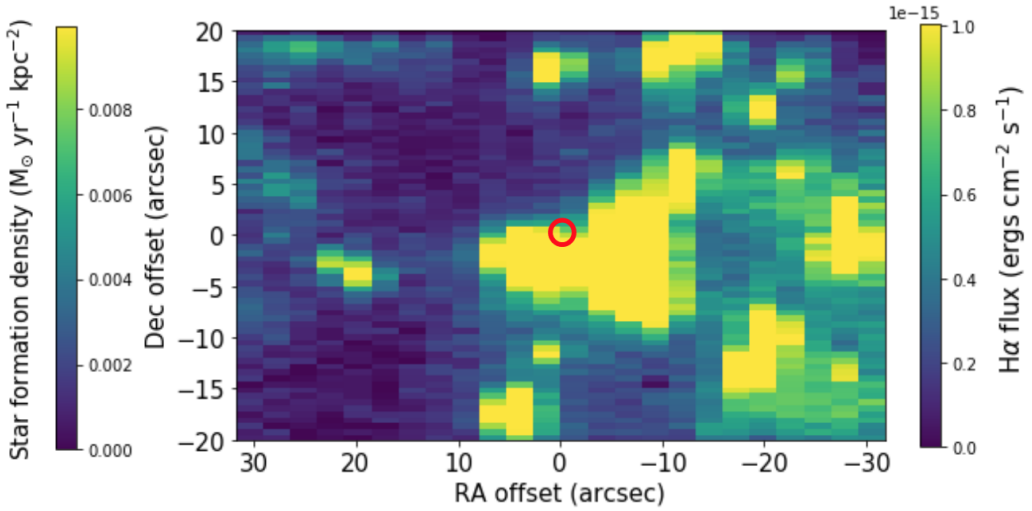

Figure 3.5: PCWI map of the host region around SPIRITS 16tn. The red circle denotes the location of the transient. The image colors correspond to the indicated Hα fluxes (right vertical axis) along with their equivalent star formation rate densities (left vertical axis).

Light curves and color evolution

SPIRITS 16tn was discovered at [4.5] = 13.04 ± 0.05 mag ($M_{[4.5]} = -16.7$ mag; $\lambda L_\lambda = 1.3 \times 10^7\ L_\odot$), as shown in the light curves in Figure 3.2. The high IR luminosity suggests an explosive event, likely an SN. At [4.5] the flux is observed to fade at a rate of 0.018 mag day^{-1} between $t = 0$ and 184.7 days. In the near-IR K_s band, SPIRITS 16tn is observed to fade more slowly at a rate of 0.013 mag day^{-1}. These are faster than the expected bolometric decline rates of 0.009 mag day^{-1} for light curves powered by the radioactive decay of ^{56}Co (see, e.g., Gehrz 1988; Gehrz and Ney 1990). In the H and J bands, the observed decline rates are somewhat slower at 0.009 ± 0.004 mag day^{-1} and 0.007 ± 0.003 mag day^{-1}, respectively.

At discovery, the IR color is [3.6]−[4.5] = 0.676 ± 0.007 mag. This corresponds to an effective blackbody temperature of $T_{\rm eff} \approx 970$ K, possibly indicating that emission from warm dust is a significant contributor to the IR luminosity. At 184.7 days, SPIRITS 16tn is observed to have faded more rapidly at [3.6] than at [4.5], and evolves to a redder IR color of [3.6]−[4.5] $\gtrsim$ 1.0 mag ($T_{\rm eff} \lesssim 700$ K).

SED

From our photometry, we constructed quasi-contemporaneous SEDs of SPIRITS 16tn at two epochs. For the first, we adopt the time of the *HST*/WFC3 detections

at $t = 41.9$ days as the nominal phase. We use a linear (in magnitudes) interpolation of the [4.5] light curve, and for the K_s band we extrapolate the observed decline back from the detection at $t = 57.5$ days. We include the earlier *Swift*/UVOT nondetections as upper limits. As we only have one detection at [3.6] and cannot interpolate an observed decline rate, we consider this point as an upper limit under the assumption that the transient faded in this band between $t = 0$ and 41.9 days. For the second epoch, we adopt the time of the second [4.5] detection (and nondetection at [3.6]) at $t = 184.7$ days as the nominal phase, using extrapolations of J- and H-band decline rates and interpolating the K_s-band light curve. The photometric magnitudes were converted to band luminosities (λL_λ) at the assumed distance to the host and correcting only for Galactic reddening. To convert the $UBVI$ optical points, we adopt Vega flux zero-points and broadband effective wavelengths for the Bessell, Castelli, and Plez (1998) Johnson–Cousins–Glass system. We adopt 2MASS system values from Cohen, Wheaton, and Megeath (2003) for our JHK_s photometry. For *Spitzer* [3.6] and [4.5] points, we use the flux zero-points and effective wavelengths listed in the IRAC instrument handbook. We show the SED evolution of SPIRITS 16tn in Figure 3.6.

Estimating the extinction

The observed SED at $t = 41.9$ days is remarkably red. It is likely that SPIRITS 16tn suffers from a high degree of host extinction given its location along an obvious dust lane in a highly inclined, late-type host galaxy. The photometry of SPIRITS 16tn cannot directly constrain the extinction parameters without some assumptions about the intrinsic SED of the source. We attempt to estimate the extinction to SPIRITS 16tn by comparing the optical/near-IR SEDs to the SEDs of well-studied SNe.

Type II-Plateau SNe (SNe IIP) are the most common of all CCSN subtypes, and we use the IJH light curves of the SN IIP SN 2004et from Maguire et al. (2010) as a template for comparison. Following Maguire et al. (2010), we adopt an explosion date of UT 2004 September 22.0 (MJD = 53, 270.0), a distance of $D = 5.9$ Mpc, and a total (Galactic and host) extinction parameterized by $E(B - V) = 0.41$ mag for SN 2004et. The light curves of SN 2004et are well sampled during each of the canonical phases of SN IIP light-curve evolution: the $\approx$ 100-day photospheric plateau phase, the rapid fall-off of the plateau, and the subsequent radioactive decline phase. The absolute phase of SPIRITS 16tn is highly uncertain, as our most constraining pre-explosion upper limit is at 82 days before discovery. Using a linear

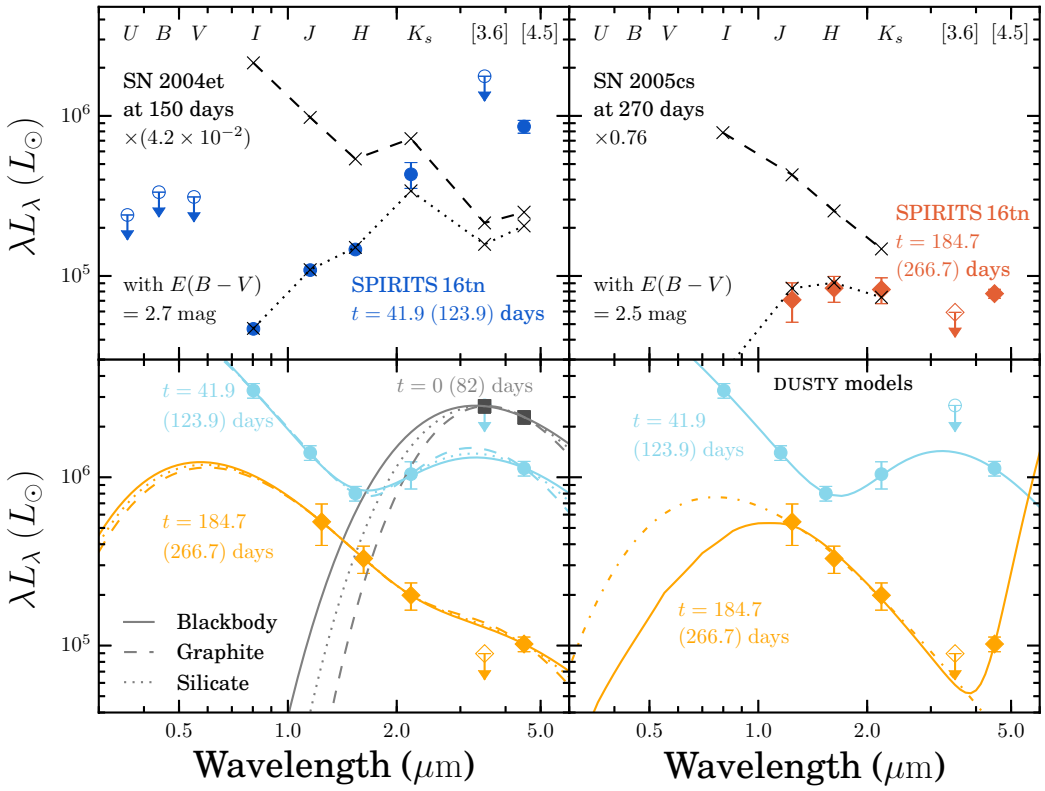

Figure 3.6: Top panels: SED evolution of SPIRITS 16tn, corrected only for Galactic extinction, constructed from the available broadband photometry at nominal phases of $t = 41.9$ days (maximum age of 123.9 days; dark-blue circles) and $t = 184.7$ days (maximum age of 266.7 days; dark-orange diamonds). Open symbols with downward-pointing arrows indicate points treated as upper limits. We compare the observed SED at $t = 41.9$ days to that of SN 2004et at a phase of 150 days as the black crosses and dashed curve, scaled down in luminosity by a factor of 4.2×10^{-2}. The black crosses and dotted curve show this SED reddened by $E(B-V) = 2.7$ mag. Similarly, we compare the observed SED of SPIRITS 16tn at $t = 187.4$ days to that of the low-luminosity SN 2005cs at a phase of 270 days scaled down by a factor of 0.76 (dashed black curve) and reddened by $E(B-V) = 2.5$ mag (dashed black curve). Bottom panels: SEDs of SPIRITS 16tn corrected for an assumed reddening of $E(B-V) = 2.5$ mag at the discovery epoch (gray squares), $t = 41.9$ days (light-blue circles), and $t = 184.7$ days (light-orange diamonds). In the bottom left panel, we show multicomponent fits to the SEDs using blackbodies (solid curves) and optically thin warm dust components with opacities appropriate for graphite (dashed curves) and silicates (dotted curves). In the bottom right panel, we show best fits to the SEDs from our dust radiative transfer modeling using DUSTY as the light-blue and light-orange solid curves. We also show an additional model for the photometry at $t = 184.7$ days as the dashed orange curve, treating the [4.5] flux as an upper limit, as it is likely enhanced by CO emission at this phase.

interpolation of the light curves, we find the host extinction parameter $E(B-V)$ that best reproduces the $I-J$ color of SN 2004et between 50 and 150 days in increments of 1 day. Even across this wide range of possible phases, the color evolution of SN 2004et is such that we find a range of 2.6 mag $< E(B-V) <$ 2.95 mag, with a mean value of $E(B-V) = 2.8$ mag.

In the top left panel of Figure 3.6, we show the observed SED of SPIRITS 16tn at $t = 41.9$ days (maximum age of 123.9 days) compared to the SED of SN 2004et at 150 days post explosion, just after the start of radioactive decline phase, but scaled down by a factor of 4.2×10^{-2}. Applying $E(B-V) = 2.7$ mag then provides a good match between the I-, J-, and H-band measurements to those of SPIRITS 16tn.

We performed a similar analysis using the light curves of SN 2005cs in nearby galaxy M51, a prototypical and well-observed low-luminosity SN IIP explosion (Pastorello et al. 2006; Pastorello et al. 2009). With a peak bolometric luminosity of $\approx 6 \times 10^{42}$ erg s^{-1}, SN 2005cs was ~ 10 times fainter than SN 2004et. We adopt a distance to SN 2005cs of 7.1 Mpc (Takáts and Vinkó 2006), a total foreground extinction (Milky Way and host) of $E(B-V) = 0.05$ mag (Baron, Branch, and Hauschildt 2007), and an explosion date of UT 2005 June 27.5 (MJD = 53,548.5) as in Pastorello et al. (2009). While the I-band light curve is well sampled throughout the plateau, fall-off, and decline tail, the available near-IR J- and H-band photometry is more limited. We compare the SED of SN 2005cs at a phase of 270 days to the late-time SED of SPIRITS 16tn at $t = 184.7$ days (maximum age of 266.7 days) in the top right panel of Figure 3.6. We find a suitable match with $E(B-V) = 2.5$ mag and scaling the SED of SN 2005cs by a factor of 0.76.

We find that assuming an SN II-like SED for SPIRITS 16tn indicates a high degree of foreground host extinction in the range of $E(B-V) \approx 2.5$–3.0 mag ($A_V \approx 7.8$–9.3 mag assuming $R_V = 3.1$), regardless of the absolute phase since explosion. This estimate is high compared to interstellar extinction for typical lines of sight in disk galaxies ($A_V \approx 1-2$ mag kpc^{-1}), but given high inclination of NGC 3556 and the coincidence of SPIRITS 16tn with a clear dust lane, it is not unreasonable. A direct comparison of the luminosity of SPIRITS 16tn is not possible in this analysis because of the large uncertainty in absolute phase. The inferred luminosity of SPIRITS 16tn at $t = 184.7$ days is comparable, however, to a late-phase, low-luminosity, SN 2005cs-like explosion, suggesting that SPIRITS 16tn is likely both heavily obscured and intrinsically faint.

Blackbody and dust component SED models

The bright IR emission associated with SPIRITS 16tn likely indicates the presence of warm dust. To model the dust emission, we assume an optically thin distribution of dust of total mass $M_{\rm d}$, composed of spherical grains of radius a, radiating thermally at a single, equilibrium temperature $T_{\rm d}$. This idealized model is described in more detail by, e.g., Hildebrand (1983), Dwek (1985), and Fox et al. (2010).

The expected flux from the warm dust is

$$F_\nu = M_{\rm d} \frac{\kappa_\nu(a) B_\nu(T_{\rm d})}{D^2}, \tag{3.1}$$

where $B_\nu(T_{\rm d})$ is the Planck blackbody function, D is the distance from the source, and $\kappa_\nu(a)$ is the dust mass absorption coefficient. In what follows, we assume a grain size of $a = 0.1$ μm and use broken power-law approximations to the dust mass absorption coefficients for dust composed entirely of either graphite or silicate (derived from Mie theory; see Figure 4 of Fox et al. 2010). To account for host extinction, we assume $E(B-V) = 2.5$ mag based on our comparison with SN 2005cs above[8].

We fit the IR photometric data for the *Spitzer* discovery epoch ($t = 0$ days) with this simple dust model for both graphite and silicate compositions to infer $T_{\rm d}$ and $M_{\rm d}$. Under the assumption of optically thin dust, the IR luminosity is not sensitive to the size of the dust cloud. In the optically thick case, however, the radius corresponding to blackbody emission provides a lower bound on the dust radius, $R_{\rm d}$. We repeat the procedure for the quasi-contemporaneous optical–IR SEDs at $t = 41.9$ and 187.4 days, including an additional, hotter blackbody component of temperature T_* and radius R_*. We note that for $E(B-V) = 2.5$ mag our optica/near-IR data do not cover the peak of the hotter SED component, and furthermore, the values inferred for T_* and R_* strongly depend on the choice of extinction. We do not attempt to make strong statements about the properties of the hotter component of the SED for these reasons, and focus our analysis on the properties of the dust component. The results are shown in the bottom left panel of Figure 3.6 and summarized in Table 3.3.

At $t = 0$ days, our best-fitting results to the IR SED give $T_{\rm dust} \approx 680$ K (880 K) and $M_{\rm dust} \approx 1.1 \times 10^{-4}$ $M_\odot$ (1.5×10^{-4} $M_\odot$) for graphite (silicate) dust. The blackbody

[8]Here we use a (Cardelli, Clayton, and Mathis 1989) extinction $R_V = 3.1$ to deredden the photometry to match our analysis using the dust radiative code DUSTY below in Section 3.3.

Table 3.3: Results of blackbody and dust component SED modeling

Phase[a] (days)	T_* (K)	$\log R_*/\mathrm{cm}$	T_d (K)	$\log R_\mathrm{d}/\mathrm{cm}$	M_d ($10^{-4}\ M_\odot$)	Dust Type
0.0	...	...	1100	15.6	...	blackbody
	...	...	680	...	1.1	graphite
	...	...	880	...	1.5	silicate
41.9	17,000	13.7	1100	15.4	...	blackbody
	14,000	13.7	730	...	0.4	graphite
	15,000	13.7	900	...	0.7	silicate
187.4	6400	13.9	960	14.9	...	blackbody
	6100	13.9	660	...	0.04	graphite
	6300	13.9	810	...	0.07	silicate

[a] Phase is number of days since the earliest detection of this event on 2016 August 15.0 (MJD = 57, 615.0).

fit to the data gives a higher temperature of $T_\mathrm{d} \approx 1100$ K and sets a lower bound on the dust radius of $R_\mathrm{d} \gtrsim 4.0 \times 10^{15}$ cm.

At $t = 41.9$ days, we find similar results for the dust temperature for each model, but we infer a somewhat lower mass of $M_\mathrm{dust} \approx 0.4 \times 10^{-4}\ M_\odot$ ($0.7 \times 10^{-4}\ M_\odot$) for graphite (silicate) dust and a smaller bound on the dust radius from the blackbody fit of $R_\mathrm{d} \gtrsim 2.5 \times 10^{15}$ cm. We note, however, that the uncertainties in interpolating the [4.5] and K_s-band light curves to construct the SED $t = 41.9$ days may have artificially lowered these values.

At $t = 187.4$ days, the data are no longer well fit by a hot source component and warm dust. The best-fitting results find $T_\mathrm{d} \approx$ 700–1000 K, but are notably inconsistent with the upper limit at [3.6]. The blackbody dust radius is smaller by a factor of 3–5 compared to the earlier epochs, and the inferred dust masses are lower by at least a factor of 10. As discussed below in the context of a CCSN the flux at [4.5] at this phase is likely enhanced by emission from the fundamental vibrational transition of CO and is not attributable solely to thermal emission from warm dust. The lack of evidence for a warm dust component at this phase may indicate that the dust has cooled, shifting the flux to longer wavelengths not probed by our data. Alternatively, as discussed below in Section 3.4, the early presence and subsequent disappearance of the warm dust component may be interpreted as a evidence for an IR echo, i.e., the reprocessing of the UV/optical emission from the luminosity peak of the transient into the thermal IR by a shell of preexisting circumstellar dust.

SED modeling with DUSTY

In addition to the simple dust models described above, we modeled the SED of SPIRITS 16tn using the dust radiative transfer code DUSTY (Ivezic and Elitzur 1997; Ivezic, Nenkova, and Elitzur 1999; Elitzur and Ivezić 2001). To find best-fitting models and allowed parameter ranges, we use a Markov chain Monte Carlo (MCMC) wrapper around DUSTY. Here we use a spherically symmetric distribution of graphite dust from Draine and Lee (1984) with a standard MRN grain size distribution ($dn/da \propto a^{-3.5}$, $0.005 < a < 0.25$ μm; Mathis, Rumpl, and Nordsieck 1977). For the central luminosity source, we assume a simple blackbody spectrum and allow the model to find best-fitting values for the source temperature T_* and luminosity L_*, the optical depth in V-band due to circumstellar dust τ_V, the dust temperature T_d, and the inner dust radius R_d. The source temperature and luminosity depend strongly on the assumed foreground extinction, but for simplicity, we again fix the extinction at $E(B-V) = 2.5$ mag as above. Our implementation of DUSTY uses a Cardelli, Clayton, and Mathis (1989) extinction law with $R_V = 3.1$, but the differences from the Fitzpatrick (1999) law assumed throughout the majority of this work are small at the wavelengths of interest in the optical and near-IR.

In this model, the dust is heated by the central source, i.e., the inferred properties of the dust are not independent of L_* and R_*. As T_d is constrained strongly by the shape of the IR SED, we do not expect it to vary strongly with the other model parameters. Furthermore, it is fairly robust to the choice of extinction, as the effects of reddening are small in the IR. We expect, however, R_d and τ_V to vary strongly with the central source properties, namely, a hotter, more luminous central source will force dust at a given temperature to larger radii and correspondingly lower optical depths. This model also does not account for light-travel time effects inherent to dust at large radii from an evolving, transient source.

The results of our DUSTY modeling at both epochs are given in Table 3.4, including both the values for each parameter for the best-fitting model, i.e., the model that minimizes χ^2, and the median value and 90% confidence interval limits from the MCMC posterior distributions. We note that the best-fitting values are sometimes near the extrema of the posterior distributions. The best-fitting SEDs are also shown in the bottom right panel of Figure 3.6 in comparison to the observations.

At $t = 41.9$ days, there is a clear IR excess requiring a warm dust component in addition to the interior, hotter source component. The MCMC results for this model have a dust temperature of $T_\mathrm{d} = 810^{+80}_{-90}$ K, consistent with the best-fitting value from

Table 3.4: Results of SED modeling with DUSTY[a]

Phase[b] (days)	$\log L_*/L_\odot$		T_* (K)		τ_V		T_d (K)		$\log R_d$/cm	
41.9	7.4	$7.1^{+0.3}_{-0.2}$	15200	10900^{+4500}_{-2700}	0.06	$0.2^{+0.2}_{-0.1}$	840	810^{+80}_{-90}	16.8	$16.7^{+0.2}_{-0.2}$
187.4	8.6	$6.2^{+2.0}_{-0.5}$	40200	5800^{+24100}_{-2600}	4.9	$0.9^{+4.5}_{-0.8}$	190	370^{+400}_{-170}	19.1	$16.9^{+1.8}_{-1.1}$
187.4[c]	6.0	$6.4^{+1.6}_{-0.7}$	48100	7600^{+23800}_{-4100}	...	...	...	...	...	...

[a] For each parameter, we give the value for the best-fitting model that minimizes χ^2, and the median value from the MCMC with the 90% confidence interval limits.
[b] Phase is number of days since the earliest detection of this event on 2016 August 15.0 (MJD = 57, 615.0).
[c] Results for t = 187.4 days when [4.5] flux treated as an upper limit including only a single blackbody component.

our simple, optically thin graphite dust model at this epoch in Section 3.3, and an inner dust radius of $R_d = 5.0^{+2.9}_{-1.9} \times 10^{16}$ cm at 90% confidence. As expected, T_d is well constrained by the K_s-band and [4.5] fluxes and does not vary strongly with the other parameters of the model. While producing a significant IR excess, the dust is optically thin at $\tau_V = 0.2^{+0.2}_{-0.1}$. Because our photometry does not cover the peak of the hot blackbody component, our measurements can only place a lower limit on the temperature and luminosity of the source, and the upper confidence limits found by the MCMC are not physically meaningful. We infer $T_* \gtrsim 8200$ K and $L_* \gtrsim 7.9 \times 10^6\ L_\odot$, but note that these limits are highly dependent on our choice of foreground host extinction, i.e., for $E(B-V)_{\rm host} < 2.5$ mag, a lower blackbody temperature and luminosity would be consistent with the data.

At t = 187.4 days, the hot component has faded by a factor of ≈ 2.7 in the J and H bands. Again, our photometric measurements do not cover the peak of this component, and thus the results of the MCMC modeling only allow us to estimate a lower limit on the source temperature of $T_* > 3200$ K. The flux in the redder bands, however, has faded more quickly. The DUSTY model fits a dust component to the excess flux at [4.5] with constraints from the MCMC at $T_d = 370^{+400}_{-170}$ K, but there is a strong degeneracy between the cooler dust temperatures at smaller radii ($\approx 6 \times 10^{15}$ cm) and warmer dust at large radii ($\approx 5 \times 10^{19}$ cm). Again, it is likely that the flux at [4.5] is enhanced by emission from the fundamental vibrational mode of CO, and therefore it is probably not attributable to thermal emission from dust. Treating the measurement at [4.5] instead as an upper limit, we find that the SED of SPIRITS 16tn at t = 187.4 days can be adequately modeled with a single blackbody component with $T_* > 4500$ K and $L_* > 5.0 \times 10^5\ L_\odot$.

The optical and near-IR spectra

At $t = 79$ days after first detection, the optical spectrum of SPIRITS 16tn is characterized by a faint, red continuum. There are no clearly discernible features. The apparent dip in the spectrum near 9300 Å is coincident with a strong telluric absorption band and is probably not intrinsic to the source.

The near-IR spectra of SPIRITS 16tn are shown in Figure 3.4. Though the Gemini N/GNIRS spectra covered the entire near-IR spectral range from 8500 to 25000 Å, we detect emission from SPIRITS 16tn only in the H and K regions of the spectrum. Due to uncertainty in the age of SPIRITS 16tn at discovery, the phase of SPIRITS 16tn is only constrained to be between 136 and 229 days since explosion at the time the spectra were taken.

As in the optical spectrum, we detect a red continuum associated with SPIRITS 16tn, but there are no unambiguous features in the near-IR. Though the spectra appear to peak near the centers of the H and K spectral windows, we suspect that this may be an artifact of low S/N and poor flux calibration, particularly near the edges of the bands, where little flux is received through the atmosphere. As expected given the high degree of reddening inferred from the SED, we detect the strongest continuum emission in the K spectral region, with an overall decrease in flux toward the blue.

3.4 Discussion

Here we compare the observed properties of SPIRITS 16tn to those of various SNe subtypes to inform our interpretation of the observations.

Comparison to SNe Ia

The deep radio nondetections of SPIRITS 16tn (Section 3.2) may be easily explained if it is an SN of Type Ia. No SN Ia has been detected as a radio source to deep limits in radio luminosity as far down as $L_\nu \lesssim 10^{24}$ erg s^{-1} Hz^{-1} for the nearest events (e.g. Panagia et al. 2006; Chomiuk et al. 2016). To test the hypothesis that SPIRITS 16tn is an SN Ia, we compare its IR color evolution and near-IR spectrum to well-studied events.

In the top right panel of Figure 3.7, we show the [4.5] light curve of SPIRITS 16tn compared to several SNe Ia from Johansson et al. (2017), who found that SNe Ia form a homogeneous class of objects at these wavelengths. The phases of the SPIRITS 16tn observations are shown as days since maximum, with $t = 0$ assumed to be at the time of the *Spitzer* discovery observations and where the uncertainty in

the time of maximum light is indicated by the horizontal error bars. SPIRITS 16tn shows a similar decline in luminosity at [4.5] to the sample of SNe Ia, but the [3.6]−[4.5] color evolution, shown in the bottom right panel of Figure 3.7, is notably inconsistent. At discovery, SPIRITS 16tn had a very red [3.6]−[4.5] color of 0.7 mag and evolved to an even redder color of [3.6]−[4.5] $>$ 1.0 mag over a period of 185 days. In contrast, SNe Ia, which may be somewhat red at early times, evolve quickly to the blue, reaching [3.6]−[4.5] ≈ -1 mag at a phase of $\approx$ 150 days. SNe Ia may evolve again to redder colors at very late times, but the observed color of SPIRITS 16tn is too extreme for SNe Ia across the entire range of phases relevant here.

Redder [3.6]−[4.5] colors have been observed during the first 400 days in some thermonuclear SNe, e.g., the interaction-powered SN Ia-CSM SN 2005gj (Fox and Filippenko 2013) and the unusual, dusty SN Iax SN 2014dt (Fox et al. 2016). We show these SNe as the the gray symbols in the top right panel of Figure 3.7. Both events have an observed late-time, IR flux excess at [4.5] over a normal SN Ia light curve extending past 200 days, indicative of emission from warm dust. In the context of SN Ia light curves, SPIRITS 16tn does not show such a late-time excess despite its red color.

We have not considered the effects of extinction from the host galaxy or local environment of the SN, e.g., from circumstellar dust. To produce a color excess of 0.7 mag between [3.6] and [4.5] would require an additional $A_V \gtrsim 40$ mag of extinction, using the empirically derived broadband extinction parameters for [3.6] and [4.5] from Chapman et al. (2009), much higher than the inferred extinction to SPIRITS 16tn from the SED of $A_V \approx 8$ mag.

Furthermore, the featureless spectrum of SPIRITS 16tn is wholly inconsistent with normal SNe Ia at comparable phases. In Figure 3.8, we show the 1.48 − 1.9 μm region ($\approx H$ band) of the spectrum of SPIRITS 16tn, along with the late-time spectra of SN Ia SN 2014J at a phase of 128 days (post B-band maximum) from Johansson et al. (2017) and the SN Ia SN 2005df at 198, 217, and 380 days (Diamond, Hoeflich, and Gerardy 2015). The phase of our near-IR spectrum is constrained to be between 136 and 229 days. The late-time spectra of SNe Ia are dominated by blended, nebular emission features, primarily forbidden transitions of Fe-peak elements (Bowers et al. 1997; Spyromilio et al. 2004). In the H-band region, Diamond, Hoeflich, and Gerardy (2015) specifically identified transitions of [Fe II], [Co II], and [Co III] in the spectra the SN Ia SN 2005df, as labeled in Figure 3.8. They noted that

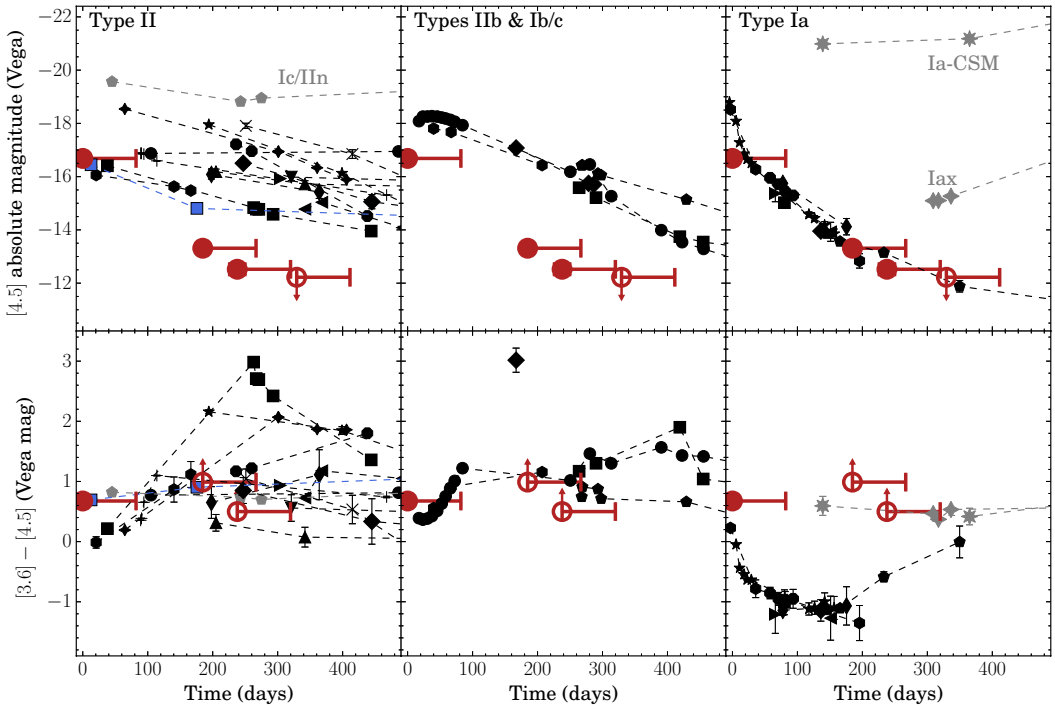

Figure 3.7: [4.5] light curves (top row) and [3.6]−[4.5] color evolution (bottom) for SPIRITS 16tn (red circles) compared to SNe II (left column), stripped-envelope SNe IIb and Ib/c (middle column), and thermonuclear SNe Ia (right column) shown in black. Lower limits in color are indicated by open circles and upward-pointing arrows. Time is given on the x-axes as days since discovery for the core-collapse events and days since B-band maximum for SNe Ia. The uncertainty in the phase for SPIRITS 16tn is indicated by the red horizontal error bars. The sample of SNe IIP shown in the right column include the *Spitzer*/IRAC measurements for SN 2004A (thick diamonds), SN 2005ad (thin diamonds), SN 2005af (stars), SN 2006my (upward-pointing triangles), SN 2006ov (downward-pointing triangles), and SN 2007oc (crosses) from Szalai and Vinkó (2013) and references therein; SN 2011ja (circles), SN 2013am (leftward-pointing triangles), SN 2013bu (rightward-pointing triangles), SN 2013ej (octagons), and SN 2014bi (squares) from Tinyanont et al. (2016) and references therein; SN 2004dj (plus signs; Kotak et al. 2005; Meikle et al. 2011; Szalai et al. 2011); SN 2004et (four-point stars; Kotak et al. 2009); and SPIRITS 14buu (hexagons; Jencson et al. 2017e). Also shown is the interaction-powered SN Ib/IIn SN 2014C (Tinyanont et al. 2016, and references therein) as the gray pentagons and the luminous infrared transient SN 2008S (Adams et al. 2016) as the blue squares. The stripped-envelope SNe shown in the middle column include SN 2011dh (circles; Type IIb), SN 2013df (squares; Type IIb), SN 2013dk (pentagons; Type Ic), and SN 2014L (hexagons, Type Ic) from Tinyanont et al. (2016) and references therein, as well as the more recent event SPIRITS 15c (diamonds; Type Ib or IIb, Jencson et al. 2017e). Measurements for SNe Ia from Johansson et al. (2017) and references therein are shown in the right column for SN 2005df (thin diamonds), SN 2006X (thick diamonds), SN 2007af (leftward-pointing triangles), SN 2007le (rightward-pointing triangles), SN 2007sr (squares), SN 2009ig (hexagons), SN 2011fe (pentagons), SN 2012cg (octagons), and SN 2014J (stars). We also show the unusual SN Iax SN 2014dt (Fox et al. 2016, and references therein) and the interaction powered SN Ia-CSM SN 2005gj (Fox and Filippenko 2013) as gray four- and eight-pointed stars, respectively. Color measurements for each object are corrected only for Galactic extinction to their respective hosts from NED. Error bars are sometimes smaller than the plotting symbols.

the spectrum became Fe dominated as the Co features faded between ≈ 200 and 380 days; however the strong, broad emission lines of [Fe II] persisted to very late phases. These features are completely absent from the near-IR spectrum of SPIRITS 16tn, and thus we definitively rule out a reddened SN Ia in this case.

Comparison to CCSNe

We compare the light curve at [4.5] of SPIRITS 16tn to CCSNe of Type II and stripped-envelope Types IIb and Ib/c the top left and middle panels of Figure 3.7. Among the hydrogen-rich SNe II, we do not distinguish between the photometric subtypes IIP and IIL, defined by the presence of a light-curve plateau or linear decline, respectively. Our dataset for SPIRITS 16tn is insufficient to make such a distinction. Furthermore, the existence of the two truly distinct subclasses is debated, and recent studies of large SN II samples have suggested that SNe IIP and SN IIL may instead form a continuous distribution in their observed properties (e.g., Anderson et al. 2014; Sanders et al. 2015; Rubin and Gal-Yam 2016).

The observed [4.5] luminosity peak of SPIRITS 16tn at −16.7 mag is in the range of SNe II, but is $\gtrsim$ 1 mag fainter than is observed for the sample of stripped-envelope events. Notably, SPIRITS 16tn fades more rapidly at [4.5] at 0.017 mag day^{-1} than any of the CCSNe for which comparable data were available. The fastest event in the comparison sample is the SN II SN 2013ej (black octagons in the top left panel of Figure 3.7) fading at a rate of 0.013 mag day^{-1}. Although the sample of stripped-envelope SNe is small, they appear relatively more homogeneous at [4.5] compared to SNe II, with typical decline rates between 0.009 and 0.012 mag day^{-1}. Given the larger degree of variation in both peak luminosity at [4.5] and the observed decline rate for SNe II, it is easier to reconcile the lower [4.5] peak and faster decline of SPIRITS 16tn with the sample of SNe II.

As shown in the bottom panels of Figure 3.7, SPIRITS 16tn develops a very red color by t = 184.7 days of [3.6]−[4.5] > 1.0 mag. Similarly red colors have been observed at comparable phases for several CCSNe, including the SNe IIP events SN 2005af (Szalai and Vinkó 2013, and references therein), SN 2004et (Kotak et al. 2009), and SN 2014bi (Tinyanont et al. 2016), and for the SN IIb/Ib event SPIRITS 15c (Jencson et al. 2017e). While a red mid-IR color may be a signature of thermal emission from warm dust ($T_{\rm eff} \lesssim$ 700 K for [3.6]−[4.5] > 1.0 mag), emission from the 1–0 vibrational transition of CO at ≈ 4.65 μm can produce excess flux at [4.5] compared to the other mid-IR bands. This emission feature has been directly

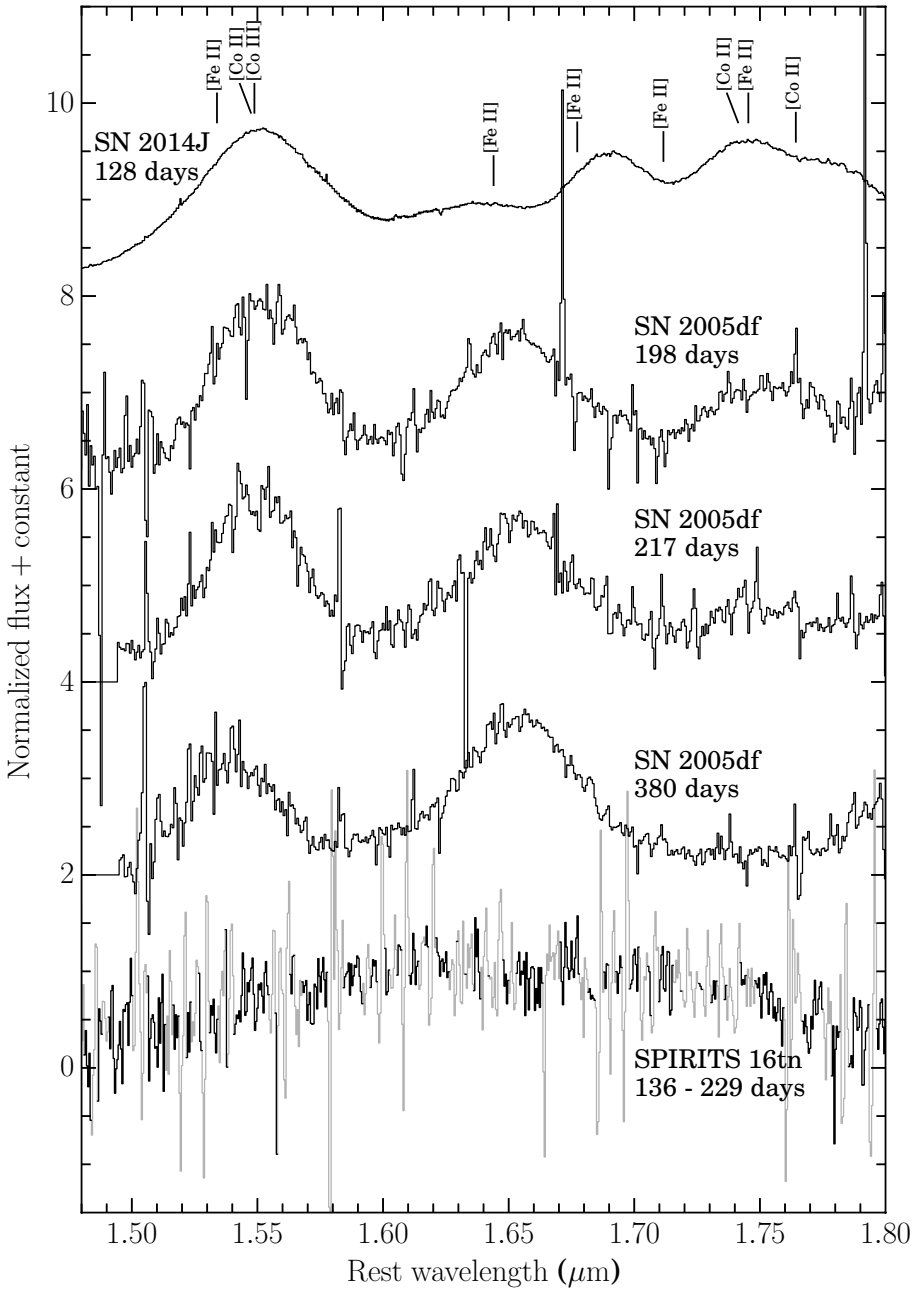

Figure 3.8: *H*-band spectrum of SPIRITS 16tn, at a phase between 136 and 229 days, compared to late-time, nebular spectra of SNe Ia SN 2014J (Johansson et al. 2017) and SN 2005df (Diamond, Hoeflich, and Gerardy 2015). The SPIRITS 16tn spectrum is the average of the two Gemini N/GNIRS spectra taken on 2016 December 29 and 2017 January 9. Spectral bins of lower S/N due to coincidence with an OH emission line of the night sky are shown in light gray. The spectra have been normalized by the flux at 1.644 μm, and each spectrum is shifted up from the one below for clarity. Forbidden transitions of Fe-peak elements identified in Diamond, Hoeflich, and Gerardy (2015) are indicated above the spectrum of SN 2014J. These broad, blended features are not present in SPIRITS 16tn.

identified in the mid-IR spectra of several SNe II including SN 1987A (e.g., Meikle et al. 1989; Wooden et al. 1993), SN 2004dj (Kotak et al. 2005), and SN 2005af (Kotak et al. 2006). Corroborating the identification of this feature, the band heads of the $\Delta v = 2$ vibrational overtones of CO, which produce excess emission beyond 2.3 μm at the end of the K band, have also been observed in, e.g., SN 1987A (Meikle et al. 1989), SN 2004dj (Kotak et al. 2005), and the stripped-envelope events SN 2011dh (Ergon et al. 2015) and SPIRITS 15c (Jencson et al. 2017e). We do not clearly detect this feature in our near-IR spectra from $t = 136$ to 145 days, but note that the $\Delta v = 2$ vibrational overtones may be significantly weaker than the fundamental band at [4.5] and hidden in our low-S/N spectra. Furthermore, the spectra were obtained at an earlier epoch, possibly before CO formed in the ejecta. In the context of CCSNe, we consider CO emission to be the most likely explanation for the observed mid-IR color evolution of SPIRITS 16tn, indicating the presence of CO in the ejecta by $t \approx 185$ days.

In Figure 3.2, we compare the multiband light curves of SPIRITS 16tn to those of the low-luminosity SN IIP SN 2005cs. The light curves of SN 2005cs are shifted to the distance of SPIRITS 16tn and reddened with $E(B-V) = 2.5$ mag, as inferred from our SED comparison in Section 3.3. For the relative phase offset shown, and with an additional offset in apparent magnitude of $\Delta m = 0.7$ mag (factor of ≈ 2 in flux), the late-time $IJHK_s$ light curves can be reasonably well matched to those of SPIRITS 16tn. In this scenario, our HST observations of SPIRITS 16tn at $t = 41.9$ days would have occurred just after the transition to the nebular phase and require a plateau duration $\lesssim 123.9$ days to be consistent with our z-band preexplosion nondetection. Given our lack of early-time data for SPIRITS 16tn and the notable gap in near-IR photometric coverage of SN 2005cs during the transition to the nebular phase, we cannot perform a more detailed light-curve comparison. Still, we find the optical–near-IR light curve evolution of SPIRITS 16tn to be largely consistent with an SN 2005cs-like, low-luminosity SN IIP event.

In Figure 3.9, we compare near-IR spectrum of SPIRITS 16tn at a phase between 136 and 229 days post maximum to those of CCSNe of various types, including the Type Ic broad-lined (Ic-BL) SN 1998bw (Patat et al. 2001), the Type IIn SN 2010jl (Borish et al. 2015), the Type IIb SN 2011dh (Ergon et al. 2015), and the Type II SN 2013ej (Yuan et al. 2016). Some of the most prominent features identified in late-phase CCSNe in the H and K bands are labeled in Figure 3.9, including Mg I at 1.504 μm, blended [Fe II] at 1.644 μm and [Si I] at 1.646 μm, He I at 2.058 μm,

Brγ at 2.166 μm, and the band heads of the $\Delta v = 2$ vibrational overtones of CO beyond 2.3 μm. Paα, a typically strong H I feature in SNe II, is unfortunately in the low atmospheric transmission region between the H and K spectral windows where we did not receive any detectable flux from SPIRITS 16tn.

As we do not detect any clear features in SPIRITS 16tn, we are unable to provide a definitive classification. However, the lack of a clear spectroscopic signature of the interaction of the SN ejecta with a dense CSM, often observed as superimposed narrow ($\sim$ few $\times$ 100 km s^{-1}) and broad ($\sim$ few $\times$ 1000 km s^{-1}) components of the H I and He I features, can rule out a strongly interacting SN IIn. We suggest that at late times it is possible that the near-IR spectral features of non-interacting CCSNe may be very weak.

Radio limits

In Figure 3.10, we show our limits on the radio luminosity of SPIRITS 16tn as a function of phase compared to the peak radio luminosities and times to peak for CCSNe. Radio emission is produced in CCSNe when the fastest SN ejecta interact with and shock the slow-moving pre-explosion CSM from the pre-explosion stellar wind of the progenitor. As the shock wave propagates through the CSM, turbulent instabilities amplify magnetic fields and accelerate relativistic electrons (Chevalier 1982). The resultant radio emission is characterized by slowly declining, optically thin, nonthermal synchrotron and early, optically thick absorption at low frequencies. Proposed absorption mechanisms include synchrotron self-absorption (SSA) or internal free-free absorption in the emitting region and free-free absorption by the external, ionized CSM (e.g., Chevalier 1982, 1998).

If one assumes that SSA is dominant, for an electron population with an energy spectral index of $p = 3$, the size of the radio-emitting region at the time of the SSA peak can be calculated as (Chevalier 1998)

$$\begin{aligned} R_{\rm s} =& 4.0 \times 10^{14} \alpha^{-1/19} \left(\frac{f}{0.5}\right)^{-1/19} \left(\frac{F_{\rm p}}{\rm mJy}\right)^{9/19} \\ & \times \left(\frac{D}{\rm Mpc}\right)^{18/19} \left(\frac{\nu}{5\ {\rm GHz}}\right)^{-1} {\rm cm}, \end{aligned} \tag{3.2}$$

where $\alpha \equiv \epsilon_e/\epsilon_B$ is the ratio of the energy density in relativistic electrons to that in the magnetic field, f is the fraction of the spherical volume filled by the radio-

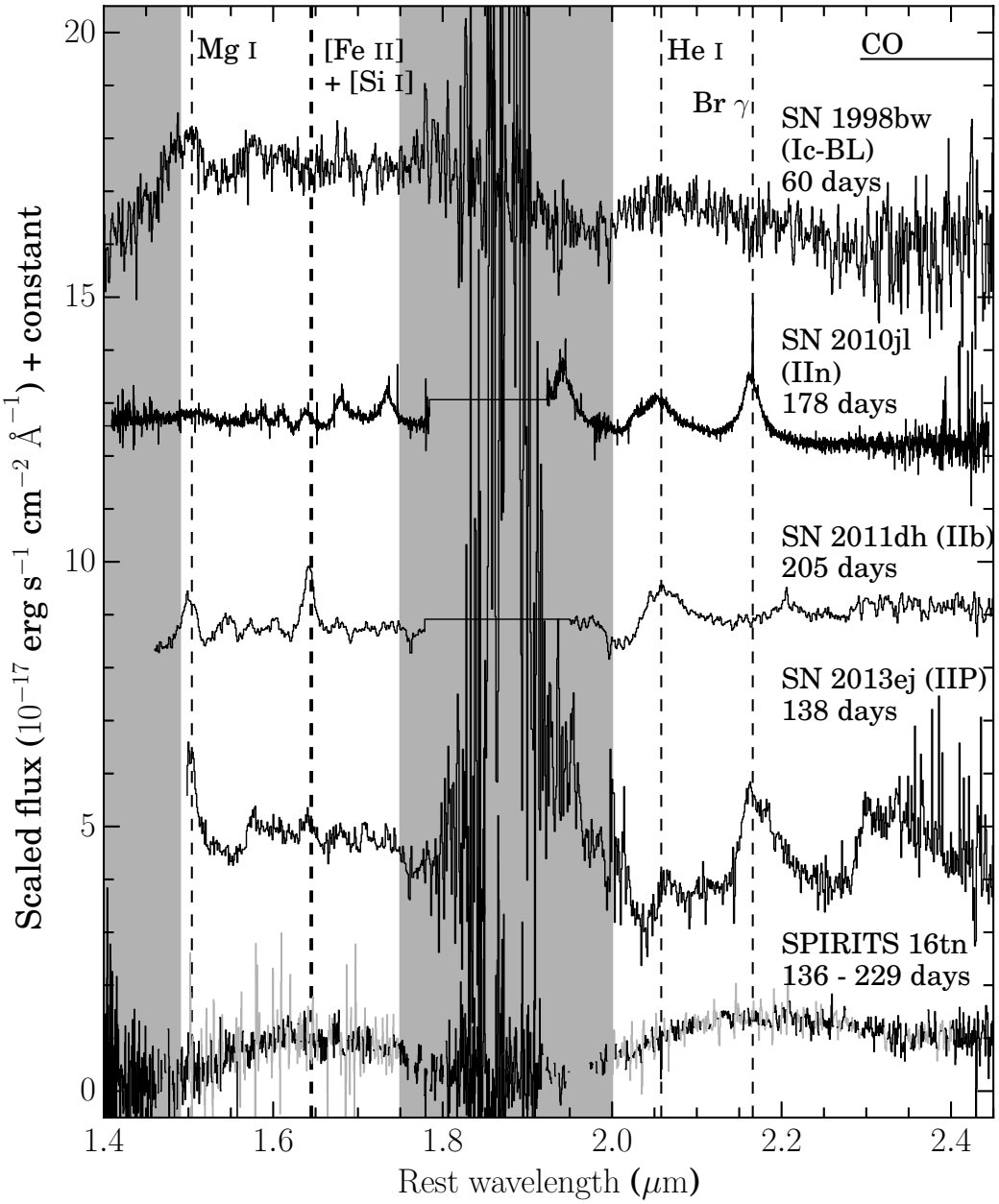

Figure 3.9: We show the H- and K-band spectra of SPIRITS 16tn at a phase between 136 and 229 days, along with the late-phase spectra of CCSNe of various types for comparison. The CCSNe spectra are scaled in flux to the distance of SPIRITS 16tn and reddened by $E(B-V) = 2.5$ mag. Each one is shifted up from the one below by an arbitrary constant for clarity. Prominent features present in the spectra of some CCSNe are indicated by the dashed vertical lines and labeled near the top of the figure.

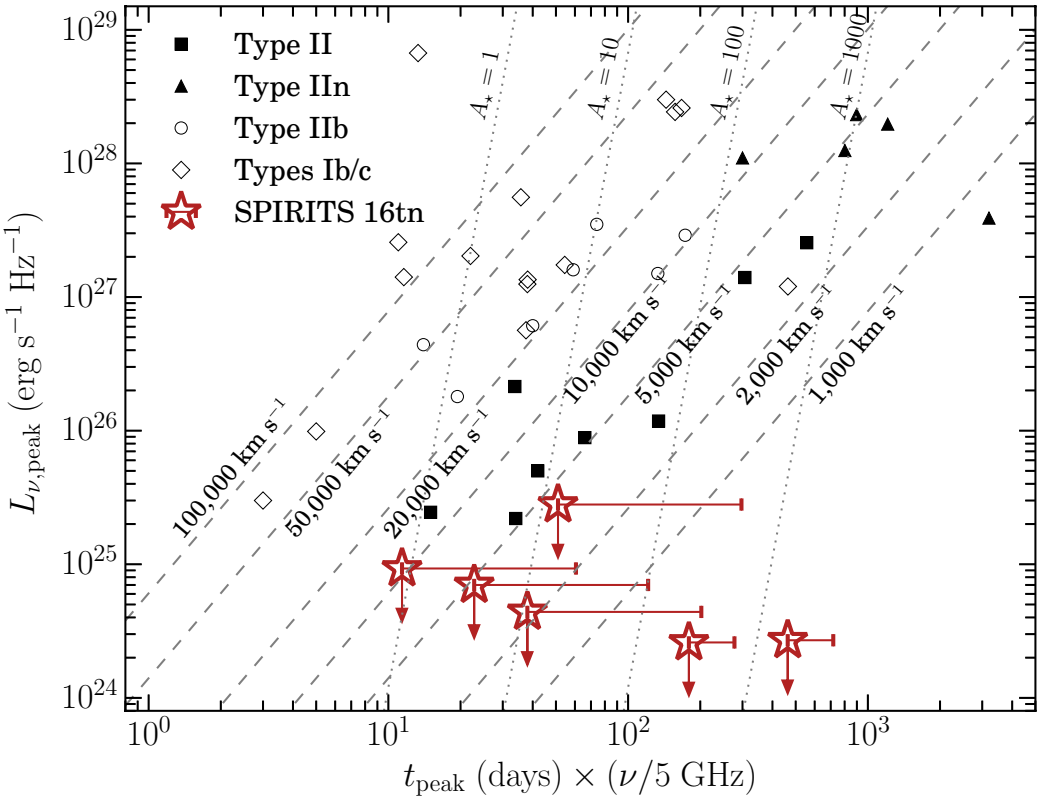

Figure 3.10: Peak radio luminosity vs. time of peak times the frequency of observation for radio CCSNe adapted from (e.g. Chevalier, Fransson, and Nymark 2006; Romero-Cañizales et al. 2014). Type IIs are shown as black squares, and interaction-powered SNe IIn are shown as black triangles. Unfilled circles and diamonds represent stripped-envelope SNe IIb and Ib/c, respectively. Upper limits on the radio luminosity of SPIRITS 16tn at a given phase from our nondetections are shown as red, unfilled stars with downward arrows, where the horizontal errorbars represent our uncertainty in the absolute phase since explosion. Assuming a SSA model with an electron distribution with $p = 3$ for the shockwave propagating through the CSM, one can infer the shock velocity (dashed lines) and CSM density parameter ($A_\star$; dotted lines) from the position on this diagram.

emitting region, F_p is the peak flux at frequency ν, and D is the distance to the source. If additional absorption mechanisms are important, this radius must be even larger. The shock wave velocities, v_s, inferred for $\alpha = 1$ (assuming equipartition) and $f = 0.5$ (as estimated in Chevalier and Fransson 2006) are shown as the dashed lines in Figure 3.10. We the note weak dependence in Eq. 3.2 of the shock radius on these parameters.

For a steady, pre-SN stellar wind, the density profile of the CSM as a function of radius, r, is $\rho_w = A/r^2 \equiv \dot{M}/(4\pi r^2 v_w)$, where $\dot{M}$ is the mass-loss rate and v_w is the wind velocity. $A \equiv \dot{M}/(4\pi v_w)$ is the normalization of the CSM density profile as in Chevalier (1982). As calculated by Chevalier and Fransson (2006), the radio emission at time t since explosion of a CCSN is sensitive to the density profile of the CSM as

$$\begin{aligned} A_\star \epsilon_{B-1} \alpha^{8/19} = 1.0 \left(\frac{f}{0.5}\right)^{-8/19} \left(\frac{F_p}{\mathrm{mJy}}\right)^{-4/19} \\ \times \left(\frac{D}{\mathrm{Mpc}}\right)^{-8/19} \left(\frac{\nu}{5\ \mathrm{GHz}}\right)^{2} \left(\frac{t}{10\ \mathrm{days}}\right)^{2}, \end{aligned} \tag{3.3}$$

where $\epsilon_{B-1} \equiv \epsilon_B/0.1$ and $A_\star \equiv A/(5 \times 10^{11}\ \mathrm{g\ cm^{-1}})$ is a dimensionless proxy for A. We show lines of constant $A_\star$ in Figure 3.10, determined largely by the strong dependence of this parameter on t_{peak}.

Our deep nondetections of SPIRITS 16tn indicate either that this event is either an intrinsically weak radio source or that the emission is heavily absorbed. Though we do not rule out radio emission arising at very late times, characteristic of strongly interacting SNe IIn with a dense CSM, this scenario is unlikely given the lack of prominent interaction features in the optical/near-IR spectra. Our observations are inconsistent with most varieties of stripped-envelope events, which tend to be more luminous radio sources. A high-velocity ($v_s \gtrsim 50,000$ km s^{-1}) SN Ic with a fast-evolving radio light curve, however, is not explicitly ruled out (cf. SN 2007gr, Soderberg et al. 2010, and PTF12gzk, Horesh et al. 2013b). Our optical–IR SED analysis and comparisons with well-studied SNe II indicate that SPIRITS 16tn falls at the low end of the SN luminosity function, and a weak SN II radio counterpart is consistent with our observations. Using Eq. 3.3, for typical SN II shock velocities of $v_s \approx$ few $\times\ 10^3$ km s^{-1}, our nondetections can constrain $A_\star \epsilon_{B-1} \alpha^{8/19} \lesssim 24$. For a steady pre-SN wind, we then infer a limit on the pre-SN mass-loss rate of $\dot{M} \lesssim 2.4 \times 10^{-6} \left(\frac{\epsilon_B}{0.1}\right)^{-1} \alpha^{-8/19} \left(\frac{v_w}{10\ \mathrm{km\ s^{-1}}}\right) M_\odot\ \mathrm{yr}^{-1}$.

Such a mass-loss rate is consistent with a low-luminosity RSG ($L \approx 10^{4.5} - 10^{5} L_{\odot}$) based on the standard observational prescriptions of de Jager, Nieuwenhuijzen, and van der Hucht (1988) (see, e.g., Smith 2014). This supports the picture of SPIRITS 16tn as a low-luminosity SN II arising from the explosion of a low-mass ($M \approx 10 - 15 M_{\odot}$) RSG progenitor. We note that, depending on the assumed explosion date of SPIRITS 16tn, for $v_{\rm s} = 10,000$ km s^{-1} and $v_{\rm w} = 10$ km s^{-1}, the timing of our radio observations probes the mass-loss history of the progenitor only in the final $\approx 50 - 600$ yr before the explosion.

Concurrent panchromatic observations spanning the radio to the X-ray have indicated deviations from energy equipartition in some SNe. For example, for SN 2011dh Soderberg et al. (2012) find $\alpha = 30$ and $\epsilon_B = 0.01$. Adopting such values results in only a modest decrease in the shock velocity (using Eq. 3.2) by a factor of 1.2 and an increase in our limit on the mass-loss rate by a factor of 2.4. Alternatively for SN 2011dh, Horesh et al. (2013a) find $\alpha \approx 500$–1700, adopting a value of 1000 as a reasonable average, and $\epsilon_{\rm B} = 3 \times 10^{-4}$. This still results in only a modest decrease in the inferred shock velocity by a factor of 1.4, and for a fixed wind velocity, the limit on the mass-loss rate increases by a factor of 20.

Origin of the observed dust component

In Section 3.3, our modeling of the SED of SPIRITS 16tn at $t = 0$ and 41.9 days suggests the presence of an IR component ($T_{\rm d} \approx 700$–900 K) powered by thermal emission by at least $M_{\rm d} \approx (1.0$–$1.5) \times 10^{-4}\ M_{\odot}$ of warm dust (our observations are not sensitive to any additional dust at cooler temperatures). By $t = 187.4$ days, we no longer see evidence for this warm dust component, indicating that either it has faded or the dust has cooled, shifting the flux to longer wavelengths.

The dust emission may arise from either preexisting circumstellar dust formed in the pre-SN wind of the progenitor or newly formed dust in the dense, rapidly cooling ejecta behind the SN shock. For a shock velocity of $v_s = 10,000$ km s^{-1}, the radius of the shock at a phase of 82.0 days (the maximum age of SPIRITS 16tn at $t = 0$ days) is $R_s = 7.1 \times 10^{15} \left(\frac{v_s}{10^4 \text{ km s}^{-1}}\right)$ cm. As we infer a lower limit on the dust radius (blackbody radius from Section 3.3) of $R_{\rm d} \gtrsim 4.0 \times 10^{15}$ cm that is smaller than the shock radius, it is plausible that the emitting dust is located in the post-shock cooling zone. Given the low observed dust temperatures, however, it is unlikely that the early dust component is due to newly formed dust in the ejecta. We would expect newly formed dust to be near the evaporation temperature, as, given

sufficiently high densities, dust grains will begin to condense as soon as the drop in temperature of the radiation environment allows. Typical values for astrophysical dust are $T_{\rm evap} \approx 1900$ K for graphite and $T_{\rm evap} \approx 1500$ K for silicate, significantly hotter than the observed dust component.

For preexisting dust, we can interpret the observed IR-excess as an IR echo. In this scenario, a preexisting shell of dust is heated by the peak luminosity of the explosion and reradiates this energy thermally in the IR. The duration of the echo is related to the size of the dust shell from geometrical arguments as $\Delta t \sim 2R_{\rm d}/c$. The observations of the warm dust component between $t = 0$ and 41.9 days, and subsequent fading by $t = 187.4$ days, when the maximum age of SPIRITS 16tn is 269.4 days, would then require 5.4×10^{16} cm $\lesssim R_{\rm d} \lesssim 3.5 \times 10^{17}$ cm.

As a consistency check, we can estimate the peak luminosity, $L_{\rm peak}$, of the transient required to heat spherical dust grains of radius a within this range of distances to the observed temperatures. The energy absorbed by a dust grain is balanced by the energy it radiates as

$$\frac{L_{\rm peak}}{4\pi R_{\rm d}^2}\pi a^2 Q_{\rm abs} = 4\pi a^2 \sigma_{\rm SB} T_{\rm d}^4 Q_{\rm em}. \tag{3.4}$$

The peak luminosity of the transient is then given by

$$L_{\rm peak} = 16\pi R_{\rm d}^2 \sigma_{\rm SB} T_{\rm d}^4 \frac{Q_{\rm em}}{Q_{\rm abs}}, \tag{3.5}$$

where $Q_{\rm em}$ and $Q_{\rm abs}$ are Planck-averaged emission and absorption efficiencies for Laor and Draine (1993) dust grains. For the temperature of the incident radiation field we assume values $T_{\rm rad} = 10,000$ K and $T_{\rm rad} = 6000$ K, characteristic of an SN at peak. We use a value of $\sigma_{\rm SB} = 5.67 \times 10^{-5}$ erg cm^{-2} K^{-4} s^{-1} for the Stefan–Boltzmann constant. For graphite grains of size $a = 0.1$ μm at $T_{\rm d} = 680$ K, we find 4.7×10^{40} erg s^{-1} $\lesssim L_{\rm peak} \lesssim 1.9 \times 10^{42}$ erg s^{-1} for $T_{\rm rad} = 10000$ K and similar values of 5.7×10^{40} erg s^{-1} $\lesssim L_{\rm peak} \lesssim 2.3 \times 10^{42}$ erg s^{-1} for $T_{\rm rad} = 6000$ K. Alternatively, for grains of silicate composition at $T_{\rm d} = 880$ K, we find a somewhat higher values of 9.9×10^{41} erg s^{-1} $\lesssim L_{\rm peak} \lesssim 4.0 \times 10^{43}$ erg s^{-1} for $T_{\rm rad} = 10,000$ K, or 2.6×10^{41} erg s^{-1} $\lesssim L_{\rm peak} \lesssim 1.0 \times 10^{43}$ erg s^{-1} for $T_{\rm rad} = 6000$ K.

While these estimates are crude, we can still compare them to the observed range of peak luminosities for SNe II. Faran, Nakar, and Poznanski (2018), for example,

estimate the bolometric luminosities of 29 SNe II and find peak values spanning at least two orders of magnitude and ranging from $L_{\rm bol} \approx 2.4 \times 10^{41}$ erg s^{-1} to 2.4×10^{43} erg s^{-1}. Similarly, the pseudo-bolometric (from $\sim U$ to I band) light curves of the sample of SNe II from Valenti et al. (2016) span $L_{\rm bol} \approx 1.0{\times}10^{41}$ erg s^{-1} to 5×10^{42} erg s^{-1}. Among the faintest SNe II known, the quasi-bolometric $UBVRI$ light curve of SN 1999br peaked at only 4.5×10^{40} erg s^{-1} (Pastorello et al. 2004; Pastorello et al. 2009). The observed range of peak luminosities for SNe II is similar to the range of luminosities estimated above to explain the IR excess of SPIRITS 16tn as a dust echo.

We can also estimate the pre-SN mass loss rate of the progenitor star necessary to support the such an echo. We assume that the dust is concentrated in a thin shell with $\Delta r/R_{\rm d} = 0.1$, a dust-to-gas ratio of $M_{\rm d}/M_{\rm g} = 0.01$, and again a pre-SN wind velocity of $v_{\rm w} = 10$ km s^{-1} and find $\dot{M} \approx 9 \times 10^{-6}$ – $6 \times 10^{-5} \left(\frac{M_{\rm d}}{10^{-4} M_\odot}\right) \left(\frac{M_{\rm d}/M_{\rm g}}{0.01}\right)^{-1} \left(\frac{\Delta r/R_{\rm d}}{0.1}\right)^{-1} \left(\frac{v_{\rm w}}{10 \text{ km s}^{-1}}\right) M_\odot$ yr^{-1} for the range of $R_{\rm d}$ allowed by the observations. These estimates are a factor of $\approx 4 - 25$ higher than that in Section 3.4 based on the radio observations, but they probe an earlier time in the mass-loss history of the progenitor of somewhere between ≈ 1700 and $11,000$ yr before explosion. While such mass-loss rates would imply a more luminous and massive RSG progenitor ($L \approx 10^{5.2} - 10^{5.5} L_\odot$, again assuming standard de Jager, Nieuwenhuijzen, and van der Hucht 1988 prescriptions), if the dust is confined to a shell, this could indicate a relatively brief episode of enhanced mass loss.

Non-SN transient scenarios

As we are unable to provide a definitive spectroscopic classification of SPIRITS 16tn as a CCSN, we briefly consider other observed classes of luminous IR transients as possible explanations for this event.

SN 2008S and NGC 300 OT2008-1-like transients

SN 2008S and the luminous 2008 optical transient in NGC 300 (NGC 300 OT2008-1) are the prototypes of a distinct class of transients. They have optically obscured progenitors but bright mid-IR pre-explosion counterparts ($M_{[4.5]} < -10$ mag), suggested to be extreme asymptotic giant branch stars of intermediate mass ($\approx$ 10–15 $M_\odot$) self-obscured by a dense, dusty wind (Prieto et al. 2008; Bond et al. 2009; Thompson et al. 2009). They are less luminous than typical CCSNe at peak ($L_{\rm bol} \approx 10^{41}$ erg s^{-1} for SN 2008S; Botticella et al. 2009). Emission lines in their

spectra indicate slow expansion velocities of 70–80 km s^{-1} (e.g., Bond et al. 2009; Humphreys et al. 2011). A proposed physical scenario is a weak explosion, possibly an electron-capture SN, or massive stellar eruption that destroys most of the obscuring dust, allowing the transient to be optically luminous. The development of a late-time IR excess, however, suggests that the dust reforms, obscuring the optical transient at late times (e.g., Thompson et al. 2009; Kochanek 2011a; Szczygieł et al. 2012). Both events are now fainter than their progenitor luminosities at [3.6] and [4.5], suggesting that the transients were terminal events (Adams et al. 2016).

The [4.5] light curve of SN 2008S is shown as the blue squares in Figure 3.7 compared to SPIRITS 16tn and several SNe II. The peak luminosity at [4.5] is similar to SPIRITS 16tn. Furthermore, the peak bolometric luminosity of SN 2008S-like events is sufficient to power the IR dust echo discussed in Section 3.4. The IR luminosity of SPIRITS 16tn declines more rapidly, and we do not observe a late-time IR excess powered by newly formed dust, inconsistent with the characteristic evolution of SN 2008S-like events.

Massive stellar mergers

The 2011 transient in NGC 4490 (hereafter NGC 4490-OT, Smith et al. 2016) and M101 2015OT-1 (Blagorodnova et al. 2017) are proposed massive analogs of the galactic contact binary merger V1309 Sco (Tylenda et al. 2011) and the B-type stellar merger V838 Mon (Bond et al. 2003; Sparks et al. 2008). These events typically have unobscured, optical progenitors; irregular, multipeaked light curves, increasingly red colors with time; and significant late-time IR excesses powered by copious dust formation. Their spectra show relatively narrow emission features of H I indicating low velocities of $\sim$ 100 km s^{-1}.

In the IR, NGC 4490-OT peaked at $M_{[4.5]} \approx -15$ mag, $\approx$ 1.7 mag fainter than SPIRITS 16tn. The inferred mass for the progenitor system of NGC 4490-OT was 20–30 $M_{\odot}$, and thus a merger origin for the more luminous SPIRITS 16tn would likely require an exceptionally massive progenitor. Furthermore, the IR light curve of NGC 4490-OT is long-lived, remaining too luminous at phases $\gtrsim$ 800 days to be powered by an IR echo (Smith et al. 2016). The relatively short-lived IR excess of SPIRITS 16tn, interpreted here as an IR echo, is generally inconsistent with the observed IR evolution typical of massive star mergers.

SN Imposters

Given the low inferred luminosity and lack of radio detection for SPIRITS 16tn, an "SN impostor" may also be a plausible explanation for the observed characteristics of SPIRITS 16tn. SN impostors are nonterminal, massive star outbursts (typically an $M \gtrsim 20$–$25\ M_{\odot}$ luminous blue variable [LBV]) that mimics the appearance of a true SN (e.g., Smith et al. 2011; Van Dyk and Matheson 2012). These events are are typically fainter in the optical fainter than true SNe ($M_V \lesssim -14$ mag). Impostors have in some cases been mistakenly classified as SNe IIn, due to the presence of "narrow" hydrogen emission lines on top of an "intermediate-width" base ($v \sim 1500$–2000 km s^{-1}). Some impostor outbursts have been observed to directly precede the death of the progenitor in the final years before the SN explosion, e.g., SN 2006jc (Pastorello et al. 2007) and SN 2009ip (Mauerhan et al. 2013; Pastorello et al. 2013). An impostor may be distinguished from a terminal SN explosion by the identification of a surviving progenitor star, or the detection of subsequent outbursts, also indicating that the progenitor has survived.

We detect no clear spectroscopic signatures of an SN or impostor in SPIRITS 16tn, and see no evidence of a subsequent outburst or variability in at least 1.5 yr of continued monitoring with *Spitzer* post discovery. We also cannot directly test for the survival of the progenitor with currently available data. Deep, high-resolution, near-IR imaging may be able to constrain the presence of a surviving star after the light from the transient completely fades.

3.5 Summary and conclusions

SPIRITS 16tn is a luminous ($M_{[4.5]} = -16.7$ mag) mid-IR transient discovered with *Spitzer*/IRAC during the ongoing SPIRITS survey in the nearby galaxy NGC 3556. We believe that SPIRITS 16tn is a possible SN. Despite being one of the nearest SNe discovered in 2016 at only 8.8 Mpc, it was completely missed by optical searches owing to heavy extinction. The transient position is coincident with a dark dust lane in the inclined, star-forming disk of the host. We estimate a total extinction of $A_V = 7.8$–9.3 mag, making SPIRITS 16tn one of the most highly obscured SNe yet discovered in the IR.

The [4.5] light curve shows a fast decline of 0.018 mag day^{-1}, and the source becomes increasingly red in the mid-IR from [3.6]−[4.5] = 0.7 mag to $\gtrsim 1.0$ mag between $t = 0$ and 184.7 days post discovery. The optical and near-IR spectra display a featureless, red continuum, ruling out an SN Ia, but preclude a definitive spectro-

scopic classification. The SED at $t = 41.9$ days post discovery is extremely red and can be matched to an SN II-like SED with $E(B-V) = 2.5 - 3.0$ mag of extinction. Furthermore, our analysis suggest that SPIRITS 16tn may be an intrinsically dim event similar to the well-studied, low-luminosity SN 2005cs. Modeling of the SED indicates the presence of a warm dust component ($T \approx 700 - 900$ K), which fades by $t = 184.7$ days. This is consistent with an IR echo powered by a circumstellar shell of dust located somewhere between 5.4×10^{16} cm and 3.5×10^{17} cm heated by a peak luminosity of $\sim 5 \times 10^{40} - 4$ erg s$^{-1} \times 10^{43}$ erg s^{-1}, similar to the range of observed peak luminosities for SNe II.

The source is not detected to deep limits in the radio across frequencies of 3–15.5 GHz, constraining the radio luminosity to $\lesssim 4 \times 10^{24}$ erg s^{-1} Hz^{-1} between $t = 19$ and 149.4 days. This effectively rules out most stripped-envelope SNe, except possibly the most rapidly evolving, high-velocity events that may peak in the radio at very early times. A late-rising, interaction-powered SN IIn may be consistent with our radio limits, but the typically strong spectroscopic signatures of interaction with a dense CSM are absent from our optical/near-IR spectra. SNe II, typically the weakest radio emitters among CCSNe, are the most consistent with our deep radio limits, and in this context we can constrain the pre-SN mass-loss rate of the progenitor to $\dot{M} \lesssim 2.4 \times 10^{-6} \left(\frac{\epsilon_B}{0.1}\right)^{-1} \left(\frac{v_w}{10 \text{ km s}^{-1}}\right) M_\odot$ yr^{-1}. This is consistent with a lower-mass RSG progenitor of $M \sim 10$–$15 M_\odot$.

We analyzed the available pre-explosion *Spitzer*/IRAC 2011 imaging and *HST*/WFPC2 F606W imaging of NGC 3556 covering the site of SPIRITS 16tn from 1994, and we do not detect a candidate progenitor star. Given the high degree of extinction inferred to SPIRITS 16tn, however, we are unable to place meaningful limits on the progenitor luminosity.

Taken together, we find the most likely explanation for the observed properties of SPIRITS 16tn to be an SN II explosion that both is highly obscured by foreground, host-galaxy dust, and is intrinsically low-luminosity. This discovery strengthens the fact that, even in the local 10 Mpc volume, SN searches appear to be incomplete. Transient surveys in the IR have the unique ability to find dust-obscured or otherwise optically dim events, allowing for the true nearby SN population to be uncovered.

We thank R. Lunnan for executing our Keck/LRIS observations. We thank D. Neill and M. Matuszewski for assistance with the PCWI observations and data reduction. We thank A. Monson for help with P200/WIRC data reduction. We thank T. Cantwell, Y. Perrott, and the AMI staff for conducting the AMI-LA observations

and data reduction. We also thank the anonymous referee for suggestions that improved the paper.

This material is based on work supported by the National Science Foundation Graduate Research Fellowship under grant no. DGE-1144469. H.E.B acknowledges support for this work provided by NASA through grants GO-13935 and GO-14258 from the Space Telescope Science Institute, which is operated by AURA, Inc., under NASA contract NAS 5-26555. R.D.G. was supported in part by the United States Air Force. A.H. acknowledges support by the I-Core Program of the Planning and Budgeting Committee and the Israel Science Foundation.

This work is based in part on observations made with the Spitzer Space Telescope, which is operated by the Jet Propulsion Laboratory, California Institute of Technology, under a contract with NASA. The work is based, in part, on observations made with the Nordic Optical Telescope, operated by the Nordic Optical Telescope Scientific Association at the Observatorio del Roque de los Muchachos, La Palma, Spain, of the Instituto de Astrofisica de Canarias.

This work is based in part on observations with the NASA/ESA *Hubble Space Telescope* obtained at the Space Telescope Science Institute and from the Mikulski Archive for Space Telescopes at STScI, which are operated by the Association of Universities for Research in Astronomy, Inc., under NASA contract NAS5-26555. These observations are associated with programs GO-14258 and SNAP-5446.

Some of the data presented herein were obtained at the W. M. Keck Observatory, which is operated as a scientific partnership among the California Institute of Technology, the University of California, and the National Aeronautics and Space Administration. The Observatory was made possible by the generous financial support of the W. M. Keck Foundation. The authors wish to recognize and acknowledge the very significant cultural role and reverence that the summit of Maunakea has always had within the indigenous Hawaiian community. We are most fortunate to have the opportunity to conduct observations from this mountain.

RATIR is a collaboration between the University of California, the Universidad Nacional Autonóma de México, NASA Goddard Space Flight Center, and Arizona State University, benefiting from the loan of an H2RG detector from Teledyne Scientific and Imaging. RATIR, the automation of the Harold L. Johnson Telescope of the Observatorio Astronómico Nacional on Sierra San Pedro Mártir, and the operation of both are funded by the partner institutions and through NASA grants

NNX09AH71G, NNX09AT02G, NNX10AI27G, and NNX12AE66G; CONACyT grant INFR-2009-01-122785; UNAM PAPIIT grant IN113810; and a UC MEXUS-CONACyT grant.

UKIRT is owned by the University of Hawaii (UH) and operated by the UH Institute for Astronomy; operations are enabled through the cooperation of the East Asian Observatory. When the data reported here were acquired, UKIRT was supported by NASA and operated under an agreement among the University of Hawaii, the University of Arizona, and Lockheed Martin Advanced Technology Center; operations were enabled through the cooperation of the East Asian Observatory.

Based on observations obtained at the Gemini Observatory acquired through the Gemini Observatory Archive and processed using the Gemini IRAF package, which is operated by the Association of Universities for Research in Astronomy, Inc., under a cooperative agreement with the NSF on behalf of the Gemini partnership: the National Science Foundation (United States), the National Research Council (Canada), CONICYT (Chile), Ministerio de Ciencia, Tecnología e Innovación Productiva (Argentina), and Ministério da Ciência, Tecnologia e Inovação (Brazil).

The National Radio Astronomy Observatory is a facility of the National Science Foundation operated under cooperative agreement by Associated Universities, Inc.

The Legacy Surveys consist of three individual and complementary projects: the Dark Energy Camera Legacy Survey (DECaLS; NOAO Proposal ID no. 2014B-0404; PIs: David Schlegel and Arjun Dey), the Beijing-Arizona Sky Survey (BASS; NOAO Proposal ID no. 2015A-0801; PIs: Zhou Xu and Xiaohui Fan), and the Mayall z-band Legacy Survey (MzLS; NOAO Proposal ID no. 2016A-0453; PI: Arjun Dey). DECaLS, BASS, and MzLS together include data obtained, respectively, at the Blanco telescope, Cerro Tololo Inter-American Observatory, National Optical Astronomy Observatory (NOAO); the Bok telescope, Steward Observatory, University of Arizona; and the Mayall telescope, Kitt Peak National Observatory, NOAO. The Legacy Surveys project is honored to be permitted to conduct astronomical research on Iolkam Du'ag (Kitt Peak), a mountain with particular significance to the Tohono O'odham Nation.

NOAO is operated by the Association of Universities for Research in Astronomy (AURA) under a cooperative agreement with the National Science Foundation.

The Legacy Survey team makes use of data products from the Near-Earth Object Wide-field Infrared Survey Explorer (NEOWISE), which is a project of the Jet

Propulsion Laboratory/California Institute of Technology. NEOWISE is funded by the National Aeronautics and Space Administration.

The Legacy Surveys imaging of the DESI footprint is supported by the Director, Office of Science, Office of High Energy Physics of the U.S. Department of Energy under Contract no. DE-AC02-05CH1123, by the National Energy Research Scientific Computing Center, a DOE Office of Science User Facility under the same contract; and by the U.S. National Science Foundation, Division of Astronomical Sciences under Contract no. AST-0950945 to NOAO.

Funding for SDSS-III has been provided by the Alfred P. Sloan Foundation, the Participating Institutions, the National Science Foundation, and the U.S. Department of Energy Office of Science. The SDSS-III website is http://www.sdss3.org/.

SDSS-III is managed by the Astrophysical Research Consortium for the Participating Institutions of the SDSS-III Collaboration, including the University of Arizona, the Brazilian Participation Group, Brookhaven National Laboratory, Carnegie Mellon University, University of Florida, the French Participation Group, the German Participation Group, Harvard University, the Instituto de Astrofisica de Canarias, the Michigan State/Notre Dame/JINA Participation Group, Johns Hopkins University, Lawrence Berkeley National Laboratory, Max Planck Institute for Astrophysics, Max Planck Institute for Extraterrestrial Physics, New Mexico State University, New York University, Ohio State University, Pennsylvania State University, University of Portsmouth, Princeton University, the Spanish Participation Group, University of Tokyo, University of Utah, Vanderbilt University, University of Virginia, University of Washington, and Yale University.

Chapter 4

CASE STUDY OF M51 OT2019-1: DISCOVERY OF AN INTERMEDIATE-LUMINOSITY RED TRANSIENT IN M51 AND ITS LIKELY DUST-OBSCURED, INFRARED-VARIABLE PROGENITOR

Jencson, Jacob E., et al. 2019. "Discovery of an Intermediate-luminosity Red Transient in M51 and Its Likely Dust-obscured, Infrared-variable Progenitor". *ApJ* 880 (2): L20–40. doi:10.3847/2041-8213/ab2c05. arXiv: 1904.07857 [astro-ph.SR].

Jacob E. Jencson[1], Scott M. Adams[1], Howard E. Bond[2,3], Schuyler D. van Dyk[4], Mansi M. Kasliwal[1], John Bally[5], Nadejda Blagorodnova[6], Kishalay De[1], Christoffer Fremling[1], Yuhan Yao[1], Andrew Fruchter[3], David Rubin[3], Cristina Barbarino[7], Jesper Sollerman[7], Adam A. Miller[8], Erin K. S. Hicks[9], Matthew A. Malkan[10], Igor Andreoni[1], Eric C. Bellm[11], Robert Buchheim[12], Richard Dekany[13], Michael Feeney[13], Sara Frederick[14], Avishay Gal-Yam[15], Robert D. Gehrz[16], Matteo Giomi[17], Matthew J. Graham[1], Wayne Green[5], David Hale[13], Matthew J. Hankins[1], Mark Hanson[18], George Helou[4], Anna Y. Q. Ho[1], T. Hung[19], Mario Jurić[11], Malhar R. Kendurkar[20], S. R. Kulkarni[1], Ryan M. Lau[21], Frank J. Masci[4], James D. Neill[1], Kevin Quin[22], Reed L. Riddle[13], Ben Rusholme[4], Forrest Sims[23], Nathan Smith[24], Roger M. Smith[13], Maayane T. Soumagnac[25], Yutaro Tachibana[1,26], Samaporn Tinyanont[1], Richard Walters[13], Stanley Watson[18], and Robert E. Williams[3,19]

[1]Division of Physics, Mathematics, and Astronomy, California Institute of Technology, Pasadena, CA 91125, USA

[2]Department of Astronomy & Astrophysics, Pennsylvania State University, University Park, PA 16802, USA

[3]Space Telescope Science Institute, 3700 San Martin Drive, Baltimore, MD 21218, USA

[4]Caltech/IPAC, Mailcode 100-22, Pasadena, CA 91125, USA

[5]Center for Astrophysics and Space Astronomy, University of Colorado, 389 UCB, Boulder, CO 80309, USA

[6]Department of Astrophysics/IMAPP, Radboud University, Nijmegen, The Netherlands

[7]The Oskar Klein Centre, Department of Astronomy, Stockholm University, AlbaNova, SE-106 91 Stockholm, Sweden

[8]Center for Interdisciplinary Exploration and Research in Astrophysics (CIERA) and Department of Physics and Astronomy, Northwestern University, Evanston, IL 60208, USA

[9]Department of Physics & Astronomy, University of Alaska Anchorage, 3211 Providence Drive, Anchorage, AK 99508, USA

[10]University of California Los Angeles, Department of Astronomy & Astrophysics, 430 Portola Plaza, Box 951547, Los Angeles, CA 90095-1547, US
[11]DIRAC Institute, Department of Astronomy, University of Washington, 3910 15th Avenue NE, Seattle, WA 98195, USA
[12]Lost Gold Observatory, Society for Astronomical Sciences, Gold Canyon, AZ 85118, USA
[13]Caltech Optical Observatories, California Institute of Technology, Pasadena, CA 91125, USA
[14]Department of Astronomy, University of Maryland, College Park, MD 20742, USA
[15]Department of Particle Physics and Astrophysics, Weizmann Institute of Science, Rehovot 76100, Israel
[16]Minnesota Institute for Astrophysics, School of Physics and Astronomy, University of Minnesota, 116 Church Street, S. E., Minneapolis, MN 55455, USA
[17]Humboldt-Universität zu Berlin, Newtonstraße 15, D-12489 Berlin, Germany
[18]Stellar Winds Observatory, Dark Sky New Mexico, Hidalgo County, NM, USA
[19]Department of Astronomy and Astrophysics, University of California, Santa Cruz, CA 95064, USA
[20]Prince George Astronomical Observatory, 7765 Tedford Road, Prince George, BC V2N 6S2, Canada
[21]Institute of Space & Astronautical Science, Japan Aerospace Exploration Agency, 3-1-1 Yoshinodai, Chuo-ku, Sagamihara,Kanagawa 252-5210, Japan
[22]Northern Virginia Astronomy Club, Fairfax, VA 22030, USA
[23]Society for Astronomical Sciences, Desert Celestial Observatory, Gilbert, AZ 85233, USA
[24]University of Arizona, Steward Observatory, 933 N. Cherry Avenue, Tucson, AZ 85721, USA
[25]Benoziyo Center for Astrophysics, Weizmann Institute of Science, Rehovot, Israel
[26]Department of Physics, Tokyo Institute of Technology, 2-12-1 Ookayama, Meguro-ku, Tokyo 152-8551, Japan

Abstract

We present the discovery of an optical transient (OT) in Messier 51, designated M51 OT2019-1 (also ZTF 19aadyppr, AT 2019abn, ATLAS19bzl), by the Zwicky Transient Facility (ZTF). The OT rose over 15 days to an observed luminosity of $M_r = -13$ ($\nu L_\nu = 9 \times 10^6\ L_\odot$), in the luminosity gap between novae and typical supernovae (SNe). Spectra during the outburst show a red continuum, Balmer emission with a velocity width of $\approx 400\,\mathrm{km\,s^{-1}}$, Ca II and [Ca II] emission, and absorption features characteristic of an F-type supergiant. The spectra and multiband light curves are similar to the so-called "SN impostors" and intermediate-luminosity red transients (ILRTs). We directly identify the likely progenitor in archival *Spitzer Space Telescope* imaging with a 4.5 μm luminosity of $M_{[4.5]} \approx -12.2$ mag and a [3.6]−[4.5] color redder than 0.74 mag, similar to those of the prototype ILRTs SN 2008S and NGC 300 OT2008-1. Intensive monitoring of M51 with *Spitzer* further reveals evidence for variability of the progenitor candidate at [4.5] in the years before the OT. The progenitor is not detected in pre-outburst *Hubble Space Telescope* optical and near-IR images. The optical colors during outburst combined with spectroscopic temperature constraints imply a higher reddening of $E(B-V) \approx 0.7$ mag and higher intrinsic luminosity of $M_r \approx -14.9$ mag ($\nu L_\nu = 5.3 \times 10^7\ L_\odot$) near peak than seen in previous ILRT candidates. Moreover, the extinction estimate is higher on the rise than on the plateau, suggestive of an

extended phase of circumstellar dust destruction. These results, enabled by the early discovery of M51 OT2019-1 and extensive pre-outburst archival coverage, offer new clues about the debated origins of ILRTs and may challenge the hypothesis that they arise from the electron-capture induced collapse of extreme asymptotic giant branch stars.

4.1 Introduction

Searches for transients in the nearby universe have uncovered a diverse array of hydrogen-rich stellar events occupying the luminosity range between that of novae and supernovae (SNe). As more well-characterized events have been found, some defined classes are beginning to emerge. Distinguishing among these classes, however, can be challenging as there is significant overlap in their observed properties. These include events often associated with luminous blue variables (LBVs; Humphreys and Davidson 1994; Smith and Owocki 2006) variably referred to as "SN impostors," "η Carinae variables," or "giant eruptions" (Humphreys, Davidson, and Smith 1999; Van Dyk et al. 2000; Pastorello et al. 2010; Smith et al. 2010; Smith 2014). The "luminous red novae" (LRNe) are believed to be associated with stellar mergers or common-envelope ejections, including the 1–3 $M_{\odot}$ contact-binary merger V1309 Sco (Tylenda et al. 2011) and the B-type stellar merger V838 Mon (Bond et al. 2003; Sparks et al. 2008). Several extragalactic events are also suggested to be members of this class, e.g., M31 RV (Rich et al. 1989; Bond and Siegel 2006; Bond 2011), M85 OT2006-1 (Kulkarni et al. 2007), NGC 4490 OT2011-1 (Smith et al. 2016), and M101 OT2015-1 (Blagorodnova et al. 2017).

We adopt the term "intermediate-luminosity red transient" (ILRT), originally suggested by Bond et al. (2009), to refer to the class of SN impostors similar to two well-characterized prototypes: SN 2008S (Prieto et al. 2008; Botticella et al. 2009; Smith et al. 2009) and the 2008 optical transient (OT) in NGC 300 (NGC 300 OT2008-1; Berger et al. 2009; Bond et al. 2009; Humphreys et al. 2011). As the name suggests, these events reach peak luminosities ($M_{r/R} \approx -13$ to -14) fainter than those of typical core-collapse SNe, but comparable to those of other impostors. The peak is followed by the monotonic decline of their optical light curves, and they also show reddened spectra suggestive of strong internal extinction from the immediate circumburst environment. Their spectra are similar to some LBV-related transients and LRNe, showing strong H, Ca II, and rare [Ca II] emission features superimposed on an absorption spectrum characteristic of an F-type supergiant. The intermediate-width H features indicate relatively low ejection velocities of a few $\times$ 100 km s^{-1}.

Both NGC 300 OT2008-1 and SN 2008S had densely self-obscured progenitor stars detected in archival imaging with the *Spitzer Space Telescope*, whose luminosities and inferred masses ($M \approx 9$–$15\ M_{\odot}$; Prieto 2008; Prieto et al. 2008; Thompson et al. 2009; Kochanek 2011a) are lower than those of classical LBVs. Both events have now faded below their pre-explosion luminosities in the IR (Adams et al. 2016), suggesting that the explosions may have been terminal. Other proposed members of this class discovered in the past decade include PTF 10fqs (Kasliwal et al. 2011), SN 2010dn (Smith et al. 2011), and AT 2017be (Cai et al. 2018), although their larger distances prevented the direct identification of progenitors.

Here, we present the discovery by the Zwicky Transient Facility (ZTF; Bellm et al. 2019a; Graham et al. 2019) of an OT in M51 with similar properties to those of previously observed ILRTs and other SN impostors. At a distance of only 8.6 Mpc (McQuinn et al. 2016, 2017), this is the closest such event in over a decade, allowing us to identify and characterize a candidate progenitor star in archival *Spitzer* images. In this Letter, we describe the discovery and early observations (Section 4.2), our analysis of available archival imaging and identification of the likely progenitor (Section 4.3), the early photometric evolution (Section 4.3), and spectroscopic properties (Section 4.3). In Section 4.4, we discuss the properties of the OT and its progenitor in the context of similar transients, and suggest it is a member of the ILRT class offering new insights on their origins.

4.2 Discovery and data collection

Discovery in M51

On UT 2019 January 22.6 (MJD = 58505.6), ZTF 19aadyppr was detected as a new OT source in the nearby galaxy M51 by ZTF with the 48 inch Samuel Oschin Telescope (P48) at Palomar Observatory as part of the public ZTF 3 day cadence survey of the visible Northern Sky. The detection passed significance (Masci et al. 2019) and machine-learning thresholds (Tachibana and Miller 2018; Mahabal et al. 2019), and was released as a public alert (Patterson et al. 2019). We refer to the phase, t, as the number of days since the first ZTF detection throughout this work. Located at an R.A. and decl. of $13^{\rm h}29^{\rm m}42\farcs41$, $+47^{\circ}11'16\farcs6$ (J2000.0), the source had an r-band AB magnitude at first detection of 19.6 ± 0.2. The source was not detected in an earlier image taken on 2019 January 19.6, to a limiting magnitude of $r > 20.5$, at $t = -3$ days. After a second detection on 2019 January 25.5 (MJD = 58508.5), ZTF 19aadyppr was autonomously selected as a high-quality transient by the AMPEL analysis framework (Nordin et al. 2019a). The discovery

was submitted to the Transient Name Server and provided the IAU designation AT 2019abn (Nordin et al. 2019b). The source passed several ZTF science-program filters and was saved by human scanners for follow-up on the GROWTH Marshal (Kasliwal et al. 2019). Early spectroscopic observations reported by De et al. (2019) on 2019 January 26 were characterized by a red continuum and strong, intermediate-width (≈ 600 km s^{-1}) Hα emission, consistent with a classification of SN impostor or young ILRT. An independent detection was reported to TNS on 2019 January 26 by the the ATLAS survey (Tonry et al. 2018), and the Las Cumbres Observatory (LCO) Global SN Project reported an additional spectrum taken on 2019 March 2 (Burke et al. 2019) and ILRT classification. We use the name M51 OT2019-1 for this event hereafter.

As shown in Figure 4.1, the transient was located in a star-forming spiral arm of M51, 108.″2 from the galaxy's center. There is a prominent dust lane at the site, indicating the source may be subject to significant host extinction. Notably, M51 has a high rate of core-collapse SNe, with three known events discovered in the last 25 yr: SN 1994I (type Ic; Schmidt et al. 1994), SN 2005cs (type II; Modjaz et al. 2005), and SN 2011dh (type IIb; Silverman, Filippenko, and Cenko 2011). The NASA/IPAC Extragalactic Database[1] (NED) lists 50 individual distance measurements to M51, with a median value in distance modulus of 29.5 mag and a large standard deviation of 0.9 mag. Throughout this work we assume a distance modulus for M51 from McQuinn et al. (2016, 2017) of $m-M = 29.67 \pm 0.02$ (statistical) ± 0.07 (systematic; Rizzi et al. 2007) mag based on the luminosity of the tip of the red giant branch (TRGB) method, and that the systematic uncertainties associated with calibrating this method dominate over the statistical measurement uncertainties. We adopt the value from NED for the Galactic extinction toward M51 of $E(B-V) = 0.03$ mag, based on the Schlafly and Finkbeiner (2011) recalibration of Schlegel, Finkbeiner, and Davis (1998), and assuming a standard (Fitzpatrick 1999) reddening law with $R_V = 3.1$.

Imaging observations

The field containing M51 OT2019-1 was regularly observed at many epochs with the ZTF camera on P48 in the g, r, and i bands. The P48 images were reduced with the ZTF Science Data System pipelines (Masci et al. 2019), which perform image subtraction based on the Zackay, Ofek, and Gal-Yam (2016) algorithm and point-

[1]NED is operated by the Jet Propulsion Laboratory, California Institute of Technology, under contract with the National Aeronautics and Space Administration.

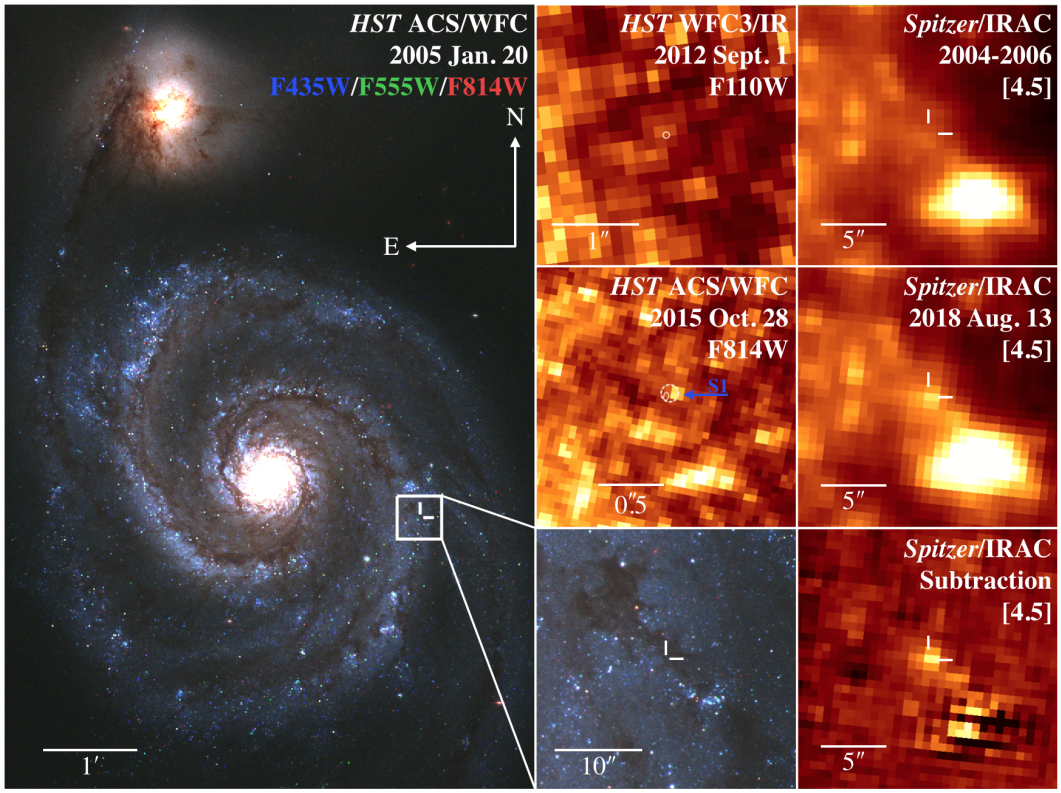

Figure 4.1: Pre-explosion *HST* and *Spitzer* imaging of M51 OT2019-1. In the leftmost panel, we show the color-composite *HST* ACS/WFC mosaics of the M51 system from 2005 in three filters (F435W in blue, F555W in green, and F814W in red; PID: GO-10451; PI: S. Beckwith). The location of M51 OT2019-1 in a prominent dust lane along a spiral arm is indicated by the white cross-hairs and shown in more detail in the $30'' \times 30''$ bottom center zoom-in panel. Above in the center column, we show the archival *HST* coverage of the site in 2015 with ACS/WFC in F814W (center row) and in 2012 with WFC3/IR in F110W (top row). The 3-σ error ellipses on the precise position of the transient from new *HST*/WFC3 (solid) and Keck/NIRC2 (dashed) imaging are shown in white at the center of these panels. The nearest star-like object in the F814W image, labeled S1 in blue, is firmly outside the *HST* error ellipse. In the rightmost column, we show the *Spitzer*/IRAC archival [4.5] Super Mosaic (top), the most recent pre-explosion [4.5] image (center), and the subtraction of the two (bottom), clearly showing the variability of the coincident IR precursor source.

spread-function (PSF) photometry on the reference-subtracted images. We utilize this photometry for data from the public ZTF survey taken after 2019 January 1. For images taken as part of the ZTF Collaboration surveys and the Caltech surveys (Bellm et al. 2019b), and images taken prior to 2019 January 1 from the first ZTF Public Data Release[2] (ZTF-DR1), we subsequently performed forced PSF-fitting photometry at the location of M51 OT2019-1, adopting a linear model for pixel values in the difference images as a function of the normalized PSF-model image values and use a Markov Chain Monte Carlo simulation to estimate the photometric uncertainties (Y. Yao et al. 2019, in preparation). Measurements for a given filter taken the same night were then averaged.

Follow-up images in the g', r', i', and Y bands were obtained with the Sinistro cameras on the Las Cumbres Observatory (LCO; Brown et al. 2013) 1 m telescopes under the program NOAO2019A-011 (PI: N. Blagorodnova). The data were reduced at LCO using the Beautiful Algorithms to Normalize Zillions of Astronomical Images (BANZAI) pipeline (McCully et al. 2018). Photometry from the LCO $g'r'i'$-band images were computed with the image-subtraction pipeline described in Fremling et al. (2016), with template images from the Sloan Digital Sky Survey (SDSS; Ahn et al. 2014). The pipeline performs PSF-fitting photometry calibrated against several SDSS stars in the field. We performed aperture photometry on M51 OT2019-1 in the LCO Y-band, with the aperture radius set by the typical full width at half maximum (FWHM) of stars in the images, calibrated against several stars in the Pan-STARRS1 (PS1; Chambers et al. 2016) DR2 catalog (Flewelling et al. 2016).

Additional ground-based follow-up images were obtained in the optical and near-IR at several epochs using the Astrophysical Research Consortium Telescope Imaging Camera (ARCTIC; Huehnerhoff et al. 2016) and Near-Infrared Camera and Fabry-Perot Spectrometer (NICFPS; Vincent et al. 2003) on the Astrophysical Research Consortium (ARC) 3.5 m Telescope at Apache Point Observatory (APO), and the Wide Field Infrared Camera (WIRC; Wilson et al. 2003) on the 200 inch Hale Telescope (P200) at Palomar Observatory. Imaging of M51 at APO was obtained as part of a program to monitor 24 galaxies in the SPitzer Infrared Intensive Transients Survey (SPIRITS; PI: M. Kasliwal; PIDs 10136, 11063, 13053). Optical $g'r'i'$ images were reduced in the standard fashion using bias, dark, and twilight flat-field frames. Our near-IR JHK_s imaging employed large dithers alternating

[2]https://www.ztf.caltech.edu/page/dr1

between the target and a blank sky field approximately every minute to allow for accurate subtraction of the bright near-IR sky background, and individual frames were flat-fielded, background-subtracted, astrometrically aligned with a catalog of Two Micron All Sky Survey (2MASS; Skrutskie et al. 2006) sources, and stacked. We performed aperture photometry at the location of the transient, and used the $g'r'i'$ or JHK_s magnitudes of several isolated stars in SDSS or 2MASS to measure the photometric zero-points in the optical and near-IR images, respectively.

We also present photometry from CCD images obtained by F. Sims, R. Buchheim, W. Green, M. Hanson, and S. Watson, in the V and R-bands, and by K. Quin and M. Kendurkar in the Astrodon LRGB filters[3]. For the LRGB frames, we performed aperture photometry on the OT calibrated to standard magnitudes in R, R, V, and B, respectively, using SDSS stars in the field and adopting the conversions of Jordi, Grebel, and Ammon (2006). Observations were obtained in the 3.6 and 4.5 μm imaging channels, [3.6] and [4.5], of the Infrared Array Camera (IRAC; Fazio et al. 2004) on board *Spitzer* (Werner et al. 2004; Gehrz et al. 2007) on 2019 April 7.6 as part of regular monitoring of M51 as part of SPIRITS. We performed image subtraction and aperture photometry as described in more detail for the archival *Spitzer*/IRAC imaging in Section 4.3.

Our photometry of M51 OT2019-1 is shown in Figure 4.2 on the AB magnitude system, corrected for Galactic extinction. Where appropriate we have converted $VRIJHK_s$ magnitudes on the Vega system to AB magnitudes using the conversions of Blanton and Roweis (2007).

We also obtained high-resolution, adaptive-optics J-band imaging of the transient on 2019 February 16.6, using the near-IR camera (NIRC2; PI: K. Matthews) on the 10 m Keck II Telescope on Maunakea. Further high-resolution imaging was obtained on 2019 March 5.0 with the *Hubble Space Telescope* (*HST*) WFC3 camera in the F275W, F336W, and F814W filters as the first target in a test program proposing a new method of *HST* observing (PI: A. Fruchter; PID SNAP-15675). This new method, called "Rolling Snapshots," allows fairly rapid response by updating a list of snapshot targets weekly; however, due to present limitations in the Astronomer's Proposal Tool (APT), the observing is done in a custom subarray mode. Data were reduced using the standard pipelines at STScI, adding a charge-transfer-efficiency (CTE) correction (which was not done by the pipeline due to the use of the custom

[3]Astrodon filter information is available here: `https://astrodon.com/products/astrodon-lrgb-gen2-i-series-tru-balance-filters/`

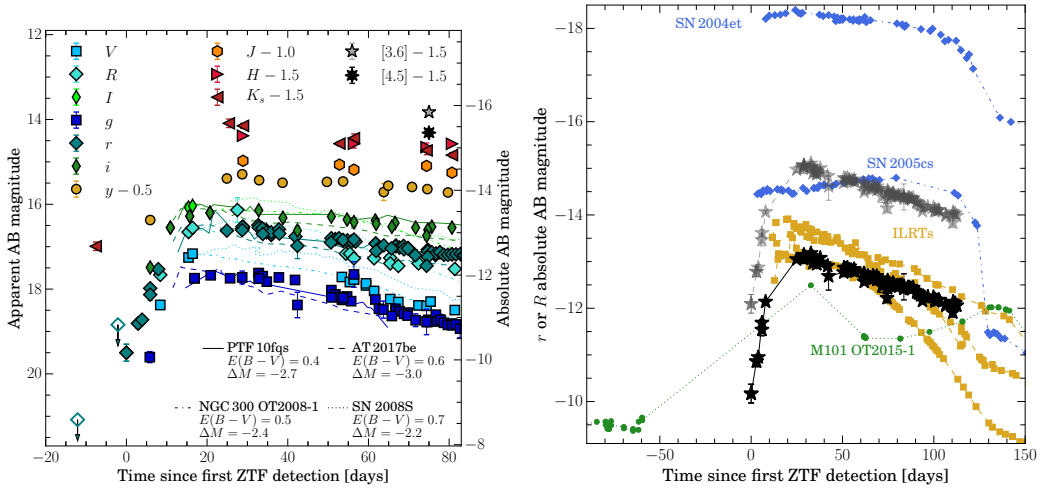

Figure 4.2: Left: multiband light curves of M51 OT2019-1 are shown as large filled symbols, and unfilled points with downward arrows represent upper limits from nondetections. Time on the x-axis is measured in days since the first detection by ZTF on 2019 January 22.6. We also show the VRI measurements reported by Pessev et al. (2019). Measurements have been corrected for Galactic extinction to M51 only, and $VRIJHK_s$ measurements have been converted from Johnson–Cousins/2MASS Vega magnitudes to AB magnitudes adopting Blanton and Roweis (2007) conversions. Absolute magnitudes at the assumed distance to M51 and assuming no host extinction are given on the y-axis to the right. For comparison, we show gri light curves of PTF10fqs (solid lines; Kasliwal et al. 2011), and the VRI light curves of SN 2008S (dotted lines; Botticella et al. 2009) and NGC 300 OT2008-1 (dashed–dotted lines, Humphreys et al. 2011). The comparison light curves have been corrected for Galactic extinction to their respective hosts from NED, then reddened to match the $g - r$ or $V - R$ colors of M51 OT2019-1 on the plateau and offset in absolute magnitude by the ΔM values indicated on the figure to match the vertical level of the M51 OT2019-1 light curves. Right: r-band light curves of M51 OT2019-1 are shown as the black stars, and corrected for our estimate of the total host/CSM extinction near peak with $E(B - V) = 0.7$ mag as lighter gray stars. The r or R light curves of the comparison ILRTs are shown as yellow squares, also corrected with an estimate for the total extinction near peak as described in the text. We compare to the r- or R-band light curves of other hydrogen-rich transients including the Type IIP SN 2004et (Maguire et al. 2010), low-luminosity Type IIP SN 2005cs (Pastorello et al. 2006), and the LRN M101 OT2015-1 (Blagorodnova et al. 2017).

subarray). CTE-corrected frames were then combined into image mosaics for each filter using AstroDrizzle within PyRAF to attempt to flag cosmic-ray hits. We performed PSF-fitting photometry for the transient using DOLPHOT (Dolphin 2000; Dolphin 2016) and obtained 23.32 ± 0.17, 20.47 ± 0.03, and 15.754 ± 0.002 mag (Vega scale) for F275W, F336W, and F814W, respectively.

Spectroscopic observations

We obtained a sequence of optical spectra of M51 OT2019-1 using several instruments covering phases from $t = 4$ to 111 days. This includes four spectra with the Alhambra Faint Object Spectrograph and Camera (ALFOSC) on the 2.56 m Nordic Optical Telescope (NOT) at the Spanish Observatorio del Roque de los Muchachos on La Palma, including two low-resolution spectra with the 300 lines mm^{-1} grism (Gr4) and an epoch of intermediate-resolution spectra using two 600 lines mm^{-1} grisms (Gr7 and Gr8), five spectra with the Double Beam Spectrograph (DBSP; Oke and Gunn 1982) on P200, one spectrum with the Gemini Multi-Object Spectrograph (GMOS; Hook et al. 2004) on the Gemini North Telescope through our Target of Opportunity program (PI: A. Miller; PID GN-2018B-Q-132), one spectrum with the Spectral Energy Distribution Machine (SEDM; Blagorodnova et al. 2018) on the Palomar 60 inch Telescope (P60), and one spectrum with the Low Resolution Imaging Spectrometer (LRIS; Goodrich and Cohen 2003) on the Keck I Telescope. The spectra were reduced using standard techniques including wavelength calibration with arc-lamp spectra and flux calibration using spectrophotometric standard stars. In particular, we made use of a custom PyRAF-based reduction pipeline[4] (Bellm and Sesar 2016) for DBSP spectra, the IDL-based reduction and pipeline LPipe[5] (Perley 2019) for the LRIS spectrum, the fully automated Python-based reduction pipeline pysedm[6] (Rigault et al. 2019) for the SEDM spectra, and standard tasks in Gemini IRAF package[7] for the GMOS spectrum following procedures provided in the GMOS Data Reduction Cookbook[8].

We also obtained an epoch of near-IR spectroscopy of M51 OT2019-1 with the TripleSpec spectrograph (Herter et al. 2008) on P200. We obtained four exposures of the transient (300 s each) while nodding the transient along the slit between exposures to allow sky subtraction. The data were reduced with a modified version of the IDL-based data reduction package Spextool[9] (Cushing, Vacca, and Rayner 2004) for P200/TripleSpec. Corrections for the strong near-IR telluric absorption features and flux calibrations were performed with observations of the A0 V standard star HIP 61471, using the method developed by Vacca, Cushing, and Rayner (2003) implemented in the IDL tool xtellcor as part of Spextool.

[4] https://github.com/ebellm/pyraf-dbsp
[5] http://www.astro.caltech.edu/~dperley/programs/lpipe.html
[6] https://github.com/MickaelRigault/pysedm
[7] http://www.gemini.edu/sciops/data-and-results/processing-software
[8] http://ast.noao.edu/sites/default/files/GMOS_Cookbook/
[9] http://irtfweb.ifa.hawaii.edu/~cushing/spextool.html

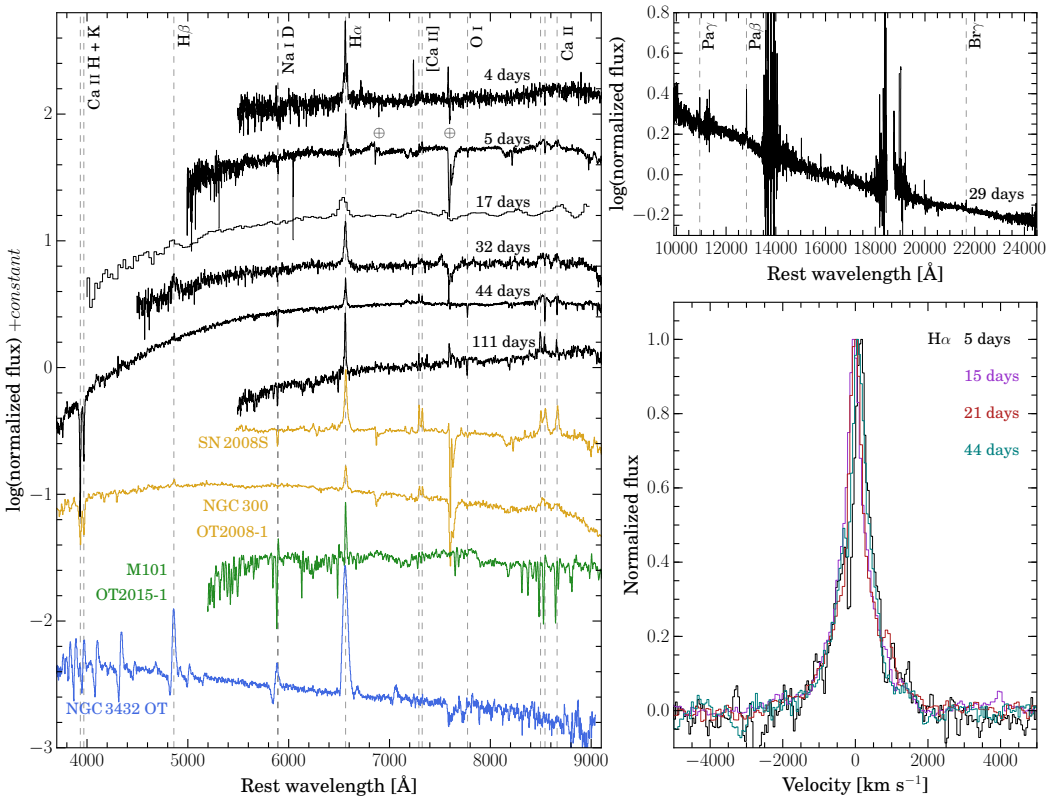

Figure 4.3: In the left panel, we show the optical spectral evolution of M51 OT2019-1 in black with the phase of each spectrum indicated along the right side of the panel. We show spectra of other ILRTs in yellow (SN 2008S from Botticella et al. 2009 and NGC 300 OT2008-1 from Bond et al. 2009), the M101 LRN (Blagorodnova et al. 2017) in green, and the 2008 LBV outburst in NGC 3432 (Pastorello et al. 2010) in blue for comparison. Each spectrum has been normalized to the continuum flux level around 7000 Å, and shifted vertically by an arbitrary constant for clarity. In the top right panel, we show the near-IR spectrum of M51 OT2019-1 from t = 29 days normalized to the continuum level around 16000 Å. We indicate the locations of several spectral features with gray, dashed vertical lines as labeled along the top of each panel. In the bottom right panel, we show the continuum-subtracted Hα velocity profiles for several epochs in the early evolution of the transient. The apparent absorption component in the t = 5 days spectrum is an artifact of the background subtraction.

A complete log of our spectroscopic observations is provided in Table 4.1, and a representative set of our spectral sequence is shown in Figure 4.3. All of our spectra will be made publicly available at the Weizmann Interactive Supernova Data Repository[10] (WISeREP; Yaron and Gal-Yam 2012).

[10] https://wiserep.weizmann.ac.il

Table 4.1: Log of spectroscopic observations of M51 OT2019-1

UT Date	MJD	Phase (days)	Tel./Instr.	Range (Å)	Resolution ($\lambda/\delta\lambda$)
2019 Jan 26	58509	4	NOT/ALFOSC	4000–9000	280
2019 Jan 26	58509	4	P200/DBSP	3500–10000	700
2019 Jan 27	58510	5	Gemini N/GMOS	5000–10000	1000
2019 Feb 6	58520	15	NOT/ALFOSC	3650–7110	500
2019 Feb 6	58520	15	NOT/ALFOSC	5680–8580	700
2019 Feb 8	58522	17	P60/SEDM	3650–10000	100
2019 Feb 12	58526	21	P200/DBSP	3500–10000	1000
2019 Feb 20	58534	29	P200/TripleSpec	10000–24000	2600
2019 Feb 23	58537	32	NOT/ALFOSC	3200–9600	280
2019 Mar 7	58549	44	Keck I/LRIS	3500–10300	600/1000[a]
2019 Mar 16	58558	53	P200/DBSP	3500–10000	1000
2019 Apr 13	58586	81	P200/DBSP	3500–10000	1000
2019 May 13	58616	111	P200/DBSP	3500–10000	1000

[a] Values given for the blue and red sides of LRIS, respectively.

4.3 Analysis

Archival imaging and progenitor constraints

Progenitor candidate identification

We searched for the presence of a progenitor star in archival imaging taken with *HST* and *Spitzer*/IRAC. To determine the precise position of the transient in the archival *HST* imaging, we registered the NIRC2 J-band image of the transient with the 2015 ACS/WFC F814W image (PID: GO-13804; PI: K. McQuinn) and 2012 WFC3/IR F110W image (PID: 12490; PI: J. Koda). Using several stars and compact background galaxies in common between the new and archival frames, we achieved rms astrometric uncertainties on the position of the transient of 0.44 ACS pixels (0.″022) in the F814W image and 0.12 WFC3/IR pixels (0.″015) in the F110W image. We identified an apparent point source at the edge of our 3σ error circle in the F814W image (object S1 in Figure 4.1), but the precision of our registration was insufficient to establish or rule out coincidence with the transient. We thus triggered the new *HST* observations with WFC3/UVIS, described above in Section 4.2, in order to obtain a more precise position.

We repeated the registrations as above, now using the new WFC3/UVIS F814W image and obtained improved rms astrometric uncertainties on the (x, y) position of the transient of (0.13, 0.20) ACS pixels or (0.″007, 0.″01) in the archival F814W image and 0.1 WFC3/IR pixels (0.″01) in the F110W image. We show the 3σ error ellipses on the position of the transient in each of these images in Figure 4.1. We performed PSF-fitting photometry on the archival *HST* images used for registration using

DOLPHOT. The nearest star detected in the 2015 F814W frame (object S1; 0.″06 from the transient location) is firmly outside the 3σ error ellipse. We note that there is an apparent source at the location of the transient in the archival F110W images, but it appears spatially extended and was not detected by DOLPHOT. Furthermore, the precise position of the transient is offset from the apparent centroid of this source. We thus find it is unlikely that the emission at the location is primarily due to the progenitor, and is more likely a blend of nearby, contaminating sources.

We then used DOLPHOT to obtain limits on the progenitor flux in the extensive archival coverage of the site with *HST*, including the images from 2005 with ACS/WFC in F435W, F555W, F814W, and F658N (PID: GO-10452; PI: S. Beckwith), 2012 with WFC3/UVIS in F689M and F673N (PID: GO-12762; PI: K. Kuntz), 2012 with WFC3/IR in F110W and F128N (PID: GO-12490; PI: J. Koda), 2014 with WFC3/UVIS in F275W and F336W (PID: GO-13340; PI: S. van Dyk), and 2015 with ACS/WFC in F606W and F814W (PID: GO-13804, PI: K. McQuinn). We adopt 5σ limiting magnitudes based on the detection significance of the faintest sources from DOLPHOT within a 100 pixel radius of the transient position. Our full set limits on the progenitor from *HST* are shown in Figure 4.4, converted to band luminosities (νL_ν) at the assumed distance to M51 and correcting for Galactic extinction.

Utilizing the extensive archival coverage in the four imaging channels of *Spitzer*/IRAC, we created deep stacks of all available images and registered them to the new *HST* imaging with an astrometric rms of 0.″4. A source consistent with the position of M51 OT2019-1 (0.″6 away) is clearly detected in the [4.5] stack. We do not see a clear point source at the location in the other channel stacks. Based on aperture photometry the source has a [4.5] flux of 0.0177 ± 0.0048 mJy and 3-σ limiting fluxes of < 0.014, < 0.073, and < 0.31 mJy in [3.6], [5.8], and [8.0], respectively. Given the high degree of crowding/blending with nearby emission at [4.5], our measurement of the flux of the putative progenitor may suffer contamination, but as we argue in more detail below and in Section 4.3, the majority of the flux is likely attributable to a single source.

We also examined archival imaging coverage of the site with the Multiband Imaging Photometer for *Spitzer* (MIPS) including 24 μm Super Mosaic (2004–2008 stack), and the 70 and 160 μm images from 2004 (PID: 159; PI: R. Kennicutt). We derive 3-σ limiting fluxes from aperture photometry of < 2.4, < 49.0, and 350.0 mJy in the three MIPS imaging bands, respectively. Similarly, we derived limits on the flux

of the progenitor from the available imaging coverage with the *Wide-field Infrared Survey Explorer* (*WISE*; Wright et al. 2010) from the AllWISE Image Atlas[11] at 3.4, 4.6, 12, and 22 μm. Our limits of 0.20, 0.41, 0.91, and 1.4 mJy in the four *WISE* channels, respectively, are typically less constraining than the corresponding limits from *Spitzer* largely due to the coarser spatial resolution in *WISE* imaging.

Using zero-magnitude fluxes (Vega system) given in the *Spitzer*/IRAC Handbook[12], we find the precursor source to have $M_{[4.5]} = -12.2$ mag and [3.6]−[4.5] $>$ 0.74 mag. Sources with these IR properties are exceptionally rare (Thompson et al. 2009; Khan et al. 2010), indicating that the [4.5] emission is likely associated with a single star, and furthermore the spatial coincidence with M51 OT2019-1 strongly suggests a physical association. The spectral energy distribution (SED) is markedly similar to those of the self-obscured progenitors of SN 2008S and NGC 300 OT2008-1 (see Figure 4.4). The best-fit blackbody, incorporating the [4.5] detection and [3.6], [5.8], and [8.0] limits, has a temperature of $T \approx 510$ K and luminosity of $L \approx 6.3 \times 10^4\ L_\odot$, though there is significant uncertainty in these parameters. Our constraints at wavelengths > 10 μm are also relatively weak. Thus, we are unable to rule out emission from cooler circumstellar dust that would indicate a more luminous (and hence more massive) progenitor.

Pre-explosion variability

We examined the considerable coverage of the location with *Spitzer*/IRAC at [3.6] and [4.5] for historical variability of the progenitor, including regular monitoring since 2014 as part of SPIRITS. The post-basic calibrated data (PBCD) level images were downloaded from the *Spitzer* Heritage Archive[13] and *Spitzer* Early Release Data Service[14] and processed through an automated image-subtraction pipeline (for details see Kasliwal et al. 2017b). For reference images, we used the Super Mosaics[15] consisting of stacks of images obtained between 2004 May 18 and 2006 January 29. In addition to the single epoch images, we performed image subtraction using

[11] Images are available here: `https://irsa.ipac.caltech.edu/applications/wise/`

[12] `https://irsa.ipac.caltech.edu/data/SPITZER/docs/irac/iracinstrumenthandbook/`

[13] `https://sha.ipac.caltech.edu/applications/Spitzer/SHA/`

[14] `http://ssc.spitzer.caltech.edu/warmmission/sus/mlist/archive/2015/msg007.txt`

[15] Super Mosaics are available as *Spitzer* Enhanced Imaging Products through the NASA/IPAC Infrared Science Archive: `https://irsa.ipac.caltech.edu/data/SPITZER/Enhanced/SEIP/overview.html`

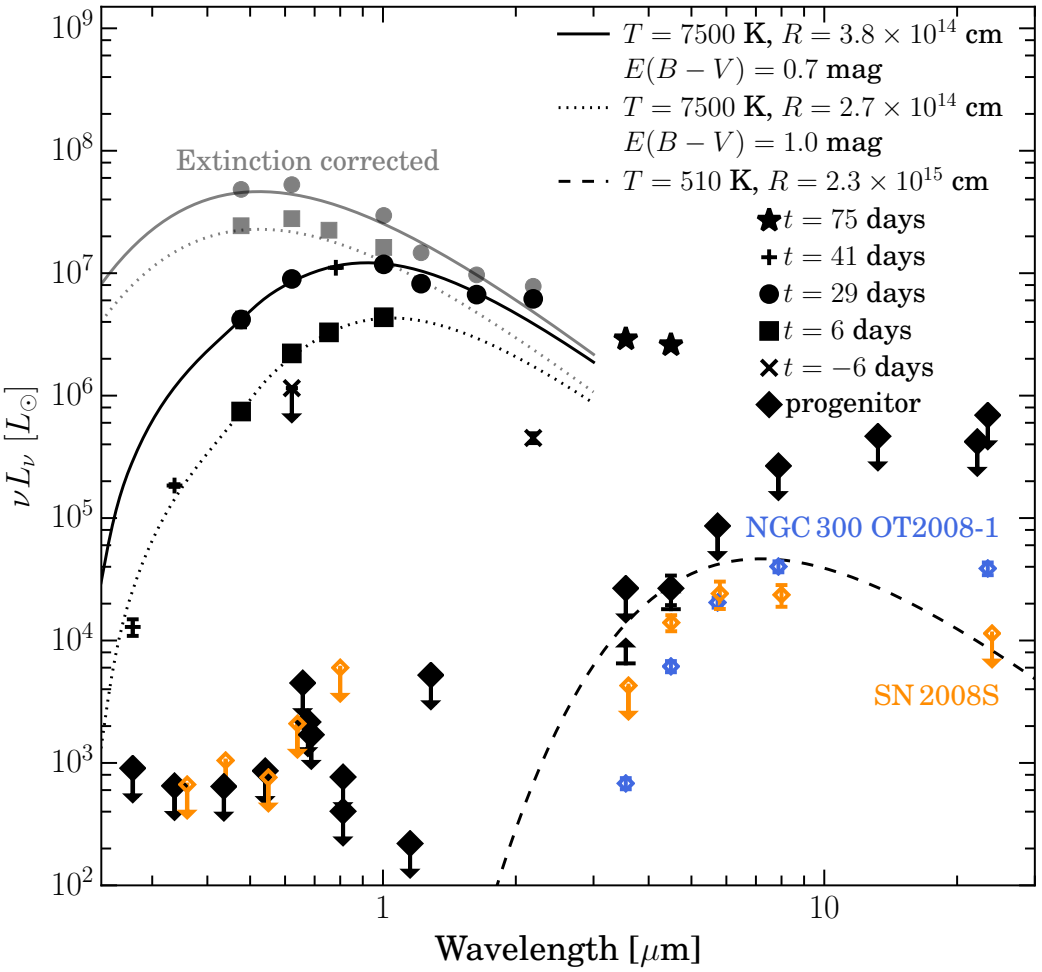

Figure 4.4: SEDs from photometry are shown in black for the M51 OT2019-1 progenitor (diamonds), and at multiple phases in the evolution of the transient (t = −6, 6, 29, 41, and 75 days as crosses, squares, circles, plusses, and stars, respectively). Upper limits from nondetections are indicated with downward arrows. Lower limits on the progenitor SED from image subtraction are also indicated by upward arrows in black. Blackbody approximations to the data are shown for the progenitor (dashed curve), t = 6 days SED on the rise (dotted) and t = 29 days SED on the plateau with radii and temperatures given in the legend. For post-discovery SEDs of the transient, the curves shown have been reddened by the amount listed. The corresponding dereddened data and blackbody curves are shown in gray. For comparison, the progenitor SED data are shown for NGC 300 OT2008-1 (open blue diamonds; Prieto 2008) and SN 2008S (open orange diamonds; Prieto et al. 2008).

the same references on our deep [3.6] and [4.5] stacks of all available pre-explosion imaging (described above in Section 4.3).

Aperture photometry was performed at the location of M51 OT2019-1 in the difference images, and our resulting differential light curves are shown in Figure 4.5, converted to band luminosities in νL_ν. During the years 2006–2008 ($\approx$ 3900–4400 days before discovery), our measurements are consistent with no change compared to the reference level within $|\Delta(\nu L_\nu)| \lesssim 10^4\ L_\odot$. In 2012 ($\approx$ 2400 days before discovery), we detect a significant, 4σ-level increase of $\Delta(\nu L_\nu) = (3.2 \pm 0.8) \times 10^4\ L_\odot$. Following this, in the time between 2014 and 2017 ($\approx$ 1600–500 days before discovery), we note a consistently elevated [4.5] flux at the location at $\Delta(\nu L_\nu) \approx 1.3 \times 10^4\ L_\odot$. In the final two epochs of *Spitzer* coverage, we detect a significant pre-explosion brightening starting sometime between $\approx$ 500 and 300 days before discovery, and rising to the level of $\Delta(\nu L_\nu) = (3.7 \pm 0.7) \times 10^4\ L_\odot$ at $t = -162.3$ days. At [3.6], the same trends in pre-explosion variability are evident, but at a lower level of significance. In the subtraction of our deep stacks, we detect significant excess flux compared to the reference level of $\Delta(\nu L_\nu) = (6.5 \pm 1.3) \times 10^3\ L_\odot$ at [3.6] and $\Delta(\nu L_\nu) = (1.8 \pm 0.4) \times 10^4\ L_\odot$ at [4.5], shown as the dashed–dotted lines and shaded regions in Figure 4.5.

While the [4.5] flux of the coincident precursor source measured in our deep pre-explosion stack may contain contamination from nearby sources (Section 4.3), the variable fluxes detected with image subtraction can be unambiguously attributed to a single source. Associating the variable precursor with the OT, these measurements are thus robust lower limits on the average, pre-explosion flux of the progenitor at [3.6] and [4.5] since 2004. We add these constraints on the progenitor SED to Figure 4.4.

We obtained constraints on pre-explosion optical variability at the location using the available coverage by the Palomar Transient Factory (Law et al. 2009; Rau et al. 2009) and its successor, the intermediate Palomar Transient Factory, (i)PTF (Cao, Nugent, and Kasliwal 2016), and ZTF on P48. For (i)PTF g and Mould-R band data taken between 2009 and 2016, we utilized forced PSF-fitting photometry at the transient location on the reference-subtracted difference images (Masci et al. 2017). The same procedure as described in Section 4.2 was used to obtain photometry from ZTF difference images for the entire set of g- and r-band images covering the site from the publicaly available ZTF-DR1, and the Caltech and Partnership surveys since the start of full operations in 2018 March. To obtain deeper limits,

we stacked our measurements from (i)PTF and ZTF within 10 day windows, and show the resulting differential optical light curves along with the IR measurements in Figure 4.5. We see no evidence for significant optical variability at the location in any of the archival P48 coverage at the level of $|\Delta(\nu L\nu)| \lesssim 2\times10^4$ and 3×10^4 $L_\odot$ in the R or r and g-bands, respectively, including during the 2012 and 2017–2018 [4.5] brightening episodes.

Photometric properties

The multiband optical and near-IR light curves of M51 OT2019-1 are shown in Figure 4.2. We observe a rise in the optical light curves over a time of $\approx$ 15 days after the first detection by ZTF, after which the source exhibits a relatively flat plateau in the g, r, i, and Y bands to at least $t = 40$ days. By $t \approx 50$ days, the light curves begin to decline, particularly noticeable in the g band. In the r band, the source is observed to peak at $M_r = -13.0$ (Galactic extinction correction only). The optical colors are remarkably red, with values on the rise of $g-r = 1.3\pm0.2$, $g-i = 1.9\pm0.2$, and $g - Y = 2.6 \pm 0.2$ mag at $t = 5.9$ days. On the plateau at $t = 25.9$ days, we observe bluer optical colors of $g - r = 0.97 \pm 0.05$, $g - i = 1.53 \pm 0.06$, and $g - Y = 1.8 \pm 0.1$ mag. In the near-IR, the source was detected 6.5 days before the earliest ZTF detection at $K_s = 18.2 \pm 0.3$, before rising to $K_s = 15.66 \pm 0.06$ at $t = 28.9$ days.

Given its red optical colors and location in a dark dust lane, it is likely that M51 OT2019-1 is subject to significant extinction. High amounts of optical extinction have also been inferred for similar transients of the ILRT class, but even among these, M51 OT2019-1 is exceptionally red. As shown in Figure 4.2, we estimate the excess reddening present in M51 OT2019-1 by comparing its optical light curves to those of the well-studied ILRTs SN 2008S (Botticella et al. 2009), NGC 300 OT2008-1 (Humphreys et al. 2011), PTF 10fqs (Kasliwal et al. 2011), and AT 2017be (Cai et al. 2018). After correcting the light curves for Galactic extinction, we require *excess* reddening of $E(B-V) \approx 0.7$, 0.5, 0.4, and 0.6 mag for each of those objects, respectively, to match the optical colors of M51 OT2019-1 near peak on the plateau.

The total extinction to M51 OT2019-1 at a given phase is likely due to a combination of attenuation by foreground dust in the host interstellar medium (ISM) as well as internal extinction by dust in the circumstellar medium (CSM). For NGC 300 OT2008-1, Humphreys et al. (2011) estimated the total extinction near

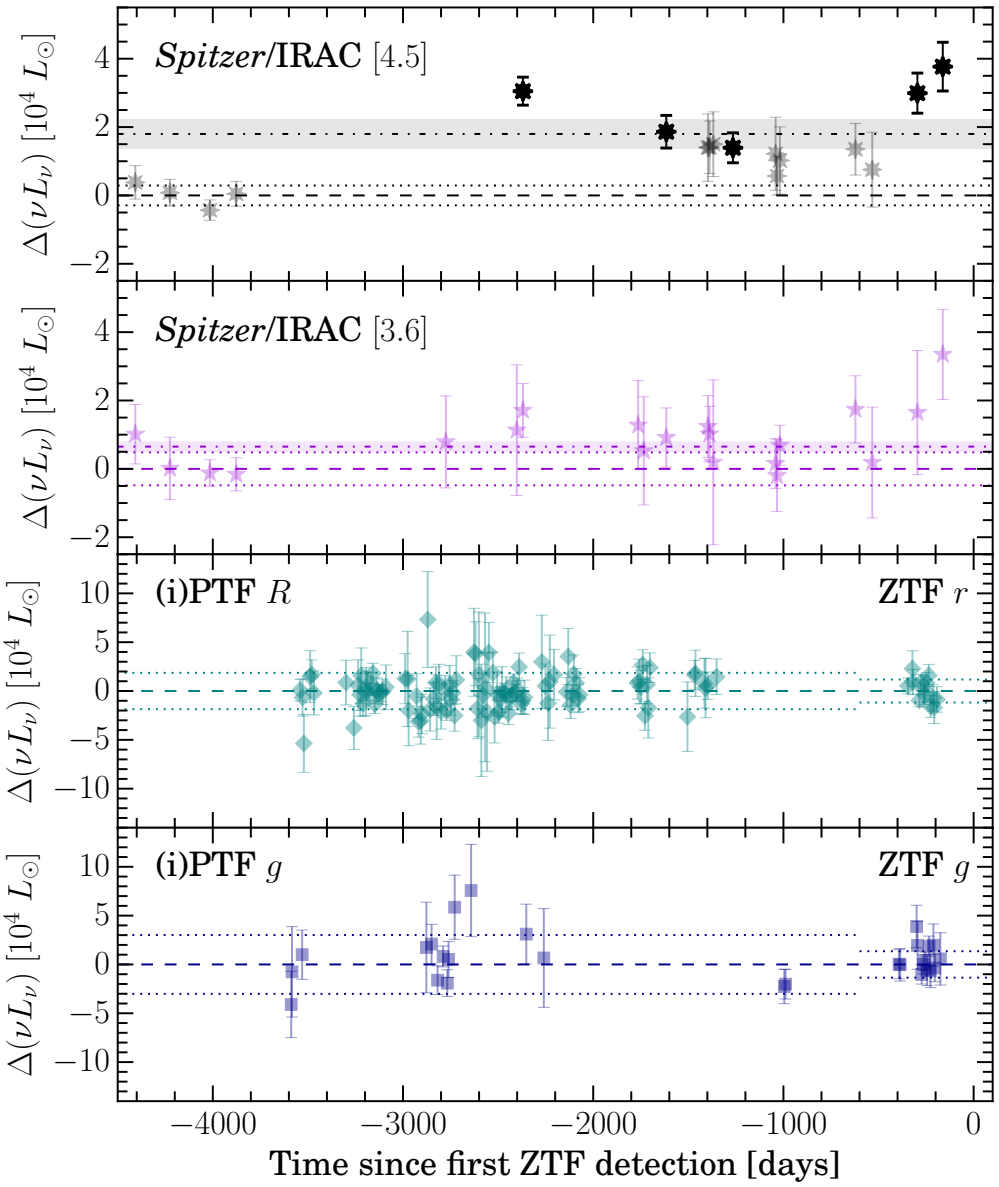

Figure 4.5: Constraints on pre-explosion variability based on image subtraction at the location of the transient in the IR with *Spitzer*/IRAC and optical with (i)PTF and ZTF. From top to bottom we show the differential light curves at the [4.5], [3.6], R or r, and g bands. The darker, solid black points in the [4.5] light curve highlight individual epochs where we detect variability of the progenitor at $>3\sigma$ significance. The dashed lines indicate the zero level, and dotted lines in each panel show the standard deviations of our measurements for the first four epochs of *Spitzer* imaging, and for the entire sets of (i)PTF and ZTF imaging. The dashed–dotted lines and shaded regions in the top two panels show the "average" differential luminosities and corresponding 1σ uncertainties measured in the subtraction of the reference Super Mosaic images from our deep stacks of all available pre-explosion *Spitzer*/IRAC [3.6] and [4.5] imaging.

the peak of the transient as $E(B-V) \approx 0.4$ mag based on comparing its optical colors to those expected for a temperature $T \approx 7500$ K inferred from the presence of F-type absorption features in the spectrum. A similar argument was made by Smith et al. (2009) to estimate a total host/CSM extinction to SN 2008S of $E(B-V) = 0.28$ mag.

As described below in Section 4.3, we observe similar absorption features in the spectra of M51 OT2019-1 throughout its evolution, and thus infer a similar temperature for the continuum emission. Our analysis of the SED derived from photometry at several phases in the evolution of the transient is shown in Figure 4.4. We observed an early brightening at $t = -6$ days in the near-IR K_s band to $\nu L_\nu \approx 4 \times 10^5\ L_\odot$ with a constraining r-band nondetection a few days later that suggests the explosion is heavily obscured at early times. At $t = 6$ days as the transient rises in the optical, comparing the SED to a reddened blackbody spectrum with $T = 7500$ K provides a good approximation to the data and suggests $E(B-V) = 1.0$ mag and a blackbody radius of $R \approx 2.7 \times 10^{14}$ cm. Near the optical peak on the plateau at $t = 29$ days, the SED appears less reddened, and can be approximated by $T = 7500$ K with $E(B-V) = 0.7$ mag and $R \approx 3.8 \times 10^{14}$ cm. The inferred expansion velocity from the evolution of the blackbody radius of ≈ 550 km s^{-1} is notably similar to the observed velocities widths of the Hα emission lines (≈ 400 km s^{-1}; Section 4.3). While some amount of extinction can likely be attributed to foreground host extinction, the variable extinction estimate from evolution of the SED indicates a significant contribution from internal CSM dust. In particular, we suggest the color evolution of the SED from rise to peak may be attributed to the continued destruction of CSM dust as the explosion emerges from the dense obscuring wind of the progenitor.

The luminosity of the corresponding unreddened blackbody is $L = 8.3 \times 10^7\ L_\odot$, which we adopt as a crude estimate of the intrinsic bolometric luminosity of the explosion at peak. In comparison, the most luminous classical novae reached peak luminosities from ≈ 3–$8 \times 10^5\ L_\odot$ (Gallagher and Ney 1976; Gehrz et al. 2015), while typical CCSNe reach 5×10^8 to $\gtrsim 10^{10}\ L_\odot$ (e.g., Valenti et al. 2016). We note, however, the reddened blackbody model significantly overpredicts the observed Y-band flux at this epoch. We also see evidence for an IR excess in the near-IR K_s-band measurement at $t = 29$ days and the later [3.6] and [4.5] measurements from *Spitzer* at $t = 75$ days, suggesting emission from dust is an important component of the SED. Finally, in the SED at $t = 41$ days from our *HST* observations (plus symbols in Figure 4.4), the measurement in F814W lies near the expectation from

the reddened blackbody approximation to the $t = 29$ day SED, consistent with the flat evolution of the i'-band light curves between these epochs; however, the F336W and F275W points are significantly below this expectation, suggesting that there may be additional suppression of the flux in the blue and UV (e.g., line blanketing and/or Balmer continuum absorption) and/or that the assumed Fitzpatrick (1999) $R_V = 3.1$ extinction law for the diffuse Milky Way ISM may not applicable for heavy internal extinction by circumstellar dust, especially at bluer wavelengths. Additional longer wavelength measurements from ongoing monitoring with *Spitzer* and self-consistent modeling of the time evolution of the SED will be necessary to better constrain the intrinsic properties of the explosion and the CSM dust.

In the right panel of Figure 4.2, we compare the r-band light curve of M51 OT2019-1 to other hydrogen-rich transients. For the sample of ILRTs, we correct for an estimate of the total extinction based on the SED near peak as described above. Assuming $E(B-V) = 0.7$ mag for M51 OT2019-1, the peak absolute magnitude is $M_r \approx -15$. This is notably more luminous than the other proposed members of this class, which fall between $M_{r/R} \approx -13$ to -14, and is near the range more typical of Type II core-collapse SNe. In fact, with our assumed extinction, M51 OT2019-1 is even more luminous than some low-luminosity Type IIP SNe, e.g., SN 2005cs (Pastorello et al. 2006).

Spectroscopic properties

Our spectroscopic observations of M51 OT2019-1 from $t = 4$ to 111 days are shown in Figure 4.3. Here, we briefly describe the important spectral properties and features observed in this event, but reserve a detailed analysis of their evolution to future, more comprehensive studies. The spectra are characterized by a very red continuum, and display prominent Hα emission along with emission features of the Ca II IR triplet ($\lambda\lambda$ 8498, 8542, 8662) and [Ca II] ($\lambda\lambda$ 7291, 7324). We detect the Ca II H and K lines ($\lambda\lambda$ 3968, 3934), the Na I D doublet ($\lambda\lambda$ 5889, 5895), and a strong O I blend near 7773 Å in absorption. Superimposed on the broader emission features, we also detect a narrower absorption component for each of the lines of the Ca II triplet. In the near-IR spectrum at $t = 29$ days (top right panel of Figure 4.3), we see additional recombination lines of H in emission including Paβ and weaker Paγ. In our latest spectrum at $t = 111$ days, the continuum has grown notably redder, and the Ca II triplet features have transitioned to predominantly narrower emission features.

These features indicate a wide range of densities in the gas producing the spectrum—reminiscent of a wind or ejected envelope with large inhomogeneities. The observed [Ca II] $\lambda\lambda$ 7291, 7324 lines have a critical density of $n_{\rm cr} \sim 10^7$ cm^{-3} (Ferland and Persson 1989) and are strongly suppressed at higher densities. On the other hand, the O I λ7773 transition, a quintet frequently observed in transients, is normally populated by collisional transfer from the O I 3p ^{3}P level, which is itself strongly excited by a wavelength coincidence between the H I Ly β and O I λ1026 transitions (Bowen 1947). The triplet-to-quintet collisional transfer is only effective at densities $n \gtrsim 10^{11}$ cm^{-3} (Williams 2012), thus demonstrating a wide range of densities in the gas ejected by the outburst.

Furthermore, as discussed by Humphreys et al. (2011) for NGC 300 OT2008-1, the Ca II and [Ca II] emission lines are sensitive to conditions in the ejecta and clearly evolve with time. The triplet emission lines are formed in the ejecta by radiative de-excitation of electrons in upper levels of the Ca II H and K absorption transitions, leaving the electrons in the upper levels of the [Ca II] lines (Ferland and Persson 1989). Typically, these electrons are collisionally de-excited to the ground state, unless the densities are low enough. Following Humphreys et al. (2011) and Humphreys et al. (2013), we can estimate the fraction of photons that are radiatively de-excited from the ratio of the equivalent widths of the [Ca II] lines to the Ca II triplet, times the ratio of the expected fluxes for the continuum emission at the corresponding wavelengths of 7300 and 8600 Å. Assuming a 7500 K blackbody for the continuum, we estimate photon fractions of ≈ 0.25 and 0.3 in our $t = 5$ and 44 day spectra, respectively, but find a lower value of ≈ 0.1 at $t = 111$ days. This is remarkably similar to the evolution for NGC 300 OT2008-1. As suggested by Humphreys et al. (2011), the decline in the photon ratio at later times may indicate an increase in the density where the [Ca II] lines are formed in the ejecta.

The Hα velocity profiles (bottom right panel of Figure 4.3) appear symmetric about their peaks, which are consistent with zero velocity in the rest frame of M51. The profiles are characterized by a FWHM velocity of ≈ 400 km s^{-1}, much lower than typical velocities observed in CCSNe of $\sim 10,000$ km s^{-1}, with broader Thomson-scattering wings extending to ≈ 2000 km s^{-1}, similar to those seen in NGC 300 OT2008-1 (Humphreys et al. 2011). The $t = 5$ days GMOS spectrum shows an apparent absorption feature near ≈ -180 km s^{-1}, but we attribute this to a data reduction artifact from oversubtraction of unrelated, background Hα emission and difficultly in finding a suitably clean region for background subtraction along

the slit. We do not see any evidence for significant evolution in the line profile shape or width for the duration of the observations presented here.

The observed absorption spectrum is reminiscent of an F-supergiant. This is expected for an eruption that produces an extended, optically thick wind (Davidson 1987), and is seen in LBVs/S Doradus variables in their cool, outburst state at maximum (Humphreys and Davidson 1994), some SN impostors and LBV giant eruptions (e.g. Smith et al. 2011), and is very similar to that of NGC 300 OT2008-1 (Bond et al. 2009; Humphreys et al. 2011) and SN 2008S (Smith et al. 2009). This suggests a temperature of $\approx$ 7500 K. The red continuum is therefore suggestive of significant extinction, and we apply this temperature estimate to our SED analysis in Section 4.3 to obtain $E(B-V) = 0.7$ mag near the peak at $t = 29$ days. Overall, the spectral features described above are generally similar to some previously observed SN impostors and ILRTs.

4.4 Discussion and conclusions

From our early observations of M51 OT2019-1, we find that the transient is characterized by a $\approx$ 15 day rise in the optical to an observed plateau luminosity of $M_r = -13$ (Galactic extinction correction only). Its spectrum shows strong Hα emission with FWHM velocities of $\approx$ 400 km s^{-1}. These basic properties are similar to those of multiple classes of transients with luminosities intermediate between those of novae and supernovae, including ILRTs, LRNe, and giant eruptions of LBVs. The photometric evolution of M51 OT2019-1 has transitioned smoothly from the rise to a plateau and subsequent smooth decline after $t \approx 50$ days, consistent with ILRTs and also similar to some SN impostors. It is more dissimilar to LRNe whose light curves are typically irregular and multi-peaked (Sparks et al. 2008; Smith et al. 2016; Blagorodnova et al. 2017) and some other LBV eruptions that may show multiple outbursts or erratic variability (Pastorello et al. 2010; Smith et al. 2010). Our optical spectra show several additional features, including Ca II and [Ca II] in emission, F-type absorption features indicating the light is escaping an optically thick wind at $\approx$ 7500 K, and a red continuum indicative of significant extinction. These features are characteristic of ILRTs, but may also be seen in LRNe and giant LBV eruptions. For example, while some LBV eruptions show bluer continua and H lines with strong P Cygni profiles (e.g., NGC 3432 OT; Pastorello et al. 2010), others are indistinguishable from ILRTs (Smith et al. 2010; Smith et al. 2011; Rest et al. 2012; Prieto et al. 2014). We identify a likely progenitor star in archival *Spitzer* imaging with $M_{[4.5]} = -12.2$ mag and $[3.6]-[4.5] > 0.74$ mag, but there

is no detected optical counterpart in archival *HST* imaging. This is reminiscent of properties of the obscured progenitors of SN 2008S and NGC 300 OT2008-1. We thus suggest M51 OT2019-1 is an ILRT, but with only weak archival constraints at longer wavelengths, we cannot rule out that the progenitor of M51 OT2019-1 is more luminous and massive than the 9–15 $M_{\odot}$ stars inferred for the ILRT prototypes.

The nature of ILRTs, the mechanism behind their outbursts, and their relation to other impostors and LBV-related transients are debated. One proposed physical scenario involves a weak explosion, possibly the electron-capture-induced collapse of an extreme asymptotic giant branch (AGB) star. In this scenario, an initial flash rapidly destroys the enshrouding circumstellar dust, which later reforms and re-obscures the optical transient (Thompson et al. 2009; Kochanek 2011a; Szczygieł et al. 2012). Thanks to the early discovery of M51 2019OT-1, we find evidence for continued dust destruction during the rise of the transient as our estimate of the reddening evolves from $E(B-V) = 1.0$ to 0.7 mag between $t = 6$ and 29 days, posing a challenge to such interpretations for this event. Alternatively, Humphreys et al. (2011) suggested that the progenitors of NGC 300 OT2008-1 and, by extension, SN 2008S may have been post-AGB stars in transition to warmer temperatures, thus near their Eddington limits and subject to a range of instabilities. Adopting $E(B-V) = 0.7$ mag at peak for M51 OT2019-1, the intrinsic luminosity is $M_r = -15$ mag, higher than previously observed ILRTs, though not unusual for some LBV-related SN impostors (Smith et al. 2011), possibly suggesting that these events may represent a continuum of related, explosive phenomena arising from evolved progenitors spanning a wide range of masses. Finally, the observed IR variability of the likely progenitor may be consistent with a long-period ($\sim$ 2000 days), thermally pulsing super-AGB (see the candidate super-AGB MSX SMC 055; Groenewegen et al. 2009), or may hint at eruptive, self-obscuring episodes occurring in the years before the explosion. A complete picture of the event awaits continued monitoring, including ongoing *Spitzer* observations, to characterize the full SED, dust properties, and energetics. Longer-term, mid-IR spectroscopic observations with the *James Webb Space Telescope* will disentangle the chemistry, and late-time imaging after the explosion fades away will provide definitive evidence on whether the explosion was terminal.

We thank J. Prieto and E. Ofek for valuable discussions in revising this work. We also thank the anonymous referee for their helpful comments, which improved the manuscript.

This material is based upon work supported by the National Science Foundation

Graduate Research Fellowship under grant No. DGE-1144469. H.E.B. acknowledges support from program numbers GO-14258 and AR-15005, provided by NASA through grants from the Space Telescope Science Institute, which is operated by the Association of Universities for Research in Astronomy, Incorporated, under NASA contract NAS5-26555. This work is part of the research programme VENI, with project number 016.192.277, which is (partly) financed by the Netherlands Organisation for Scientific Research (NWO). A.G.-Y. is supported by the EU via ERC grant No. 725161, the ISF, the BSF Transformative program and by a Kimmel award. R.D.G. was supported by NASA and the United States Air Force. Based on observations obtained with the Samuel Oschin Telescope 48 inch and the 60 inch Telescope at the Palomar Observatory as part of the Zwicky Transient Facility project. ZTF is supported by the National Science Foundation under grant No. AST-1440341 and a collaboration including Caltech, IPAC, the Weizmann Institute for Science, the Oskar Klein Center at Stockholm University, the University of Maryland, the University of Washington, Deutsches Elektronen-Synchrotron and Humboldt University, Los Alamos National Laboratories, the TANGO Consortium of Taiwan, the University of Wisconsin at Milwaukee, and Lawrence Berkeley National Laboratories. Operations are conducted by COO, IPAC, and UW. This work was supported by the GROWTH project funded by the National Science Foundation under grant No. 1545949. SED Machine is based upon work supported by the National Science Foundation under Grant No. 1106171. The work presented here is based on observations obtained with the Apache Point Observatory 3.5 m telescope, which is owned and operated by the Astrophysical Research Consortium. We thank the Apache Point Observatory Observing Specialists for their assistance during the observations. The data presented here were obtained in part with ALFOSC, which is provided by the Instituto de Astrofisica de Andalucia (IAA) under a joint agreement with the University of Copenhagen and NOTSA. Based on observations obtained at the Gemini Observatory acquired through the Gemini Observatory Archive and processed using the Gemini IRAF package, which is operated by the Association of Universities for Research in Astronomy, Inc., under a cooperative agreement with the NSF on behalf of the Gemini partnership: the National Science Foundation (United States), National Research Council (Canada), CONICYT (Chile), Ministerio de Ciencia, Tecnología e Innovación Productiva (Argentina), Ministério da Ciência, Tecnologia e Inovação (Brazil), and Korea Astronomy and Space Science Institute (Republic of Korea). Some of the data presented herein were obtained at the W. M. Keck Observatory, which is operated as a scientific partnership among

the California Institute of Technology, the University of California and the National Aeronautics and Space Administration. The Observatory was made possible by the generous financial support of the W. M. Keck Foundation. The authors wish to recognize and acknowledge the very significant cultural role and reverence that the summit of Maunakea has always had within the indigenous Hawaiian community. We are most fortunate to have the opportunity to conduct observations from this mountain. This work is based in part on observations made with the *Spitzer Space Telescope*, which is operated by the Jet Propulsion Laboratory, California Institute of Technology under a contract with NASA. Based on observations made with the NASA/ESA *Hubble Space Telescope*, obtained from the Data Archive at the Space Telescope Science Institute, which is operated by the Association of Universities for Research in Astronomy, Inc., under NASA contract NAS 5-26555. Some of these observations are associated with program #15675. This publication makes use of data products from the *Wide-field Infrared Survey Explorer*, which is a joint project of the University of California, Los Angeles, and the Jet Propulsion Laboratory/California Institute of Technology, funded by the National Aeronautics and Space Administration. This research has made use of the NASA/IPAC Extragalactic Database (NED), which is operated by the Jet Propulsion Laboratory, California Institute of Technology, under contract with the National Aeronautics and Space Administration.

Chapter 5

THE SPIRITS 2014–2018 SAMPLE OF LUMINOUS INFRARED TRANSIENTS: UNCOVERING HIDDEN SUPERNOVAE AND DUSTY STELLAR OUTBURSTS IN NEARBY GALAXIES

Jencson, Jacob E., et al. 2019. "The SPIRITS Sample of Luminous Infrared Transients: Uncovering Hidden Supernovae and Dusty Stellar Outbursts in Nearby Galaxies". *ApJ* 886 (1): 40. doi:10.3847/1538-4357/ab4a01. arXiv: 1901.00871 [astro-ph.HE].

Jacob E. Jencson[1], Mansi M. Kasliwal[1], Scott M. Adams[1], Howard E. Bond[2,3], Kishalay De[1], Joel Johansson[4], Viraj Karambelkar[5], Ryan M. Lau[1,6], Samaporn Tinyanont[1], Stuart D. Ryder[7,8], Ann Marie Cody[9], Frank J. Masci[10], John Bally[11], Nadejda Blagorodnova[12], Sergio Castellón[13], Christoffer Fremling[1], Robert D. Gehrz[14], George Helou[10], Charles D. Kilpatrick[15], Peter A. Milne[16], Nidia Morrell[13], Daniel A. Perley[17], M. M. Phillips[13], Nathan Smith[16], Schuyler D. van Dyk[10], and Robert E. Williams[3,15]

[1]Division of Physics, Mathematics and Astronomy, California Institute of Technology, Pasadena, CA 91125, USA
[2]Department of Astronomy & Astrophysics, Pennsylvania State University, University Park, PA 16802, USA
[3]Space Telescope Science Institute, 3700 San Martin Dr., Baltimore, MD 21218, USA
[4]Department of Physics and Astronomy, Division of Astronomy and Space Physics, Uppsala University, Box 516, SE 751 20 Uppsala, Sweden
[5]Department of Physics, Indian Institute of Technology Bombay, Mumbai 400076, India
[6]Institute of Space & Astronautical Science, Japan Aerospace Exploration Agency, 3-1-1 Yoshinodai, Chuo-ku, Sagamihara, Kanagawa 252-5210, Japan
[7]Australian Astronomical Observatory, 105 Delhi Road, North Ryde, NSW 2113, Australia
[8]Department of Physics & Astronomy, Macquarie University, NSW 2109, Australia
[9]NASA Ames Research Center, Moffet Field, CA 94035, USA
[10]Caltech/IPAC, Mailcode 100-22, Pasadena, CA 91125, USA
[11]Astrophysical and Planetary Sciences Department University of Colorado, UCB 389, Boulder, CO 80309, USA
[12]Department of Astrophysics/IMAPP, Radboud University, Nijmegen, The Netherlands
[13]Las Campanas Observatory, Carnegie Observatories, Casilla 601, La Serena, Chile
[14]Minnesota Institute for Astrophysics, School of Physics and Astronomy, University of Minnesota, 116 Church Street SE, Minneapolis, MN 55455, USA
[15]Department of Astronomy and Astrophysics, University of California, Santa Cruz, CA 95064, USA
[16]University of Arizona, Steward Observatory, 933 N. Cherry Avenue, Tucson, AZ 85721, USA
[17]Astrophysics Research Institute, Liverpool John Moores University, IC2, Liverpool Science Park, 146 Brownlow Hill, Liverpool L3 5RF, UK

Abstract

We present a systematic study of the most luminous ($M_{\rm IR}$ [Vega mag] brighter than -14) infrared (IR) transients discovered by the *SPitzer* InfraRed Intensive Transients Survey (SPIRITS) between 2014 and 2018 in nearby galaxies ($D < 35$ Mpc). The sample consists of nine events that span peak IR luminosities of $M_{[4.5],\rm peak}$ between -14 and -18.2, show IR colors between $0.2 < ([3.6]-[4.5]) < 3.0$, and fade on timescales between 55 days $< t_{\rm fade} <$ 480 days. The two reddest events ($A_V > 12$) show multiple, luminous IR outbursts over several years and have directly detected, massive progenitors in archival imaging. With analyses of extensive, multiwavelength follow-up, we suggest the following possible classifications: five obscured core-collapse supernovae (CCSNe), two erupting massive stars, one luminous red nova, and one intermediate luminosity red transient. We define a control sample of all optically discovered transients recovered in SPIRITS galaxies and satisfying the same selection criteria. The control sample consists of eight CCSNe and one Type Iax SN. We find that 7 of the 13 CCSNe in the SPIRITS sample have lower bounds on their extinction of $2 < A_V < 8$. We estimate a nominal fraction of CCSNe in nearby galaxies that are missed by optical surveys of $38.5^{+26.0}_{-21.9}$% (90% confidence). This study suggests that a significant fraction of CCSNe may be heavily obscured by dust and therefore undercounted in the census of nearby CCSNe from optical searches.

5.1 Introduction

While there are now several known classes of stellar transient phenomena for which the observable emission is predominantly infrared (IR), exploration of the landscape of IR-dominated transients is just beginning. Often due to the effects of astrophysical dust, a host of eruptive and explosive stellar phenomena may be best observed in the IR. In particular, otherwise optically luminous transients such as supernovae (SNe) may be significantly obscured by dust in their host galaxies and/or local environments. Dust in the immediate circumstellar environment of a luminous transient, which may have condensed in a steady wind of the progenitor or formed during previous eruptive mass-loss events, may also efficiently reprocess shorter-wavelength emission into the IR. Some transients, particularly those associated with cool, low-velocity outflows, are themselves copious dust producers, leading to IR-dominated spectral energy distributions (SEDs).

Since 2014, we have been conducting the *SPitzer* InfraRed Intensive Transients Survey (SPIRITS; PIDs 11063, 13053, 14089; PI M. Kasliwal, Kasliwal et al. 2017b)

to discover transients in nearby $D \lesssim 35$ Mpc galaxies using the 3.6 and 4.5 μm imaging bands ([3.6] and [4.5]) of the Infrared Array Camera (IRAC; Fazio et al. 2004) on board the warm *Spitzer* Space Telescope (*Spitzer*; Werner et al. 2004; Gehrz et al. 2007). In this paper, we focus on a thorough investigation of all luminous ($M_{[4.5]}$ [Vega mag] brighter than -14) IR transients discovered by SPIRITS in the past 5 yr (Section 5.2). We compare this sample to a well-defined control sample of all optically discovered and spectroscopically classified transients hosted by SPIRITS galaxies and satisfying the same selection criteria (Section 5.2). Our sample of luminous infrared transients may represent diverse origins, including obscured core-collapse supernovae (CCSNe) and other known classes of IR-dominated transients such as stellar mergers or massive-star eruptions (MSEs).

CCSNe, the explosive deaths of stars of initial masses $\gtrsim 8\ M_{\odot}$, are now found in numbers exceeding several hundreds of events per year by numerous, primarily optical, searches. Arising from recently formed, massive stars, CCSNe may be subject to significant extinction from the dusty regions of active star formation in their host galaxies. The fraction of CCSNe missed optically owing to the obscuring effects of dust is therefore an important consideration for measurements of the CCSN rate (e.g., Grossan et al. 1999; Maiolino et al. 2002). Horiuchi et al. (2011) claimed that half of all SNe were missing from observed CCSN rate estimates in comparison to the rate of massive star formation both locally and across cosmic time from redshifts $0 < z < 1$; however, other studies have found better agreement (e.g., Cappellaro et al. 2015). Accounting for obscured or otherwise optically dim CCSNe may also resolve this discrepancy (e.g., Mannucci, Della Valle, and Panagia 2007; Mattila et al. 2012). Direct searches for CCSNe at wavelengths less sensitive to extinction are thus required to accurately measure the CCSN rate. Significant work (e.g., Varenius et al. 2017; Kool et al. 2018, and references therein; see discussion in Section 5.7) has been dedicated to uncovering extinguished CCSNe in the densely obscured and highly star forming regions of starburst and (ultra)luminous infrared galaxies (U/LIRGS). In contrast, our SPIRITS sample focuses on local galaxies encompassing a wide variety of galaxy morphologies, masses, and star-formation rates with unbiased sampling of all environments within galaxies (Section 5.2).

Other categories of luminous IR transients include intermediate luminosity red transients (ILRTs), luminous red novae (LRNe), and giant eruptions of luminous blue variables (LBVs)[1]. The prototypical objects for ILRTs are the "impostor" SN 2008S

[1]Distinguishing among classes of hydrogen-rich, intermediate-luminosity transients is difficult,

and the 2008 transient in NGC 300 (NGC 300 OT2008-1; Bond et al. 2009), suggested to be explosions of ≈10–15 $M_\odot$ stars, possibly extreme asymptotic giant branch (AGB) stars, self-obscured by a dusty wind (Prieto et al. 2008; Bond et al. 2009; Thompson et al. 2009). Extragalactic LRNe are believed to be massive analogs of stellar mergers observed in the Galaxy, including the striking example of the ≈1–3 $M_\odot$ contact binary merger V1309 Sco (Tylenda et al. 2011) and the B-type stellar merger V838 Mon (Bond et al. 2003; Sparks et al. 2008). While sharing many observational properties with, e.g., ILRTs, a key difference is that LRNe have surviving remnants (e.g., NGC 4490 OT2011-1; Smith et al. 2016). Surviving dust in the circumstellar environments of LBVs may also result in an observed IR excess during some nonterminal giant eruptions (e.g., η Carinae and other "η Carinae variables"; Humphreys, Davidson, and Smith 1999, UGC 2773OT; Smith et al. 2010).

It is particularly telling that known examples and even class prototypes of known IR-dominated events have almost exclusively been identified via their optical emission. It has been proposed, for example, that early dust formation in some LRNe may even entirely obscure or dramatically shorten the optical luminosity peak, while still producing a bright, long-lived infrared transient (e.g., Metzger and Pejcha 2017). Kashi and Soker (2017) have also suggested that dense, equatorial material may obscure transients driven by strong binary interactions, but that dust formation in polar outflows may still power IR emission in these events. As suggested by Bally and Zinnecker (2005), dynamical interactions of massive, compact-multiple systems in star-forming regions may also produced luminous transients, the energy released likely emerging in the IR given their densely obscured environments (see also recent events in the Galactic star-forming regions Sh2-255 and NGC 6334; Caratti o Garatti et al. 2017; Hunter et al. 2017; Brogan et al. 2018). SPIRITS overcomes the selection biases of optical discovery and is sensitive to redder events that may

as they may share many observational properties, and the nomenclature referring to these classes varies throughout the literature. We use the term "giant eruption" to refer to the class of events associated with LBVs, also variously referred to as "SN impostors" or "η Carina variables" (Humphreys, Davidson, and Smith 1999; Van Dyk et al. 2000; Pastorello et al. 2010; Smith et al. 2010; Smith 2014). We use the term "intermediate-luminosity red transient" (ILRT; originally suggested by Bond et al. 2009) specifically to refer the class of impostors similar to the prototypes SN 2008S and NGC 300 OT2008-1, whose self-obscured progenitors are believed to be less massive than classical LBVs. We use the term "luminous red nova" (LRN; e.g. Kulkarni et al. 2007) to specifically to refer to events believed to be associated with stellar mergers or common envelope ejections. This is similar to the nomenclature used by, e.g., Kashi and Soker (2016), who also adopted the umbrella term "intermediate-luminosity optical transient" of Berger et al. (2009) to refer to all three of these classes together.

lack optical counterparts altogether (e.g., the recently discovered eSPecially Red Intermediate-luminosity Transient Events [SPRITEs]; Kasliwal et al. 2017b).

We have undertaken extensive follow-up, including optical/IR photometry, spectroscopy, and radio imaging to characterize the nature of each luminous IR transient presented in this work (Section 5.3). We describe our analysis of the full data set, including host galaxy properties, progenitor constraints, photometric evolution, spectroscopic feature identification, and extinction estimates, in Section 5.4. In Section 5.5, we combine all available observational constraints in comparison to well-studied objects and attempt classify each luminous SPIRITS transient. In Section 5.6, we discuss the A_V distribution of nearby, luminous IR transients and CCSNe in particular, and in Section 5.7, we derive statistically robust estimates of the rate of CCSNe missed in nearby galaxies relative to the control sample of optically discovered CCSNe in SPIRITS galaxies. Finally, in Section 5.8, we summarize the main results and conclusions of this work.

5.2 Survey design and sample selection

Galaxy sample and imaging cadence

A full description of the SPIRITS survey design is given in Kasliwal et al. (2017b). It is a targeted search of nearby galaxies using the $5 \times 5'$ field of view of the IRAC camera. SPIRITS monitored a sample of 190 nearby galaxies for 3 yr from 2014 to 2016. The sample was selected based on the following criteria: (1) The 37 galaxies within 5 Mpc including both early- and late-type galaxies, dwarf galaxies, and giant galaxies, (2) the 116 most luminous galaxies between 5 and 15 Mpc, including 83% of the B-band starlight within 15 Mpc, and (3) the 37 most luminous and massive galaxies in the Virgo Cluster at 17 Mpc.

In 2014, each galaxy was observed 3 times at ~1-month and ~6-month intervals. In 2015-2016, baselines of 1- and 3-week timescales were added. In 2017–2018, the galaxy sample was reduced to focus on only the 105 galaxies most likely to host new transients and SNe, including the 58 galaxies that had previously hosted at least one IR transient, and the 47 remaining most luminous and star-forming galaxies ($L > 2 \times 10^{10}\ L_{\odot}$). Our cadence was also reduced to ~6-month intervals, typically with one observation per galaxy per visibility window. Each SPIRITS observation consists of seven dithered 100 s exposures in both IRAC bands. The nominal 5σ point-source limiting magnitudes of these observations are 20.0 and 19.1 at [3.6] and [4.5], respectively, using the zero-magnitude fluxes given in the IRAC instrument

handbook[2] of $F_{\nu 0}$ = 280.9 Jy for [3.6] and $F_{\nu 0}$ = 179.7 Jy for [4.5].

Image subtraction and transient identification

For reference images, we make use of archival *Spitzer* frames, including Super Mosaics[3] or S4G (*Spitzer* Survey of Stellar Structure in Galaxies; PID 61065; PI K. Sheth; Sheth et al. 2010; Muñoz-Mateos et al. 2013; Querejeta et al. 2015), or stacks of archival "bcd" images (where Super Mosaics or S4G images were not available). Further details of our image subtraction and transient identification pipelines are provided in Kasliwal et al. (2017b). Transient candidates automatically identified in by our pipeline in reference-subtracted images are vetted by human scanners, and sources passing human vetting are saved to our database and assigned a SPIRITS name.

Photometry is performed at the location of SPIRITS transients in the reference-subtracted images using a 4 mosaicked pixel (2.″4) aperture and background annulus from 4 to 12 pixels (2.″4–7.″2). The extracted flux is multiplied by the aperture corrections of 1.215 for [3.6] and 1.233 for [4.5], as described in the IRAC instrument handbook, and converted to Vega system magnitudes using the handbook-defined zero-magnitude fluxes for each IRAC channel.

Luminous IR transient sample selection

We selected events that peaked at $M_{\rm IR}$ brighter than −14 ($\nu L_\nu > 1.5 \times 10^5\ L_\odot$ at [4.5]) in either the [3.6] channel or [4.5] channel of *Spitzer*/IRAC during SPIRITS observations[4]. We further required at least two SPIRITS detections, to ensure that each event is astrophysically real and that the transients were not present in the first epoch of SPIRITS imaging, so that the age of the event is constrained by SPIRITS data. We list basic properties for these objects in Table 5.1. SPIRITS 14buu (first presented in Jencson et al. 2017e) was identified in the first epoch of SPIRITS imaging of the galaxy IC 2163. As such, we have no constraint on the age of this object from SPIRITS data, and thus we exclude it from the primary sample. The

[2] `http://irsa.ipac.caltech.edu/data/SPITZER/docs/irac/iracinstrumenthandbook/`

[3] Super Mosaics are available as Spitzer Enhanced Imaging Products through the NASA/IPAC Infrared Science Archive: `https://irsa.ipac.caltech.edu/data/SPITZER/Enhanced/SEIP/overview.html`

[4] The full sample of SPIRITS transients includes many lower-luminosity events, including IR detections of classical novae (e.g., M81 possible nova AT 2018akh; Jencson et al. 2018d), and events belonging to the diverse and mysterious class of objects called SPRITEs, first described by Kasliwal et al. (2017b). These events are outside the scope of this work and will be studied in future publications.

sample then consists of nine events discovered in SPIRITS between 2014–2018 that, to our knowledge, were not identified and spectroscopically classified by any other survey[5]. The *Spitzer*/IRAC [4.5] discovery images for each object, including the new science frame, reference image, and science-minus-reference subtractions, are shown in Figure 5.1.

Optically discovered control sample

To place our sample of luminous IR transients in context, we define a control sample of optically discovered and classified transients recovered during normal operation of the SPIRITS survey, employing the same selection criteria as for the IR-selected sample. A total of 14 such transients hosted by SPIRITS galaxies and discovered at optical wavelengths have been reported since the start of the survey in 2014. We summarize basic properties of these events in Table 5.2.

Three events, SN 2014C (Type Ib/IIn), SN 2014J (Type Ia), and SN 2014L (Type Ic), were present in the first epoch of SPIRITS observations such that we would not have a meaningful constraint on the explosion epoch from SPIRITS data alone. Two additional events were not recovered in SPIRITS by our automated image subtraction and transient identification pipeline owing to saturation of the IRAC detector at the location of the transient. SN 2014bc (Type II) was located only $3\farcs4$ from the bright nucleus of NGC 4258, which is saturated in all epochs of SPIRITS imaging. SN 2016adj (Type Ib), the nearest object in the optically discovered sample at only 3.7 Mpc, is itself saturated in all epochs where the SN is present in SPIRITS imaging and was not recovered by the SPIRITS pipeline.

Thus, we define our primary comparison sample as the nine objects that were recovered by SPIRITS and have constraints on their explosion dates from SPIRITS data. By optical spectroscopic subtype this sample includes six SNe II, two SNe Ib, and one SN Iax.

Our photometry from *Spitzer*/IRAC imaging for both the IR-discovered sample of luminous IR transients and the optically discovered control sample in SPIRITS is given in Table 5.3 and shown in Figure 5.2 (see Section 5.4 for further discussion).

[5]An optical transient at the location of SPIRITS 15ade was first discovered on 2015 September 11.5 and reported by M. Aoki as PSN J15220552+0503160 through the Central Bureau for Astronomical Telegrams (CBAT; `http://www.cbat.eps.harvard.edu/unconf/followups/J15220552+0503160.html`). To our knowledge, no spectroscopy for classification or host confirmation was reported before this work.

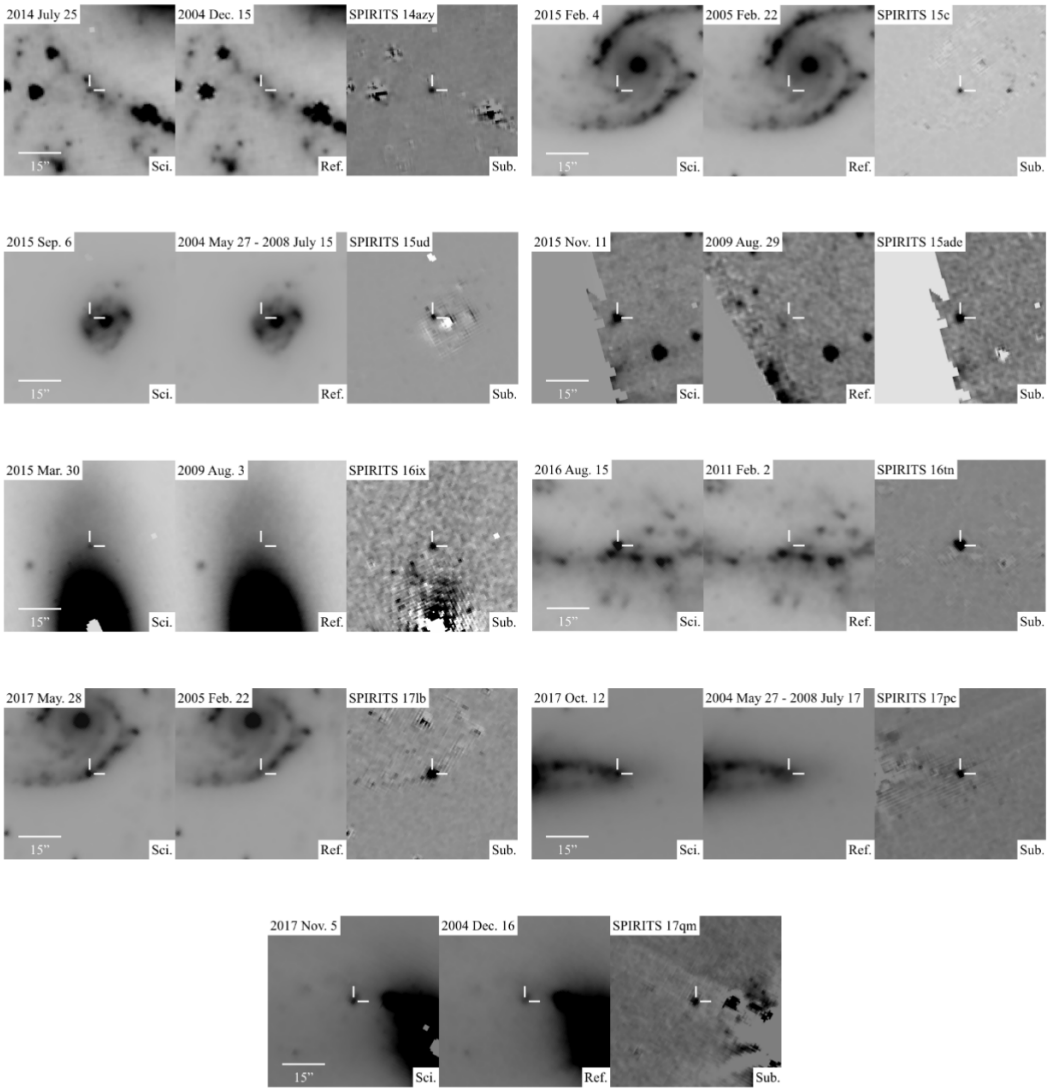

Figure 5.1: We show the *Spitzer*/IRAC [4.5] discovery images for each luminous SPIRITS-discovered transient in our sample. In each panel, from left to right, we show the new science frame, reference frame, and science-minus-reference subtraction image. The dates of each image and labels for each object are shown along the top of each panel, and the locations of the transients are indicated by white crosshairs. Each image is $1' \times 1'$, oriented with N up and E left.

Table 5.1: Luminous, IR-discovered SPIRITS transients

Name	R.A. (J2000)	Decl. (J2000)	Host (Type)	$m - M$[a] (mag)	Distance (Mpc)	$E(B-V)_{\rm MW}$[b] (mag)	UT Discovery	Host Offset (arcsec)	(kpc)
SPIRITS 14buu	06:16:27.2	–21:22:29.2	IC 2163 (SBc pec)	32.75 ± 0.4	35.5	0.077	2014 Jan 13.9[c]	11.5	2.0
SPIRITS 14azy	09:45:40.92	–31:12:07.8	NGC 2997 (SABc)	30.43 ± 0.16	12.2	0.027	2014 Jul 26.0	48.4	2.9
SPIRITS 15c	06:16:28.49	–21:22:42.2	IC 2163 (SBc pec)	32.75 ± 0.4	35.5	0.077	2015 Feb 04.4	11.6	2.0
SPIRITS 15ud	12:22:55.29	+15:49:22.0	M100 (SABbc)	30.72 ± 0.06	13.9	0.023	2015 Sep 06.7	7.5	0.5
SPIRITS 15ade	15:22:05.55	+05:03:15.9	NGC 5921 (SBbc)	31.9 ± 0.2	24.0	0.036	2015 Nov 11.9	146.3	17.0
SPIRITS 16ix	12:29:03.16	+13:11:30.7	NGC 4461 ($SB0^+$)	31.48 ± 0.25	19.8	0.02	2016 Mar 30.9	29.2	2.8
SPIRITS 16tn	11:11:20.40	+55:40:17.3	NGC 3556 (SBcd)	29.7 ± 0.4	8.7	0.015	2016 Aug 15.0	89.9	3.8
SPIRITS 17lb	06:16:27.78	–21:22:51.7	IC 2163 (SBc pec)	32.75 ± 0.4	35.5	0.077	2017 May 28.7	18.8	3.2
SPIRITS 17pc	12:25:44.43	+12:39:44.5	NGC 4388 (SAb)	31.3 ± 0.4	18.2	0.029	2017 Oct 12.8	33.9	3.0
SPIRITS 17qm	03:33:38.85	–36:08:09.4	NGC 1365 (SBb)	31.31 ± 0.06	18.3	0.018	2017 Nov 05.2	34.1	3.0

[a] References for distance moduli: NGC 2997 (Hess et al. 2009), IC 2163 (Theureau et al. 2007), M100 and NGC 4461 (Tully et al. 2013), NGC 5921 (Rodríguez, Clocchiatti, and Hamuy 2014), NGC 3556 and NGC 4388 (Sorce et al. 2014), NGC 1365 (Riess et al. 2016).

[b] Galactic extinction estimates taken from NED using the Schlafly and Finkbeiner (2011) recalibration of the Schlegel, Finkbeiner, and Davis (1998) IR-based dust map assuming a Fitzpatrick (1999) extinction law with $R_V = 3.1$.

[c] Transient present in first 2014 SPIRITS epoch and therefore excluded from the primary sample.

Table 5.2: Optically discovered and classified transients in SPIRITS

Name	SPIRITS Name[a]	R.A. (J2000)	Decl. (J2000)	Host (Type)	$m - M$[b] (mag)	D (Mpc)	$E(B-V)$[c] (MW; mag)	A_V[d] (mag)	UT Discovery[e]	Host Offset (arcsec)	Host Offset (kpc)	Type[f]
SN 2014C	14aom	22:37:05.60	+34:24:31.9	NGC 7331 (SAb)	30.71 ± 0.08	13.9	0.08	0.22	2014 Jan 05.1[g]	31.0	2.1	Ib/IIn
SN 2014J	14pw	09:55:42.14	+69:40:26.0	M82 (I0)	27.74 ± 0.08	3.5	0.14	0.98	2014 Jan 21.8[g]	58.6	1.0	Ia
SN 2014L	14we	12:18:48.68	+14:24:43.5	NGC 4254 (SAc)	30.7 ± 0.2	13.8	0.11	...	2014 Jan 26[g]	20.8	1.4	Ic
SN 2014bc	...	12:18:57.71	+47:18:11.3	NGC 4258 (SABbc)	29.32 ± 0.05	7.3	0.01	...	2014 May 19.3	3.7	0.1	II
SN 2014bi	15bx	12:06:02.99	+47:29:33.5	NGC 4096 (SABc)	30.4 ± 0.4	12.1	0.02	4.3	2014 May 31.3	54.4	3.2	IIP
SN 2014df	14bsc	03:44:23.99	–44:40:08.1	NGC 1448 (SAcd)	31.31 ± 0.05	18.3	0.01	~ 0	2014 Jun 03.2	121.1	10.7	Ib
ASASSN-14ha	15yp	04:20:01.41	–54:56:17.0	NGC 1566 (Sab pec?)	31.1 ± 0.4	16.8	0.01	~ 0	2014 Sep 10.3	8.6	0.7	II
SN 2014dt	15sd	12:21:57.57	+04:28:18.5	M61 (SABbc)	31.43 ± 0.07	19.3	0.02	~ 0	2014 Oct 29.8	40.5	3.8	Iax
SN 2016C	16ot	13:38:05.30	–17:51:15.3	NGC 5247 (SAbc)	31.7 ± 0.4	21.9	0.07	~ 0.2	2016 Jan 03.8	111.9	11.9	IIP
SN 2016adj	...	13:25:24.11	–43:00:57.5	Cen A (S0 pec)	27.82 ± 0.06	3.7	0.10	0.23	2016 Feb 08.6	40.1	0.7	Ib
SN 2016bau	16is	11:20:59.02	+53:10:25.6	NGC 3631 (SAc)	31.2 ± 0.4	17.4	0.01	~ 3.3	2016 Mar 14.0	37.8	3.2	Ib
SN 2016bkv	17eb	10:18:19.31	+41:25:39.3	NGC 3184 (SABcd)	30.79 ± 0.05	14.4	0.01	0.0	2016 Mar 21.7	30.3	2.1	IIP
SN 2016cok	17ft	11:20:19.10	+12:58:56.0	M66 (SABb)	29.78 ± 0.07	9.0	0.03	0.16	2016 May 28.5	69.1	3.0	IIP
SN 2017eaw	18k	20:34:44.24	+60:11:35.9	NGC 6946 (SABcd)	28.73 ± 0.05	5.6	0.30	$\lesssim 0.13$	2017 May 14.2	154.1	4.2	IIP

[a] SN 2014bc was located near the saturated nucleus of NGC 4258 in the *Spitzer*/IRAC images and not detected in SPIRITS. SN 2016adj itself was saturated in the *Spitzer*/IRAC images of Centaurus A and not recovered by the SPIRITS pipeline.

[b] References for distance moduli: NGC 7331, M82, NGC 4254, NGC 4258, Centaurus A, M66 (Tully et al. 2013), NGC 4096, (Sorce et al. 2014), NGC 1448 (Riess et al. 2016), NGC 1566 (Nasonova, de Freitas Pacheco, and Karachentsev 2011), M61 and NGC 6946 (Rodríguez, Clocchiatti, and Hamuy 2014), NGC 5247 (Tully 1988), NGC 3631 (Theureau et al. 2007), NGC 3184 (Ferrarese et al. 2000).

[c] Galactic extinction estimates taken from NED using the Schlafly and Finkbeiner (2011) recalibration of the Schlegel, Finkbeiner, and Davis (1998) IR-based dust map assuming a Fitzpatrick (1999) extinction law with $R_V = 3.1$.

[d] References for host extinction estimates: SN 2014C (Milisavljevic et al. 2015), SN 2014J (with $R_V = 1.4$; Amanullah et al. 2014), SN 2014bi (J. Johansson et al. 2019, in preparation), SN 2014dt (Foley et al. 2015), SN 2016adj (with $R_V = 2.57$; Banerjee et al. 2018), SN 2016bkv (Hosseinzadeh et al. 2018), SN 2016cok (Kochanek et al. 2017), SN 2017eaw (Kilpatrick and Foley 2018).

[e] References for SN discovery: SN 2014C (Kim et al. 2014), SN 2014J (Fossey et al. 2014), SN 2014L (Zhang et al. 2014), SN 2014bc (Smartt et al. 2014), SN 2014bi (Kumar et al. 2014), SN 2014df (Monard et al. 2014), ASASSN-14ha (Kiyota et al. 2014), SN 2014dt (Nakano et al. 2014), SN 2016C (Aoki 2016), SN 2016ajd (Marples, Bock, and Parker 2016), SN 2016bau (Arbour 2016), SN 2016bkv (Itagaki 2016), SN 2016cok (Bock et al. 2016), and SN 2017eaw (Wiggins 2017).

[f] References for SN classification: SN 2014C (Kim et al. 2014; Milisavljevic et al. 2015), SN 2014J (Cao et al. 2014), SN 2014L (Li et al. 2014), SN 2014bc (Cortini et al. 2014); SN 2014bi (Kumar et al. 2014), SN 2014df (Monard et al. 2014), ASASSN-14ha (Arcavi et al. 2014), SN 2014dt (Ochner et al. 2014), SN 2016C (Sahu et al. 2016), SN 2016adj (Stritzinger et al. 2016), SN 2016bau (Granata et al. 2016), SN 2016bkv (Hosseinzadeh et al. 2016), SN 2016cok (Zhang et al. 2016), and SN 2017eaw (Cheng, Chen, and Prentice 2017).

[g] SN present in first 2014 SPIRITS epoch and therefore excluded from the control sample.

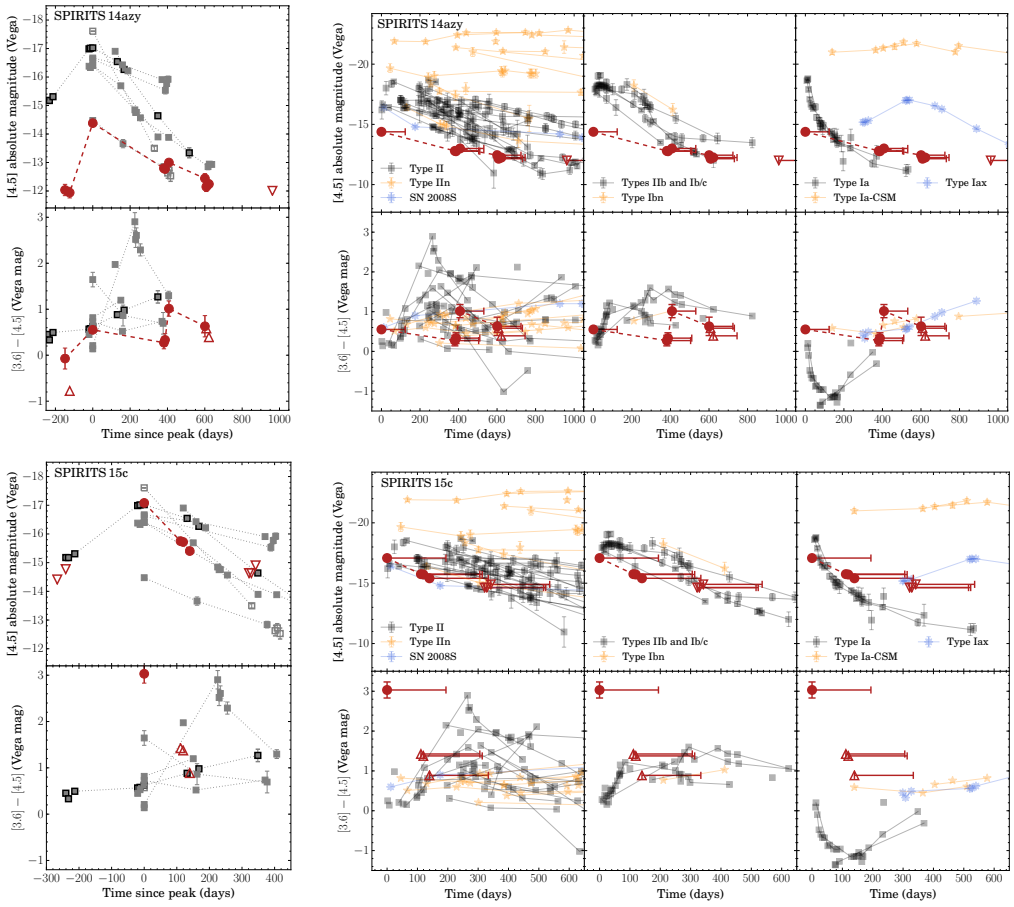

Figure 5.2: For each luminous IR SPIRITS transient, we show the [4.5] light curve (top row) and [3.6]−[4.5] color curve (bottom row) as the large red circles. In the left panel for each object, the phase is measured in days since the observed IR peak, and we compare to the control sample of optically discovered SNe recovered in SPIRITS as described in Section 5.2, including SNe II (light-gray squares), stripped-envelope SNe Ib (open squares), and the Type Iax SN 2014dt (black outlined squares). In the right panel for each object, we compare to the full sample of SNe detected by *Spitzer* compiled by Szalai et al. (2019a), including previous compilations by Szalai and Vinkó (2013), Tinyanont et al. (2016), and Johansson et al. (2017), and references therein. Additionally, we include the SNe observed by SPIRITS since 2014 and presented in this work. From left to right, we compare to SNe II (IIn), stripped-envelope SNe IIb and Ib/c (Ibn), and SNe Ia (Ia-CSM) as light-grey squares (orange stars). The blue, eight-pointed stars indicate the prototypical for its class SN 2008S, and the unusual, dusty Type Iax SN 2014dt. The phase for comparison SNe is measured as days since discovery, and for obscured SN candidates we represent our uncertainty in the phase of the primary outburst by the horizontal error bars. Upper (lower) limits from nondetections are indicated by unfilled, downward-pointing (upward-pointing) triangles.

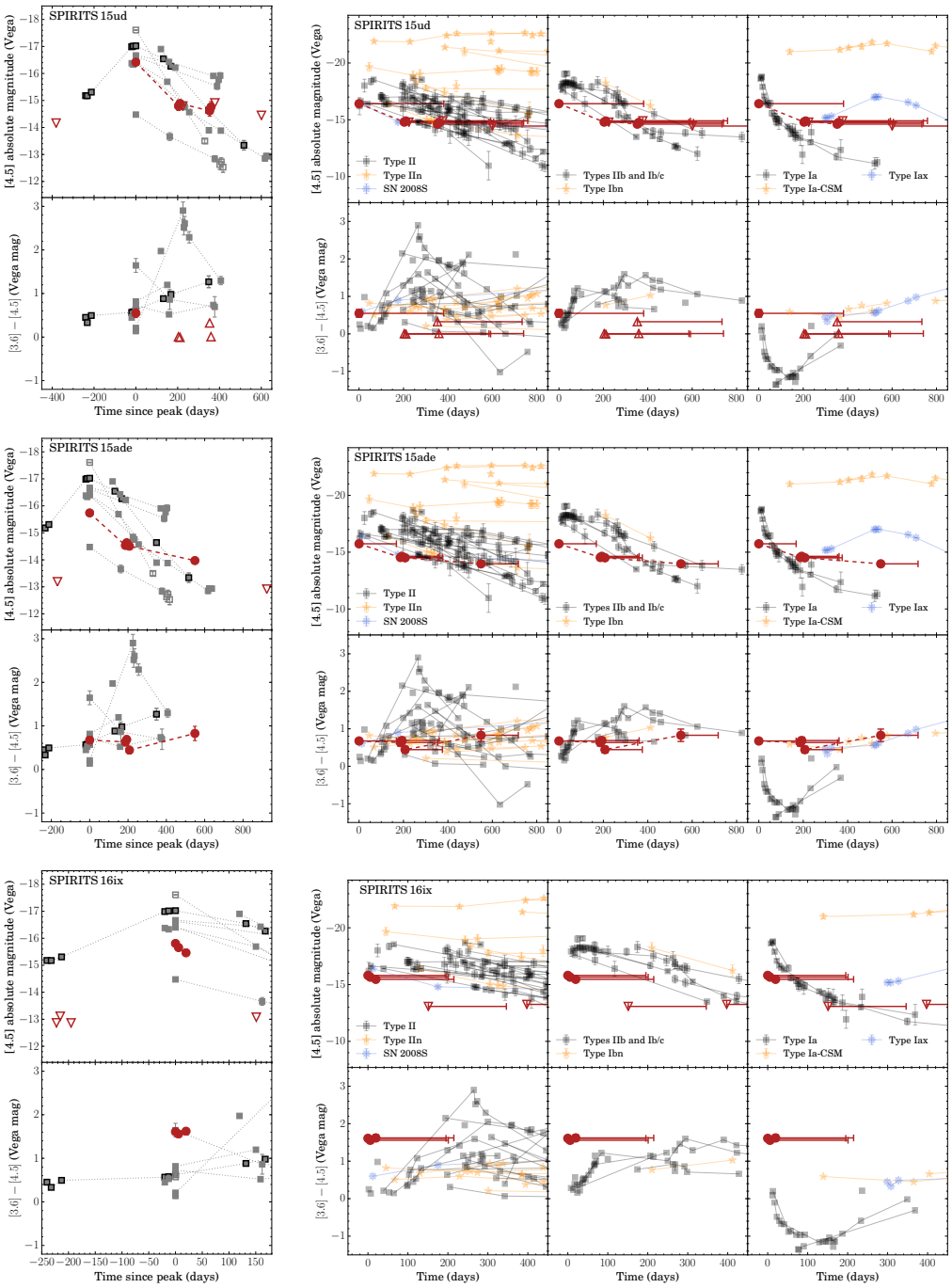

Figure 5.2: Continued.

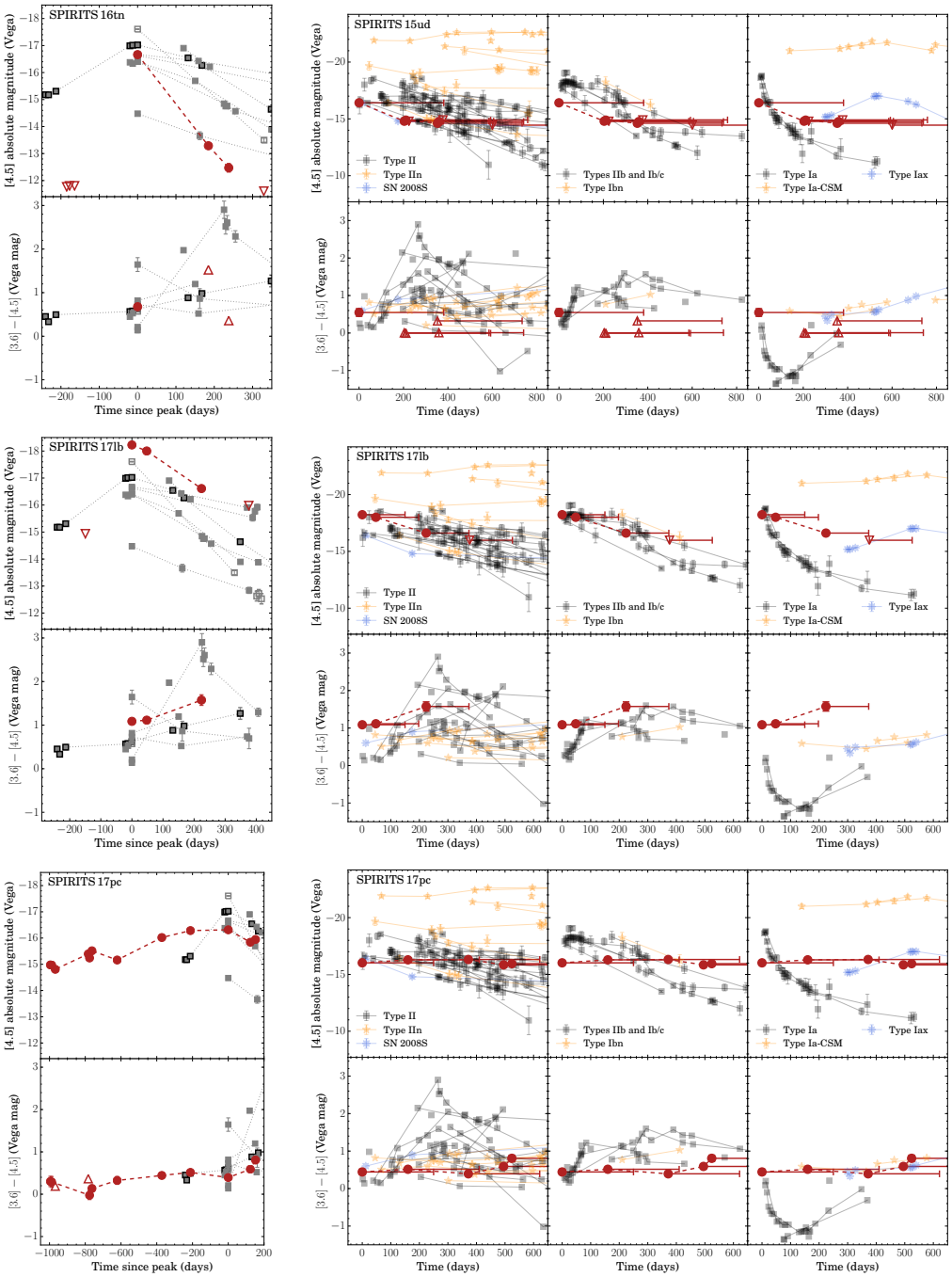

Figure 5.2: Continued.

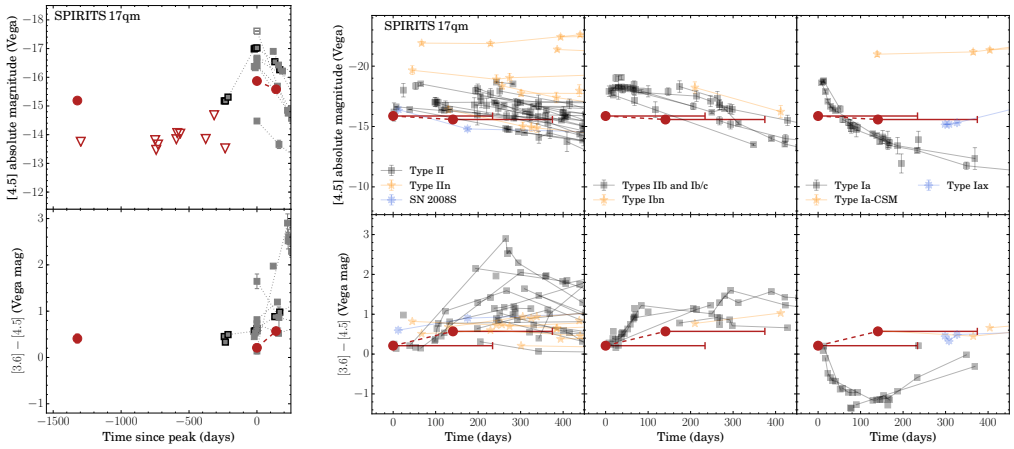

Figure 5.2: Continued.

Table 5.3: *Spitzer*/IRAC Photometry of Luminous, IR Transients in SPIRITS[a]

Name	MJD	Phase[b] (days)	$f_{\nu,[3.6]}$ (μJy)	$f_{\nu,[4.5]}$ (μJy)	[3.6] (Vega mag.)	[4.5] (Vega mag.)	$M_{[3.6]}$	$M_{[4.5]}$
SPIRITS 14azy	56,715.5	-56.5	13.5 ± 1.4	8.1 ± 1.5	18.29 ± 0.11	18.37 ± 0.20	−12.1	−12.1
	56,740.5	-31.5	< 23.8	7.4 ± 1.3	> 17.7	18.46 ± 0.19	> −12.8	−12.0
	56,864.0	92.0	66.1 ± 1.8	70.3 ± 1.4	16.57 ± 0.03	16.02 ± 0.02	−13.9	−14.4
	57,245.1	473.1	19.9 ± 1.7	16.3 ± 1.4	17.88 ± 0.09	17.60 ± 0.09	−12.6	−12.8
	57,251.0	479.0	18.3 ± 1.6	15.9 ± 1.4	17.96 ± 0.09	17.63 ± 0.10	−12.5	−12.8
	57,271.8	499.8	12.1 ± 1.6	19.7 ± 1.5	18.41 ± 0.14	17.40 ± 0.08	−12.0	−13.0
	57,464.6	692.6	10.3 ± 1.5	11.8 ± 1.8	18.59 ± 0.16	17.96 ± 0.17	−11.8	−12.5
	57,472.0	700.0	< 8.2	9.0 ± 1.4	> 18.8	18.25 ± 0.17	> −11.6	−12.2
	57,486.0	714.0	< 10.7	9.8 ± 1.3	> 18.5	18.16 ± 0.14	> −11.9	−12.3
	57,826.1	1054.1	< 7.3	< 7.9	> 19.0	> 18.4	> −11.5	> −12.0
	57,974.2	1202.2	< 8.2	< 6.6	> 18.8	> 18.6	> −11.6	> −11.9
SN 2014bi[c]	56737.5	-70.8	< 8.9	< 9.8	> 18.8	> 18.2	> −11.6	> −12.2
(SPIRITS 15bx)	56,847.1	38.8	585.3 ± 10.8	453.7 ± 8.4	14.20 ± 0.02	13.99 ± 0.02	−16.2	−16.4
	57,072.5	264.2	11.7 ± 2.1	108.1 ± 2.0	18.45 ± 0.20	15.55 ± 0.02	−11.9	−14.8
	57,076.8	268.5	15.2 ± 2.4	99.1 ± 2.0	18.17 ± 0.17	15.65 ± 0.02	−12.2	−14.8
	57,080.5	272.2	14.1 ± 2.1	99.6 ± 1.8	18.25 ± 0.16	15.64 ± 0.02	−12.2	−14.8
	57,102.2	293.9	15.8 ± 1.9	83.6 ± 1.8	18.12 ± 0.13	15.83 ± 0.02	−12.3	−14.6
	57,253.6	445.3	21.0 ± 1.6	44.4 ± 1.9	17.81 ± 0.08	16.52 ± 0.05	−12.6	−13.9
	57,464.4	656.1	< 8.4	17.2 ± 1.7	> 18.8	17.55 ± 0.11	> −11.6	−12.9
	57,470.9	662.6	< 8.8	18.7 ± 1.5	> 18.8	17.46 ± 0.09	> −11.6	−12.9
	57,484.4	676.1	< 8.8	18.5 ± 1.4	> 18.8	17.47 ± 0.08	> −11.6	−12.9
	57,842.9	1034.6	< 8.8	< 11.0	> 18.8	> 18.0	> −11.6	> −12.4
	57,963.7	1155.4	< 7.5	< 9.1	> 18.9	> 18.2	> −11.5	> −12.2

[a] We show measurements for SPIRITS 14azy and SN 2014bi to illustrate the form and content of this table. A full version including all nine objects in each of IR-discovered and optical control samples will be available in the electronic version of the published article.
[b] Time since t_0 as reported in Table 5.8 for the IR-discovered sample, and time since discovery as reported in Table 5.2 for the optical control sample.
[c] Measurements through MJD = 57253.6 were previously reported in Tinyanont et al. (2016).

5.3 Follow-up and supplementary observations

Space-based imaging

For transients that were inaccessible to ground-based observing at the time of discovery with *Spitzer*, we attempted to trigger Target of Opportunity (ToO) observations with the *Neil Gehrels Swift Observatory* UV/Optical Telescope (*Swift*/UVOT; Gehrels et al. 2004; Nousek 2004; Roming et al. 2005) to detect an optical counterpart or obtain limits on the contemporaneous optical flux. For SPIRITS 16tn we triggered a 2000 s observation on 2016 August 29.1 split between the U, B, and V bands, with limits reported in Adams, Jencson, and Kasliwal (2016) and Jencson et al. (2018e). For SPIRITS 17lb we obtained a 1200 s integration in the V band on 2017 June 9.4 and derived a 5σ limiting magnitude of $V > 17.7$. For SPIRITS 17pc we obtained a 2000 s observation on 2017 November 9.1 split between U, B, and V. NGC 4388 was previously observed by *Swift*/UVOT 1 yr prior on 2016 November 8.8, but with shorter integrations of only $\approx$60 s in each band. We find no evidence of significant variability at the location of SPIRITS 17pc between the two epochs. We derive limits for the earlier (later) epochs of $U > 18.0$ (18.8), $B > 18.2$ (18.8), and $V > 17.2$ (18.0).

We also executed *Hubble Space Telescope* (*HST*) ToO observations of SPIRITS 16tn using the Wide Field Camera 3 (WFC3) in the UVIS channel with the F814W filter and the IR channel with the F110W and F160W filters as part of our program to follow up SPIRITS transients (GO-14258; PI: H. Bond) on 2016 September 25 as described in Jencson et al. (2018e).

Ground-based imaging

SPIRITS galaxies were regularly monitored from the ground in the optical and near-IR with several telescopes. For the SPIRITS transient host galaxies discussed here, sequences of optical $g'r'i'$-band images of IC 2163, M100, NGC 4461, NGC 3556, and NGC 4388 were obtained with the CCD camera on the fully automated Palomar 60-inch telescope (P60; Cenko et al. 2006) throughout 2014–2018 and reduced by a fully automated pipeline. Where available, we used Sloan Digital Sky Survey (SDSS) images as templates for image subtraction to remove host galaxy background emission and obtain deeper limits on optical emission from the transients.

Similarly for SPIRITS galaxies located in the southern hemisphere, namely, NGC 2997, IC 2163, and NGC 1365, sequences of optical gri-band images were obtained with the CCD camera on the 1 m Swope Telescope at Las Campanas Observatory (LCO)

throughout 2014–2015. Near-IR YJH-band images were also obtained throughout 2014-2015 with the RetroCam IR camera (Morgan et al. 2005) on the 2.5 m du Pont Telescope at LCO. Photometry was performed at the locations of the transients by fitting the point-spread function (PSF) of the images, measured using stars in the field, simultaneously with the background emission, modeled using low-order polynomials.

We also obtained and performed PSF photometry on the images of NGC 5921 reported at CBAT for PSN J15220552+0503160 (SPIRITS 15ade), including unfiltered CCD images obtained by M. Aoki, G. Masi, and T. Noguchi, along with post-discovery images of this galaxy in the R band from the Hiroshima One-shot Wide-field Polarimeter (HOWpol; Kawabata et al. 2008) on the Kanata 1.5 m telescope at Higashi-Hiroshima Observatory and in the r band with the Dark Energy Camera (DECam) on the Blanco 4 m telescope at Cerro Tololo Inter-American Observatory (CTIO).

Post-discovery, ground-based follow-up imaging in the optical and near-IR was also obtained for several SPIRITS transients. Near-IR JHK_s-band images were obtained with the Multi-object Spectrometer for Infra-red Exploration (MOSFIRE; McLean et al. 2010; McLean et al. 2012) on the 10 m Keck I Telescope of the W. M. Keck Observatory on the summit of Maunakea, the Wide Field Infrared Camera (WIRC; Wilson et al. 2003) on the 200-inch telescope at Palomar Observatory (P200), and the FourStar IR camera (Persson et al. 2013) on the Magellan Baade Telescope at LCO. Flat-fielding, background subtraction, astrometric alignment, and final stacking of images in each filter were performed using a custom pipeline. Additional near-IR imaging for SPIRITS 17lb was obtained with the FLAMINGOS-2 imaging spectrograph on the 8.1 m Gemini S Telescope (PID GS-2017B-Q-15; PI J. Jencson) and reduced using the Gemini IRAF package following procedures online in the FLAMINGOS-2 Data Reduction Cookbook[6]. Optical imaging was obtained for SPIRITS 17pc using the DEep Imaging Multi-Object Spectrograph (DEIMOS; Faber et al. 2003) on the 10 m Keck II Telescope and reduced using standard tasks in IRAF.

Additional near-IR imaging was obtained with the Wide Field Camera (WFCAM; Casali et al. 2007) on the United Kingdom Infrared Telescope (UKIRT) at Maunakea Observatories. Simultaneous optical/near-IR $rizYJH$ were obtained with the

[6]Data reduction procedures for FLAMINGOS-2 are found at `https://gemini-iraf-flamingos-2-cookbook.readthedocs.io/en/latest/`

Table 5.4: Supplementary photometry[a]

Name	MJD	Phase[b] (days)	Tel./Inst.	Band	Apparent Mag.	Absolute Mag.[c]
SPIRITS 14azy	56,772.0	0.0	Swope/CCD	g	21.94 ± 0.47	-8.8
	56,772.0	0.0	Swope/CCD	r	20.49 ± 0.18	-10.2
	56,772.0	0.0	Swope/CCD	i	19.81 ± 0.18	-10.8
	56,804.0	32.0	Swope/CCD	g	20.04 ± 0.10	-10.7
	56,804.0	32.0	Swope/CCD	r	19.02 ± 0.06	-11.7
	56,804.0	32.0	Swope/CCD	i	18.73 ± 0.06	-11.9
	56,828.0	56.0	Swope/CCD	g	20.79 ± 0.27	-10.0
	56,828.0	56.0	Swope/CCD	r	19.63 ± 0.10	-11.0
	56,828.0	56.0	Swope/CCD	i	19.20 ± 0.10	-11.4
	56,829.0	57.0	Swope/CCD	g	21.09 ± 0.19	-9.7
	56,829.0	57.0	Swope/CCD	r	19.69 ± 0.07	-11.0
	56,829.0	57.0	Swope/CCD	i	19.17 ± 0.07	-11.4
	56,996.8	224.8	du Pont/RetroCam	H	19.83 ± 0.05	-10.6
	57,053.7	281.7	du Pont/RetroCam	H	20.32 ± 0.19	-10.2
	57,066.7	294.7	du Pont/RetroCam	H	20.11 ± 0.19	-10.4
	57,069.7	297.7	Baade/FourStar	J	21.11 ± 0.27	-9.4
	57,069.7	297.7	Baade/FourStar	K_s	18.58 ± 0.27	-11.9
	57,089.7	317.7	du Pont/RetroCam	H	20.42 ± 0.22	-10.1
	57,115.6	343.6	du Pont/RetroCam	H	20.41 ± 0.11	-10.1

[a] We show measurements for SPIRITS 14azy to illustrate the form and content of this table. A full version including all of our supplementary photometry will be available in the electronic version of the published article.
[b] Time since t_0 as reported in Table 5.8 for the IR-discovered sample.
[c] Absolute magnitudes corrected for Galactic extinction to the host from NED.

Reionization and Transients InfraRed camera (RATIR; Butler et al. 2012) on the 1.5 m Johnson Telescope at the Mexican Observatorio Astronomico Nacional on the Sierra San Pedro Martir in Baja California, Mexico (Watson et al. 2012).

For our follow-up imaging, we performed simple aperture photometry at the location of the transients with the aperture size defined by the seeing in each image. Our photometry (including PSF photometry above) was calibrated using $\gtrsim 10$ isolated stars in SDSS for the optical images and in the Two Micron All Sky Survey (2MASS) for the near-IR images. Where necessary, we adopt the conversions of Jordi, Grebel, and Ammon (2006) to convert from the Sloan $ugriz$ system to $UBVRI$ magnitudes. For Y-band images, we adopt the conversion from 2MASS used for the UKIRT/WFCAM from Hodgkin et al. (2009). Unfiltered CCD images of NGC 5921 were calibrated to the SDSS r band. Our supplementary photometry is included in Table 5.4 and shown for each object in Figure 5.12.

Spectroscopy

We obtained near-IR spectroscopy of the luminous IR SPIRITS transients at several epochs using the Folded-port InfraRed Echellette spectrograph (FIRE; Simcoe et

al. 2008; Simcoe et al. 2013) on the Magellan Baade Telescope at LCO, MOSFIRE on the Keck I Telescope, the Near-Infrared Echellette Spectrometer[7] (NIRES) on the Keck II Telescope, the Gemini Near-InfraRed Spectrograph (GNIRS; Elias et al. 2006) on the 8.1 m Gemini N Telescope (PIDs GN-2016B-FT-25, GN-2017B-Q-14; PI J. Jencson), and the FLAMINGOS-2 spectrograph (Eikenberry et al. 2006) on the 8.1 m Gemini S Telescope (PID GS-2017B-Q-15; PI J. Jencson). Optical spectroscopy was obtained for SPIRITS 16tn, SPIRITS 17pc, and SPIRITS 17qm with the Low Resolution Imaging Spectrometer (LRIS; Goodrich and Cohen 2003) on the Keck I telescope. Our spectroscopic observations, including the integration times used, are summarized in Table 5.5.

The FIRE and MOSFIRE spectra of SPIRITS 15c and the GNIRS and LRIS spectra of SPIRITS 16tn, as well as details of the data reduction procedures, were previously published in Jencson et al. (2017e) and Jencson et al. (2018e).

For the LRIS observations of SPIRITS 17pc and SPIRITS 17qm, we used the D560 dichroic to split the light between the red and blue sides, and we used a 1″ long slit with the 400/8500 grating on the red side and the 400/3400 grism on the blue side providing the resolution and wavelength coverage given in Table 5.5. Spectroscopic reductions for LRIS were performed using the analysis pipeline LPIPE[8] developed by D. Perley. For SPIRITS 17pc, a weak trace is visible at the position of the transient on the red-side camera. For SPIRITS 17qm, there is no obvious continuum trace; however we detect several emission lines associated with the transient on the red side. No emission was detected on the blue side for either object. The 1D spectra were extracted at these positions along the slit and flux-calibrated using observations of the standard stars G191-B2B and BD +75°325. Our optical spectra of SPIRITS 16tn, SPIRITS 17pc, and SPIRITS 17qm are shown in Figure 5.3.

For observations with the near-IR spectrographs the target was nodded along the slit between exposures to allow for accurate subtraction of the sky background. Observations of an A0V telluric standard star near the target location were also taken immediately before or after each science target observation for flux calibration and correction of the strong near-IR telluric absorption features. For MOSFIRE, we used a 0.″7 slit with the standard grating/filter setups for each of the $YJHK$ spectral regions, providing the wavelength coverage and resolution listed for each observation in Table 5.5. For GNIRS, we used the cross-dispersed (XD), multiorder

[7] `https://www2.keck.hawaii.edu/inst/nires/`

[8] Software available at `http://www.astro.caltech.edu/~dperley/programs/lpipe.html`.

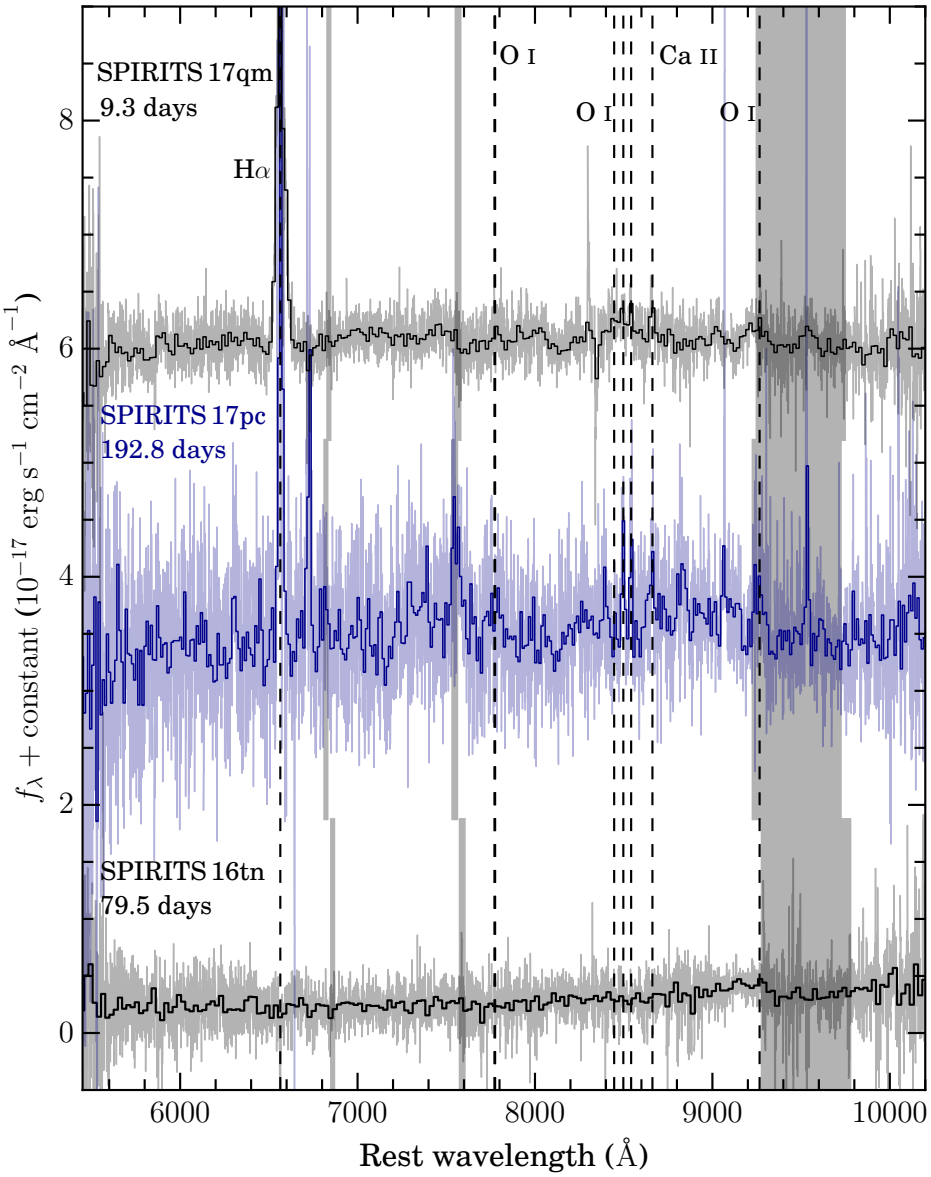

Figure 5.3: Optical spectroscopy from Keck I/LRIS of SPIRITS 16tn, SPIRITS 17pc, and SPIRITS 17qm in alternating colors and offset in flux by an arbitrary constant so that spectra for each object may be easily distinguished. Spectra are labeled for each object along with their respective phases along the left side of the figure. Data are shown in light gray or light blue, with binned data for each object overplotted in black or dark blue, respectively. Regions contaminated by telluric absorption are indicated by the light-gray vertical bands. Atomic emission features detected in the spectra, including broad $\approx$1000 km s^{-1} Hα and lines of O I in SPIRITS 17qm, and the Ca II IR triplet in SPIRITS 17qm and SPIRITS 17pc, are indicated by the dashed black vertical lines and labeled near the top of the figure.

Table 5.5: Spectroscopic Observations

Name	UT Date	MJD	Phase (days)	Tel./Instr.	Range (Å)	Resolution ($\lambda/\delta\lambda$)	Integration
SPIRITS 15c	2015 Mar 14.1	57,095.1	204.7	Baade/FIRE	8000–24000	300–500	4×120 s
	2015 Mar 31.2	57,112.2	221.8	Keck I/MOSFIRE	9700–11100	3400	8×180 s
	2015 Mar 31.3	57,112.3	221.9	Keck I/MOSFIRE	11400–13100	3300	6×120 s
	2015 Mar 31.3	57,112.3	221.9	Keck I/MOSFIRE	14500–17500	3700	10×120 s
	2015 Mar 31.3	57,112.3	221.9	Keck I/MOSFIRE	19500–23500	3600	6×180 s
	2015 Sep 19.3	57,284.6	394.2	Keck I/MOSFIRE	9700–11100	3400	10×180 s
SPIRITS 15ud	2016 Jan 23.6	57,410.6	138.9	Keck I/MOSFIRE	19500–23500	3600	12×180 s
SPIRITS 15ade	2016 Jan 23.6	57,410.6	134.1	Keck I/MOSFIRE	19500–23500	3600	30×180 s
	2016 Apr 16.6	57,494.6	218.1	Keck I/MOSFIRE	9700–11100	3400	2×180 s
	2016 Apr 16.6	57,494.6	218.1	Keck I/MOSFIRE	11400–13100	3300	10×120 s
	2016 May 30.5	57,538.5	262.0	Keck I/MOSFIRE	14500–17500	3700	6×120 s
SPIRITS 16ix	2016 Apr 16.5	57,494.5	16.6	Keck I/MOSFIRE	19500–23500	3600	10×180 s
SPIRITS 16tn	2016 Nov 2.6	57,694.6	79.5	Keck I/LRIS	3500–6000	600	1800 s
	2016 Nov 2.6	57,694.6	79.5	Keck I/LRIS	5500–10300	1000	2×860 s
	2016 Dec 29.5	57,751.5	136.4	Gemini N/GNIRS	8500–25000	1200	14×300 s
	2017 Jan 9.6	57,762.6	147.5	Gemini N/GNIRS	8500–25000	1200	10×300 s
SPIRITS 17lb	2017 Sep 28.6	58,024.6	122.9	Keck I/MOSFIRE	19500–23500	3600	24×180 s
	2017 Nov 1.3	58,058.3	156.6	Gemini S/FLAMINGOS-2	13500–24000	600	24×150 s
	2017 Nov 20.6	58,077.6	175.9	Keck I/MOSFIRE	11400–13100	3300	6×120 s
	2017 Nov 20.6	58,077.6	175.9	Keck I/MOSFIRE	19500–23500	3600	8×180 s
SPIRITS 17pc	2017 Nov 11.6	58,071.6	192.8	Keck I/LRIS	3500–6000	600	1200 s
	2017 Nov 11.6	58,071.6	192.8	Keck I/LRIS	5500–10300	1000	2×560 s
	2017 Nov 20.6	58,077.6	198.8	Keck I/MOSFIRE	9700–11100	3400	6×180 s
	2017 Nov 20.7	58,077.7	198.9	Keck I/MOSFIRE	19500–23500	3600	4×180 s
	2017 Dec 7.6	58,094.6	215.8	Gemini N/GNIRS	8500–25000	1200	4×180 s
	2017 Dec 8.6	58,095.6	216.8	Gemini N/GNIRS	8500–25000	1200	8×180 s
	2017 Dec 11.6	58,098.6	219.8	Gemini N/GNIRS	8500–25000	1200	12×180 s
	2018 Jan 8.5	58,126.5	247.7	Keck I/MOSFIRE	9700–11100	3400	6×180 s
	2018 Jan 8.6	58,126.6	247.8	Keck I/MOSFIRE	11400–13100	3300	6×120 s
	2018 Jan 8.6	58,126.6	247.8	Keck I/MOSFIRE	14500–17500	3700	6×120 s
	2018 Jan 8.6	58,126.6	247.8	Keck I/MOSFIRE	19500–23500	3600	6×180 s
	2018 May 4.4	58,242.4	363.6	Keck II/NIRES	9500–24600	2700	6×300 s
SPIRITS 17qm	2017 Nov 11.5	58,071.5	9.3	Keck I/LRIS	3500–6000	600	2×1200 s
	2017 Nov 11.5	58,071.5	9.3	Keck I/LRIS	5500–10300	1000	4×560 s
	2017 Nov 20.5	58,077.5	15.3	Keck I/MOSFIRE	9700–11100	3400	14×180 s
	2018 Jan 8.2	58,126.2	64.0	Keck I/MOSFIRE	9700–11100	3400	8×180 s
	2018 Jan 8.3	58,126.3	64.1	Keck I/MOSFIRE	11400–13100	3300	12×120 s
	2018 Jan 8.3	58,126.3	64.1	Keck I/MOSFIRE	14500–17500	3700	12×120 s
	2018 Jan 8.3	58,126.3	64.1	Keck I/MOSFIRE	19500–23500	3600	10×180 s

mode providing coverage of the full near-IR spectral region at once, with a 0.″45 slit, the 32 line mm^{-1} grating, and the short blue camera with its XD prism, providing an average spectral resolution of $R = 1200$. For, FLAMINGOS-2 we use the long-slit mode and the low-resolution HK grism with a 3 pixel, 0.″54 slit providing wavelength coverage from 13,500 to 24,000 Å and an average spectral resolution of $R = 600$. NIRES employs a 0.″55 slit and provides wavelength coverage from 9500 to 24,600 Å across five spectral orders at a mean resolution of $R = 2700$.

Reductions for MOSFIRE, including flat-fielding, the wavelength solution, background subtraction, and frame stacking for each object on a given night, were

performed with the MOSFIRE Data Reduction Pipeline[9]. 1D extractions, where the continuum trace of the target and/or emission lines were visible in the reduced 2D spectra, were performed using standard tasks in IRAF[10]. For GNIRS and FLAMINGOS-2 reductions, including detector pattern noise cleaning and radiation event removal (GNIRS only), flat-fielding, background subtraction, spatial distortion corrections (GNIRS only), wavelength calibration, and 1D extractions, we used standard tasks in the Gemini IRAF package following procedures outlined on the Gemini webpage[11]. NIRES data were reduced, including flat-fielding, wavelength calibration, background subtraction, and 1D spectral extractions steps, using a version of the IDL-based data reduction package Spextool developed by Cushing, Vacca, and Rayner (2004), updated by M. Cushing specifically for NIRES. Corrections for the strong near-IR telluric absorption features and flux calibrations for spectra from all instruments were performed with the A0V standard-star observations using the method developed by Vacca, Cushing, and Rayner (2003) implemented with the IDL tools XTELLCOR or XTELLCOR_GENERAL developed by Cushing, Vacca, and Rayner (2004) as part of Spextool.

We did not detect any line emission or a discernible continuum trace from the transients in the MOSFIRE spectrum of SPIRITS 15ud, the MOSFIRE 2016 April 16.6 *Y*-band and 2016 May 30.5 *H*-band spectra of SPIRITS 15ade, the MOSFIRE spectrum of SPIRITS 16ix, or the 2017 November 20.6 MOSFIRE spectrum of SPIRITS 17lb. The full sequence of near-IR spectra for which we detected emission from the transient, either a continuum trace or specific emission lines, is shown in Figure 5.4.

Radio Observations

We obtained radio continuum imaging observations of each of our luminous IR transients, primarily using the Karl G. Jansky Very Large Array (VLA) between 2017 June and 2018 April in the C, B, and A configurations with 3.4, 11.1, and 36.4 km maximum baselines, respectively (PIDs 16B-388, 17A-365, 17B-331, 18A-418; PI J. Jencson). The bulk of our observations were carried out in 1 hr blocks in *C* band (6 GHz central frequency) using the full, wide-band capabilities of the

[9] `https://keck-datareductionpipelines.github.io/MosfireDRP/`

[10] IRAF is distributed by the National Optical Astronomy Observatory, which is operated by the Association of Universities for Research in Astronomy (AURA) under a cooperative agreement with the National Science Foundation.

[11] Procedures for reducing GNIRS XD spectra are found at `http://www.gemini.edu/sciops/instruments/gnirs/data-format-and-reduction/reducing-xd-spectra`

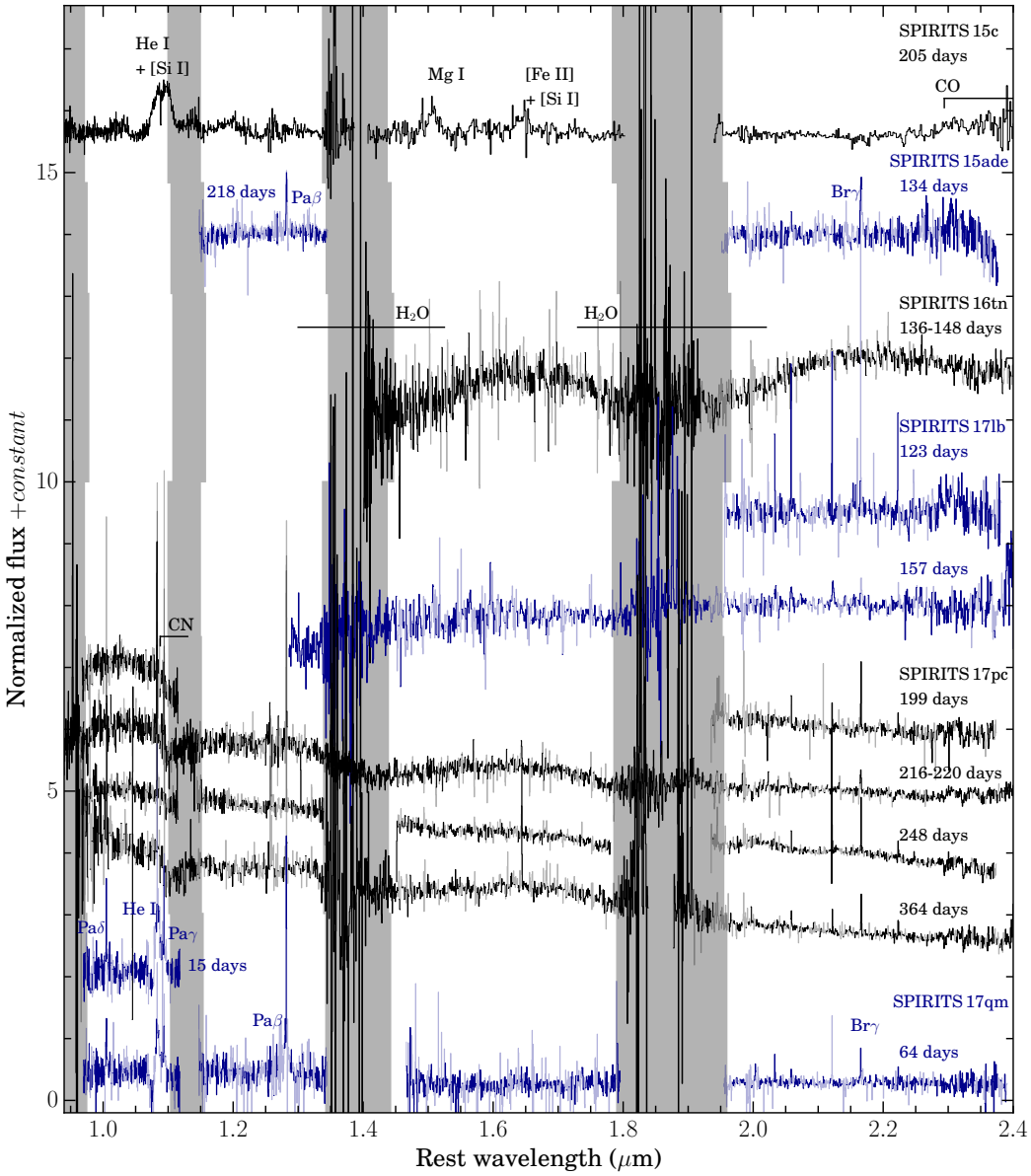

Figure 5.4: Full sequence of near-IR spectra obtained for the SPIRITS luminous IR transient sample. Spectra correspond to the objects and phases (measured from t_0 as in Table 5.8) listed along the right side of the figure, shown in alternating colors so that spectra for separate objects may be easily distinguished. The spectra for each object are shifted to the rest frame of their respective host galaxies, and regions of low S/N due to coincidence with OH airglow emission lines are shown in lighter colors. The spectra have been scaled in flux and shifted by arbitrary constants for clarity. The major features identified in each spectrum and discussed in the text are labeled, including the SN Ib/IIb emission features in the spectrum of SPIRITS 15c, the ~200 km s^{-1} width emission lines of H I in the spectra of SPIRITS 15ade, the possible broad H_2O absorption features in the spectrum of SPIRITS 16tn, the broader ~2000 km s^{-1} features of H I and He I in the spectrum of SPIRITS 17qm, and the CO $\delta v = 2$ vibrational transition band heads detected in the spectra of SPIRITS 15c, SPIRITS 17lb, and SPIRITS 17pc.

upgraded VLA with 3-bit samplers offering 4 GHz bandwidth. For some objects and epochs, we split the block between multiple bands including the *S* (3 GHz central frequency, 2 GHz bandwidth with 8 bit samplers), *X* (10 GHz central frequency, 4 GHz bandwidth), and *Ku* bands (15.5 GHz central frequency, 4 GHz bandwidth). Each observing block included observations of the VLA standard calibrators 3C 286 or 3C 138 for calibration of the flux density scale and instrument bandpass. For complex gain calibrations, we took observations of a nearby calibrator source, cycling between the calibrator and science target at sufficient intervals for the given array configuration and observing frequency based on recommendations in the VLA observing guide[12].

We also analyzed the 2016 February 19 observations of IC 2163 targeting the unrelated event SN 2010jp, but fortuitously covering the sites of SPIRITS 14buu, SPIRITS 15c, and SPIRITS 17lb (PID 16A-101; PI C. Kilpatrick). These observations used the 8-bit sampler setup providing 2×1 GHz bandwidth tuned to the ranges 4.5–5.5 GHz and 6.9–7.9 GHz in *C* band and 8.0–9.0 GHz and 10.5–11.5 GHz in *X* band.

The data for each observation were run through the VLA CASA calibration pipeline,[13] suitable for automated flagging and calibration of Stokes *I* continuum data sets. The calibrated data were carefully inspected, and additional flagging and recalibration were performed as necessary. We imaged our data using the standard CLEAN task in CASA. First-pass images of SPIRITS 17pc in NGC 4388 were limited in sensitivity owing to artifacts from residual phase errors of the bright nucleus of the host, a known Seyfert 2 active galactic nucleus. We performed self-calibration of the visibility phases on the nucleus, which significantly improved the final images, reaching near the theoretical thermal noise sensitivity for our observations.

We inspected the location of the transients in each image for the presence of a coincident point source and report our flux measurements with 1σ errors, estimated as the rms noise in a relatively clean region of the image, in Table 5.6. In several cases, the location of the transients suffered significant contamination from extended emission from the host galaxy or nearby star-forming regions, particularly in the lower-resolution *C*-configuration observations. For nondetections or when possible emission from the transient cannot be distinguished from background contamination,

[12]VLA calibration information available here: `https://science.nrao.edu/facilities/vla/docs/manuals/obsguide/calibration`

[13]`https://science.nrao.edu/facilities/vla/data-processing/pipeline/scripted-pipeline`

Table 5.6: Radio Observations

Name	UT Date	MJD	Phase (days)	Inst.	D[a] (km)	Freq. (GHz)	Flux (mJy)	Lum. (erg s^{-1} Hz^{-1})
SPIRITS 14buu	2016 Feb 19.1	57,437.1	786.8	VLA	3.4	10.0	< 0.04	$< 6.0 \times 10^{25}$
	2016 Feb 19.1	57,437.1	786.8	VLA	3.4	6.0	< 0.13	$< 2.0 \times 10^{26}$
	2017 Jun 10.8	57,914.8	1264.5	VLA	3.4	6.0	< 0.12	$< 1.8 \times 10^{26}$
	2017 Sep 4	58,000	1349.7	ATCA	4.5	9.0	< 22	$< 3.3 \times 10^{28}$
	2017 Sep 4	58,000	1349.7	ATCA	4.5	5.5	< 25	$< 3.8 \times 10^{28}$
	2018 Jan 6.2	58,124.2	1473.9	VLA	11.1	6.0	< 0.039	$< 5.9 \times 10^{25}$
	2018 May 9.0	58,247.0	1596.7	VLA	36.4	6.0	< 0.035	$< 5.3 \times 10^{25}$
	2018 May 9.0	58,247.0	1596.7	VLA	36.4	6.0	< 0.055	$< 8.3 \times 10^{25}$
SPIRITS 14azy	2017 Jun 12.9	57,916.9	1144.9	VLA	3.4	6.0	< 0.075	$< 1.3 \times 10^{25}$
SPIRITS 15c	2016 Feb 19.1	57,437.1	546.7	VLA	3.4	10.0	0.12 ± 0.01	1.8×10^{26}
	2016 Feb 19.1	57,437.1	546.7	VLA	3.4	6.0	$0.23^{+0.01}_{-0.09}$	3.5×10^{26}
	2017 Jun 10.8	57,914.8	1024.4	VLA	3.4	6.0	< 0.11	$< 1.7 \times 10^{26}$
	2017 Sep 4	58,000	1110	ATCA	4.5	9.0	< 1.7	$< 2.6 \times 10^{27}$
	2017 Sep 4	58,000	1110	ATCA	4.5	5.5	< 7.6	$< 1.1 \times 10^{28}$
	2018 Jan 6.2	58,124.2	1233.8	VLA	11.1	6.0	0.055 ± 0.007	8.3×10^{25}
	2018 May 9.0	58,247.0	1356.6	VLA	36.4	6.0	0.051 ± 0.008	7.7×10^{25}
	2018 May 9.0	58,247.0	1356.6	VLA	36.4	3.0	0.082 ± 0.014	1.2×10^{26}
SPIRITS 15ud	2017 Jun 14.1	57,918.1	646.4	VLA	3.4	6.0	< 1.1	$< 2.5 \times 10^{26}$
SPIRITS 15ade	2017 Jun 16.0	57,920.0	643.5	VLA	3.4	6.0	< 0.045	$< 3.1 \times 10^{25}$
SPIRITS 16ix	2017 Jun 16.0	57,920.0	442.1	VLA	3.4	6.0	< 0.025	$< 1.2 \times 10^{25}$
SPIRITS 16tn	2016 Sep 3	57,634	19	AMI-LA	0.11	15.0	< 0.3	$< 2.8 \times 10^{25}$
	2016 Sep 4.0	57,635.0	20.0	VLA	11.1	10.0	< 0.047	$< 4.4 \times 10^{24}$
	2016 Sep 4.0	57,635.0	20.0	VLA	11.1	6.0	< 0.075	$< 7.0 \times 10^{24}$
	2016 Sep 4.0	57,635.0	20.0	VLA	11.1	3.0	< 0.10	$< 9.3 \times 10^{24}$
	2017 Jan 12.4	57,765.4	150.4	VLA	36.4	15.5	< 0.029	$< 2.7 \times 10^{24}$
	2017 Jan 12.4	57,765.4	150.4	VLA	36.4	6.0	< 0.029	$< 2.7 \times 10^{24}$
	2018 Jan 23.6	58,141.6	526.6	VLA	11.1	15.5	< 0.030	$< 2.8 \times 10^{24}$
	2018 Jan 23.6	58,141.6	526.6	VLA	11.1	6.0	< 0.030	$< 2.8 \times 10^{24}$
SPIRITS 17lb	2017 Jun 10.8	57,914.8	13.1	VLA	3.4	6.0	< 0.25	$< 3.8 \times 10^{26}$
	2017 Sep 4	58,000	99	ATCA	4.5	9.0	< 1.7	$< 2.6 \times 10^{27}$
	2017 Sep 4	58,000	99	ATCA	4.5	5.5	< 6.5	$< 9.8 \times 10^{27}$
	2018 Jan 6.2	58,124.2	222.5	VLA	11.1	6.0	0.059 ± 0.006	8.9×10^{25}
	2018 May 9.0	58,247.0	345.3	VLA	36.4	6.0	0.039 ± 0.009	5.9×10^{25}
	2018 May 9.0	58,247.0	345.3	VLA	36.4	3.0	0.067 ± 0.013	1.0×10^{26}
SPIRITS 17pc	2017 Oct 30.5	58,056.5	177.7	VLA	11.1	6.0	< 0.090	$> 3.6 \times 10^{25}$
	2018 Jan 21.7	58,139.7	260.9	VLA	11.1	6.0	< 0.13	$> 5.2 \times 10^{25}$
	2018 Apr 14.2	58,222.1	343.3	VLA	36.4	6.0	< 0.025	$> 9.9 \times 10^{24}$
SPIRITS 17qm	2017 Nov 23.3	58,080.3	18.1	VLA	11.1	6.0	< 0.05	$> 2.0 \times 10^{25}$
	2018 Apr 16.8	58,224.8	162.6	VLA	36.4	6.0	< 0.025	$> 1.0 \times 10^{25}$

[a] Maximum baseline of array configuration.

we report upper limits on the transient flux as either 5σ ($5 \times$ image rms), or the level of the contaminating flux at the location plus $2 \times$ image rms, whichever is larger.

Specifically for the 2016 February 19.1 *C*-band measurement of SPIRITS 15c, a source is clearly detected at the position and has faded significantly in the subsequent image on 2017 June 10.8 (taken in the same configuration with similar resolution),

confirming its association with the transient. We note, however, that possible residual emission from the transient in the later epoch is blended with a nearby, somewhat extended contaminating source. We adopt the flux at the transient location as an estimate of the maximum contamination for our previous measurement and adopt this as a lower bound on the flux in Table 5.6. In the subsequent epochs in the larger B and A configurations, the contaminating emission appears resolved out, and the radio counterpart to SPIRITS 15c is clearly detected as a relatively isolated, fading point source.

Radio observations of SPIRITS 16tn were also obtained with the Arcminute Microkelvin Image Large Array (AMI-LA), which were previously reported in Jencson et al. (2018e). Additional observations of IC 2163 containing SPIRITS 14buu, SPIRITS 15c, and SPIRITS 17lb were obtained with the Australia Telescope Compact Array (ATCA) over 6 hr on 2017 September 4 at 9.0 and 5.5 GHz simultaneously. The ATCA primary flux calibrator, PKS B1934≡638, was used to set the absolute flux scale, as well as define the bandpass calibration in each 2 GHz band. Frequent observations of the nearby source PKS 0606≡223 allowed us to monitor and correct for variations in gain and phase throughout each run. The data were processed using the Miriad package (Sault, Teuben, and Wright 1995) and using procedures outlined in Section 4.3 of the ATCA User Guide[14]. After editing and calibrating the data, images at each frequency were made using robust weighting (robust = 0.5) and then cleaned down to 3× the rms noise level. No point sources exactly matching the locations of these three SNe were evident at either frequency within the clumpy disk structure. Fitting a Gaussian point source to the nearest peak of emission in each case yielded the upper limits on flux densities shown in Table 5.6.

Limits from wide-field optical surveys

We obtained limits on the optical emission from SPIRITS transients that were fortuitously covered by the intermediate Palomar Transient Factory (iPTF) survey during their outbursts in the g, R, and/or i filters. The iPTF operated from 2013 January 1 to 2017 March 2 using a wide-field camera with a 7.26 deg^2 field of view on the 48-inch Samuel Oschin Schmidt Telescope at Palomar Observatory (P48). During its operation, iPTF images were processed through a real-time image subtraction pipeline (Cao, Nugent, and Kasliwal 2016) to search for transients and variables. We ran forced PSF photometry at the locations of our SPIRITS transients

[14] http://www.narrabri.atnf.csiro.au/observing/users_guide/html/atug.html

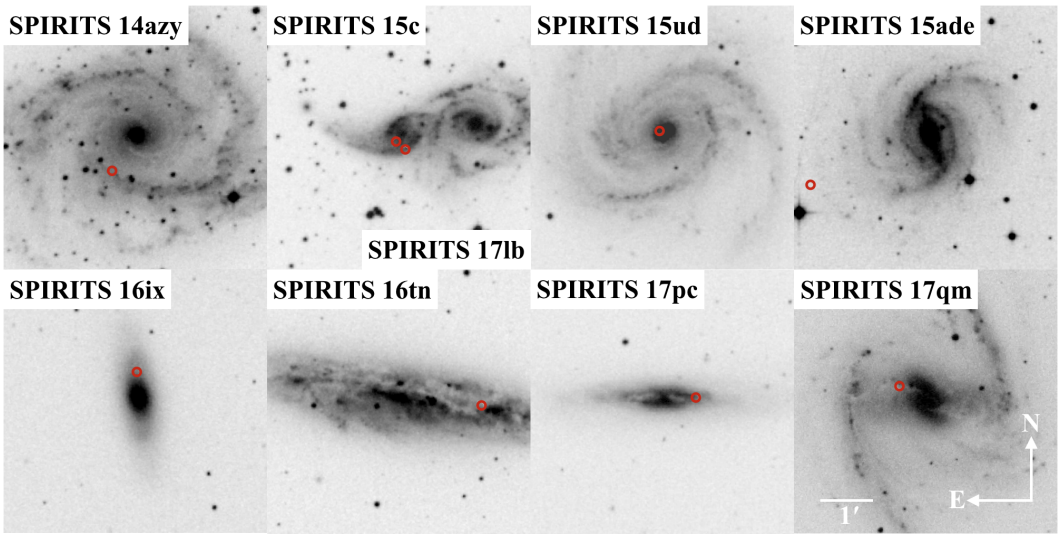

Figure 5.5: We show the DSS2-red images of the host galaxies of the IR-selected sample of SPIRITS transients. The location of the transient(s) in each panel is indicated by the red circle. The orientation and scale are the same in each panel as indicated in the bottom right panel.

on iPTF reference-subtracted images using the PTF IPAC/iPTF Discovery Engine (PTFIDE) tool (Masci et al. 2017). To obtain deeper constraints, we stacked limits from individual observations within 10-day windows. Constraints on the optical emission from our sample transients from the iPTF are included in Figure 5.12.

5.4 Analysis

Host environments and archival imaging

The host galaxy morphological types (obtained from NED) of our sample of IR-selected transients are given in Table 5.1. With the exception of SPIRITS 16ix in the lenticular SB0$^+$ galaxy NGC 4461, these events were found in late-type, star-forming galaxies. Similarly, the entire control sample of optically discovered SNe was also found in star-forming galaxies (Table 5.2). In Figure 5.5, we indicate the locations of the IR-selected transients in the Digitized Sky Survey 2 (DSS2) images of their host galaxies, showing a clear trend of positional associations with the active star-forming regions of the hosts' spiral arms. This indicates a likely physical association of the bulk of the sample to ongoing star formation and young, massive stars. Of particular note, SPIRITS 15ade was discovered in the outskirts of NGC 5921 at a projected distance from the galaxy center of 146.″3 (17.0 kpc), while SPIRITS 15ud was found very near the nucleus of M100 at a projected distance of only 7.″5 (0.5 kpc).

We examined the location of each source in the IR-selected sample in the archival *Spitzer*/IRAC [3.6] and [4.5] reference images for the presence of possible IR progenitor stars. The regions near the objects in our sample were typically crowded by several sources or dominated by the bright, spatially variable background emission from the host galaxy. To identify possible progenitors, we constructed source catalogs and performed PSF photometry for each *Spitzer*/IRAC reference image using the DAOPHOT/ALLSTAR package (Stetson 1987), where a model of the PSF was constructed using isolated stars in the image. The PSF-fitting and photometry procedure, including corrections for the finite radius of the PSF (using the method of Khan 2017), is described in Karambelkar et al. (2019).

With the exception of SPIRITS 17qm, there are no sources in our catalogs consistent with the transient positions in *Spitzer*/IRAC reference images. We estimate upper limits on the progenitor flux as 5 times the standard deviation in a 25×25 pixel box at the transient position. The limits at [3.6] and [4.5] on the progenitor flux of each object in our sample are given in Table 5.7.

For SPIRITS 17qm, we identified a source in the [3.6] and [4.5] reference image PSF catalogs of NGC 1365, separated from the location of the transient by only $0\farcs12$ and $0\farcs24$, respectively, less than one IRAC mosaicked pixel. However, we note that this source is heavily blended with several other sources in our catalogs, and its centroid is slightly offset from the optical progenitor star identified in archival *HST* imaging below. While the coincident IR PSF catalog sources likely contain flux from the progenitor, we consider the PSF magnitudes given in Table 5.7 as upper limits given the possibility of significant contamination from nearby sources.

We also examined the available archival *Hubble Space Telescope* (*HST*) imaging for each source in our sample. To determine the precise locations of our transients in the archival *HST* frames, we registered the archival images with a detection image of the transient, usually a *Spitzer*/IRAC image where the transient is strongly detected. We used higher-resolution images of the active transients where they were available and where registration with *Spitzer* frames was insufficient to determine a precise location of the transient. To perform the registrations, we used centroid measurements of several (at least 10) relatively isolated, bright stars detected in both frames. We then determined the geometric transformations from the archival *HST* frame to the frame containing the transient using the Space Telescope Science Data Analysis System (STSDAS)[15] GEOMAP task. By applying the GEOTRAN task

[15]STSDAS is a product of STScI, which is operated by AURA for NASA.

Table 5.7: Archival imaging progenitor constraints

Name	UT Date	Tel./Inst.	Program/PI	Band	Vega Mag.	Abs. Mag.[a]
SPIRITS 14azy	2004 Dec 16.7	*Spitzer*/IRAC	PID 3333/M. Barlow	[3.6]	> 16.7	> −13.8
	2004 Dec 16.7	*Spitzer*/IRAC	PID 3333/M. Barlow	[4.5]	> 16.5	> −14.0
	2010 Oct 28.8	*HST*/WFC3 UVIS	SNAP-12229/L. Smith	F336W	> 25.5	> −5.4
SPIRITS 15c	2005 Feb 22.7	*Spitzer*/IRAC	Super Mosaic	[3.6]	> 15.5	> −17.3
	2005 Feb 22.7	*Spitzer*/IRAC	Super Mosaic	[4.5]	> 15.5	> −17.3
	1998 Nov 11.7	*HST*/WFPC2 WFC	GO-6483/D. Elmegreen	F555W	> 25.1	> −7.9
	1998 Nov 11.7	*HST*/WFPC2 WFC	GO-6483/D. Elmegreen	F814W	> 24.0	> −8.9
SPIRITS 15ud	2004 May 27.5 –2008 Jul 15.7	*Spitzer*/IRAC	Super Mosaic	[3.6]	> 12.8	> −17.9
	2004 May 27.5 –2008 Jul 15.7	*Spitzer*/IRAC	Super Mosaic	[4.5]	> 12.7	> −18.0
	2001 Nov 12.1	*HST*/WFC3 UVIS	GO-11646/A. Crotts	F775W	> 24.5	> −6.3
	2005 May 31.0	*HST*/ACS HRC	GO-9776/D. Richstone	F814W	> 24.4	> −6.4
SPIRITS 15ade	2009 Aug 29.4	*Spitzer*/IRAC	S4G/K. Sheth	[3.6]	> 19.7	> −12.2
	2009 Aug 29.4	*Spitzer*/IRAC	S4G/K. Sheth	[4.5]	> 19.1	> −12.8
SPIRITS 16ix	2010 Aug 3.5	*Spitzer*/IRAC	S4G/K. Sheth	[3.6]	> 16.3	> −15.2
	2010 Aug 3.5	*Spitzer*/IRAC	S4G/K. Sheth	[4.5]	> 16.3	> −15.2
SPIRITS 16tn	2011 Feb 7.6	*Spitzer*/IRAC	S4G/K. Sheth	[3.6]	> 15.0	> −14.7
	2011 Feb 7.6	*Spitzer*/IRAC	S4G/K. Sheth	[4.5]	> 14.8	> −14.9
	1994 Jul 4.8	*HST*/WFPC2 WFC	SNAP-5446/G. Illingworth	F606W	> 24.5	> −5.2
SPIRITS 17lb	2005 Feb 22.7	*Spitzer*/IRAC	Super Mosaic	[3.6]	> 14.9	> −17.9
	2005 Feb 22.7	*Spitzer*/IRAC	Super Mosaic	[4.5]	> 14.8	> −18.0
	2012 Dec 4.5	*HST*/WFC3 UVIS	SNAP-13029/A. Filippenko	F625W	> 26.8	> −9.4
	2012 Dec 4.5	*HST*/WFC3 UVIS	SNAP-13029/A. Filippenko	F814W	> 26.2	> −8.9
SPIRITS 17pc	2004 May 27.6 –2008 Jul 17.7	*Spitzer*/IRAC	Super Mosaic	[3.6]	> 14.6	> −16.7
	2004 May 27.6 –2008 Jul 17.7	*Spitzer*/IRAC	Super Mosaic	[4.5]	> 14.4	> −16.9
	2011 Jun 8.3	*HST*/WFC3 UVIS	GO-12185/J. Greene	F336W	> 26.06	> −5.4
	2011 Jun 8.4	*HST*/WFC3 UVIS	GO-12185/J. Greene	F438W	> 26.2	> −5.2
	2011 Jun 8.4	*HST*/WFC3 UVIS	GO-12185/J. Greene	F814W	24.21 ± 0.05	−7.1
	2011 Jun 8.2	*HST*/WFC3 IR	GO-12185/J. Greene	F110W	21.76 ± 0.04	−9.6
	2011 Jun 8.2	*HST*/WFC3 IR	GO-12185/J. Greene	F160W	20.60 ± 0.02	−10.7
SPIRITS 17qm	2004 Dec 16.4	*Spitzer*/IRAC	Super Mosaic	[3.6]	> 15.3	> −16.0
	2004 Dec 16.4	*Spitzer*/IRAC	Super Mosaic	[4.5]	> 14.9	> −16.5
	2001 Mar 8.3	*HST*/WFPC2 PC	SNAP-8597/M. Regan	F606W	22.45	−9.3
	2001 Jun 9.1	*HST*/WFPC2 WFC	SNAP-8597/M. Regan	F606W	20.77	−11.0

[a] Corrected for Galactic extinction only.

to the archival frames and blinking these transformed images against the transient detection images, we verified the quality of the registrations. We then examined the precise location of each transient in the available archival frames to search for the presence of a possible progenitor star.

For SPIRITS 15c and SPIRITS 16tn, we discussed the limits we obtained on their progenitors from this procedure in Jencson et al. (2017e) and Jencson et al. (2018e). We obtained precise registrations of the *HST*/WFPC2 F555W and F814W images taken 1998 November 11.7 with program GO-6483 (PI: D. Elmegreen) using a Baade/IMACS WB6226-7171 image of the SPIRITS 15c from 2015 January 20.0. We derived 5σ limiting magnitudes on the progenitor of $V > 25.1$ and $I > 24.0$, cor-

responding to limits on the absolute magnitude of the progenitor of $M_V > -7.9$ and $M_I > -8.9$, correcting for Galactic extinction to IC 2163 only. We constrained the flux from the progenitor of SPIRITS 16tn to $V \gtrsim 24.5$ in an archival WFPC2/WFC F606W frame from 1994 July 4.8 (PID SNAP-5446; PI: G. Illingworth), corresponding to limits on the absolute magnitude of $M_V > -5.2$ (correcting for Galactic extinction only; $L < 2.9 \times 10^4\ L_\odot$ for a red supergiant [RSG] progenitor of spectral type M0); however the limit is not constraining for an SN II progenitor if one assumes heavy extinction of $A_V \sim 8$ as was inferred for SPIRITS 16tn in Jencson et al. (2018e) based on the optical/near-IR SED of the transient.

The location of SPIRITS 14azy was imaged with WFC3/UVIS in the F336W filter on 2010 October 28.8 with program SNAP-12229 (PI L. Smith), nearly 4 yr before the discovery of the transient, which we registered with the *Spitzer*/IRAC [4.5] discovery image of the transient. The rms uncertainty in the registration is 0.9 WFC3 pixels (0.″036) in both the x- and y-directions. As shown in Figure 5.6, the location is within an apparent dust lane, completely devoid of stars consistent with the transient position. The limiting magnitude in the image is $U \gtrsim 25.5$, which we adopt as a limit on the progenitor flux, corresponding to a limit on the absolute magnitude of the progenitor star of $M_U \gtrsim -5.4$ (Galactic extinction correction only).

SPIRITS 15ud is located near the nucleus of M100 and was covered in several bands at several epochs with *HST*/WFPC2 and WFC3. We selected the WFC3/UVIS F775W image from 2001 November 12.1 (PID GO-11646; PI A. Crotts) for registration with the *Spitzer*/IRAC [4.5] discovery image, for which we obtained an rms uncertainty on the position of the transient of 0.84 WFC3 pixels (0.″034). The transient is located in a prominent, nearly opaque dust lane (see Figure 5.6), and we detect no source consistent with the transient position to a limiting depth of $I \gtrsim 24.5$ ($M_I \gtrsim -6.3$; Galactic extinction only). We also examined this position in the ACS/HRC F814W frame from 2005 May 31.0 (PID GO-9776; PI D. Richstone), deriving a limit on the flux from the progenitor of $I \gtrsim 24.4$ ($M_I \gtrsim -6.4$).

SPIRITS 17lb is located near the edge of the southern spiral arm of IC 2163, with possible extinction by the foreground spiral arm of the companion galaxy NGC 2207. This location was covered in WFC3/UVIS F625W and F814W images taken on 2012 December 4.5 (PID SNAP-13029; PI A. Filippenko). We selected the F814W image for registration with the *Spitzer*/IRAC [4.5] discovery image, for which we obtained an rms uncertainty of 0.94 WFC3 pixels (0.″038). The transient location is coincident with a patch of unresolved, diffuse starlight, characterized by variable extinction in

the vicinity. The limits on the progenitor flux from these images are $I \gtrsim 26.2$ and $R \gtrsim 26.8$, corresponding to limits in absolute magnitude of $M_I \gtrsim -8.9$ and $M_R \gtrsim -9.4$.

We reported on the analysis of the WFC3/UVIS and IR frames covering the site of SPIRITS 17pc and SPIRITS 17qm in Jencson et al. (2018a) and Jencson et al. (2018b), respectively. The site of SPIRITS 17pc was covered in WFC3/UVIS and IR F336W, F438W, F814W, F110W, and F160W images taken on 2011 June 8 (PID GO-12185; PI J. Greene). We registered the F110W frame with a high-resolution, J-band image taken with the Keck II/NIRC2 adaptive optics image of the active transient from 2017 December 8.6, obtaining a registration rms uncertainty of 0.15 WFC3 pixels (0.″02). There are several blended sources near the location of SPIRITS 17pc in the WFC3 frames. We analyzed the sources near the location using PSF-fitting photometry with DOLPHOT (Dolphin 2000; Dolphin 2016). We identify a source consistent with the precise transient position and rated as a "good star" by DOLPHOT in the F814W, F110W, and F160W images. There is coincident emission in the F336W and F438W frames, but it is not point-like and is blended with nearby objects. Our PSF-photometry from DOLPHOT on the candidate progenitor gives F336W > 26.06 mag, F438W > 26.18 mag, F814W $= 24.21 \pm 0.05$ mag, F110W $= 21.76 \pm 0.04$ mag, and F160W $= 20.60 \pm 0.02$ mag. At the distance to NGC 4388, the photometry can be well fit by a single blackbody component of $T = 1900 \pm 100$ K and $L = 2.1^{+0.4}_{-0.3} \times 10^5\ L_\odot$.

There are two epochs of WFPC2 F606W images taken on 2001 March 8.3 and 2001 June 9.1 (PID SNAP-8597; PI M. Regan) covering the site of SPIRITS 17qm. We registered the first WFPC2 image with the *Spitzer*/IRAC [3.6] discovery image and obtained an rms uncertainty of 3.0 WFPC2 pixels (0.″3). As shown in Figure 5.6, there is a single, isolated point source consistent with the location of SPIRITS 17qm in both WFPC2 frames. We obtained magnitudes from the Hubble Legacy Archive source catalogs of $V = 22.45$ (2001 March 8) and $V = 20.77$ (2001 June 9), indicating that the source is highly variable and brightened by $\approx$1.7 mag during the 3 months between the two epochs. The absolute magnitudes then are $V \approx -9.3$ and -11.0 for each epoch, respectively, indicating that the star is highly luminous. While the localization of SPIRITS 17qm in the WFPC2 frames is coarse, the marked variability of the coincident star strongly suggests a physical association.

There is no archival *HST* imaging available for the sites of SPIRITS 15ade in NGC 5921 or SPIRITS 16ix in NGC 4461.

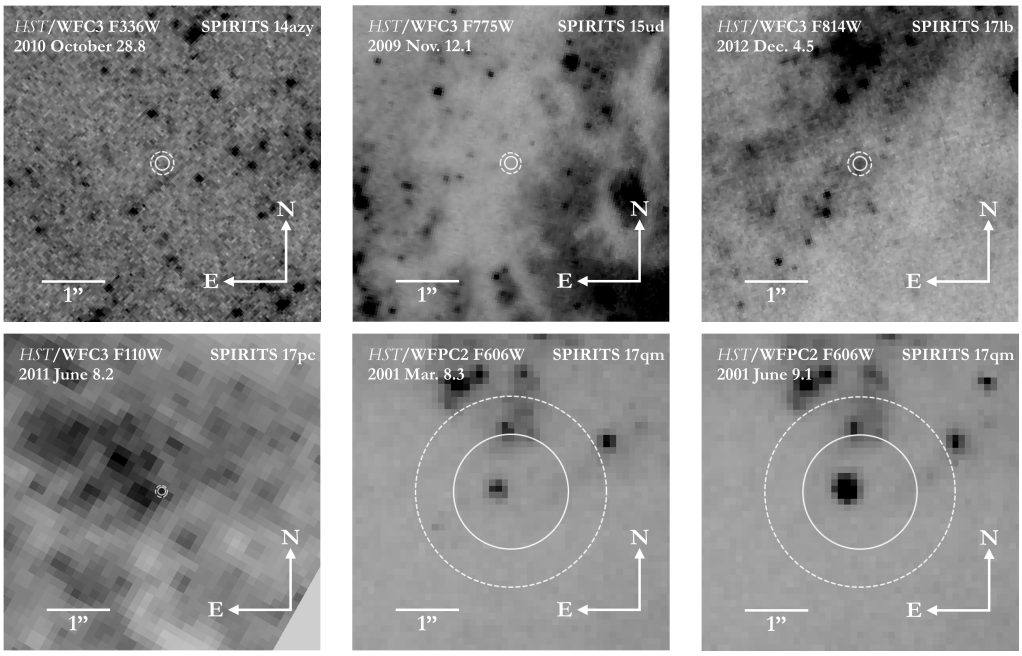

Figure 5.6: Archival *HST* images of the locations, from left to right, of SPIRITS 14azy, SPIRITS 15ud, and SPIRITS 17lb (top row), and SPIRITS 17pc and the two epochs covering SPIRITS 17qm (bottom row). The portion of each image shown is a $5'' \times 5''$ box, oriented with north up and east to the left. The 3σ (5σ) error circles on the locations of the transients in each image are shown as the solid (dashed) white circles. Each image is labeled with the instrument/filter combination used and the date of the observation.

Spitzer light curves

The [4.5] light curves and [3.6]−[4.5] color curves of the IR-selected obscured SN candidate sample are shown in Figure 5.2. In the left panel for each object, we compare to those of the optically discovered control sample. We define zero phase in a uniform way for each object across both samples as the time of peak brightness in the *Spitzer*/IRAC bands. For SN 2017eaw, we adopt 2017 September 13.6 as the observed time of peak brightness; however, the SN was saturated in the images taken on this date, and we do not have a reliable flux measurement of the peak.

The [4.5] light curves of the IR-selected sample appear broadly similar to those of the control sample, usually showing a luminous initial peak and subsequent fade over a timescale of ≈200–600 days. SPIRITS 17pc and SPIRITS 17qm represent notable exceptions, as both sources underwent previous luminous IR outbursts, up to nearly 1500 days before the observed peak in the case of SPIRITS 17qm. While both sources have begun to decline in IR brightness since their discovery, we will continue to monitor their IR with *Spitzer* throughout Cycle 14 ending in 2020 January.

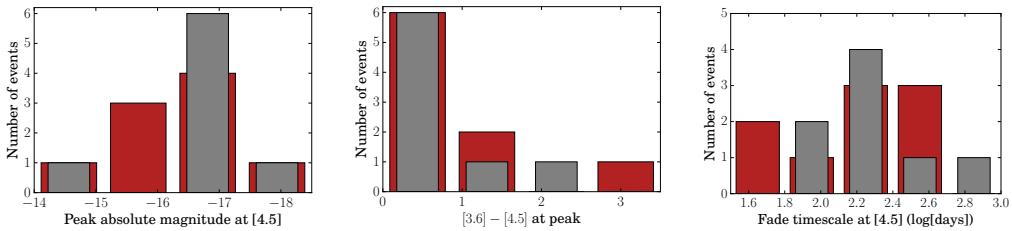

Figure 5.7: Observed distributions of peak absolute magnitude at [4.5] (left), [3.6]−[4.5] color at time of peak (middle), and fade timescale at [4.5] (right) for the IR-discovered sample (red) and the optically discovered control sample (gray).

Table 5.8: Properties derived from light curves and suggested classifications

Name	t_0 (MJD)	Max Age days	$t_{\rm peak}$ (MJD)	$M_{[4.5],\rm peak}$ (mag)	[3.6]−[4.5][a] (mag)	$t_{\rm fade,[4.5]}$ (days)	A_V (mag)	Classification
SPIRITS 14azy	56,772.0	27.9	57,245.1	-14.4	0.55 ± 0.04	270	3.2	LRN[b]
SPIRITS 15c	56,890.4	27.0	57,057.4	-17.1	3.0 ± 0.2	85	2.2	SN Ib/IIb
SPIRITS 15ud	57,271.7	381.4	57,271.7	-16.4	0.5 ± 0.1	170	$\gtrsim$ 3.7	SN II[b]
SPIRITS 15ade	57,276.5	34.0	57,337.9	-15.7	0.67 ± 0.03	220	2.7	ILRT
SPIRITS 16ix	57,477.9	195.2	57,477.9	-15.8	1.61 ± 0.05	55	$\gtrsim$ 5.5	SN II[b]
SPIRITS 16tn	57,615.0	82.0	57,615.1	-16.7	0.68 ± 0.03	55	7.8	SN II[b]
SPIRITS 17lb	57,901.7	149.8	57,901.7	-18.2	1.09 ± 0.03	160	$\gtrsim$ 2.5	SN II[b,c]
SPIRITS 17pc	57,878.8	249.9	58,250.4	-16.3	0.39 ± 0.04	...	12.5	MSE
SPIRITS 17qm	58,062.2	234.0	58,062.2	-15.9	0.21 ± 0.04	480	12.1	MSE/LBV

[a] Measured at time $t_{\rm peak}$.
[b] Suggested classification for these sources is not spectroscopically confirmed.
[c] SPIRITS 17lb was confirmed as a CCSN via the detection of its radio counterpart.

The [3.6]−[4.5] color curves are also qualitatively similar between the two samples. Most objects are found with red colors between $0 \lesssim$ [3.6]−[4.5] $\lesssim 1$ throughout their evolution, with a few events achieving even redder colors up to ≈3 mag The reddest object we observe is SPIRITS 15c with [3.6]−[4.5] = 3.0 ± 0.2 at the time of the observed IR peak, rivaled by SN 2014bi with [3.6]−[4.5] = 2.9 ± 0.2 at 225.5 days post-peak.

We can make a more quantitative comparison between the IR-selected and optically selected control samples based on properties derived from the [3.6] and [4.5] light curves. In Figure 5.7, we show histograms for both samples of their peak absolute magnitudes at [4.5], $M_{[4.5],\rm peak}$, their [3.6]−[4.5] colors at peak, and the characteristic fade timescales of their [4.5] light curve, $t_{\rm fade,[4.5]}$, defined as the time in days for the light curve to decline by 1 mag from a linear (in magnitudes) fit to the post-peak light curve. These properties for IR-selected events are also summarized in Table 5.8.

Both samples span a range in peak [4.5] luminosity, $M_{[4.5],\rm peak}$, between −14 and

-18.5. The distributions in $M_{[4.5],\mathrm{peak}}$ appear similar, with both peaking between ≈ -16.3 and -17.4. We note that there is a larger fraction of low-luminosity events in the IR-selected sample, i.e., three of nine objects ($\approx$33%) have $M_{[4.5],\mathrm{peak}}$ fainter than -16, while there is only one such object of eight ($\approx$13%) in the control sample. In [3.6]$-$[4.5] color at peak, the two samples again show similar distributions that peak in the range $0.0 \lesssim$ [3.6]$-$[4.5] $\lesssim 0.9$ with one-sided tails extending to redder colors. Finally, in the distributions of $t_{\mathrm{fade},[4.5]}$, we once again note the broad similarity between the two samples. The distributions extend between $\approx$50 and 500 days, with peaks between $\approx$130 and 250 days. Notably, though, the two most rapidly fading events in either sample are SPIRITS 16ix and SPIRITS 16tn, both from the IR discovered sample, with $t_{\mathrm{fade},[4.5]} = 55$ days for both, while the next-fastest events are SPIRITS 15c and SN 2016bau (Type Ib) with $t_{\mathrm{fade},[4.5]} \approx 80$ days.

We performed Kolmogorov–Smirnov tests between the two samples in each of the light-curve-derived parameters discussed above. For the distributions in $M_{[4.5],\mathrm{peak}}$, [3.6]$-$[4.5] color at peak, and $t_{\mathrm{fade},[4.5]}$, the tests return p-values of 0.31, 0.91, and 0.97, respectively. Thus, we are unable to reject the null hypotheses that the IR-selected and optically discovered samples are drawn from the same parent distribution in all three parameters. The overall similarity of the two samples in their IR properties supports the suggestion that the IR-selected objects presented in this work may represent a population of SNe that were systematically missed by optical transient searches.

Comparison to *Spitzer* SNe

In the right panel for each object in Figure 5.2, we compare the SPIRITS transients to the entire sample of SNe so far detected by *Spitzer*/IRAC. A large compilation including every available *Spitzer*/IRAC detection of known SNe through 2014 was recently presented by Szalai et al. (2019a), including the previously published compilations of Szalai and Vinkó (2013), Tinyanont et al. (2016), and Johansson et al. (2017); detections of individual SNe originally reported by several authors; and new, previously unpublished detections. To this, we add new detections since 2014 of the optically discovered SNe in our control sample.

We divide this large comparison sample by subtype into hydrogen-rich SNe II (and interacting SNe IIn), stripped-envelope SNe IIb and SNe Ib/c (and interacting SNe Ibn), and thermonuclear SNe Ia (and interacting SNe Ia-CSM) to demonstrate the diagnostic utility of IR light curves.

In the IR, as found by Johansson et al. (2017), SNe Ia are clearly separated from CCSNe by their rapidly declining [4.5] light curves and evolution to blue [3.6]−[4.5] colors for the first 200 days. The IR emission of SNe Ia is powered by the tail of the hot thermal component of the SN peaking in the optical, and Johansson et al. (2017) placed stringent limits on the presence of dust within $\lesssim 10^{17}$ cm of $M_{\rm dust} \lesssim 10^{-5}\ M_{\odot}$ for the SNe Ia SN 2014J, SN 2006X, and SN 2007le. Characterized by strong interaction with a dense circumstellar medium (CSM), SNe Ia-CSM may display redder colors from $0.0 \lesssim$ [3.6]−[4.5] $\lesssim 1.0$, and show a clear IR excess over a normal SN Ia in their [4.5] light curves. Similarly, the unusual, dusty Type Iax SN 2014dt showed redder colors and developed a clear dust excess at [4.5] peaking at ≈500 days. With the exception of the ongoing outburst SPIRITS 17pc that shows an initial rise, all of the SPIRITS transients are characterized by declining [4.5] light curves and red IR colors throughout their evolution, inconsistent with the characteristic evolution of SNe Ia and largely dissimilar to the thermonuclear SN subtypes of SNe Ia-CSM and SNe Iax that have been now been characterized by *Spitzer*.

CCSNe, on the other hand, are characterized by more slowly declining IR light curves and redder IR colors with $0 \lesssim$ [3.6]−[4.5] $\lesssim 3$. The IR emission of CCSNe may be powered by thermal emission from the SN itself, or warm circumstellar dust that may be newly formed in the ejecta or preexisting dust heated by the light from the explosion. Additionally, if CO has formed in the ejecta as in the case of Banerjee et al. (2018), the emission at [4.5] may be additionally powered by the fundamental CO vibrational transition in this band, producing a significant [4.5] excess over the other IR bands. This likely contributes to the extreme observed [3.6]−[4.5] colors in several cases. Among the sample of CCSNe, stripped-envelope events (including the interacting subtype Ibn) are relatively more homogeneous in their IR properties, characterized by monotonically declining [4.5] light curves with $M_{[4.5]}$ peaking between −17.5 and −19, and fading at a typical rate of ≈0.01 mag day^{-1}. SNe II show a larger spread in both peak luminosity, spanning $M_{[4.5]}$ between −16 and −19, and decay rates, with some objects having nearly constant [4.5] flux for the first ≈500 days. Strongly interacting SNe IIn may exhibit extreme [4.5] luminosities of $M_{[4.5]}$ brighter than −22, though some SNe IIn have IR light curves similar to more typical SNe II.

Now, for each IR-selected SPIRITS transient, we discuss inferences on possible classifications by comparing their IR light curves directly to the *Spitzer*-observed

SNe. Where appropriate, we also provide context for our final, suggested classifications based on all available observational data provided in the rightmost column of Table 5.8 and discussed in more detail in Section 5.5.

SPIRITS 14azy, peaking at only $M_{[4.5]} = -14.4 \pm 0.2$, is fainter than any previously observed CCSN. While consistent with the luminosity of an SN Ia at a phase of $\approx$120 days, the [4.5] fade rate is much slower, and the source is overluminous compared to an SN Ia by 400 days post-discovery. Furthermore, its color evolution is inconsistent with an SN Ia. Based only on the IR light curves and considering only SN subtypes, SPIRITS 14azy would be most consistent with a faint SN II; however, as discussed below in Sections 5.4 and 5.5, optical light curves bear strong similarity to the LRN M101 OT2015-1, arguing against SPIRITS 14azy as a true CCSN.

SPIRITS 15c, spectroscopically confirmed as an SN Ib/IIb in Jencson et al. (2017e), is fully consistent with the sample of stripped-envelope SNe in its [4.5] light curve. At [3.6]−[4.5] = 3.0 at peak light, it is the reddest stripped-envelope SN yet observed by *Spitzer*. The extreme IR color is likely attributable to CO emission at [4.5], corroborated by the detection of emission from the CO $\Delta v = 2$ vibrational overtone transitions in the K band also reported in Jencson et al. (2017e).

The [4.5] light curve of SPIRITS 15ud appears most similar to the sample of SNe II. With an observed peak at $M_{[4.5]} = -16.4$, however, it may also be consistent with the class of SN 2008S-like transients (also including NGC 300 OT2008-1; Adams et al. 2016). Given the large uncertainty in the phase of SPIRITS 15ud of $\gtrsim$ 400 days, however, it is likely that the transient was significantly more luminous than SN 2008S, but the IR peak was missed by our observations.

SPIRITS 15ade again appears consistent with either a low-luminosity SN II or an SN 2008S-like event in both its [4.5] light curve and [3.6]−[4.5] color evolution. We examine the classification of this object as an SN 2008S-like event also considering its near-IR spectrum and limits on the presence of an IR progenitor star in Section 5.5.

SPIRITS 16ix and SPIRITS 16tn, with largely similar IR properties, are unique among the SPIRITS IR transients presented here, and among all SNe previously observed by *Spitzer*. Their light curves at [4.5] decline more rapidly than any CCSN yet observed and appear consistent with the decline of an SN Ia. However, their red colors at [3.6]−[4.5] $\gtrsim$ 0.7 rule out an SN Ia scenario. In Jencson et al. (2018e), we argued that the properties of SPIRITS 16tn were most consistent with a weak

SN II, where the early bright IR emission was powered by a luminous dust echo, and the redder [3.6]−[4.5] color at later times was likely attributable to a [4.5] excess from CO emission. This interpretation may also apply to SPIRITS 16ix given the similarity of these objects in the *Spitzer* bands.

SPIRITS 17lb is our most luminous transient at $M_{[4.5]} = -18.2 \pm 0.4$, and its light curve and color evolution are consistent with either a luminous SN II or stripped-envelope SN IIb or Ib/c. While we are unable to distinguish between CCSN subtypes based on the *Spitzer* data alone, we discuss the likely classification of SPIRITS 17lb as an SN II based on the rest of our follow-up data at optical, near-IR, and radio wavelengths in Section 5.5.

SPIRITS 17pc and SPIRITS 17qm are remarkable among the SPIRITS sample owing to the presence of multiple IR outbursts in the *Spitzer* light curves over the last ≈1000–1500 days. As reported in Jencson et al. (2018a), SPIRITS 17pc shows three distinct IR peaks at [3.6] and [4.5], growing progressively more luminous and longer in duration. During the current, ongoing outburst, SPIRITS 17pc brightened to $M_{[4.5]} = -16.3 \pm 0.4$ over a period of at least 400 days, with a fairly constant color between [3.6]−[4.5] = 0.2 and 0.4. The increasing IR emission may indicate ongoing interaction of an SN blast wave with the surrounding CSM, or alternatively, active dust formation during a less extreme, nonterminal outburst.

SPIRITS 17qm, as reported in Jencson et al. (2018b), underwent a previous IR outburst ≈1300 days at $M_{[4.5]} = -15.2 \pm 0.1$ before the discovery by SPIRITS. The observed peak at discovery of $M_{[4.5]} = -15.9 \pm 0.1$ and subsequent slow decline are consistent with an SN II, or even some previously observed interacting SN IIn. Given its eruptive history, however, the discovery outburst of SPIRITS 17qm may be due to a more intense nonterminal outburst, rather than a true SN explosion.

Optical/near-IR spectroscopic properties

Our optical spectroscopy of SPIRITS 16tn (79.5 days), SPIRITS 17pc (192.8 days), and SPIRITS 17qm (9.3 days) is shown in Figure 5.3. The spectrum of SPIRITS 16tn, previously presented in Jencson et al. (2018e), shows only a featureless red continuum beyond ≈8000 Å. The spectrum of SPIRITS 17qm is dominated by strong Hα emission with an FWHM velocity of 2400 km s^{-1} (top left panel of Figure 5.8), consistent with ejecta velocities of giant LBV eruptions. We do not detect any broader components that would indicate higher, explosive velocities of an interacting SN IIn. Additionally, in SPIRITS 17qm we detect weaker emission

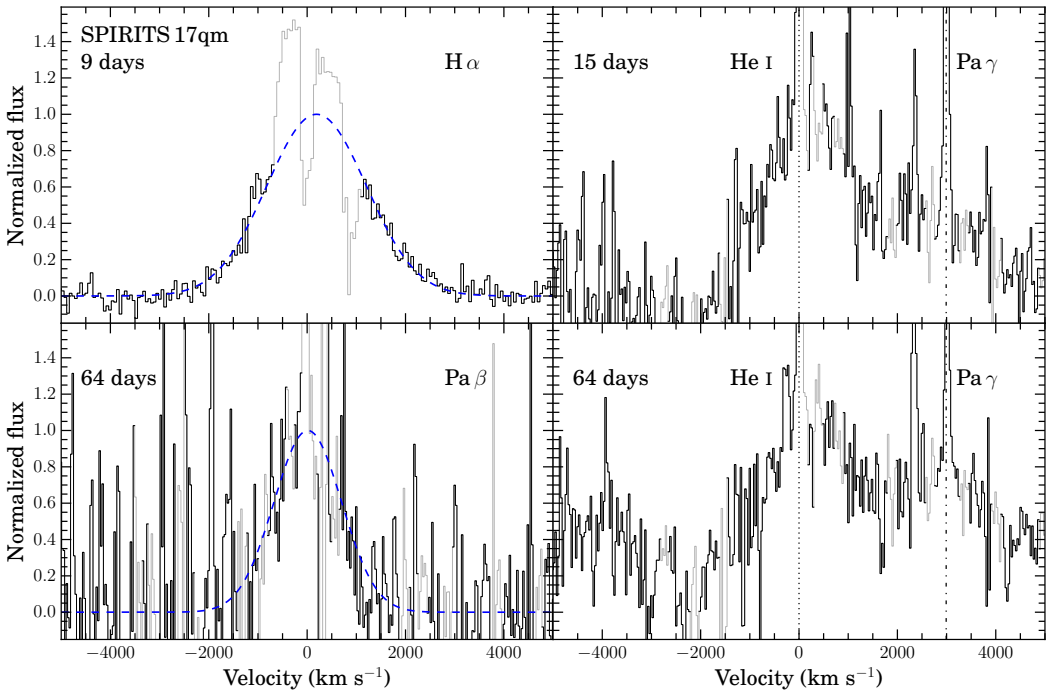

Figure 5.8: In the left panels we show the Hα (top; 9 days) and Paβ (bottom; 64 days) velocity profiles of SPIRITS 17qm in black. Gaussian fits to the data with FWHM velocities of 2400 and 1600 km s^{-1}, respectively, are plotted as blue dashed curves, where spectral bins contaminated by emission features of the underlying star-forming region or bright OH airglow emission lines are shown in light gray and excluded from the fits. In the right 2 panels, we show the velocity profiles of He I (λ10830; dotted vertical lines) at 15 days (top) and 64 days (bottom), with FWHM velocities of $\approx$2000 km s^{-1}. The red wing of the line is blended with emission from Paγ (dashed-dotted vertical lines)

.

features of O I ($\lambda\lambda$8446, 9266), but with no clear detection of the O I λ7771 line, as well as detections of the Ca II IR triplet ($\lambda\lambda$8498, 8542, 8662). In contrast, for SPIRITS 17pc, we detect narrow, unresolved emission features of the underlying star-forming region (including Hα), along with the Ca II triplet in emission, but no significant O I emission or broader components of Hα associated with the transient. We confirmed the veracity of the weaker features reported here by close inspection of the reduced 2D spectra.

A zoom-in to the region around O I (λ8446) and the Ca II triplet in the spectra of SPIRITS 17pc and SPIRITS 17qm is shown in Figure 5.9. The Ca II lines in SPIRITS 17pc are each double peaked, with a blueshifted component at $\approx -$ 240 km s^{-1} and a redshifted component at $\approx$100 km s^{-1}. For SPIRITS 17qm, the lines show a single component centered at a velocity consistent with the host and

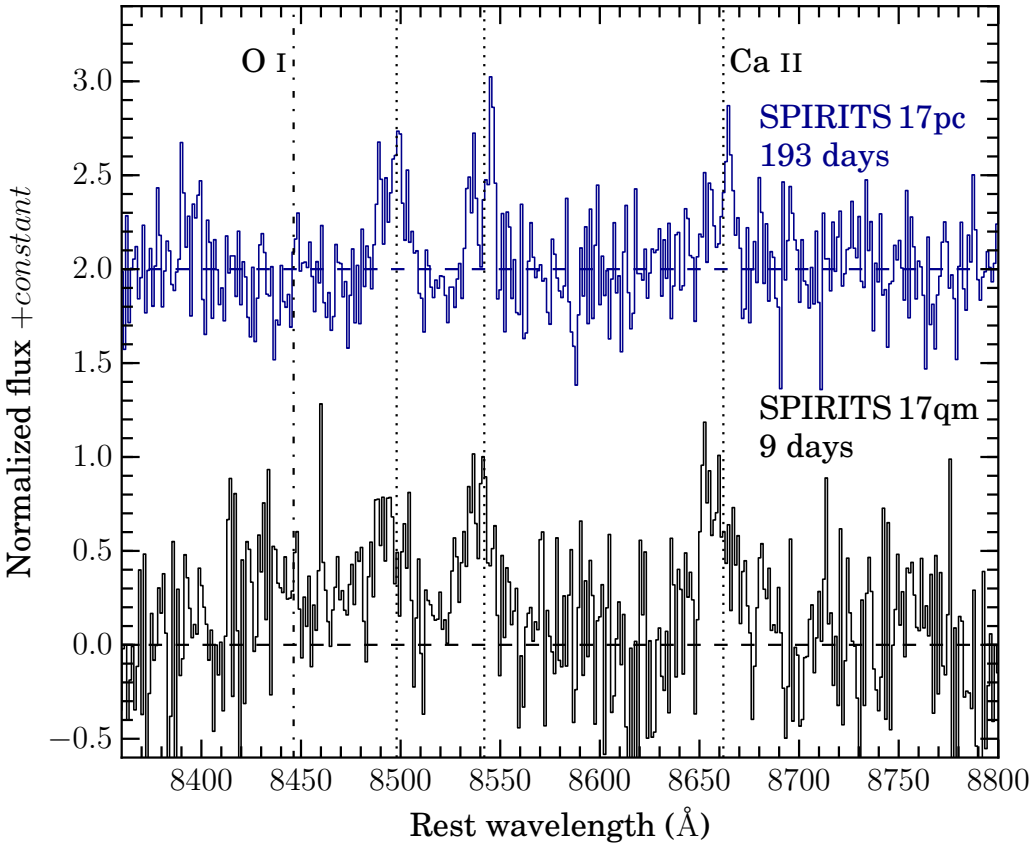

Figure 5.9: Comparison of the spectral region around O I (λ8446; dashed-dotted vertical line) and the Ca II IR triplet (dotted vertical lines) in the optical spectra of SPIRITS 17pc (193 days) and SPIRITS 17qm (9 days). A linear approximation to the continuum emission has been subtracted from the spectra. The spectra were then normalized in flux, and the SPIRITS 17pc spectrum has been shifted vertically for clarity. The dashed blue and black horizontal lines show the zero-levels for SPIRITS 17pc and SPIRITS 17qm, respectively.

with an FWHM velocity of $\approx$230 km s^{-1}. We also note that the O I line at 8446 Å present in SPIRITS 17qm, is absent or much weaker in SPIRITS 17pc.

The full set of our near-IR spectroscopy is shown in Figure 5.4, including spectra of six of the nine IR-discovered transients. In the near-IR, these objects are spectroscopically diverse, showing a range of properties and features. Our clearest example of a spectroscopically confirmed CCSN is SPIRITS 15c. In Jencson et al. (2017e), we compared the near-IR spectra of SPIRITS 15c to those of the well-studied type IIb SN 2011dh. We found strong similarities and identified several features in SPIRITS 15c based on the comparison, including He I (10830 Å), emission features of neutral or singly ionized intermediate-mass elements and Fe, and emission from the

$\Delta v = 2$ vibrational overtone transitions of CO (see Figure 5.10 in comparison to SPIRITS 17lb and SPIRITS 17pc). We do not detect any hydrogen in the spectrum but cannot rule out the presence of hydrogen at earlier times. Thus, we find the spectrum to be consistent with a Type Ib or IIb classification.

Our near-IR spectroscopy of SPIRITS 16tn was first presented in Jencson et al. (2018e), where the spectrum was characterized as a largely featureless red continuum. The spectrum, however, displays broad bumps in each of the H and K bands that we originally believed may have been due to difficulty in properly flux-calibrating low-S/N data, especially in the regions of strong telluric H_2O absorption where little to no flux from the transient is received through the atmosphere. Here, after carefully checking our calibrations, we suggest a real, astrophysical origin for these broad features as absorption by water vapor at higher temperatures than the narrower telluric features. Such features have been observed in the atmospheres of cool giants with spectral types no earlier than M6 (Rayner, Cushing, and Vacca 2009), where models of pulsating Mira variables show the formation of water in the dense, cool (< 1000 K) layers formed beyond periodic, outward-propagating shocks in their extended atmospheres (Bessell et al. 1989; Bessell, Scholz, and Wood 1996). To our knowledge, this would be the first detection of water vapor absorption associated with a luminous transient or SN, and we discuss possible interpretations in Section 5.5. As we detected no unambiguous SN features, however, we cannot definitively classify SPIRITS 16tn.

For SPIRITS 17lb, we detect a red continuum in the H and K regions, plausibly attributable to emission from warm dust. We note only possible excess emission beyond 23000 Å from CO in the 123-day spectrum, but which appears to fade by 157 days. As with SPIRITS 16tn, there are no clear, broad features indicative of an SN. We find, however, that a lack of such features does not rule out an SN altogether for these objects. As discussed below in Section 5.4, nonthermal synchrotron emission from the interaction of high-velocity ejecta with CSM was detected in SPIRITS 17lb, confirming the core-collapse nature of this event. The strength of the radio emission suggests an SN II classification, possibly indicating that SNe II may be characterized by only weak or absent near-IR features at late phases. It is relevant to note here that we have not attempted to remove contamination from the host galaxy background from our spectra, and that the absence of strong, clear features may also be attributable to the inclusion of galaxy light as sources become faint at late times.

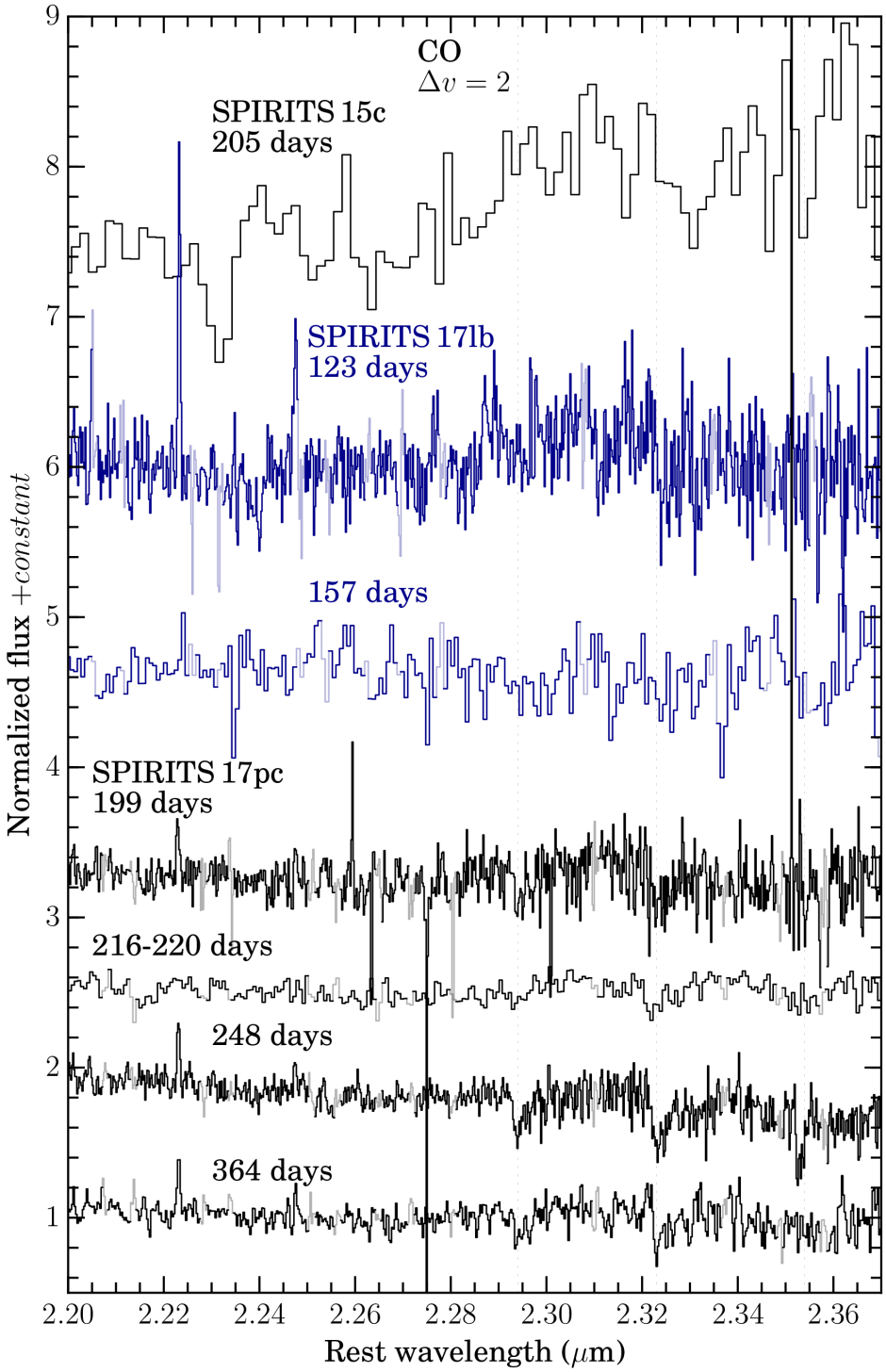

Figure 5.10: Comparison of the region of the K band between 2.2 and 2.37 μm in the near-IR spectra of SPIRITS 15c, SPIRITS 17lb, and SPIRITS 17pc. The spectra, shown in alternating colors for each object, are labeled on the figure along with their respective phases. Spectral bins of low S/N due to coincidence with bright OH airglow emission lines are plotted in lighter colors. The band heads of the $\Delta v = 2$ vibrational transitions of CO are indicated by the dotted vertical lines.

The spectra of SPIRITS 15ade show only the H I recombination lines Brγ in the K band and Paβ in the J band. As shown in Figure 5.11, the peak velocities are consistent with the recession velocity of the host, and the velocity profiles can be approximated by simple Gaussians with FWHM velocities of ≈360 and 390 km s^{-1}, respectively. These are similar to the low expansion velocities seen in the H I lines in optical spectra of the prototypical members of the class of ILRTs SN 2008S (e.g., Botticella et al. 2009) and NGC 300 OT2008-1 (Bond et al. 2009; Humphreys et al. 2011). The similarity of the [4.5] light curve of SPIRITS 15ade to that of SN 2008S (Section 5.4) strengthens its association with this class. There is also an apparent secondary peak in the Brγ and Paβ velocity profiles in SPIRITS 15ade at ≈300 km s^{-1}, possibly indicative of a bipolar or toroidal outflow geometry. Double-peaked profiles were also seen in the H I and Ca II emission features in NGC 300 OT2008-1 (Bond et al. 2009), but at lower velocities of ≈70–80 km s^{-1}.

The near-IR spectra of SPIRITS 17pc, taken between 199 and 364 days, show a relatively smooth continuum, with a few notable features. We identify an absorption band of molecular CN at 1.1 μm along with the CO $\Delta v = 2$ band heads beyond 2.3 μm (shown in more detail in Figure 5.10). These features are characteristic of mid-G to early K-type stellar spectra, and the spectra bear particular resemblance to G6 Ia–Ib supergiants (see the NASA Infrared Telescope Facility; IRTF spectral library of cool stars; Rayner, Cushing, and Vacca 2009). Despite good coverage of several near-IR H I recombination lines, we detect only narrow H lines from the underlying star-forming region and no broader features associated with the transient (also for He I $\lambda\lambda$10830, 20581). As described above, the Ca II IR triplet emission (seen in absorption in mid-G to early K-type stellar spectra) suggests an outflow with velocities of ≈100–240 km s^{-1}. While we do not detect H recombination features from the transient, this is consistent with a temperature of ≈5400–5600 K inferred by the presence of CN/CO absorption and the presence of Ca II in the spectrum, as such temperatures are too low for a significant fraction of the hydrogen to be ionized. The relatively low outflow velocities observed for SPIRITS 17pc and cooler, stellar-like spectrum suggest that this event is likely associated with nonterminal outbursts or eruptions of its progenitor, rather than a true SN.

In the near-IR, SPIRITS 17qm shows emission features of H I, as well as the He I λ10830 line. As shown in Figure 5.8, these lines are relatively broad. The Paγ line at 64 days, well approximated by a gaussian with an FWHM velocity of 1600 km s^{-1}, is somewhat narrower than the Hα emission line observed at an earlier phase of

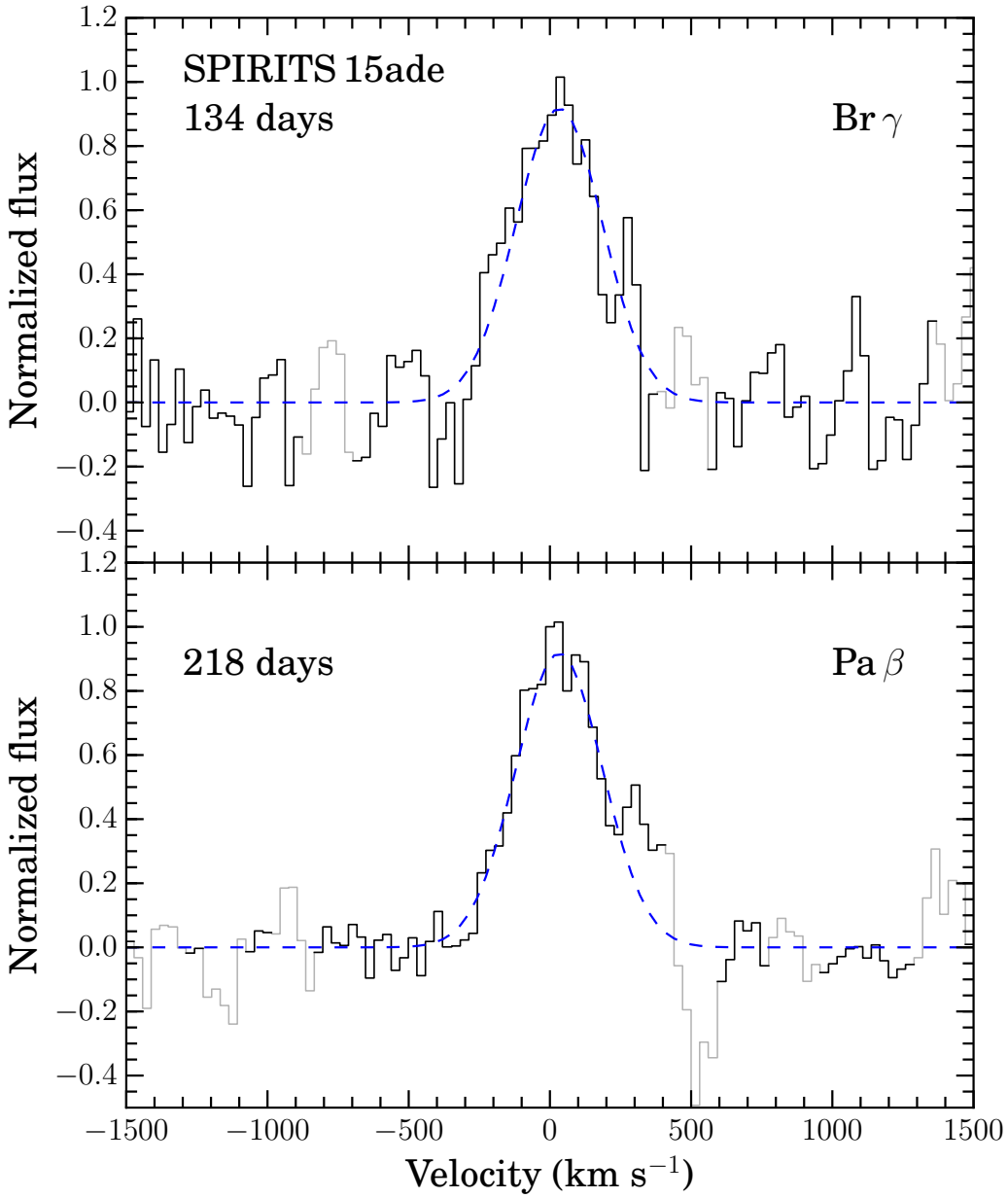

Figure 5.11: Velocity profiles of Brγ (134 days) and Paβ (218 days) in the spectra of SPIRITS 15ade are shown as the black solid lines in the top and bottom panels, respectively, in the rest frame of the host galaxy, NGC 5921. Gaussian fits to the profiles, excluding velocity bins of low S/N due to coincidence with bright OH airglow emission lines (plotted in light gray), are shown as the blue dashed curves.

9 days. The spectra are consistent with a giant eruption from an LBV, and while a low-energy SN IIn may also be possible, the lack of higher-velocity features argues against the terminal explosion of the progenitor.

Multiband light curves and extinction estimates

Using available data, we compiled multiband light curves from the optical to near-IR for each luminous SPIRITS transient in our sample. Theses light curves are shown in Figure 5.12. We then estimate the visible extinction, A_V (after correcting for the Galactic contribution), which may come from the foreground interstellar medium (ISM) of the host galaxy, from the local circumstellar environment of the progenitor, or by dust formed in the event itself. We provide our estimates, based on the analysis below, in Table 5.8. In most cases, we are unable to make strong statements about the origin of the extinction, and throughout this section we assume a standard Milky Way ISM extinction law with $R_V = 3.1$ (Fitzpatrick 1999). To obtain A_V estimates where we have a reasonably secure classification of the transient, we attempt to make a direct comparison with template light curves from a well-studied object. Where the classification of a transient is less secure, or where good template light curves were not available, we adopt $m_X - m_{[4.5]}$ near the observed peak of the transient as an estimate of A_X, the extinction in broadband filter X (preferably optical), and convert to A_V with our assumed extinction law.

The light curves of SPIRITS 15c were discussed in detail in Jencson et al. (2017e), where we estimated $A_V \approx 2.2$ based on comparison to the well-studied Type IIb SN 2011dh. Similarly, for SPIRITS 16tn we estimated $A_V \approx 7.8$ based on a comparison to the low-luminosity Type IIP SN 2005cs (Jencson et al. 2018e).

The light curves of SPIRITS 14azy are shown in Figure 5.12 in comparison to the 2015 LRN in M101 (M101 OT2015-1), a well-studied example of a common-envelope ejection in a merging stellar binary system (Blagorodnova et al. 2017, , and 2019, in preparation). SPIRITS 14azy, shows a short-lived, optical counterpart peaking at $g' = 20.0$ ($M_{g'} = -10.7$), which rises to peak and fades within $\lesssim 60$ days. The optical, broadband colors near peak are red, with $g' - r' = 0.9$ and $g' - i' = 1.1$. The transient displays a longer-lived, IR excess detected out to $\gtrsim 300$ days in the near-IR and to $\gtrsim 700$ days in the *Spitzer*/IRAC bands. Shifted in apparent magnitude to the distance of SPIRITS 14azy in NGC 2997, we see that the light curves of M101 OT2015-1 are similar to SPIRITS 14azy both in the absolute brightness of the transient in g' and the *Spitzer*/IRAC IR bands and in the timescale of the

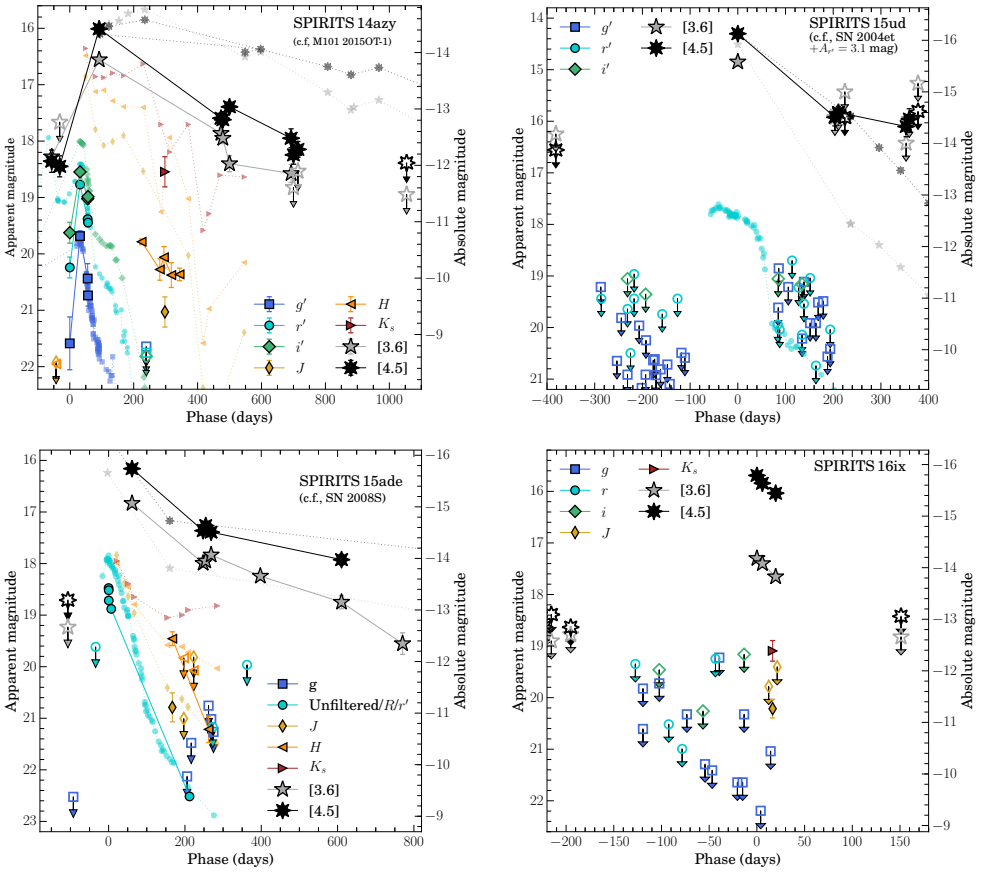

Figure 5.12: Multiband light curves of the SPIRITS sample of luminous, IR-discovered transients. The large, black-outlined, filled symbols are detections of the SPIRITS transient indicated in the upper right corner of each panel. Upper limits from nondetections are shown as the large, open symbols with downward-pointing arrows. The smaller, faint symbols show corresponding light curves of a well-studied comparison object, also listed in parentheses in the upper right corner of each panel. All light curves have been corrected for Galactic extinction, and comparison light curves are also corrected for additional host/intrinsic reddening as described in the text. Comparison light curves are then shifted in apparent magnitude to the distance of their corresponding SPIRITS event. The SN 2004et light curves, in comparison to SPIRITS 15ud, have additionally been shifted in apparent magnitude to match in [4.5] peak luminosity and then reddened by $A_V = 3.7$ to be consistent with our r'-band limits. Similarly, in comparison to SPIRITS 17lb, the SN 2004et light curves have been reddened by $A_V = 2.5$ to be consistent with our V-band limit.

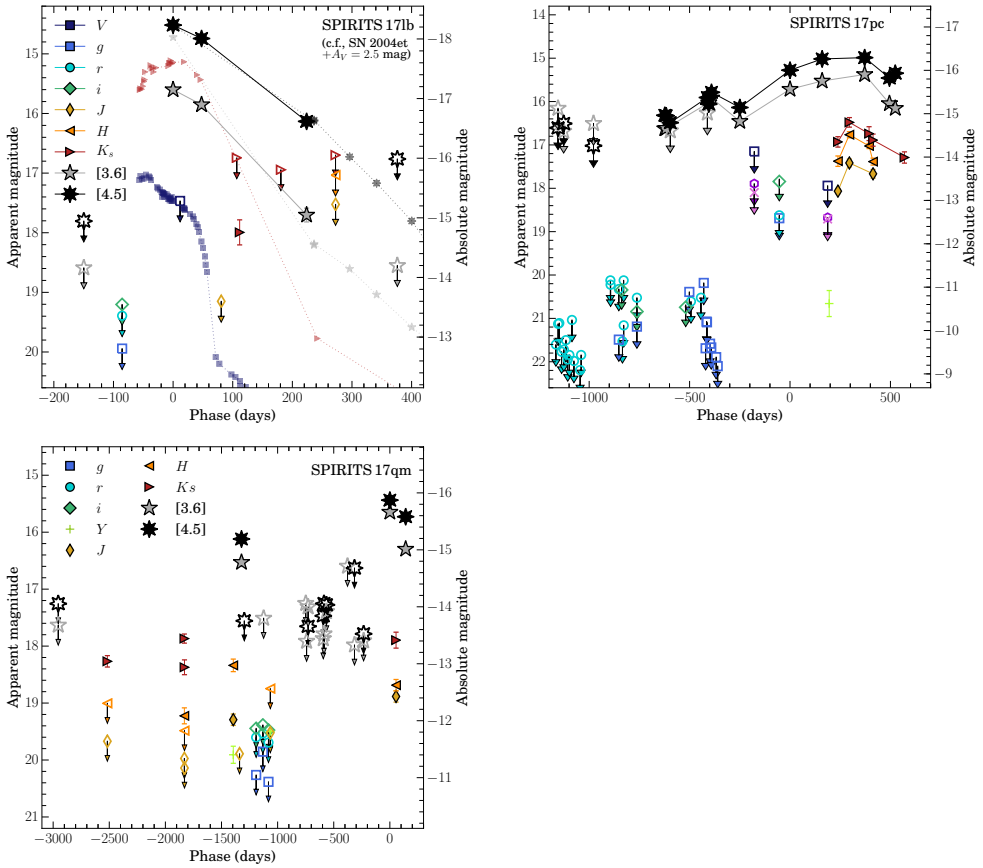

Figure 5.12: Continued.

optical transient. While M101 OT2015-1 is characterized by somewhat redder optical colors and an even longer-lived IR excess, the overall similarity of the two events is readily apparent. We characterize the reddening for SPIRITS 14azy as $A_{g'} \approx g'_{\rm peak} - [4.5]_{\rm peak} = 3.7$, corresponding to $A_V = 3.2$. We caution that this estimate should not be directly interpreted as a measurement of the extinction from the host galaxy or local environment, and it may also be indicative of "intrinsic" reddening of the transient due to dust formation or the relatively cool effective temperatures associated with LRN-like events.

SPIRITS 15ud was inaccessible for ground-based observing owing to its proximity to the sun from Earth at the time of the *Spitzer* discovery, and thus our constraints on any optical emission associated with the transient are only from phases before/after $\approx\pm100$ days. As discussed below in Section 5.5, we find the most likely interpretation of the IR light curves of this event to be an SN II. Our deepest limits on the post-peak optical flux of SPIRITS 15ud are in the r' band, and we compare to the light curve in this band of the Type IIP SN 2004et from Maguire et al. (2010) to obtain a

constraint on the extinction. We shift the light curves in phase to match the time of the observed [4.5] peak of SPIRITS 15ud and in apparent magnitude to match the observed [4.5] brightness, and we find that our optical limits then require $A_{r'} \gtrsim 3.1$ to be consistent with the declining light curve of SN 2004et. This corresponds to $A_V \gtrsim 3.7$, which we adopt as a lower limit on the extinction to SPIRITS 15ud.

The *Spitzer* light curves of SPIRITS 15ade, as discussed above in Section 5.4, show a distinct similarity those of SN 2008S, a prototype of the class of ILRTs, in both IR luminosity at $M_{[4.5],\mathrm{peak}} \approx -16$ and the subsequent IR light-curve decline. The first detection of the source was in in an unfiltered optical CCD image taken on 2015 September 11.5, where the transient was identified as PSN J15220552+0503160 by M. Aoki. Calibrated to the SDSS r band, our photometry yields an observed optical peak at $r = 18.6 \pm 0.2$ ($M_r = -13.4$) 61.3 days before the first detection by SPIRITS. The optical luminosity is similar to the R-band peak of SN 2008S (from Botticella et al. 2009, assuming $A_V \approx 1$ in excess of the Galactic contribution as in Botticella et al. 2009 and Szczygieł et al. 2012), and our late-time optical measurements are consistent with the optical fading of SN 2008S within ≈200 days. We detect a near-IR excess in the J, H, and K_s bands at a phase of ≈170 days, again similar to that observed in SN 2008S. We characterize the reddening to SPIRITS 15ade, though it may be intrinsic to the source, as $A_r = R_{\mathrm{peak}} - [4.5]_{\mathrm{peak}} = 2.3$, corresponding to $A_V = 2.7$.

SPIRITS 16ix is a near twin to SPIRITS 16tn in both their observed peak IR luminosities at $M_{[4.5],\mathrm{peak}} \approx -16$ and their rapid IR decline rates (Section 5.4). Furthermore, both objects are remarkably red, as shown for SPIRITS 16ix in Figure 5.12. Our deepest optical limit during the IR observed peak of SPIRITS 16ix reached $g \gtrsim 22.2$ ($M_g \gtrsim -9.3$), indicating $A_g \gtrsim 6.3$. Corresponding to $A_V \gtrsim 5.5$, we adopt this as a lower limit on the extinction to SPIRITS 16ix.

Similar to our analysis for SPIRITS 15ud, we compare our photometric data for SPIRITS 17lb to those of SN 2004et. Shifting SN 2004et in phase to match the time of the observed [4.5] peak and in apparent magnitude to the distance of SPIRITS 17lb, we find that their [4.5] light curves track each other remarkably well, though SPIRITS 17lb is significantly redder than SN 2004et in [3.6]−[4.5] until $\gtrsim$ 150 days. Applying reddening with $A_V \gtrsim 2.5$ is then required for the SN 2004et light curves to be consistent with our V-band limit at 11.7 days, which we adopt as a lower limit on the extinction to SPIRITS 17lb.

As discussed in Section 5.4, the *Spitzer* light curves of SPIRITS 17pc are charac-

terized by multiple outbursts over the past ≈4 yr that appear to be progressively increasing in both brightness and duration. Deep optical limits constrain the optical variability of the source between ≈ − 1200 and −300 days, and we note that the IR outburst peaking at [4.5] = 15.8 near −400 days was extremely red with $g' - [4.5] > 5.9$. During the brightest, longest-duration IR outburst seen in the *Spitzer*/IRAC bands lasting $\gtrsim$ 500 days, we detected underlying near-IR variability peaking at $K_s = 16.5$ at 295.6 days with a red near-IR color of $J - K_s = 0.9$ with a comparatively shorter duration of $\lesssim$ 200 days. We also obtained our only optical detection of SPIRITS 17pc at $Z = 20.7$ at 195.1 days, indicating $A_Z = Z - [4.5] = 5.7$. To estimate the extinction in Table 5.8, we convert this to $A_V = 12.5$ but again caution that the extreme optical−IR color may be intrinsic to the source and is not necessarily indicative of extinction by the host ISM or local environment of the progenitor.

The light curves of SPIRITS 17qm also indicate multiple epochs of significant variability across the near-IR and *Spitzer*/IRAC bands extending back to at least a phase of −2500 days before the discovery detection and observed IR peak at [4.5] = 15.4 ($M_{[4.5]} = -15.9$). During the pre-discovery outburst detected by *Sptizer*, our photometry indicates a notably red SED with $Y - [4.5] = 3.8$. Similarly, our near-IR follow-up observations during the post-peak decline at $t = 55.1$ days indicate $A_J = J - [4.5] = 3.3$, corresponding to $A_V = 12.1$. As with SPIRITS 17pc, rather than indicating host or environmental extinction, the extreme colors we observe may be intrinsic to the SED of the source or caused by dust formation.

Radio constraints

Radio observations of CCSNe probe the nonthermal emission generated when the fastest ejecta interact with the CSM produced by the pre-explosion stellar wind of the progenitor. The spectrum is dominated by synchrotron emission as the blast wave propagates through the CSM, where turbulent instabilities may accelerate electrons to relativistic energies and amplify magnetic fields (Chevalier 1982). At early times, the synchrotron spectrum is self-absorbed at high frequencies, with possible additional contributions from internal free-free absorption, and free-free absorption by the external, pre-shocked, ionized CSM (e.g., Chevalier 1982, 1998). As the shock propagates out into the CSM, the peak in the spectrum, below which the source is opaque, shifts to lower frequencies. As no SN Ia has been detected in the radio to deep limits in radio luminosity of $L_\nu \lesssim 10^{24}$ erg s^{-1} Hz^{-1}, detection of this characteristic signature could provide strong confirmation our sources as

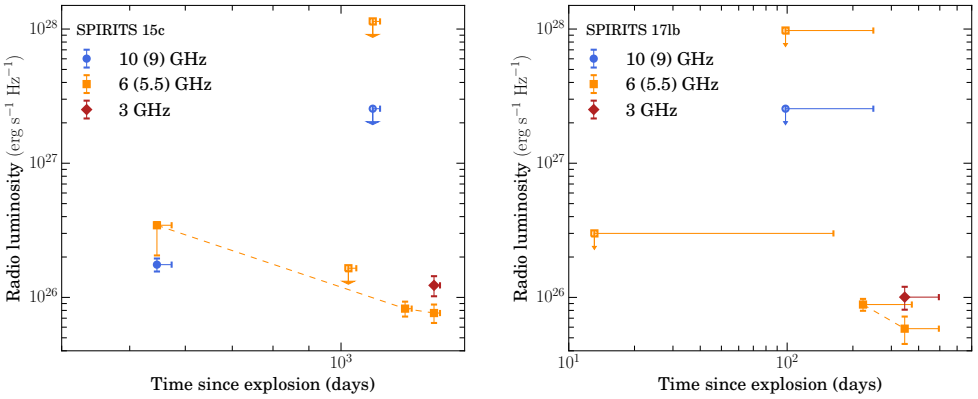

Figure 5.13: Radio light curves of SPIRITS 15c (left) and SPIRITS 17lb (right) in multiple frequency bands. Detections are indicated by filled symbols, while upper limits from non-detection are indicated by open symbols with downward-pointing arrows. Horizontal error bars indicate the uncertainty in the absolute phase since explosion for these events.

CCSNe.

In Figure 5.13, we show the radio light curves of SPIRITS 15c and SPIRITS 17lb. For both sources, we detect a declining radio source consistent with optically thin synchrotron emission. At $t = 546.7$ days for SPIRITS 15c, the transient is detected at both 10 and 6 GHz, with a spectral index $\alpha = 1.32^{+0.05}_{-1.01}$, where the flux density is given by $S_\nu \propto \nu^{-\alpha}$. The source is observed to fade at 6 GHz, with a spectral index of $\alpha = 0.7 \pm 0.1$ between 3 and 6 GHz at $t = 1356.6$ days. We infer from these observations that SPIRITS 15c peaked at a 6 GHz radio luminosity of $L_\nu \gtrsim 3.5 \times 10^{26}$ erg s^{-1} Hz^{-1} at time $t \lesssim 546.7$ days (maximum age $\lesssim 573.7$ days). For SPIRITS 17lb, the source fades at 6 GHz between $t = 222.5$ and 345.3 days, with a spectral index of $\alpha = 0.78 \pm 0.13$ between 3 and 6 GHz at the later epoch. SPIRITS 17lb thus peaked at 6 GHz at $L_\nu \gtrsim 8.8 \times 10^{25}$ erg s^{-1} Hz^{-1} at time $t \lesssim 222.5$ days (maximum age $\lesssim 372.3$ days). The remaining SPIRITS events were undetected in our radio follow-up observations.

In Figure 5.14, we show the peak luminosities of radio CCSNe of various subtypes and the time to peak times the frequency of observation compared to our constraints for SPIRITS 15c and SPIRITS 17lb, as well as our limits on the radio luminosity of the rest of the sample. Following our discussion in Section 4.2.1 of Jencson et al. (2018e), we use the self-similar solution for the propagation of the SN blast wave into the CSM described in Chevalier (1998) and Chevalier and Fransson (2006). If synchrotron self-absorption (SSA) is the dominant absorption mechanism, and

assuming that the emitting electron population is described by a power law with an energy spectral index $p = 3$, then, as calculated by Chevalier (1998), the size of the radio-emitting region is given by

$$R_{\rm s} = 4.0 \times 10^{14} q^{-1/19} \left(\frac{f}{0.5}\right)^{-1/19} \left(\frac{F_{\rm p}}{\rm mJy}\right)^{9/19} \times \left(\frac{D}{\rm Mpc}\right)^{18/19} \left(\frac{\nu}{5\ {\rm GHz}}\right)^{-1} {\rm cm}, \tag{5.1}$$

where $q \equiv \epsilon_e/\epsilon_B$ is the ratio of the energy density in relativistic electrons to that in the magnetic field, f is the filling factor of the radio-emitting region, F_p is the peak flux at frequency ν, and D is the distance to the source. We show the inferred shock velocities assuming energy equipartition ($q = 1$) and $f = 0.5$ (as estimated by Chevalier and Fransson 2006) as the dashed lines in Figure 5.14.

Assuming that the CSM was produced by a steady pre-SN stellar wind, its density profile as a function of radius, r, will be given by $\rho_{\rm w} = A/r^2 \equiv \dot{M}/(4\pi r^2 v_{\rm w})$, where $\dot{M}$ is the mass-loss rate and $v_{\rm w}$ is the wind velocity. We define $A \equiv \dot{M}/(4\pi v_{\rm w})$ as the normalization of the CSM density profile, and $A_\star \equiv A/(5 \times 10^{11}\ {\rm g\ cm^{-1}})$ is a dimensionless proxy for A as in Chevalier (1982). The radio emission at time t since explosion is then sensitive to the density profile of the CSM as

$$A_\star \epsilon_{B-1} q^{8/19} = 1.0 \left(\frac{f}{0.5}\right)^{-8/19} \left(\frac{F_{\rm p}}{\rm mJy}\right)^{-4/19} \times \left(\frac{D}{\rm Mpc}\right)^{-8/19} \left(\frac{\nu}{5\ {\rm GHz}}\right)^{2} \left(\frac{t}{10\ {\rm days}}\right)^{2}, \tag{5.2}$$

where $\epsilon_{B-1} \equiv \epsilon_B/0.1$ (Chevalier and Fransson 2006). The inferred value of A_* depends very sensitively on $t_{\rm peak}$, shown in Figure 5.14 as the nearly vertical dotted lines.

Our constraint on the peak radio luminosity for SPIRITS 15c is consistent with its spectroscopic classification as an SN IIb or SN Ib, which tend to be more luminous radio sources ($10^{26} \lesssim L_{\nu,{\rm peak}} \lesssim 10^{28}$ erg s^{-1} Hz^{-1}) peaking on timescales between 10 and 100 days. Because our radio observations were post-peak, we are only able to place limits on the relevant parameters. Our observations require

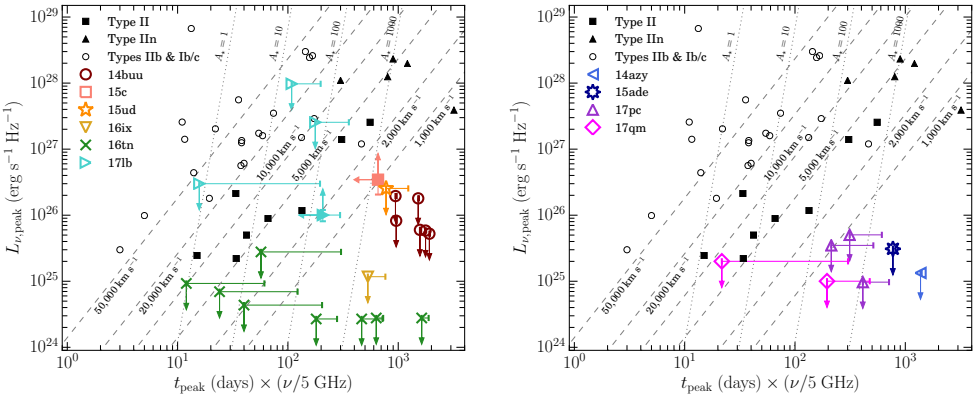

Figure 5.14: In each panel, we show the peak radio luminosity vs. time of peak times the frequency of observation for radio CCSNe adapted from, e.g., Chevalier, Fransson, and Nymark (2006) and Romero-Cañizales et al. (2014). This is an updated version of Figure 10 from Jencson et al. (2018e). SNe II are shown as black squares, and strongly interacting SNe IIn are shown as black triangles. Open circles represent stripped-envelope SNe IIb and Ib/c. Upper limits on the radio luminosity of SPIRITS transients at a given phase are shown as multi-color, open symbols with downward-pointing arrows, where the horizontal error bars represent our uncertainty in the absolute phase since explosion. The possible CCSNe are shown in the left panel, while the non-SN events are shown in the right panel. Filled symbols for SPIRITS 15c and SPIRITS 17lb represent constraints on t_{peak} and $L_{\nu,\mathrm{peak}}$ from detections of the transients. Symbols corresponding to each object are labeled in the legend on the left side of the figure. Assuming an SSA model with an electron distribution with p = 3 for the shock wave propagating through the CSM, one can infer the shock velocity (dashed lines) and CSM density parameter (A_*; dotted lines) from the position on this diagram.

$v_s \gtrsim 1000\,\mathrm{km\ s^{-1}}$ and $A_* \lesssim 1400$. This translates to a limit on the pre-SN mass-loss rate of $\dot{M} \lesssim 1.4 \times 10^{-3} \left(\frac{\epsilon_B}{0.1}\right) \left(\frac{v_w}{100\ \mathrm{km\ s^{-1}}}\right) M_\odot\ \mathrm{yr}^{-1}$.

SPIRITS 17lb, despite its younger phase at the time of first observation with the VLA, is notably less luminous, more consistent with the population of radio SNe II. We find $v_s \gtrsim 800\,\mathrm{km\ s^{-1}}$ and $A_* \lesssim 800$, corresponding to a limit on the pre-SN mass-loss rate of $\dot{M} \lesssim 8.0 \times 10^{-4} \left(\frac{\epsilon_B}{0.1}\right) \left(\frac{v_w}{100\ \mathrm{km\ s^{-1}}}\right) M_\odot\ \mathrm{yr}^{-1}$.

As discussed in Jencson et al. (2018e), our deep radio nondetections for SPIRITS 16tn rule out a stripped-envelope classification, except possibly the most rapidly evolving, high-velocity events that may have fast-peaking radio light curves. The new late-time limits beyond $t \gtrsim 500$ days presented here also argue against a strongly interacting SN IIn, unless the radio emission is still strongly self-absorbed at this phase. A weak SN II is the most consistent with our observations for SPIR-

ITS 16tn, and specifically, our inferred constraint on the pre-SN mass-loss rate of $\dot{M} \lesssim 2.4 \times 10^{-5} \left(\frac{\epsilon_B}{0.1}\right) \left(\frac{v_w}{100 \text{ km s}^{-1}}\right) M_\odot \text{ yr}^{-1}$ may suggest a RSG progenitor of lower initial mass (10–15 $M_\odot$). Similarly, the late-time limit for SPIRITS 16ix is significantly deeper than observed radio-luminous SN IIn and stripped-envelope SNe and is most consistent with an SN II. Our weaker constraint for SPIRITS 15ud may be consistent with either an SN II or stripped-envelope classification.

As discussed below in Section 5.5, based on the sum of all available observational data, we do not believe that SPIRITS 14azy, SPIRITS 15ade, SPIRITS 17pc, and SPIRITS 17qm were terminal CCSN explosions. Thus, we do not expect strong radio counterparts for these events, but show our radio limits in the right panel of Figure 5.14 for completeness. Specifically for SPIRITS 17qm, while the most likely interpretation is a giant LBV eruption, an SN IIn is consistent with the optical/IR data but may be disfavored by the lack of radio emission detected thus far.

5.5 Putting it all together: suggested transient classifications

Here we discuss suggested classifications for each SPIRITS event in our sample based on the combined observational constraints across radio, IR, and optical wavelengths. We find that five of our nine IR events are confirmed or plausible CCSNe, while the remaining four are more likely non-SN massive-star outbursts of various origins. Our suggested classification for each event is given in Table 5.8.

The confirmed and plausible CCSNe

As discussed in detail in Jencson et al. (2017e), SPIRITS 15c is a clear example of a confirmed, moderately obscured CCSN. Our assessment is based primarily on near-IR spectroscopy showing distinct similarity to the Type IIb SN 2011dh, and in particular the presence of a broad ($\approx$8400 km s^{-1}) double-peaked emission line of He I at 1.0830 μm. The optical/near-IR light curves were well matched to those of SN 2011dh assuming $A_V = 2.2$ and a standard Milky Way ISM extinction law with $R_V = 3.1$. In this work we present new radio observations of SPIRITS 15c, which are characterized by the detection of a declining, optically thin synchrotron source consistent with the radio counterparts of other, previously observed stripped-envelope CCSNe.

SPIRITS 17lb, our most luminous IR transient at $M_{[4.5]} = -18.2$, clearly falls in the IR luminosity range of CCSNe (see Figure 5.2), and is more luminous than any other class of known IR transient. The IR light curves and color evolution are consistent with either a hydrogen-rich Type II or stripped-envelope Type Ib/c or IIb.

The near-IR spectra, taken at phases of 123 and 157 days, show no strong features indicative of a CCSN or specific SN subtype. There is a possible weak detection of the CO $\Delta v = 2$ features in the 123 day K-band spectrum, which is not present at 157 days. We note that some SNe II, including the recent SN 2017eaw, have shown strong CO K-band features that may fade on timescales of months (e.g., Tinyanont et al. 2019), but this does not provide a definitive classification for SPIRITS 17lb. As discussed in Section 5.4, we detected a declining, optically thin synchrotron source at the location of SPIRITS 17lb, confirming this source as a CCSN. Our constraints on the peak radio luminosity and time of the synchrotron peak are most consistent with previously observed radio SNe of Type IIP. This rules out a strongly interacting SN IIn, as the observed emission is optically thin and thus not strongly self-absorbed by a dense wind, and disfavors a typically more luminous stripped-envelope event. Assuming a steady pre-SN wind, we derive constraints on the mass-loss rate of $\dot{M} \lesssim 8.0 \times 10^{-4} \left(\frac{\epsilon_B}{0.1}\right) \left(\frac{v_w}{100 \text{ km s}^{-1}}\right) M_\odot \text{ yr}^{-1}$, consistent with an RSG progenitor. We infer a lower limit on the extinction to SPIRITS 17lb of $A_V \gtrsim 2.5$ in Section 5.12 comparing to the Type IIP SN 2004et.

The evidence for SPIRITS 15ud, SPIRITS 16ix, and SPIRITS 16tn is more circumstantial, but we find a reddened CCSN to be a plausible interpretation for each of these events. For SPIRITS 15ud, at $M_{[4.5],\text{peak}} = -16.4$ the IR light curves are broadly consistent with an SN II, stripped-envelope Type Ib/c or IIb, or alternatively, an SN 2008S-like ILRT. Given the large uncertainty in the age of SPIRITS 15ud at discovery (< 381.4 days), it is likely that our *Spitzer* observations missed the peak of this event and that its true peak luminosity was substantially higher. This would place SPIRITS 15ud firmly in the IR luminosity range characteristic of CCSNe and disfavors the ILRT interpretation. Despite the large uncertainty in its age in Section 5.12 and under the assumption that SPIRITS 15ud was an SN II, we placed a lower limit on the extinction of $A_V \gtrsim 3.7$. This interpretation is further supported by the location of SPIRITS 15ud in a prominent, nearly opaque dust lane in archival *HST* imaging.

We examined the observational constraints for SPIRITS 16tn in Jencson et al. (2018e) and again found an SN II, possibly a low-luminosity event similar to SN 2005cs, heavily obscured by $A_V = 7 - 9$ to be the most likely interpretation of this event. A new piece of the puzzle is the possible identification of water vapor absorption in the near-IR spectrum of SPIRITS 16tn (Section 5.4). In the CCSN scenario, a possibility is that the progenitor was encased in a dense molecular cloud, and

water in the vicinity was heated by the explosion to produce the observed, broad absorption. The high extinction for SPIRITS 16tn is consistent with this interpretation. This would constitute the first direct identification of a CCSN associated with a molecular cloud, though Galactic candidates for SN remnants interacting with molecular gas have been previously noted (e.g., W44 and IC 443, Chevalier 1999). Interestingly, Chevalier (1999) argued that the progenitors of such events must be relatively low mass, i.e., early B-type stars on the main sequence (8–12 $M_{\odot}$), as the ionizing flux from a more massive O-type progenitor will clear a region $\approx$15 pc in radius of molecular material. Our inferred limit on the pre-SN mass-loss rate from radio observations of SPIRITS 16tn was also consistent with a lower-mass RSG progenitor, which may add further support to this hypothesis.

Alternatively, given the apparent similarity of the water absorption features to those of late-type Mira variables, SPIRITS 16tn may represent a previously unknown class of transient associated with such stars. It is unclear, however, that water in the atmosphere would survive a luminous outburst or mass-loss event. Finally, an additional, though unlikely, possibility is chance positional coincidence between SPIRITS 16tn and an unrelated Mira variable. Continued monitoring for ongoing Mira-like variability in the near-IR is required to confirm or rule out this possibility.

SPIRITS 16ix is a near twin of SPIRITS 16tn in their IR properties, and thus we also consider a CCSN, possibly another weak or low-luminosity SN II, as a plausible interpretation. SPIRITS 16tn was clearly associated with active star-formation, indicating a likely massive-star origin further suggestive of a CCSN. We note that for SPIRITS 16ix, however, there is no clear evidence of star-formation at the site, and given the classification of the host as a lenticular S0 galaxy, the association is more ambiguous. We noted in Jencson et al. (2018e) that given the low explosion energy inferred for SPIRITS 16tn and lack of spectroscopic features distinctive of a CCSN, a nonterminal "impostor" explosion or eruption remains a viable scenario. Neither SPIRITS 16ix nor SPIRITS 16tn has shown any evidence of prior or subsequent IR variability other than the singular events described in this work. This further supports our interpretation that they were isolated, and possibly terminal, events in the lives of their progenitors. It is particularly notable that SPIRITS 16ix and SPIRITS 16tn, while distinctly similar to each other in their IR light curves, are also unique compared to the rest of the IR- and optically discovered transients. Furthermore, they are the two most severely reddened possible CCSNe ($A_V \gtrsim 5.5$) presented in this work. We thus speculate that they may represent a new class

of IR-dominated transients, possibly associated with low-energy CCSNe arising preferentially in particularly extinguished environments and/or from progenitors that are directly associated with or encased in dense molecular clouds.

ILRT: SPIRITS 15ade

As a distinct class of IR-dominated events, the nature of ILRTs remains unclear. The prototypical objects are the "impostor" SN 2008S and NGC 300 2008OT-1 (Bond et al. 2009). ILRTs are observed to have dust-obscured, IR-luminous ($M_{[4.5]} < -10$; $\nu L_\nu > 3.7 \times 10^3$) pre-explosion counterparts, suggested to be extreme AGB stars of intermediate mass ($\approx$10–15 $M_\odot$) self-obscured by a dusty wind (Prieto et al. 2008; Bond et al. 2009; Thompson et al. 2009). The recently discovered transient in M51 (M51 OT2019-1) was also proposed as a new member of this class. Its likely progenitor was a similar dust-obscured star, with significant IR variability detected in archival *Spitzer*/IRAC imaging over the past $\approx$12 yr (Jencson et al. 2019c). Less luminous than typical CCSNe at peak, emission lines in their spectra (including H recombination and strong [Ca II] and Ca II features) also indicate lower velocities up to few $\times$100 km s^{-1} (e.g., Bond et al. 2009; Botticella et al. 2009; Humphreys et al. 2011). A suggested physical scenario involves weak explosion, possibly an electron-capture SN (disfavored for the slow rise and extended phase of early destruction observed in M51 OT2019-1; Jencson et al. 2019c), or massive stellar eruption that initially destroys the obscuring, circumstellar dust and produces a short-lived optical transient. In the aftermath, the development of a significant IR excess indicates the recondensation of dust and consequent reobscuration of the transient (Thompson et al. 2009; Kochanek 2011a; Szczygieł et al. 2012). There is currently no evidence that the progenitor stars survive such events, as both prototypes have now faded below their pre-explosion luminosities in the IR (Adams et al. 2016).

SPIRITS 15ade shares several properties with this class. While we do not directly detect a progenitor star, our limit from archival *Spitzer*/IRAC imaging at $M_{[4.5]}$ fainter than -12.8 is consistent with the IR progenitors of SN 2008S and NGC 300 OT2008-1. As we found in Section 5.12, the IR light curves (peaking at $M_{[4.5]} = -15.7$) and the observed peak and duration of the associated optical transient are also very similar to known ILRTs. Finally, we detect H recombination emission in our near-IR spectra, suggestive of an outflow at 300–400 km s^{-1}, similar to the low expansion velocities of known ILRTs (e.g., Bond et al. 2009; Botticella et al. 2009; Humphreys et al. 2011).

Possible LRN: SPIRITS 14azy

The class of extragalactic transients referred to as luminous red novae (LRNe) are believed to be more massive analogs of the population of stellar mergers observed in the Galaxy, including the striking example of the ≈1–3 $M_\odot$ contact binary merger V1309 Sco (Tylenda et al. 2011; McCollum et al. 2014) and the B-type stellar merger V838 Mon (Bond et al. 2003; Sparks et al. 2008). While sharing several properties with ILRTs, LRNe are distinctly characterized by multipeaked, irregular light curves. At early times, their spectra show H emission features, but they develop red optical colors, atomic and molecular absorption features, and significant IR excesses as they evolve. Recent examples include the 2011 transient in NGC 4490 (NGC 4490 OT2011-1; Smith et al. 2016), and the 2015 event in M101 (M101 OT2015-1; Blagorodnova et al. 2017). Specifically in the case of NGC 4490 OT2011-1, the late-time IR excess was too luminous to be explained as an IR echo, indicating the presence of a surviving, merged remnant. With unobscured, directly detected progenitor systems in archival imaging estimated at 20–30 $M_\odot$ for NGC 4490 OT2011-1 and ≈18 $M_\odot$ for M101 OT2015-1, these events extend a correlation noted by Kochanek, Adams, and Belczynski (2014) for LRNe between progenitor masses and the transient peak luminosity. Specifically, the progenitor of M101 OT2015-1 was identified in archival imaging as having properties of an F-type supergiant with $L \approx 8.7 \times 10^4\ L_\odot$ and $T_{\rm eff} \approx 7000$ K, likely having recently evolved off the main sequence and crossing the Hertzsprung gap as it expands.

Based primarily on our analysis of its multiband light curves, we find that SPIRITS 14azy is most consistent with the LRN class of IR transients, and in particular bears strong similarity to M101 OT2015-1 in its peak luminosity at both [4.5] and g'. Thus, we suggest that it may have a similar mass progenitor system. In Section 5.4, we placed a limit on the flux of the progenitor in the HST/WFC3 UVIS F336W filter corresponding to M_U fainter than −5.4. As the transient is located in a prominent dust lane of the host, the foreground extinction in U band may be significant. Even in the absence of host extinction, and assuming bolometric corrections from Flower (1996), with corrections by Torres (2010) using a consistent choice of $M_{\rm bol,\odot} = 4.73$ and Crowther (1997) filter transformations, this limit is approximately consistent with a zero-age main-sequence O9 star ($T_{\rm eff} \approx 30,000$ K, $L \approx 40,000\ L_\odot$) of similar mass to the progenitor of M101 OT2015-1.

MSEs: SPIRITS 17pc and SPIRITS 17qm

SPIRITS 17pc has undergone multiple, IR-dominated outbursts over a time period spanning at least 1100 days. These outbursts are extremely red (we infer $A_V \approx 12.5$), possibly indicative of copious dust formation. Near-IR spectra taken during the most recent, longest-duration, and most luminous outburst show features similar to a mid- to late G-type supergiant spectrum, including CN and CO absorption. An optical spectrum shows double-peaked Ca textscii emission, but no H or He features, indicative of a cool, $\times 100$ km s^{-1} outflow. We identified a luminous ($L \approx 2 \times 10^5\ L_\odot$) star detected in 2011 archival, multiband *HST* imaging at the precise location of SPIRITS 17qm as a likely progenitor. The luminosity is lower than that of a classical LBV but still likely indicates a very massive progenitor. The progenitor photometry is consistent with a blackbody temperature of $T = 1900 \pm 100$ K, likely indicating active dust formation was occurring around the underlying star. Given the previous history of strong IR variability, cool spectral features, low outflow velocities, and lack of strong radio emission, we argue that the most recent outburst of SPIRITS 17pc represents a more intense mass-loss event or eruption, rather than a terminal SN explosion.

Similar to SPIRITS 17pc, SPIRITS 17qm has also undergone multiple IR outbursts in SPIRITS, and furthermore was also extremely red (estimated $A_V = 12.1$). However, we highlight several notable differences. The spectra of SPIRITS 17qm were dominated by broader ($v \approx$ 1500-2000 km $^{-1}$) features of H and He and also showed prominent Ca II emission, consistent with a giant LBV eruption. Again, the lack of strong radio emission argues against the interpretation of SPIRITS 17qm as a terminal, Type IIn CCSN explosion. The presumed progenitor of SPIRITS 17qm detected in multiepoch *HST* imaging was highly luminous and variable ($L \approx 2 \times 10^6\ L_\odot$, $\Delta V = 1.7$), also consistent with the properties of an LBV. Assuming that the progenitor was undergoing S Doradus-like variability, the foreground extinction (host or circumstellar) was likely no larger than $A_V \approx 0.5$ at the time of the *HST* observations in 2001. Thus, we suggest that the extreme optical/IR color observed for SPIRITS 17qm may be due to the formation of copious dust in the intervening years and/or during the observed giant eruption. Incorporating ongoing monitoring, the physical details of SPIRITS 17qm and SPIRITS 17pc as self-obscuring MSEs will be explored more fully in a future publication.

5.6 The "redness" distribution of luminous IR transients

In Figure 5.15, we show the distribution of A_V (including lower limits) inferred for our sample of luminous SPIRITS transients. This includes confirmed and plausible CCSNe as the filled portions of the histograms, as well the Type Iax SN 2014dt from the optical control sample and the non-SN IR transients as the unfilled portions. For the non-SN transients, we emphasize that our A_V estimates are only a proxy for the observed optical−IR color and may be indicative of internal reddening (due to dust formation) or the intrinsically cool SEDs, rather than external extinction. We note that our IR-discovered events are overall much redder, all nine objects having $A_V \gtrsim 2$, compared to the optical control sample with seven of nine objects having $A_V \lesssim 2$. In particular, the MSEs SPIRITS 17pc and SPIRITS 17qm stand out as the reddest events in our sample with $A_V > 12$. For the five IR-discovered events interpreted as possible CCSNe, the estimates range from $2.2 \lesssim A_V \lesssim 7.8$. The optically discovered CCSNe in our control sample are again notably less reddened, ranging from $A_V \sim 0$ up to 4.3, with six of the eight events having $A_V \lesssim 2$. This suggests that the IR-selected sample of luminous SPIRITS transients may represent populations of much redder events that are largely inaccessible to optical searches, namely, heavily obscured CCSNe and exceptionally red or self-obscuring transients associated with massive-star outbursts of various origins.

The sample of all known CCSNe discovered between 2000 and the end of 2011 hosted by galaxies within 12 Mpc along with literature estimates of their host extinction compiled by Mattila et al. (2012, hereafter M12) provides another useful comparison for the SPIRITS sample. In Figure 5.16, we directly compare the distribution of host A_V for the SPIRITS sample of confirmed and plausible CCSNe (both optically and IR-selected events) to the M12 sample. We note that M12 excluded five SNe in galaxies with inclinations $>60^\circ$ from their primary analysis, as they believed that their volume-limited sample was incomplete for SNe in highly inclined hosts. We first include these events here for a more direct comparison to the SPIRITS sample, which includes some highly inclined galaxies. In the SPIRITS sample, 7 of the 13 CCSNe (58.3%) have $A_V \gtrsim 2$, and the median value is 2.2. For M12, only 6 of 18 events (33.3%) have $A_V \gtrsim 2$, and the median is significantly lower at $A_V = 0.25$. Shown as cumulative distributions in the right panel of Figure 5.16, we find that the M12 sample is bracketed between the optically known CCSNe in SPIRITS and the full SPIRITS sample including the IR-discovered events, where again a larger fraction of events were found with large host extinction. Here, it is particularly important to reemphasize that for three of the five IR-discovered CCSNe

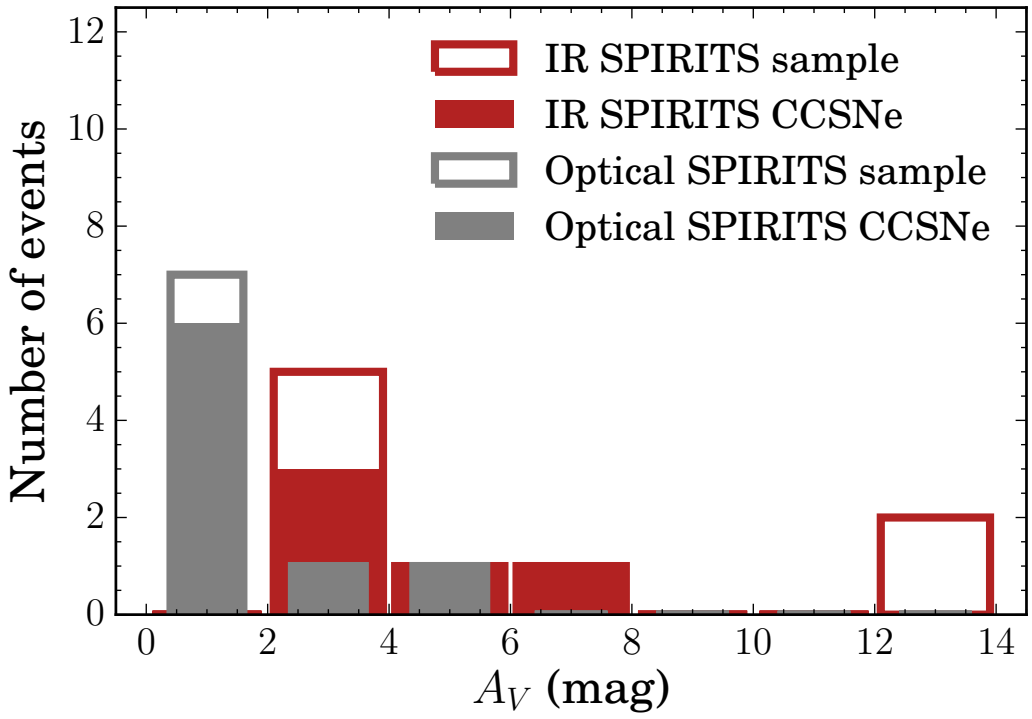

Figure 5.15: Distribution of A_V inferred for the IR-selected sample of luminous SPIRITS transients (red) and the optically selected control sample (gray). The filled regions of the histograms represent confirmed or possible CCSNe. The unfilled regions include the Type Iax SN 2014dt from the control sample and the non-SN stellar outbursts from the IR sample.

in the SPIRITS sample, our A_V estimates are only lower limits, meaning that the true distribution may be even more skewed to large host extinctions.

If we now compare only those events in normal galaxies at inclinations <60°, the M12 sample contained 2 of 13 SNe (15%) that appeared as outliers above the A_V distribution expected for dust smoothly distributed in disk galaxies with $A_V \gtrsim 3.5$ mag. The fraction in the SPIRITS sample (excluding events in highly inclined hosts and IC 2163, which is part of an interacting pair and a borderline LIRG; see our discussion of galaxy selection biases below in Section 5.7) is twice as high, with two of six events (33%) with $A_V > 3.5$ mag (SPIRITS 15ud and SN 2016bau). It is difficult to draw strong conclusions from this comparison given the small number of events included. It may hint, however, that the fraction of CCSNe suffering high host extinction, above that expected solely from inclination effects, and thus missing from optical searches, may be higher than previously estimated.

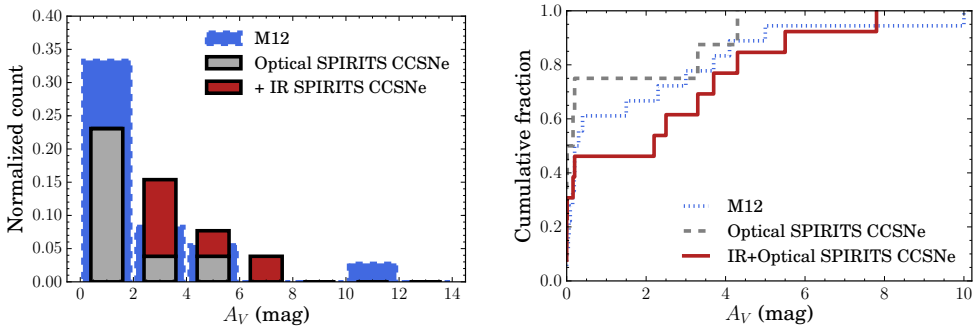

Figure 5.16: Left: normalized distribution of A_V for CCSNe from M12 sample, and the sample of confirmed/possible CCSNe in SPIRITS (filled histogram), including events from the optically discovered control sample (gray) and IR-discovered events (red). Right: cumulative distribution functions in host A_V estimates for M12 (blue short-dashed curve), optically known SPIRITS CCSNe from the control sample (gray dashed curve), and the full sample of likely SPIRITS CCSNe including both optically known and IR-discovered events (red solid curve).

5.7 SPIRITS constraints on the optically missed fraction of nearby CCSNe

We now consider constraints from our sample on the fraction of optically missed CCSNe in nearby galaxies, an important consideration for measurements of the local CCSN rate. $N_{\rm CCSNe} = 13$ confirmed/plausible CCSNe were recovered by SPIRITS and pass our selection criteria, with $N_{\rm mCCSNe} = 5$ events unreported by any optical search. If we assume that the completeness of our IR survey to optically discovered and optically missed SNe is the same (we examine this assumption in more detail below), then the fraction of missing CCSNe, f, is given by the binomial distribution

$$P(f) \propto (1-f)^{N_{\rm CCSNe}} f^{N_{\rm mCCSNe}} \tag{5.3}$$

and the requirement that $\int_0^1 P(f)\,df = 1$ sets the normalization. The nominal, observed missed fraction is 0.385 with a 90% confidence interval of $0.166 < f < 0.645$.

Since 2 of 10 optically discovered and classified CCSNe, SN 2014bc and SN 2016adj, were not recovered in SPIRITS and selected as part of our sample with the criteria outlined in Sections 5.2 and 5.2, our selection efficiency for optically known CCSNe is 0.8. SN 2016adj in Cen A was itself flagged as a saturated source in our transient identification pipeline. An optically obscured CCSN in a galaxy as near as Cen A at a similar IR brightness would have been similarly flagged, and it is natural to assume that our survey incompleteness to optically bright and optically obscured

CCSNe in the nearest galaxies ($D \lesssim 5$ Mpc) is the same. SN 2014bc was located in the saturated core of NGC 4285, and again we may expect our incompleteness to optically missed events located near the core of their host galaxies to be the same. Still, we may obtain a more conservative estimate of f if we assume that our sample was complete in optically missed events. With $N_{\rm CCSNe} = 15$ total CCSNe in SPIRITS galaxies, and again with $N_{\rm mCCSNe} = 5$, we obtain a missed fraction of 0.333 with a 90% confidence interval of $0.142 < f < 0.577$.

Next, we consider the effects of selection biases in our galaxy sample. For the first 3 yr (2014–2016), the full sample of 190 SPIRITS galaxies was more representative across galaxy types, though primarily composed of luminous and massive galaxies beyond 5 Mpc. IC 2163, producing both SPIRITS 15c and SPIRITS 17lb, also stands out from the sample in that with recent distance estimates, it lies much farther than the rest of the sample at 35.5 Mpc, is currently undergoing strong tidal interactions with its companion galaxy, NGC 2207, and is a borderline LIRG at $L_{\rm IR} \approx 10^{11}\ L_{\odot}$ (Sanders et al. 2003). Including only events discovered during the original 3 yr survey, and further excluding SPIRITS 15c in IC 2163, we have $N_{\rm CCSNe} = 8$ and $N_{\rm mCCSNe} = 3$, giving $f = 0.375$ with a 90% confidence interval of $0.111 < f < 0.711$. This is notably similar to our nominal estimate from the full sample, but with a larger 90% confidence interval due to the smaller number of events.

Finally, we consider the possibility that some events interpreted here as CCSNe have been misclassified. SPIRITS 16tn and SPIRITS 16ix have uniquely fast-fading IR light curves compared to the full sample of CCSNe observed by *Spitzer*, and while SPIRITS 16tn is clearly associated with a region of active star formation, there is not such a clear association for SPIRITS 16ix. Excluding these two events, we have $N_{\rm CCSNe} = 11$ and $N_{\rm mCCSNe} = 3$, giving $f = 0.273$ with a 90% confidence interval of $0.079 < f < 0.564$.

Our data suggest an optically missed fraction of about $1/3$ and cannot rule out a value twice as high. Such a large missing fraction could help explain the claimed factor of 2 discrepancy by Horiuchi et al. (2011) between the measured rate of CCSNe and rate of cosmic star formation at $z = 0$, but the precision of our measurement is limited by our small sample size and remaining ambiguous classifications. We also note that more recent volumetric CCSN rate estimates from the Supernova Diversity and Rate Evolution (SUDARE; Botticella et al. 2013) have challenged the claim by Horiuchi et al. (2011) and suggest better agreement between CCSN and

star-formation rates at medium redshift ($0.2 < z < 0.8$; Cappellaro et al. 2015). In the other direction, some local studies have even suggested that CCSNe may be overproduced compared to Hα- and UV-inferred star formation rates (Botticella et al. 2012; Horiuchi et al. 2013; Xiao and Eldridge 2015), and interestingly, accounting for the population of heavily obscured nearby events uncovered by SPIRITS may further increase this tension.

We also now place our estimate in the context of other recent work to constrain the missing CCSN fraction and uncover events buried in densely obscured environments. M12 estimated that locally $18.9^{+19.2}_{-9.5}$% of CCSNe are missed by optical surveys, substantially higher than previous estimates by Mannucci, Della Valle, and Panagia (2007) at 5%–10%. Our nominal estimate of $38.5^{+26.0}_{-21.9}$% of CCSNe missed in nearby galaxies is even higher, falling at the upper end of the allowed range by M12, but with substantial overlap with our 90% confidence interval. The estimates of Mannucci, Della Valle, and Panagia (2007) and M12 rise steeply to > 30% and ~ 40% by $z = 1$, respectively, and substantial work has also been dedicated to uncovering missing supernovae at higher redshift, particularly in the densely obscured and highly star-forming nuclear regions of starburst galaxies and (U)LIRGs. With seeing-limited imaging (e.g. Mannucci et al. 2003; Miluzio et al. 2013) and high-resolution space- or ground-based adaptive optics imaging (Cresci et al. 2007; Mattila et al. 2007; Kankare et al. 2008; Kankare et al. 2012; Kool et al. 2018), a total of 16 individual CCSNe have been uncovered in the IR in these galaxies. Radio very long baseline interferometry (VLBI) imaging of multiple (U)LIRGs (e.g., Lonsdale et al. 2006; Pérez-Torres et al. 2009; Romero-Cañizales et al. 2011; Romero-Cañizales et al. 2014; Bondi et al. 2012; Varenius et al. 2017, and references therein) has also revealed scores of radio sources interpreted as SN and SN remnants. Even with the resolution of the upcoming *James Webb Space Telescope*, probing the innermost nuclear regions of such systems will remain challenging, and recently Yan et al. (2018) undertook a successful pilot study examining the spatially integrated IR light curves of high-redshift (U)LIRGS for variability suggestive of ongoing SN explosions. Finally, deep, targeted optical searches of nearby galaxies may also achieve the sensitivity necessary to uncover heavily extinguished events, e.g., SN 2016ija uncovered by the $D < 40$ Mpc (DLT40) SN search in NGC 1532 with $A_V \approx 6$ (Tartaglia et al. 2018). In this context, we emphasize that our work represents the first attempt to uncover the obscured population and directly constrain the missing fraction of CCSNe in nearby galaxies in the IR.

5.8 Summary and conclusions

We have presented a sample of nine luminous IR transients discovered in nearby ($D \lesssim 35$ Mpc) galaxies by the SPIRITS survey between 2014 and 2018. These events were selected as having $M_{\rm IR}$ brighter than -14 ($\nu L_\nu > 1.5 \times 10^5\ L_\odot$ at [4.5]) in either the [3.6] or [4.5] channels of *Spitzer*/IRAC, and we required at least two SPIRITS detections and that these events were not present in the first epoch of SPIRITS imaging. Combining archival imaging constraints from *Spitzer* and *HST*, concomitant monitoring of SPIRITS galaxies with several ground-based telescopes, coverage in the iPTF survey from Palomar Observatory, and a dedicated ground- and space-based follow-up effort for our transients at optical, near-IR, and radio wavelengths, we construct detailed observational characterizations and attempt to determine their nature. Here we summarize our analysis of the sample and primary conclusions:

1. The IR-discovered sample of transients were predominantly found in the spiral arms of star-forming hosts, except for one event, SPIRITS 16ix, in a lenticular S0 galaxy. This strongly suggests an association with young stellar populations and massive stars. They span IR luminosities with $M_{\rm [4.5],peak}$ between -14 and -18.2, show IR colors between $0.2 <$ [3.6]$-$[4.5] < 3.0, and fade on timescales between 55 days $< t_{\rm fade} <$ 480 days.

2. We define a control sample of optically discovered and classified transients recovered in SPIRITS using the same selection criteria (as outlined in Section 5.2). The control sample also consists of nine events, including known eight CCSNe and one SN Iax. Overall, the control sample and the IR-selected sample are similar in their IR properties, with similar distributions in $M_{\rm [4.5],peak}$, their [3.6]$-$[4.5] colors at peak, and $t_{\rm fade}$.

3. Of the nine IR-discovered events, we suggest that five may be significantly dust-obscured CCSNe. SPIRITS 15c was confirmed via a near-IR spectrum similar to the Type IIb SN 2011dh and detection of a radio counterpart consistent with an SN Ib/IIb (Jencson et al. 2017e). SPIRITS 17lb, as the most luminous IR transient in our sample, and despite a lack of unambiguous SN features in its near-IR spectrum, was confirmed via its radio counterpart most consistent with an SN II. Our radio data constrain the pre-SN mass-loss rates of the progenitors of SPIRITS 15c and SPIRITS 17lb to $\dot{M} \lesssim 1.4 \times 10^{-3} \left(\frac{\epsilon_B}{0.1}\right) \left(\frac{v_w}{100\ \rm km\ s^{-1}}\right) M_\odot\ \rm yr^{-1}$ and $\dot{M} \lesssim 8.0 \times 10^{-4} \left(\frac{\epsilon_B}{0.1}\right) \left(\frac{v_w}{100\ \rm km\ s^{-1}}\right) M_\odot\ \rm yr^{-1}$,

respectively. The IR light curve of SPIRITS 15ud is also most consistent with a CCSN classification. SPIRITS 16ix and SPIRITS 16tn may constitute a previously unknown class of rapidly fading, luminous IR transients occurring in the most densely obscured environments. We suggest these that two events are also CCSNe, possibly directly associated with or occurring within dense molecular clouds.

4. The four remaining luminous IR SPIRITS transients represent a diverse array of IR-dominated events arising from massive-star progenitor systems. The multiband optical and IR light curves of SPIRITS 14azy and SPIRITS 15ade are most similar to an LRN (possible massive stellar merger similar to M101 OT2015-1) and ILRT (possible weak or electron-capture SN similar to SN 2008S), respectively. SPIRITS 17pc underwent multiple, extremely red outbursts over several years, now showing G-type spectral features in the near-IR, and double-peaked Ca II emission indicative of a few $\times 100$ km s^{-1} outflow. We identified a luminous ($L \approx 2 \times 10^5\ L_\odot$) star detected in multiband archival *HST* imaging as a likely progenitor. SPIRITS 17qm, also undergoing multiple IR-dominated outbursts, showed high-velocity ($\sim$ 1500–2000 km s^{-1}) H and He features consistent with a giant LBV eruption. We identified a visually luminous ($L \approx 10^6\ L_\odot$), highly variable progenitor in archival *HST* imaging. Future observations and continued monitoring of SPIRITS 17pc and SPIRITS 17qm may determine the physical origin of their IR outbursts and constrain the ultimate fate of their progenitors.

5. We estimated the visual extinction, A_V—either as a direct estimate of the host extinction (in the case of a CCSN) or as a proxy for the optical−IR color for non-SN transients that may be self-obscured or intrinsically red—for each event in our sample based on their multiband optical and IR light curves. All nine IR-discovered events, including the five confirmed/plausible CCSNe, have $A_V \gtrsim 2$, while only two of the nine objects in the optically discovered control sample have extinction estimates so high. Compared to a volume- and time-limited sample of CCSNe within 12 Mpc compiled by Mattila et al. (2012), we find that the SPIRITS sample of optically known and newly IR discovered CCSNe contains a larger fraction of significantly obscured events ($A_V \gtrsim 2$). Furthermore, seven out of the 13 plausible CCSNe detected by SPIRITS were significantly obscured. This makes it likely that optical transient/SN searches at larger distances are very incomplete because

they miss highly obscured events.

6. A total of 13 confirmed/plausible CCSNe recovered in SPIRITS passed our selection criteria, including 8 optically discovered events in the control sample and 5 IR-discovered events presented here. For our galaxy sample, this implies that a large fraction, nominally $38.5^{+26.0}_{-21.9}$% (90% confidence), of CCSNe are being missed by optical surveys in nearby galaxies.

We thank the anonymous referee for their thorough read of the paper and helpful comments. We thank C. Contreras and the staff of Las Campanas Observatory for help with conducting observations and data reduction. We thank E. Hsiao for helpful commentary and advice in the analysis and discussion of the spectra. We thank K. Mooley, D. Dong, M. Anderson, M. Eastwood, and A. Horesh for helpful advice and assistance with VLA data reduction. We thank S. Mattila and T. Reynolds for valuable discussions in revising this work.

This material is based on work supported by the National Science Foundation Graduate Research Fellowship under grant No. DGE-1144469. H.E.B. acknowledges that support for *HST* program Nos. GO-13935, GO-14258, and AR-15005 was provided by NASA through grants from the Space Telescope Science Institute, which is operated by the Association of Universities for Research in Astronomy, Incorporated, under NASA contract NAS5-26555. R.D.G. was supported by NASA and the United States Air Force. This work is part of the research program VENI, with project No. 016.192.277, which is (partly) financed by the Netherlands Organisation for Scientific Research (NWO).

This work is based in part on observations made with the *Spitzer Space Telescope*, which is operated by the Jet Propulsion Laboratory, California Institute of Technology, under a contract with NASA. This work is based in part on observations with the NASA/ESA *Hubble Space Telescope* obtained at the Space Telescope Science Institute and from the Mikulski Archive for Space Telescopes at STScI, which are operated by the Association of Universities for Research in Astronomy, Inc., under NASA contract NAS5-26555. We acknowledge the use of public data from the *Swift* data archive.

Some of the data presented herein were obtained at the W. M. Keck Observatory, which is operated as a scientific partnership among the California Institute of Technology, the University of California, and the National Aeronautics and Space

Administration. The Observatory was made possible by the generous financial support of the W. M. Keck Foundation. The authors wish to recognize and acknowledge the very significant cultural role and reverence that the summit of Maunakea has always had within the indigenous Hawaiian community. We are most fortunate to have the opportunity to conduct observations from this mountain.

Part of the optical and near-infrared photometric data included in this paper were obtained by the Carnegie Supernova Project through the support of NSF grant AST-1008343.

Based on observations obtained at the Gemini Observatory acquired through the Gemini Observatory Archive and processed using the Gemini IRAF package, which is operated by the Association of Universities for Research in Astronomy, Inc., under a cooperative agreement with the NSF on behalf of the Gemini partnership: the National Science Foundation (United States), National Research Council (Canada), CONICYT (Chile), Ministerio de Ciencia, Tecnología e Innovación Productiva (Argentina), Ministério da Ciência, Tecnologia e Inovação (Brazil), and Korea Astronomy and Space Science Institute (Republic of Korea).

UKIRT is owned by the University of Hawaii (UH) and operated by the UH Institute for Astronomy; operations are enabled through the cooperation of the East Asian Observatory. When the data reported here were acquired, UKIRT was supported by NASA and operated under an agreement among the University of Hawaii, the University of Arizona, and Lockheed Martin Advanced Technology Center; operations were enabled through the cooperation of the East Asian Observatory.

Some of the data used in this paper were acquired with the RATIR instrument, funded by the University of California and NASA Goddard Space Flight Center, and the 1.5 m Harold L. Johnson telescope at the Observatorio Astronómico Nacional on the Sierra de San Pedro Mártir, operated and maintained by the Observatorio Astronómico Nacional and the Instituto de Astronomía of the Universidad Nacional Autónoma de México. We acknowledge the contribution of Leonid Georgiev and Neil Gehrels to the development of RATIR.

The National Radio Astronomy Observatory is a facility of the National Science Foundation operated under cooperative agreement by Associated Universities, Inc.

The Australia Telescope Compact Array is part of the Australia Telescope National Facility, which is funded by the Australian Government for operation as a National Facility managed by CSIRO. This paper includes archived data obtained through the

Australia Telescope Online Archive (http://atoa.atnf.csiro.au).

The Digitized Sky Surveys were produced at the Space Telescope Science Institute under U.S. Government grant NAG W-2166. The images of these surveys are based on photographic data obtained using the Oschin Schmidt Telescope on Palomar Mountain and the UK Schmidt Telescope. The plates were processed into the present compressed digital form with the permission of these institutions. The Second Palomar Observatory Sky Survey (POSS-II) was made by the California Institute of Technology with funds from the National Science Foundation, the National Geographic Society, the Sloan Foundation, the Samuel Oschin Foundation, and the Eastman Kodak Corporation. The Oschin Schmidt Telescope is operated by the California Institute of Technology and Palomar Observatory. The UK Schmidt Telescope was operated by the Royal Observatory Edinburgh, with funding from the UK Science and Engineering Research Council (later the UK Particle Physics and Astronomy Research Council), until 1988 June, and thereafter by the Anglo-Australian Observatory. The blue plates of the southern Sky Atlas and its Equatorial Extension (together known as the SERC-J), as well as the Equatorial Red (ER) and the Second Epoch [red] Survey (SES), were all taken with the UK Schmidt. Supplemental funding for sky-survey work at the STScI is provided by the European Southern Observatory.

Funding for SDSS-III has been provided by the Alfred P. Sloan Foundation, the Participating Institutions, the National Science Foundation, and the U.S. Department of Energy Office of Science. The SDSS-III website is http://www.sdss3.org/. SDSS-III is managed by the Astrophysical Research Consortium for the Participating Institutions of the SDSS-III Collaboration, including the University of Arizona, the Brazilian Participation Group, Brookhaven National Laboratory, Carnegie Mellon University, University of Florida, the French Participation Group, the German Participation Group, Harvard University, the Instituto de Astrofisica de Canarias, the Michigan State/Notre Dame/JINA Participation Group, Johns Hopkins University, Lawrence Berkeley National Laboratory, Max Planck Institute for Astrophysics, Max Planck Institute for Extraterrestrial Physics, New Mexico State University, New York University, Ohio State University, Pennsylvania State University, University of Portsmouth, Princeton University, the Spanish Participation Group, University of Tokyo, University of Utah, Vanderbilt University, University of Virginia, University of Washington, and Yale University.

This publication makes use of data products from the Two Micron All Sky Survey,

which is a joint project of the University of Massachusetts and the Infrared Processing and Analysis Center/California Institute of Technology, funded by the National Aeronautics and Space Administration and the National Science Foundation.

Chapter 6

NEW FRONTIERS: SUMMARY AND LOOKING AHEAD

6.1 Landscape of infrared transients in 2019

We are now approaching six years of a dedicated exploration of the dynamic IR sky with *Spitzer*/IRAC. Substantial progress, largely enabled by SPIRITS, has been made in uncovering the rich diversity of IR transients. Returning to the diagram of the IR luminosity time evolution of transients in Figure 6.1, we have witnessed a true explosion in the sheer number of and range of properties observed for known events. The sample of well-characterized, mid-IR light curves of CCSNe has more than doubled, enabling large systematic studies of their circumstellar environments and dust emission in the IR for the first time (e.g., Tinyanont et al. 2016; Szalai et al. 2019a). The first compilation of IR light curves of thermonuclear Type Ia SNe as well placed stringent limits on the presence of circumstellar dust (Johansson et al. 2017)—a notable exception is the unusual, dusty Type Iax SN 2014dt (Fox et al. 2016). Eight years of monitoring the enigmatic prototypes of the ILRT class of SN "impostors", SN 2008S and NGC 300 OT2008-1, showed they have faded well below their progenitor luminosities, and may indicate they were terminal explosions after all (Adams et al. 2016). A first sampling of the IR light curves of LRNe associated with stellar mergers and common-envelope ejections have now been obtained for a range of progenitor system masses, providing new insights on dust formation in their explosive outflows, and the merged remnants powering their long-lived IR excesses (e.g., Smith et al. 2016; Blagorodnova et al. 2017).

But of course, the story does not end there. In the final chapter of this thesis, I will take a first look at the full sample of new transient discoveries uncovered by SPIRITS in the IR, including a summary of the major findings and conclusions of my work to date, and offer a brief view to the future of time-domain astrophysics in the IR.

6.2 The full sample of SPIRITS transients: exceptionally red events evolving on timescales of weeks to years

Overlaid on the 2019 landscape of known IR transients, I show the IR light curves all transients discovered by the SPIRITS survey (events listed in Table 1.1). The light curves for each event individually are provided in Appendix A, also in-

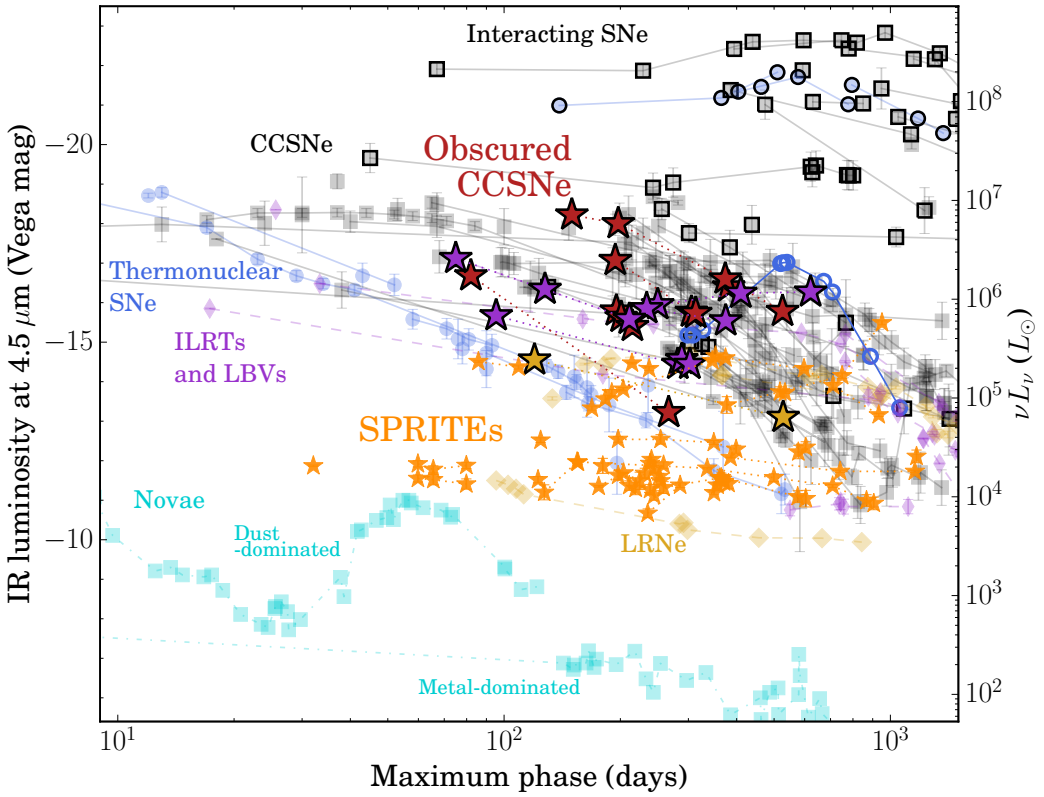

Figure 6.1: The mid-IR 4.5 μm light curves of transients of various classes as they are known in 2019. Luminous SPIRITS events ($M_{[4.5]} < -14$ mag) discussed in detail in this thesis are shown as large stars, including five confirmed and plausible obscured CCSNe (red), four new ILRTs and LBV-like massive star eruptions (purple), and a candidate LRN (yellow). The full SPIRITS sample of transients including all events brighter than $M_{[4.5]} < -11$ mag are shown as the small orange stars. The phase on the x-axis is the maximum age of the event from the most constraining, pre-outburst nondetection. Additionally, to those objects shown in Figure 1.1, we add all SNe detected by *Spitzer*/IRAC to date, including recent compiliations by Tinyanont et al. (2016), Johansson et al. (2017), Szalai et al. (2019a), Jencson et al. (2019d), and references therein. New data on ILRTs include the full light curves of SN 2008S and NGC 300 OT2008-1 (Adams et al. 2016) and the SPIRITS light curve of SN 2010dn. We also include the SPIRITS light curves of the LBVs SNHunt225 and the recent transient in M74 (AT 2018krl; Szalai et al. 2019b). New LRN light curves include those of the NGC 4490 OT (Smith et al. 2016), M101 OT2015-1 (Blagorodnova et al. 2017), and the recent 2018 LRN in NGC 45 (AT 2018bwo; N. Blagorodnova, et al., in preparation), all obtained as part of SPIRITS.

cluding constraints on any associated optical emission from wide-field surveys at Palomar. I divide these events into basic categories based on their IR luminosities, namely the luminous ($M_{[4.5]} \lesssim -14$ mag) transients and eruptions, and the less luminous SPRITEs (eSPecially Red Intermediate-luminosity Transient Events; $-11 \gtrsim M_{[4.5]} \gtrsim -14$ mag; Kasliwal et al. 2017b). I further examine the SPRITEs in terms of the timescale of their IR evolution, and discuss each group in turn, below.

Luminous IR transients: Obscured CCSNe

The sample of luminous ($M_{[4.5]} \lesssim -14$ mag) IR transient and eruptive stellar outbursts discovered by SPIRITS have been the primary focus of this thesis. These events include five candidate obscured CCSNe discovered between 2014-2018 (red stars in Figure 6.1), discussed in Chapters 2, 3, and 5, that, despite their high IR luminosities, were completely missed by any optical search. I find that compared to a control sample of the optically discovered events recovered as luminous IR transients in SPIRITS, including eight CCSNe and one SN Iax, the IR-discovered events are systematically redder in their optical–IR colors. All five had extinction estimates of $A_V \gtrsim 2$–9 mag, and compared to the time- and volume-limited sample of CCSNe within 12 Mpc of Mattila et al. (2012), the SPIRITS sample suggests a higher fraction of CCSNe may suffer significant host extinction than previously thought. Quantitatively, I estimate that 38^{+14}_{-11}% of CCSNe in nearby galaxies are being missed by optical searches due to heavy extinction.

SPIRITS 16tn, discussed in detail in Chapter 3, is the most heavily extinguished object in the sample at $A_V \approx 8$–9 mag. Its near-IR spectrum shows broad water absorption features, never before seen in an SN, that together with the high extinction inferred for this event, may suggest the progenitor was encased in a dense molecular cloud heated by the energetic explosion. Intriguingly, SPIRITS 16ix is a near twin to SPIRITS 16tn. Both are characterized by fast IR fade rates compared to previously observed CCSNe, and SPIRITS 16ix is similarly heavily obscured ($A_V \gtrsim 5$ mag). Though this is speculative, they could represent a previously unknown subclass of events, systematically missed in the optical due to their low intrinsic luminosities and apparent preference for the most densely obscured environments.

Luminous IR transients: LRNe, ILRTs, and LBVs

The four remaining luminous IR SPIRITS transients presented in Chapter 5 represent a diverse array of IR-dominated events likely arising from massive stellar systems. SPIRITS 14azy is a candidate LRN, and may have arisen from a similar mass

system to the $M \approx 18\ M_{\odot}$ F-type supergiant progenitor of the common-envelope ejection event M101 OT2015-1. The newly discovered SPIRITS 19fi, peaking at $M_{[4.5]} = -14.5$, may also be related to the LRNe, with possible evidence for early dust formation given the short ≈10-day duration of its associated optical counterpart (see *Spitzer* and ZTF light curves in Figure A.1).

In addition to the candidate ILRT SPIRITS 15ade, the discovery of the most recent member of this class, M51 OT2019-1, is discussed in detail in Chapter 4. Twelve years of monitoring M51 with *Spitzer*, including substantial coverage in the last 5 years from SPIRITS, showed significant IR variability of its directly identified progenitor. This may suggest prior episodes of eruptive, dust-forming outbursts, or may be consistent with the periodic thermal pulsations expected of super-AGB stars. The extended phase of early circumstellar dust destruction observed in the early optical light curves for M51 OT2019-1 disfavors a terminal explosion scenario, and may strengthen the connection between the ILRTs and the giant, non-terminal eruptions of LBVs.

SPIRITS 17pc and SPIRITS 17qm, discussed in Chapter 5 underwent multiple, extremely red outbursts over several years and have directly identified, massive progenitors likely to be LBVs. Together with the newly discovered SPIRITS 19bh, these events may be the first LBV-associated transients identified only via their infrared emission, expanding the landscape of the eruptive phenomena associated with these enigmatic stars.

Fast and faint SPRITEs: Dusty, IR-luminous novae?

The majority of SPIRITS transients fainter than $M_{[4.5]} > 14$ mag (17 of 21 events) are detected in *Spitzer*/IRAC imaging during only a single visibility window, implying that these events evolve on timescales shorter than the primary ≈6 month cadence of the SPIRITS survey. This is born out further for a handful of transients showing significant evolution during higher cadence observations within a visibility window (e.g., SPIRITS 14bmc, SPIRITS 16rs, and SPIRITS 19bl rise over a week to two months, while SPIRITS 15bh and SPIRITS 15lq fade within a week to a month). The bulk of these fast transients are relatively dim, with 15 events fainter than $M_{[4.5]} > -12.5$ mag at peak (I return to the brighter, fast events below), and all of them have red IR colors at peak of [3.6]−[4.5] between 0.5 and 1.2 mag. Where contemporaneous optical data are available from iPTF and ZTF, we see that these events have remarkably red optical–IR SEDs, with colors in excess of $r - [4.5] \gtrsim$

5 mag in some cases. Two events, SPIRITS 15bb and SPIRITS 15bh, were preceded by short ($\lesssim$2 months), faint ($M_g \approx -8$ mag) optical outbursts recovered in stacked, archival iPTF images.

All 15 fast and faint IR transients in SPIRITS were found in just seven galaxies within $\approx$ 5 Mpc, and nearly half of them were in M81. The high rate of these events from such a small number of nearby galaxies suggests they are very common. An attractive scenario for the origin of these events is thus classical novae, of which the rate in large galaxies like the Milky Way is estimated to be $\approx$50 yr^{-1} (e.g., Shafter 2017). The optical precursors detected for SPIRITS 15bb and SPIRITS 15bh are in the luminosity range typical of novae, further supporting this hypothesis. Classical novae of the DQ Her class, originating from a binary system with a carbon-oxygen white dwarf primary star, form optically thick circumstellar dust shells, powering IR-dominated SEDs. Some faster carbon-oxygen novae as well, while forming less dust in optically thin shells, still produce strong IR emission peaking on a timescale of $\approx$ 50–80 days at $M_{[4.5]} \approx -11$ to -12 mag (e.g., V1668 Cyg; Gehrz et al. 1995). These properties are generally consistent with the those of the fast and faint IR transients discovered by SPIRITS. Further study on the implications of this population for the rate of strongly dust-forming novae and their impact on the chemical enrichment and dust budget of galaxies (e.g., Gehrz 1988; Gehrz et al. 2007) is certainly warranted.

Slow SPRITEs: self-obscured stellar mergers?

Four transients fainter than $M_{[4.5]} > 14$ mag, in contrast, evolve much more slowly, with IR light curve lasting longer than one year. SPIRITS 15bk, SPIRITS 17fe, and SPIRITS 18nu were first detected on the rise, reaching their peak IR luminosities of $M_{[4.5]} \approx -12$ mag between about 30 and 200 days later. All four events, also including SPIRITS 17ar, then begin to slowly decline. Optical constraints again indicate extreme optical–IR colors of $r - [4.5] \gtrsim$ 5–6 mag, though we cannot rule out the possibility of faint, short-duration optical precursors, like those seen in the faint and fast events, SPIRITS 15bb and SPIRITS 15bh, or the more luminous transient, SPIRITS 19fi.

A distinguishing feature in the optical light curves of many LRN is the presence of a second peak, which cannot be easily explained in the stellar merger scenario by a single energy source such as recombination in a shell of dynamically ejected mass, nor as cooling emission from hot ejecta (e.g., MacLeod et al. 2017). A

new model by (Metzger and Pejcha 2017), suggests that, while cooling emission from the freely expanding ejecta in the polar direction may power the first peak, the second is powered by the shock-interaction of the dynamically-ejected mass and equatorially concentrated mass ejected prior to the dynamical merger phase (as in Pejcha, Metzger, and Tomida 2016a, 2016b). The dense regions behind radiative shocks is a favorable location for dust nucleation, provided the shock luminosity is sufficiently low for the gas to cool (e.g., Smith et al. 2011; Derdzinski, Metzger, and Lazzati 2017). Intriguingly, Metzger and Pejcha (2017) find that for some binary systems, namely those involving giant stars with extended phases of pre-dynamical mass-loss, dust formation can occur early enough to completely obscure, or dramatically shorten, the secondary optical peak, reprocessing the shock luminosity into a long-lived IR transient. Overcoming the inherent selection effects of optical discovery, the slow SPRITEs, in addition to the more luminous candidate LRNe, SPIRITS 14azy and SPIRITS 19fi, may represent the first *unbiased* census of stellar mergers and common-envelope events.

While the self-obscuring stellar merger scenario may neatly explain the properties of slow SPRITEs, alternative models are also possible. For example, massive, compact-multiple systems in star-forming regions undergoing dynamical interactions can release as much as 10^{51} erg, and could power IR transients given their densely obscured environments (Bally and Zinnecker 2005). Kashi and Soker (2017) have also suggested more generally that equatorial material can obscure transients driven by strong binary interactions, but that dust formation in polar outflows may still power IR transients. Conclusively determining the physical nature of slow SPRITEs is only possibly with infrared spectroscopy. Given their long-lived, ongoing IR emission, these events will be prime targets for early observations with the *James Webb Space Telescope* (*JWST*) following its planned launch in 2021.

Bright, fast SPRITEs: A new and unexpected mystery

Similar to the class of faint, fast SPRITEs described above, SPIRITS 14bug and SPIRITS 18dz evolve on timescales shorter than ≈6 months, each appearing in observations during only a single *Spitzer* visibility window. In fact, SPIRITS 18dz is one of the fastest fading events in the entire sample, disappearing within $\lesssim 40$ days. These events, peaking at $M_{[4.5]} \lesssim -13$ to -14 mag, are too luminous to be novae. The IR luminosity of a dust-forming nova is limited by the Eddington luminosity of the explosion at peak, corresponding to a peak magnitude at [3.6] of ≈ -11 when the optically thick dust shell forms at $\approx$ 50-80 days later (Gehrz et al. 1995). The

most luminous novae at [4.5] show IR colors up to [3.6]−[4.5] $\lesssim$ 1.5 mag, limiting the [4.5] peak to ≈ -12.5 mag (Gehrz et al. 1980). Given their fast timescale, the physics of these events may be similar to novae, but requiring a more luminous underlying power source. I speculate as well, that they could be related to the fast-fading, more luminous SPIRITS events, SPIRITS 16tn and SPIRITS 16ix, possibly associated with weak core-collapse explosions or even the elusive electron-capture SNe. Elucidating the nature of these mysterious transients will require faster cadence experiments in the IR to better characterize their light curves and IR spectroscopy to reveal the detailed physics.

6.3 Beyond *Spitzer*: the future of exploring the dynamic infrared sky

As Project Scientist for SPIRITS, I will continue to oversee the successful carrying-out of the survey through the end of the more than 16-year *Spitzer* mission in January 2020. As the first dedicated search for infrared transients in nearby galaxies, SPIRITS has laid the ground work for continued exploration of the dynamic infrared sky. The first ground-based, synoptic transients searches in the near-IR are already underway (e.g., Palomar Gattini-IR; Moore et al. 2016, K. De et al., in preparation). The launch of *JWST* will bring the first opportunities—and at unprecedented sensitivity—to gain access to the detailed physics of IR-dominated transients with mid-IR spectroscopy since the end of *Spitzer*'s cryogenic mission in 2009. The Wide-Field Infrared Survey Telescope (WFIRST), planned to launch in the mid 2020s, with its large field of view and increased sensitivity over ground-based facilities will be another unique discovery machine for transient phenomena in the near-IR. Even as SPIRITS comes to a close, the future is undoubtedly bright for time-domain astrophysics in the IR.

BIBLIOGRAPHY

Adams, S. M., J. E. Jencson, and M. M. Kasliwal. 2016. "Swift follow-up of SPIRITS16tn". *The Astronomer's Telegram* 9441 ().

Adams, S. M., et al. 2016. "Almost gone: SN 2008S and NGC 300 2008OT-1 are fainter than their progenitors". *MNRAS* 460 (): 1645–1657. doi:10.1093/mnras/stw1059. arXiv: 1511.07393 [astro-ph.HE].

Ahn, C. P., et al. 2014. "The Tenth Data Release of the Sloan Digital Sky Survey: First Spectroscopic Data from the SDSS-III Apache Point Observatory Galactic Evolution Experiment". *ApJS* 211, 17 (): 17. doi:10.1088/0067-0049/211/2/17. arXiv: 1307.7735 [astro-ph.IM].

Alam, S., et al. 2015. "The Eleventh and Twelfth Data Releases of the Sloan Digital Sky Survey: Final Data from SDSS-III". *ApJS* 219, 12 (): 12. doi:10.1088/0067-0049/219/1/12. arXiv: 1501.00963 [astro-ph.IM].

Amanullah, R., et al. 2014. "The Peculiar Extinction Law of SN 2014J Measured with the Hubble Space Telescope". *ApJL* 788, L21 (): L21. doi:10.1088/2041-8205/788/2/L21. arXiv: 1404.2595 [astro-ph.HE].

Anderson, J. P., et al. 2014. "Characterizing the V-band Light-curves of Hydrogen-rich Type II Supernovae". *ApJ* 786, 67 (): 67. doi:10.1088/0004-637X/786/1/67. arXiv: 1403.7091 [astro-ph.HE].

Andrews, J. E., et al. 2011. "Evidence for Pre-existing Dust in the Bright Type IIn SN 2010jl". *AJ* 142, no. 2, 45 (): 45. doi:10.1088/0004-6256/142/2/45. arXiv: 1106.0537 [astro-ph.CO].

Andrews, J. E., et al. 2010. "SN 2007od: A Type IIP Supernova with Circumstellar Interaction". *ApJ* 715, no. 1 (): 541–549. doi:10.1088/0004-637X/715/1/541. arXiv: 1004.1209 [astro-ph.SR].

Aoki, M. 2016. "Transient Discovery Report for 2016-01-04". *Transient Name Server Discovery Report* 4 ().

Arbour, R. 2016. "Transient Discovery Report for 2016-03-14". *Transient Name Server Discovery Report* 215 ().

Arcavi, I., et al. 2012. "Caltech Core-Collapse Project (CCCP) Observations of Type II Supernovae: Evidence for Three Distinct Photometric Subtypes". *ApJL* 756, L30 (): L30. doi:10.1088/2041-8205/756/2/L30. arXiv: 1206.2029.

Arcavi, I., et al. 2014. "FLOYDS Classification of ASASSN-14ha as a Young Type II SN". *The Astronomer's Telegram* 6466 ().

Bally, John, and Hans Zinnecker. 2005. "The Birth of High-Mass Stars: Accretion and/or Mergers?" *AJ* 129, no. 5 (): 2281–2293. doi:10.1086/429098. arXiv: astro-ph/0502485 [astro-ph].

Banerjee, D. P. K., et al. 2018. "Early formation of carbon monoxide in the Centaurus A supernova SN 2016adj". *ArXiv e-prints* (). arXiv: 1808.04766 [astro-ph.SR].

Barnes, Jennifer, and Daniel Kasen. 2013. "Effect of a High Opacity on the Light Curves of Radioactively Powered Transients from Compact Object Mergers". *ApJ* 775, no. 1, 18 (): 18. doi:10.1088/0004-637X/775/1/18. arXiv: 1303.5787 [astro-ph.HE].

Baron, E., D. Branch, and P. H. Hauschildt. 2007. "Reddening, Abundances, and Line Formation in SNe II". *ApJ* 662 (): 1148–1155. doi:10.1086/517961. eprint: astro-ph/0703068.

Bellm, E. C., and B. Sesar. 2016. *pyraf-dbsp: Reduction pipeline for the Palomar Double Beam Spectrograph*. Astrophysics Source Code Library. ascl: 1602.002.

Bellm, E. C., et al. 2019a. "The Zwicky Transient Facility: System Overview, Performance, and First Results". *PASP* 131, no. 1 (): 018002. doi:10.1088/1538-3873/aaecbe. arXiv: 1902.01932 [astro-ph.IM].

Bellm, Eric C., et al. 2019b. "The Zwicky Transient Facility: Surveys and Scheduler". *PASP* 131, no. 1000 (): 068003. doi:10.1088/1538-3873/ab0c2a. arXiv: 1905.02209 [astro-ph.IM].

Berger, E., et al. 2009. "An Intermediate Luminosity Transient in NGC 300: The Eruption of a Dust-Enshrouded Massive Star". *ApJ* 699 (): 1850–1865. doi:10.1088/0004-637X/699/2/1850. arXiv: 0901.0710 [astro-ph.HE].

Bessell, M. S., F. Castelli, and B. Plez. 1998. "Model atmospheres broad-band colors, bolometric corrections and temperature calibrations for O - M stars". *A&A* 333 (): 231–250.

Bessell, M. S., M. Scholz, and P. R. Wood. 1996. "Phase and cycle dependence of the photospheric structure and observable properties of Mira variables." *A&A* 307 (): 481–499.

Bessell, M. S., et al. 1989. "The effects of photospheric extension upon the spectra of M-type Mira variables". *A&A* 213 (): 209–225.

Blagorodnova, N., et al. 2017. "Common Envelope Ejection for a Luminous Red Nova in M101". *ApJ* 834, 107 (): 107. doi:10.3847/1538-4357/834/2/107. arXiv: 1607.08248 [astro-ph.SR].

Blagorodnova, N., et al. 2018. "The SED Machine: A Robotic Spectrograph for Fast Transient Classification". *PASP* 130, no. 3 (): 035003. doi:10.1088/1538-3873/aaa53f. arXiv: 1710.02917 [astro-ph.IM].

Blanton, M. R., and S. Roweis. 2007. "K-Corrections and Filter Transformations in the Ultraviolet, Optical, and Near-Infrared". *AJ* 133 (): 734–754. doi:10.1086/510127. eprint: astro-ph/0606170.

Blinnikov, S. I., et al. 1998. “A Comparative Modeling of Supernova 1993J”. *ApJ* 496 (): 454–472. doi:10.1086/305375. eprint: astro-ph/9711055.

Bock, G., et al. 2016. “ASASSN-16fq: Discovery of A Probable Supernova in M66”. *The Astronomer’s Telegram* 9091 ().

Bode, M. F., and A. Evans. 1980. “Infrared emission by dust grains near variable primary sources. III - Type II supernovae”. *MNRAS* 193 (): 21P–24P. doi:10.1093/mnras/193.1.21P.

Bond, H. E. 2011. “Hubble Space Telescope Imaging of the Outburst Site of M31 RV. II. No Blue Remnant in Quiescence”. *ApJ* 737, 17 (): 17. doi:10.1088/0004-637X/737/1/17. arXiv: 1105.4595 [astro-ph.SR].

Bond, H. E., and M. H. Siegel. 2006. “Hubble Space Telescope Imaging of the Outburst Site of M31 RV”. *AJ* 131 (): 984–989. doi:10.1086/498896. eprint: astro-ph/0510401.

Bond, H. E., et al. 2003. “An energetic stellar outburst accompanied by circumstellar light echoes”. *Nature* 422 (): 405–408. eprint: astro-ph/0303513.

Bond, H. E., et al. 2009. “The 2008 Luminous Optical Transient in the Nearby Galaxy NGC 300”. *ApJL* 695 (): L154–L158. doi:10.1088/0004-637X/695/2/L154. arXiv: 0901.0198 [astro-ph.SR].

Bondi, M., et al. 2012. “The nuclear starburst in Arp 299-A: from the 5.0 GHz VLBI radio light-curves to its core-collapse supernova rate”. *A&A* 539, A134 (): A134. doi:10.1051/0004-6361/201118446. arXiv: 1201.3220.

Borish, H. J., et al. 2015. “Near-infrared Spectroscopy of the Type IIn SN 2010jl: Evidence for High Velocity Ejecta”. *ApJ* 801, 7 (): 7. doi:10.1088/0004-637X/801/1/7. arXiv: 1406.5531 [astro-ph.SR].

Botticella, M. T., et al. 2012. “A comparison between star formation rate diagnostics and rate of core collapse supernovae within 11 Mpc”. *A&A* 537, A132 (): A132. doi:10.1051/0004-6361/201117343. arXiv: 1111.1692.

Botticella, M. T., et al. 2009. “SN 2008S: an electron-capture SN from a super-AGB progenitor?” *MNRAS* 398 (): 1041–1068. doi:10.1111/j.1365-2966.2009.15082.x. arXiv: 0903.1286 [astro-ph.SR].

Botticella, M. T., et al. 2013. “SUDARE at the VST”. *The Messenger* 151 (): 29–32.

Bowen, I. S. 1947. “Excitation by Line Coincidence”. *PASP* 59 (): 196–198. doi:10.1086/125951.

Bowers, E. J. C., et al. 1997. “Infrared and optical spectroscopy of Type IA supernovae in the nebular phase”. *MNRAS* 290 (): 663–679. doi:10.1093/mnras/290.4.663. eprint: astro-ph/9707119.

Brogan, C. L., et al. 2018. "The Extraordinary Outburst in the Massive Protostellar System NGC 6334I-MM1: Flaring of the Water Masers in a North-South Bipolar Outflow Driven by MM1B". *ApJ* 866, no. 2, 87 (): 87. doi:10.3847/1538-4357/aae151. arXiv: 1809.04178 [astro-ph.SR].

Brown, T. M., et al. 2013. "Las Cumbres Observatory Global Telescope Network". *PASP* 125 (): 1031. doi:10.1086/673168. arXiv: 1305.2437 [astro-ph.IM].

Brunthaler, A., et al. 2009. "Discovery of a bright radio transient in M 82: a new radio supernova?" *A&A* 499, no. 2 (): L17–L20. doi:10.1051/0004-6361/200912327. arXiv: 0904.2388 [astro-ph.CO].

Brunthaler, A., et al. 2010. "VLBI observations of SN 2008iz. I. Expansion velocity and limits on anisotropic expansion". *A&A* 516, A27 (): A27. doi:10.1051/0004-6361/201014133. arXiv: 1003.4665 [astro-ph.CO].

Burke, J., et al. 2019. "Global SN Project Transient Classification Report for 2019-03-05". *Transient Name Server Classification Report* 328 ().

Butler, N., et al. 2012. "First Light with RATIR: An Automated 6-band Optical/NIR Imaging Camera". In *Ground-based and Airborne Instrumentation for Astronomy IV*, 8446:844610. Proc. SPIE. doi:10.1117/12.926471.

Cai, Y.-Z., et al. 2018. "AT 2017be - a new member of the class of intermediate-luminosity red transients". *MNRAS* 480 (): 3424–3445. doi:10.1093/mnras/sty2070. arXiv: 1807.11676 [astro-ph.HE].

Cao, Y., P. E. Nugent, and M. M. Kasliwal. 2016. "Intermediate Palomar Transient Factory: Realtime Image Subtraction Pipeline". *PASP* 128, no. 11 (): 114502. doi:10.1088/1538-3873/128/969/114502. arXiv: 1608.01006 [astro-ph.IM].

Cao, Y., et al. 2014. "Classification of Supernova in M82 as a young, reddened Type Ia Supernova". *The Astronomer's Telegram* 5786 ().

Cappellaro, E., et al. 2015. "Supernova rates from the SUDARE VST-OmegaCAM search. I. Rates per unit volume". *A&A* 584, A62 (): A62. doi:10.1051/0004-6361/201526712. arXiv: 1509.04496.

Caratti o Garatti, A., et al. 2017. "Disk-mediated accretion burst in a high-mass young stellar object". *Nature Physics* 13, no. 3 (): 276–279. doi:10.1038/nphys3942. arXiv: 1704.02628 [astro-ph.SR].

Cardelli, J. A., G. C. Clayton, and J. S. Mathis. 1989. "The relationship between infrared, optical, and ultraviolet extinction". *ApJ* 345 (): 245–256. doi:10.1086/167900.

Casali, M., et al. 2007. "The UKIRT wide-field camera". *A&A* 467 (): 777–784. doi:10.1051/0004-6361:20066514.

Cenko, S. B., et al. 2006. "The Automated Palomar 60 Inch Telescope". *PASP* 118 (): 1396–1406. doi:10.1086/508366. eprint: astro-ph/0608323.

Chambers, K. C., et al. 2016. "The Pan-STARRS1 Surveys". *arXiv e-prints* (). arXiv: 1612.05560 [astro-ph.IM].

Chapman, N. L., et al. 2009. "The Mid-Infrared Extinction Law in the Ophiuchus, Perseus, and Serpens Molecular Clouds". *ApJ* 690, 496-511 (): 496–511. doi:10.1088/0004-637X/690/1/496. arXiv: 0809.1106.

Cheng, Y.-C., T.-W. Chen, and S. Prentice. 2017. "LOT spectroscopic classification of AT 2017eaw in NGC 6946 as a Type II SN". *The Astronomer's Telegram* 10374 ().

Chevalier, R. A. 1999. "Supernova Remnants in Molecular Clouds". *ApJ* 511 (): 798–811. doi:10.1086/306710. eprint: astro-ph/9805315.

– . 1998. "Synchrotron Self-Absorption in Radio Supernovae". *ApJ* 499 (): 810–819. doi:10.1086/305676.

– . 1982. "The radio and X-ray emission from type II supernovae". *ApJ* 259 (): 302–310. doi:10.1086/160167.

Chevalier, R. A., and C. Fransson. 2006. "Circumstellar Emission from Type Ib and Ic Supernovae". *ApJ* 651 (): 381–391. doi:10.1086/507606. eprint: astro-ph/0607196.

Chevalier, R. A., C. Fransson, and T. K. Nymark. 2006. "Radio and X-Ray Emission as Probes of Type IIP Supernovae and Red Supergiant Mass Loss". *ApJ* 641 (): 1029–1038. doi:10.1086/500528. eprint: astro-ph/0509468.

Chomiuk, L., et al. 2016. "A Deep Search for Prompt Radio Emission from Thermonuclear Supernovae with the Very Large Array". *ApJ* 821, 119 (): 119. doi:10.3847/0004-637X/821/2/119. arXiv: 1510.07662 [astro-ph.HE].

Ciatti, F., and R. Barbon. 1971. "Observations of six supernovae". *Mem. Soc. Astron. Italiana* 42:145.

Cohen, M., W. A. Wheaton, and S. T. Megeath. 2003. "Spectral Irradiance Calibration in the Infrared. XIV. The Absolute Calibration of 2MASS". *AJ* 126 (): 1090–1096. doi:10.1086/376474. eprint: astro-ph/0304350.

Conseil, E., et al. 2013. "Supernova 2013ai in NGC 2207 = Psn J06161835-2122329". *Central Bureau Electronic Telegrams* 3431 ().

Cortini, G., et al. 2014. "Supernova 2014bc in M106 = Psn J12185771+4718113". *Central Bureau Electronic Telegrams* 3876 ().

Cresci, G., et al. 2007. "A NICMOS search for obscured supernovae in starburst galaxies". *A&A* 462 (): 927–931. doi:10.1051/0004-6361:20065364. eprint: astro-ph/0610783.

Crockett, R. M., et al. 2008. "The type IIb SN 2008ax: the nature of the progenitor". *MNRAS* 391 (): L5–L9. doi:10.1111/j.1745-3933.2008.00540.x. arXiv: 0805.1913.

Crowther, P. A. 1997. “The effective temperatures of hot stars.” In *IAU Symposium*, ed. by T. R. Bedding, A. J. Booth, and J. Davis, 189:137–146. IAU Symposium.

Cushing, M. C., W. D. Vacca, and J. T. Rayner. 2004. “Spextool: A Spectral Extraction Package for SpeX, a 0.8-5.5 Micron Cross-Dispersed Spectrograph”. *PASP* 116 (): 362–376. doi:10.1086/382907.

Davidson, K. 1987. “The relation between apparent temperature and mass-loss rate in hypergiant eruptions”. *ApJ* 317 (): 760–764. doi:10.1086/165324.

Davies, M. L., et al. 2009. “Follow-up observations at 16 and 33GHz of extragalactic sources from WMAP 3-yr data: I - Spectral properties”. *MNRAS* 400 (): 984–994. doi:10.1111/j.1365-2966.2009.15518.x. arXiv: 0907.3707.

de Jager, C., H. Nieuwenhuijzen, and K. A. van der Hucht. 1988. “Mass loss rates in the Hertzsprung-Russell diagram”. *A&AS* 72 (): 259–289.

De, K., et al. 2019. “Spectroscopic follow-up of ZTF 19aadyppr: A young and red transient in M51”. *The Astronomer’s Telegram* 12433 ().

Derdzinski, Andrea M., Brian D. Metzger, and Davide Lazzati. 2017. “Radiative shocks create environments for dust formation in classical novae”. *MNRAS* 469, no. 2 (): 1314–1329. doi:10.1093/mnras/stx829. arXiv: 1610.02401 [astro-ph.SR].

Diamond, T. R., P. Hoeflich, and C. L. Gerardy. 2015. “Late-time Near-infrared Observations of SN 2005df”. *ApJ* 806, 107 (): 107. doi:10.1088/0004-637X/806/1/107. arXiv: 1410.6759 [astro-ph.SR].

Dolphin, A. 2016. *DOLPHOT: Stellar photometry*. Astrophysics Source Code Library. ascl: 1608.013.

Dolphin, A. E. 2000. “WFPC2 Stellar Photometry with HSTPHOT”. *PASP* 112 (): 1383–1396. doi:10.1086/316630. eprint: astro-ph/0006217.

Draine, B. T., and H. M. Lee. 1984. “Optical properties of interstellar graphite and silicate grains”. *ApJ* 285 (): 89–108. doi:10.1086/162480.

Dwek, E. 1983. “The infrared echo of a type II supernova with a circumstellar dust shell - Applications to SN 1979c and SN 1980k”. *ApJ* 274 (): 175–183. doi:10.1086/161435.

– . 1985. “The infrared echo of Type II supernovae with circumstellar dust shells. II - A probe into the presupernova evolution of the progenitor star”. *ApJ* 297 (): 719–723. doi:10.1086/163571.

Eikenberry, S., et al. 2006. “FLAMINGOS-2: the facility near-infrared wide-field imager and multi-object spectrograph for Gemini”. In *Society of Photo-Optical Instrumentation Engineers (SPIE) Conference Series*, 6269:626917. Proc. SPIE. doi:10.1117/12.672095. eprint: astro-ph/0604577.

Eisenstein, D. J., et al. 2011. "SDSS-III: Massive Spectroscopic Surveys of the Distant Universe, the Milky Way, and Extra-Solar Planetary Systems". *AJ* 142, 72 (): 72. doi:10.1088/0004-6256/142/3/72. arXiv: 1101.1529 [astro-ph.IM].

Elias, J. H., et al. 2006. "Design of the Gemini near-infrared spectrograph". In *Society of Photo-Optical Instrumentation Engineers (SPIE) Conference Series*, 6269:62694C. Proc. SPIE. doi:10.1117/12.671817.

Elitzur, M., and Ž. Ivezić. 2001. "Dusty winds - I. Self-similar solutions". *MNRAS* 327 (): 403–421. doi:10.1046/j.1365-8711.2001.04706.x. eprint: astro-ph/0106096.

Elmegreen, B. G., et al. 2016. "High Star Formation Rates in Turbulent Atomic-dominated Gas in the Interacting Galaxies IC 2163 and NGC 2207". *ApJ* 823, 26 (): 26. doi:10.3847/0004-637X/823/1/26. arXiv: 1603.04533.

Elmegreen, B. G., et al. 2000. "Hubble Space Telescope Observations of the Interacting Galaxies NGC 2207 and IC 2163". *AJ* 120 (): 630–644. doi:10.1086/301462. eprint: astro-ph/0007200.

Elmegreen, D. M., et al. 2001. "Hubble Space Telescope Observations of Dust and Star-forming Regions in the Ocular Galaxy IC 2163 and Its Spiral Companion NGC 2207". *AJ* 121 (): 182–197. doi:10.1086/318036.

Ergon, M., et al. 2014. "Optical and near-infrared observations of SN 2011dh - The first 100 days". *A&A* 562, A17 (): A17. doi:10.1051/0004-6361/201321850. arXiv: 1305.1851 [astro-ph.SR].

Ergon, M., et al. 2015. "The Type IIb SN 2011dh: Two years of observations and modelling of the lightcurves". *A&A* 580, A142 (): A142. doi:10.1051/0004-6361/201424592. arXiv: 1408.0731 [astro-ph.SR].

Fabbri, J., et al. 2011. "The effects of dust on the optical and infrared evolution of SN 2004et". *MNRAS* 418, no. 2 (): 1285–1307. doi:10.1111/j.1365-2966.2011.19577.x. arXiv: 1110.3166 [astro-ph.GA].

Faber, S. M., et al. 2003. "The DEIMOS spectrograph for the Keck II Telescope: integration and testing". In *Instrument Design and Performance for Optical/Infrared Ground-based Telescopes*, ed. by M. Iye and A. F. M. Moorwood, 4841:1657–1669. Proc. SPIE. doi:10.1117/12.460346.

Faran, T., E. Nakar, and D. Poznanski. 2018. "The evolution of temperature and bolometric luminosity in Type II supernovae". *MNRAS* 473 (): 513–537. doi:10.1093/mnras/stx2288. arXiv: 1707.07695 [astro-ph.HE].

Fazio, G. G., et al. 2004. "The Infrared Array Camera (IRAC) for the Spitzer Space Telescope". *ApJS* 154 (): 10–17. doi:10.1086/422843. eprint: astro-ph/0405616.

Ferland, G. J., and S. E. Persson. 1989. "Implications of CA II emission for physical conditions in the broad-line region of active galactic nuclei". *ApJ* 347 (): 656–673. doi:10.1086/168156.

Ferrarese, L., et al. 2000. “The Hubble Space Telescope Key Project on the Extragalactic Distance Scale. XXVI. The Calibration of Population II Secondary Distance Indicators and the Value of the Hubble Constant”. *ApJ* 529 (): 745–767. doi:10.1086/308309. eprint: astro-ph/9908192.

Filippenko, A. V., et al. 2003. “Supernovae 2001co, 2003H, 2003dg, and 2003dr”. *IAU Circ.* 8159 ().

Fitzpatrick, E. L. 1999. “Correcting for the Effects of Interstellar Extinction”. *PASP* 111 (): 63–75. doi:10.1086/316293. eprint: astro-ph/9809387.

Flewelling, H. A., et al. 2016. “The Pan-STARRS1 Database and Data Products”. *arXiv e-prints* (). arXiv: 1612.05243 [astro-ph.IM].

Flower, P. J. 1996. “Transformations from Theoretical Hertzsprung-Russell Diagrams to Color-Magnitude Diagrams: Effective Temperatures, B-V Colors, and Bolometric Corrections”. *ApJ* 469 (): 355. doi:10.1086/177785.

Foley, R. J., et al. 2015. “On the Progenitor System of the Type Iax Supernova 2014dt in M61”. *ApJL* 798, L37 (): L37. doi:10.1088/2041-8205/798/2/L37. arXiv: 1412.1088 [astro-ph.HE].

Fossey, S. J., et al. 2014. “Supernova 2014J in M82 = Psn J09554214+6940260”. *Central Bureau Electronic Telegrams* 3792 ().

Fox, O. D., and C. Casper. 2015. “A Spitzer Search for the Missing Supernovae in the Galactic Nuclei of ULIRGS”. *IAU General Assembly* 22, 2258045 (): 2258045.

Fox, O. D., and A. V. Filippenko. 2013. “The Late-time Rebrightening of Type Ia SN 2005gj in the Mid-infrared”. *ApJL* 772, L6 (): L6. doi:10.1088/2041-8205/772/1/L6. arXiv: 1304.4934 [astro-ph.HE].

Fox, O. D., et al. 2011. “A Spitzer Survey for Dust in Type IIn Supernovae”. *ApJ* 741, 7 (): 7. doi:10.1088/0004-637X/741/1/7. arXiv: 1104.5012 [astro-ph.SR].

Fox, O. D., et al. 2016. “An Excess of Mid-infrared Emission from the Type Iax SN 2014dt”. *ApJL* 816, L13 (): L13. doi:10.3847/2041-8205/816/1/L13. arXiv: 1510.08070 [astro-ph.HE].

Fox, O. D., et al. 2010. “Disentangling the Origin and Heating Mechanism of Supernova Dust: Late-time Spitzer Spectroscopy of the Type IIn SN 2005ip”. *ApJ* 725, 1768-1778 (): 1768–1778. doi:10.1088/0004-637X/725/2/1768. arXiv: 1005.4682 [astro-ph.HE].

Fox, O. D., et al. 2013. “Late-time Circumstellar Interaction in a Spitzer Selected Sample of Type IIn Supernovae”. *AJ* 146, 2 (): 2. doi:10.1088/0004-6256/146/1/2. arXiv: 1304.0248 [astro-ph.SR].

Fremling, C., et al. 2016. “PTF12os and iPTF13bvn. Two stripped-envelope supernovae from low-mass progenitors in NGC 5806”. *A&A* 593, A68 (): A68. doi:10.1051/0004-6361/201628275. arXiv: 1606.03074 [astro-ph.HE].

Fukugita, M., et al. 1996. “The Sloan Digital Sky Survey Photometric System”. *AJ* 111 (): 1748. doi:10.1086/117915.

Gallagher, J. S., and E. P. Ney. 1976. “The early infrared development of Nova Cygni 1975”. *ApJL* 204 (): L35–L39. doi:10.1086/182049.

Gallagher, Joseph S., et al. 2012. “Optical and Infrared Analysis of Type II SN 2006bc”. *ApJ* 753, no. 2, 109 (): 109. doi:10.1088/0004-637X/753/2/109. arXiv: 1205.5517 [astro-ph.CO].

Gal-Yam, Avishay, et al. 2006. “Radio and Optical Follow-up Observations of a Uniform Radio Transient Search: Implications for Gamma-Ray Bursts and Supernovae”. *ApJ* 639, no. 1 (): 331–339. doi:10.1086/499157. arXiv: astro-ph/0508629 [astro-ph].

Gandhi, P., et al. 2013. “SN 2009js at the Crossroads between Normal and Subluminous Type IIP Supernovae: Optical and Mid-infrared Evolution”. *ApJ* 767, no. 2, 166 (): 166. doi:10.1088/0004-637X/767/2/166. arXiv: 1303.1565 [astro-ph.SR].

Gehrels, N., et al. 2004. “The Swift Gamma-Ray Burst Mission”. *ApJ* 611 (): 1005–1020. doi:10.1086/422091.

Gehrz, R. D. 1988. “Casting light on the ejecta”. *Nature* 333 (): 705–706. doi:10.1038/333705a0.

Gehrz, R. D., and E. P. Ney. 1990. “Confirmation of Dust Condensation in the Ejecta of Supernova 1987a”. *Proceedings of the National Academy of Science* 87 (): 4354–4357. doi:10.1073/pnas.87.11.4354.

Gehrz, R. D., et al. 2015. “The Early Infrared Temporal Development of Nova Delphini 2013 (V339 DEL) Observed with the Stratospheric Observatory for Infrared Astronomy (SOFIA) and from the Ground”. *ApJ* 812, 132 (): 132. doi:10.1088/0004-637X/812/2/132.

Gehrz, R. D., et al. 2007. “The NASA Spitzer Space Telescope”. *Review of Scientific Instruments* 78, no. 1 (): 011302–011302. doi:10.1063/1.2431313.

Gehrz, R. D., et al. 1995. “The Neon Nova. III. The Infrared Light Curves of Nova QU Vulpeculae (Nova VUL 1984#2)”. *AJ* 110 (): 325. doi:10.1086/117523.

Gehrz, R. D., et al. 1980. “The optically thin dust shell of nova CYG 1978.” *ApJ* 239 (): 570–580. doi:10.1086/158143.

Goobar, A., et al. 2014. “The Rise of SN 2014J in the Nearby Galaxy M82”. *ApJL* 784, no. 1, L12 (): L12. doi:10.1088/2041-8205/784/1/L12. arXiv: 1402.0849 [astro-ph.GA].

Goodrich, R., and M. Cohen. 2003. “LRIS imaging spectropolarimeter at the W.M. Keck Observatory”. In *Polarimetry in Astronomy*, ed. by S. Fineschi, 4843:146–155. Proc. SPIE. doi:10.1117/12.458652.

Graham, Matthew J., et al. 2019. "The Zwicky Transient Facility: Science Objectives". *PASP* 131, no. 1001 (): 078001. doi:10.1088/1538-3873/ab006c. arXiv: 1902.01945 [astro-ph.IM].

Granata, V., et al. 2016. "Asiago spectroscopic and photometric observations of AT2016bau". *The Astronomer's Telegram* 8818 ().

Groenewegen, M. A. T., et al. 2009. "Luminosities and mass-loss rates of SMC and LMC AGB stars and red supergiants". *A&A* 506, no. 3 (): 1277–1296. doi:10.1051/0004-6361/200912678. arXiv: 0908.3087 [astro-ph.SR].

Grossan, B., et al. 1999. "An Infrared Search for Extinguished Supernovae in Starburst Galaxies". *AJ* 118 (): 705–718. doi:10.1086/300962. eprint: astro-ph/9812253.

Hamuy, M. 2003. "Observed and Physical Properties of Core-Collapse Supernovae". *ApJ* 582 (): 905–914. doi:10.1086/344689. eprint: astro-ph/0209174.

Helou, G., et al. 2013. "The Mid-infrared Light Curve of Nearby Core-collapse Supernova SN 2011dh (PTF 11eon)". *ApJL* 778, L19 (): L19. doi:10.1088/2041-8205/778/1/L19. arXiv: 1309.4891 [astro-ph.SR].

Herrero-Illana, R., M. Á. Pérez-Torres, and A. Alberdi. 2012. "Evidence of nuclear disks in starburst galaxies from their radial distribution of supernovae". *A&A* 540, L5 (): L5. doi:10.1051/0004-6361/201118545. arXiv: 1203.2927 [astro-ph.CO].

Herter, T. L., et al. 2008. "The performance of TripleSpec at Palomar". In *Ground-based and Airborne Instrumentation for Astronomy II*, 7014:70140X. Proc. SPIE. doi:10.1117/12.789660.

Hess, K. M., et al. 2009. "Anomalous H I in NGC 2997". *ApJ* 699 (): 76–88. doi:10.1088/0004-637X/699/1/76. arXiv: 0904.3494 [astro-ph.GA].

Hewett, P. C., et al. 2006. "The UKIRT Infrared Deep Sky Survey ZY JHK photometric system: passbands and synthetic colours". *MNRAS* 367, no. 2 (): 454–468. doi:10.1111/j.1365-2966.2005.09969.x. arXiv: astro-ph/0601592 [astro-ph].

Hildebrand, R. H. 1983. "The Determination of Cloud Masses and Dust Characteristics from Submillimetre Thermal Emission". *QJRAS* 24 (): 267.

Hodgkin, S. T., et al. 2009. "The UKIRT wide field camera ZYJHK photometric system: calibration from 2MASS". *MNRAS* 394 (): 675–692. doi:10.1111/j.1365-2966.2008.14387.x. arXiv: 0812.3081.

Hoffman, D., et al. 2011. "WISE Detections of Luminous Red Novae". *The Astronomer's Telegram* 3160 (): 1.

Hook, I. M., et al. 2004. "The Gemini-North Multi-Object Spectrograph: Performance in Imaging, Long-Slit, and Multi-Object Spectroscopic Modes". *PASP* 116 (): 425–440. doi:10.1086/383624.

Horesh, A., et al. 2013a. "An early and comprehensive millimetre and centimetre wave and X-ray study of SN 2011dh: a non-equipartition blast wave expanding into a massive stellar wind". *MNRAS* 436 (): 1258–1267. doi:10.1093/mnras/stt1645. arXiv: 1209.1102.

Horesh, A., et al. 2013b. "PTF 12gzk—A Rapidly Declining, High-velocity Type Ic Radio Supernova". *ApJ* 778, 63 (): 63. doi:10.1088/0004-637X/778/1/63. arXiv: 1306.5755 [astro-ph.HE].

Horiuchi, S., et al. 2013. "Effects of Stellar Rotation on Star Formation Rates and Comparison to Core-collapse Supernova Rates". *ApJ* 769, 113 (): 113. doi:10.1088/0004-637X/769/2/113. arXiv: 1302.0287 [astro-ph.SR].

Horiuchi, S., et al. 2011. "The Cosmic Core-collapse Supernova Rate Does Not Match the Massive-star Formation Rate". *ApJ* 738, 154 (): 154. doi:10.1088/0004-637X/738/2/154. arXiv: 1102.1977 [astro-ph.CO].

Horne, K. 1986. "An optimal extraction algorithm for CCD spectroscopy". *PASP* 98 (): 609–617. doi:10.1086/131801.

Hosseinzadeh, G., et al. 2016. "FLOYDS Classification of AT 2016bkv as a Young Type II Supernova". *The Astronomer's Telegram* 8859 ().

Hosseinzadeh, G., et al. 2018. "Short-lived Circumstellar Interaction in the Low-luminosity Type IIP SN 2016bkv". *ApJ* 861, 63 (): 63. doi:10.3847/1538-4357/aac5f6. arXiv: 1801.00015 [astro-ph.HE].

Huehnerhoff, J., et al. 2016. "Astrophysical Research Consortium Telescope Imaging Camera (ARCTIC) facility optical imager for the Apache Point Observatory 3.5m telescope". In *Ground-based and Airborne Instrumentation for Astronomy VI*, vol. 9908, 99085H. Proc. SPIE. doi:10.1117/12.2234214.

Humphreys, R. M., and K. Davidson. 1994. "The luminous blue variables: Astrophysical geysers". *PASP* 106 (): 1025–1051. doi:10.1086/133478.

Humphreys, R. M., K. Davidson, and N. Smith. 1999. "η Carinae's Second Eruption and the Light Curves of the η Carinae Variables". *PASP* 111 (): 1124–1131. doi:10.1086/316420.

Humphreys, R. M., et al. 2011. "The Photometric and Spectral Evolution of the 2008 Luminous Optical Transient in NGC 300". *ApJ* 743, 118 (): 118. doi:10.1088/0004-637X/743/2/118. arXiv: 1109.5131 [astro-ph.SR].

Humphreys, Roberta M., et al. 2013. "Luminous and Variable Stars in M31 and M33. I. The Warm Hypergiants and Post-red Supergiant Evolution". *ApJ* 773, no. 1, 46 (): 46. doi:10.1088/0004-637X/773/1/46. arXiv: 1305.6051 [astro-ph.SR].

Hunter, T. R., et al. 2017. "An Extraordinary Outburst in the Massive Protostellar System NGC6334I-MM1: Quadrupling of the Millimeter Continuum". *ApJL* 837, no. 2, L29 (): L29. doi:10.3847/2041-8213/aa5d0e. arXiv: 1701.08637 [astro-ph.SR].

Itagaki, K. 2016. “Transient Discovery Report for 2016-03-22”. *Transient Name Server Discovery Report* 234 ().

Ivezic, Z., and M. Elitzur. 1997. “Self-similarity and scaling behaviour of infrared emission from radiatively heated dust - I. Theory”. *MNRAS* 287 (): 799–811. doi:10.1093/mnras/287.4.799. eprint: astro-ph/9612164.

Ivezic, Z., M. Nenkova, and M. Elitzur. 1999. “User Manual for DUSTY”. *ArXiv Astrophysics e-prints* (). eprint: astro-ph/9910475.

Jencson, J. E., et al. 2017a. “Additional SPIRITS Discoveries of Infrared Transients and Variables with Counterparts in Reference Imaging”. *The Astronomer’s Telegram* 10171 (): 1.

– . 2017b. “Additional SPIRITS Discoveries of Infrared Transients and Variables without Counterparts in Reference Imaging”. *The Astronomer’s Telegram* 10172 (): 1.

Jencson, J. E., et al. 2017c. “New SPIRITS discoveries of Infrared Transients and Variables”. *The Astronomer’s Telegram* 10903 (): 1.

Jencson, J. E., et al. 2018a. “Pre-discovery detections and progenitor candidate for SPIRITS17pc in NGC 4388”. *The Astronomer’s Telegram* 11577 (): 1.

– . 2018b. “Pre-discovery detections and progenitor candidate for SPIRITS17qm in NGC 1365”. *The Astronomer’s Telegram* 11579 (): 1.

Jencson, J. E., et al. 2017d. “Recent Discoveries of Infrared Transients and Variables by SPIRITS”. *The Astronomer’s Telegram* 10488 (): 1.

Jencson, J. E., et al. 2018c. “Recent SPIRITS discoveries of Infrared Transients and Variables with Spitzer/IRAC”. *The Astronomer’s Telegram* 11575 (): 1.

Jencson, J. E., et al. 2019a. “SPIRITS discoveries of 8 Infrared Transients and Eruptive Variables with Spitzer/IRAC”. *The Astronomer’s Telegram* 12675 (): 1.

Jencson, J. E., et al. 2016a. “SPIRITS Discoveries of Infrared Transients and Variables with Spitzer Early Release Data”. *The Astronomer’s Telegram* 8688 (): 1.

Jencson, J. E., et al. 2016b. “SPIRITS Discoveries of New Infrared Transients and Variables”. *The Astronomer’s Telegram* 8940 (): 1.

Jencson, J. E., et al. 2015. “SPIRITS Discoveries of Recent Infrared Transients with Spitzer Early Release Data”. *The Astronomer’s Telegram* 7929 (): 1.

Jencson, J. E., et al. 2016c. “SPIRITS16tn: Spitzer Discovery of a Possible Supernova in Messier 108 at 8.8 Mpc”. *The Astronomer’s Telegram* 9434 (): 1.

Jencson, J. E., et al. 2018d. “Spitzer detections and pre-discovery archival limits for AT 2018akh in M81”. *The Astronomer’s Telegram* 11803 (): 1.

Jencson, J. E., et al. 2019b. "Spitzer detections and pre-discovery limits for nova candidate PNV J09552547+6903458 in M81". *The Astronomer's Telegram* 12679 (): 1.

Jencson, Jacob E., et al. 2019c. "Discovery of an Intermediate-luminosity Red Transient in M51 and Its Likely Dust-obscured, Infrared-variable Progenitor". *ApJL* 880, no. 2, L20 (): L20. doi:10.3847/2041-8213/ab2c05. arXiv: 1904.07857 [astro-ph.SR].

Jencson, Jacob E., et al. 2017e. "SPIRITS 15c and SPIRITS 14buu: Two Obscured Supernovae in the Nearby Star-forming Galaxy IC 2163". *ApJ* 837, no. 2, 167 (): 167. doi:10.3847/1538-4357/aa618f. arXiv: 1609.04444 [astro-ph.HE].

Jencson, Jacob E., et al. 2018e. "SPIRITS 16tn in NGC 3556: A Heavily Obscured and Low-luminosity Supernova at 8.8 Mpc". *ApJ* 863, no. 1, 20 (): 20. doi:10.3847/1538-4357/aacf8b. arXiv: 1803.00574 [astro-ph.HE].

Jencson, Jacob E., et al. 2019d. "The SPIRITS sample of Luminous Infrared Transients: Uncovering Hidden Supernovae and Dusty Stellar Outbursts in Nearby Galaxies". *arXiv e-prints*, arXiv:1901.00871 (): arXiv:1901.00871. arXiv: 1901.00871 [astro-ph.HE].

Jerkstrand, A., et al. 2015. "Late-time spectral line formation in Type IIb supernovae, with application to SN 1993J, SN 2008ax, and SN 2011dh". *A&A* 573, A12 (): A12. doi:10.1051/0004-6361/201423983. arXiv: 1408.0732 [astro-ph.HE].

Jha, S., et al. 1999. "Supernova 1999ec in NGC 2207". *IAU Circ.* 7269 ().

Johansson, J., et al. 2017. "Spitzer observations of SN 2014J and properties of mid-IR emission in Type Ia supernovae". *MNRAS* 466 (): 3442–3449. doi:10.1093/mnras/stw3350. arXiv: 1411.3332 [astro-ph.HE].

Jordi, K., E. K. Grebel, and K. Ammon. 2006. "Empirical color transformations between SDSS photometry and other photometric systems". *A&A* 460 (): 339–347. doi:10.1051/0004-6361:20066082. eprint: astro-ph/0609121.

Kankare, E., et al. 2008. "Discovery of a Very Highly Extinguished Supernova in a Luminous Infrared Galaxy". *ApJL* 689, L97 (): L97. doi:10.1086/595820. arXiv: 0810.2885.

Kankare, E., et al. 2012. "Discovery of Two Supernovae in the Nuclear Regions of the Luminous Infrared Galaxy IC 883". *ApJL* 744, L19 (): L19. doi:10.1088/2041-8205/744/2/L19. arXiv: 1112.0777 [astro-ph.SR].

Kankare, E., et al. 2014. "The nature of supernovae 2010O and 2010P in Arp 299 - I. Near-infrared and optical evolution". *MNRAS* 440, no. 2 (): 1052–1066. doi:10.1093/mnras/stt2289. arXiv: 1311.6408 [astro-ph.SR].

Karambelkar, V. R., et al. 2019. "SPIRITS Catalog of Infrared Variables: Identification of Extremely Luminous Long Period Variables". *arXiv e-prints* (). arXiv: 1901.07179 [astro-ph.SR].

Kasen, Daniel, N. R. Badnell, and Jennifer Barnes. 2013. "Opacities and Spectra of the r-process Ejecta from Neutron Star Mergers". *ApJ* 774, no. 1, 25 (): 25. doi:10.1088/0004-637X/774/1/25. arXiv: 1303.5788 [astro-ph.HE].

Kashi, Amit, and Noam Soker. 2016. "Operation of the jet feedback mechanism (JFM) in intermediate luminosity optical transients (ILOTs)". *Research in Astronomy and Astrophysics* 16, no. 6, 99 (): 99. doi:10.1088/1674-4527/16/6/099. arXiv: 1508.00004 [astro-ph.SR].

– . 2017. "Type II intermediate-luminosity optical transients (ILOTs)". *MNRAS* 467, no. 3 (): 3299–3305. doi:10.1093/mnras/stx240. arXiv: 1611.05855 [astro-ph.SR].

Kasliwal, M. M., et al. 2017a. "Illuminating gravitational waves: A concordant picture of photons from a neutron star merger". *Science* 358, no. 6370 (): 1559–1565. doi:10.1126/science.aap9455. arXiv: 1710.05436 [astro-ph.HE].

Kasliwal, M. M., et al. 2011. "PTF 10fqs: A Luminous Red Nova in the Spiral Galaxy Messier 99". *ApJ* 730, 134 (): 134. doi:10.1088/0004-637X/730/2/134. arXiv: 1005.1455 [astro-ph.SR].

Kasliwal, M. M., et al. 2014. "SPIRITS Discoveries of Infrared Transients with Spitzer". *The Astronomer's Telegram* 6644 (): 1.

Kasliwal, M. M., et al. 2017b. "SPIRITS: Uncovering Unusual Infrared Transients with Spitzer". *ApJ* 839, 88 (): 88. doi:10.3847/1538-4357/aa6978. arXiv: 1701.01151 [astro-ph.HE].

Kasliwal, M. M., et al. 2019. "The GROWTH Marshal: A Dynamic Science Portal for Time-domain Astronomy". *PASP* 131, no. 3 (): 038003. doi:10.1088/1538-3873/aafbc2. arXiv: 1902.01934 [astro-ph.IM].

Kato, M., H. Saio, and I. Hachisu. 1989. "Stellar wind during helium nova outburst". *ApJ* 340 (): 509–517. doi:10.1086/167413.

Kaufman, Michele, et al. 2016. "Ocular Shock Front in the Colliding Galaxy IC 2163". *ApJ* 831, no. 2, 161 (): 161. doi:10.3847/0004-637X/831/2/161. arXiv: 1608.02130 [astro-ph.GA].

Kawabata, K. S., et al. 2008. "Wide-field one-shot optical polarimeter: HOWPol". In *Ground-based and Airborne Instrumentation for Astronomy II*, 7014:70144L. Proc. SPIE. doi:10.1117/12.788569.

Kelson, D. D. 2003. "Optimal Techniques in Two-dimensional Spectroscopy: Background Subtraction for the 21st Century". *PASP* 115 (): 688–699. doi:10.1086/375502. eprint: astro-ph/0303507.

Kennicutt, R. C., Jr. 1998. "Star Formation in Galaxies Along the Hubble Sequence". *ARA&A* 36:189–232. doi:10.1146/annurev.astro.36.1.189. eprint: astro-ph/9807187.

Kennicutt, R. C., Jr., et al. 2009. "Dust-corrected Star Formation Rates of Galaxies. I. Combinations of Hα and Infrared Tracers". *ApJ* 703, 1672-1695 (): 1672–1695. doi:10.1088/0004-637X/703/2/1672. arXiv: 0908.0203 [astro-ph.CO].

Khan, R. 2017. "Spitzer Photometry of ˜1 Million Stars in M31 and 15 Other Galaxies". *ApJS* 228, 5 (): 5. doi:10.3847/1538-4365/228/1/5. arXiv: 1612.02009.

Khan, R., et al. 2010. "Census of Self-obscured Massive Stars in Nearby Galaxies with Spitzer: Implications for Understanding the Progenitors of SN 2008S-like Transients". *ApJ* 715 (): 1094–1108. doi:10.1088/0004-637X/715/2/1094. arXiv: 1001.3681 [astro-ph.SR].

Kilpatrick, C. D., and R. J. Foley. 2018. "The Dusty Progenitor Star of the Type II Supernova 2017eaw". *ArXiv e-prints* (). arXiv: 1806.00348 [astro-ph.SR].

Kim, M., et al. 2014. "Supernova 2014C in NGC 7331 = Psn J22370560+3424319". *Central Bureau Electronic Telegrams* 3777 ().

Kirshner, R. P., H. C. Arp, and J. R. Dunlap. 1976. "Observations of supernovae - 1975a in NGC 2207 and 1975b in the Perseus cluster". *ApJ* 207 (): 44. doi:10.1086/154465.

Kiyota, S., et al. 2014. "ASAS-SN Discovery of A Possible Supernova in NGC 1566". *The Astronomer's Telegram* 6460 ().

Kochanek, C. S. 2011a. "Dusty Explosions from Dusty Progenitors: The Physics of SN 2008S and the 2008 NGC 300-OT". *ApJ* 741, 37 (): 37. doi:10.1088/0004-637X/741/1/37. arXiv: 1106.4722 [astro-ph.SR].

– . 2011b. "The Astrophysical Implications of Dust Formation during the Eruptions of Hot, Massive Stars". *ApJ* 743, no. 1, 73 (): 73. doi:10.1088/0004-637X/743/1/73. arXiv: 1109.2596 [astro-ph.SR].

Kochanek, C. S., S. M. Adams, and K. Belczynski. 2014. "Stellar mergers are common". *MNRAS* 443 (): 1319–1328. doi:10.1093/mnras/stu1226. arXiv: 1405.1042 [astro-ph.SR].

Kochanek, C. S., D. M. Szczygiel, and K. Z. Stanek. 2011. "The Supernova Impostor Impostor SN 1961V: Spitzer Shows That Zwicky Was Right (Again)". *ApJ* 737, no. 2, 76 (): 76. doi:10.1088/0004-637X/737/2/76. arXiv: 1010.3704 [astro-ph.SR].

Kochanek, C. S., et al. 2017. "Supernova progenitors, their variability and the Type IIP Supernova ASASSN-16fq in M66". *MNRAS* 467 (): 3347–3360. doi:10.1093/mnras/stx291. arXiv: 1609.00022 [astro-ph.SR].

Kool, E. C., et al. 2018. "First results from GeMS/GSAOI for project SUNBIRD: Supernovae UNmasked By Infra-Red Detection". *MNRAS* 473 (): 5641–5657. doi:10.1093/mnras/stx2463. arXiv: 1709.08307.

Kotak, R., et al. 2009. "Dust and The Type II-Plateau Supernova 2004et". *ApJ* 704 (): 306–323. doi:10.1088/0004-637X/704/1/306. arXiv: 0904.3737 [astro-ph.SR].

Kotak, R., et al. 2005. "Early-Time Spitzer Observations of the Type II Plateau Supernova SN 2004dj". *ApJL* 628 (): L123–L126. doi:10.1086/432719. eprint: astro-ph/0506407.

Kotak, R., et al. 2006. "Spitzer Measurements of Atomic and Molecular Abundances in the Type IIP SN 2005af". *ApJL* 651 (): L117–L120. doi:10.1086/509655. eprint: astro-ph/0609706.

Kulkarni, S. R., et al. 2007. "An unusually brilliant transient in the galaxy M85". *Nature* 447 (): 458–460. doi:10.1038/nature05822. arXiv: 0705.3668.

Kumar, S., et al. 2014. "Supernova 2014bi in NGC 4096 = Psn J12060299+4729335". *Central Bureau Electronic Telegrams* 3892 ().

Laor, A., and B. T. Draine. 1993. "Spectroscopic constraints on the properties of dust in active galactic nuclei". *ApJ* 402 (): 441–468. doi:10.1086/172149.

Law, N. M., et al. 2009. "The Palomar Transient Factory: System Overview, Performance, and First Results". *PASP* 121 (): 1395. doi:10.1086/648598. arXiv: 0906.5350 [astro-ph.IM].

Levesque, E. M., et al. 2005. "The Effective Temperature Scale of Galactic Red Supergiants: Cool, but Not As Cool As We Thought". *ApJ* 628 (): 973–985. doi:10.1086/430901. eprint: astro-ph/0504337.

Li, W., et al. 2005. "On the Progenitor of the Type II Supernova 2004et in NGC 6946". *PASP* 117 (): 121–131. doi:10.1086/428278. eprint: astro-ph/0412487.

Li, W., et al. 2014. "Supernova 2014H = Psn J03370148+3205017". *Central Bureau Electronic Telegrams* 3788 ().

Lonsdale, C. J., et al. 2006. "VLBI Images of 49 Radio Supernovae in Arp 220". *ApJ* 647 (): 185–193. doi:10.1086/505193. eprint: astro-ph/0604570.

MacLeod, Morgan, et al. 2017. "Lessons from the Onset of a Common Envelope Episode: the Remarkable M31 2015 Luminous Red Nova Outburst". *ApJ* 835, no. 2, 282 (): 282. doi:10.3847/1538-4357/835/2/282. arXiv: 1605.01493 [astro-ph.SR].

Maeda, K., et al. 2008. "Asphericity in Supernova Explosions from Late-Time Spectroscopy". *Science* 319 (): 1220. doi:10.1126/science.1149437. arXiv: 0801.1100.

Maeda, K., et al. 2002. "Explosive Nucleosynthesis in Aspherical Hypernova Explosions and Late-Time Spectra of SN 1998bw". *ApJ* 565 (): 405–412. doi:10.1086/324487.

Maguire, K., et al. 2010. "Optical and near-infrared coverage of SN 2004et: physical parameters and comparison with other Type IIP supernovae". *MNRAS* 404 (): 981–1004. doi:10.1111/j.1365-2966.2010.16332.x. arXiv: 0912.3111 [astro-ph.SR].

Mahabal, A., et al. 2019. "Machine Learning for the Zwicky Transient Facility". *PASP* 131, no. 3 (): 038002. doi:10.1088/1538-3873/aaf3fa. arXiv: 1902.01936 [astro-ph.IM].

Maiolino, R., et al. 2002. "Discovery of two infrared supernovae: A new window on the SN search". *A&A* 389 (): 84–92. doi:10.1051/0004-6361:20020604. eprint: astro-ph/0204107.

Mannucci, F., M. Della Valle, and N. Panagia. 2007. "How many supernovae are we missing at high redshift?" *MNRAS* 377 (): 1229–1235. doi:10.1111/j.1365-2966.2007.11676.x. eprint: astro-ph/0702355.

Mannucci, F., et al. 2003. "The infrared supernova rate in starburst galaxies". *A&A* 401 (): 519–530. doi:10.1051/0004-6361:20030198. eprint: astro-ph/0302323.

Marples, P., G. Bock, and S. Parker. 2016. "Bright PSN in NGC5128 (Centaurus A) Discovered By Backyard Observatory Supernova Search (BOSS)". *The Astronomer's Telegram* 8651 ().

Martin, D. C., et al. 2014. "Intergalactic Medium Emission Observations with the Cosmic Web Imager. I. The Circum-QSO Medium of QSO 1549+19, and Evidence for a Filamentary Gas Inflow". *ApJ* 786, 106 (): 106. doi:10.1088/0004-637X/786/2/106. arXiv: 1402.4816.

Martini, Paul, et al. 1999. "Nova Sagittarii 1994 1 (V4332 Sagittarii): The Discovery and Evolution of an Unusual Luminous Red Variable Star". *AJ* 118, no. 2 (): 1034–1042. doi:10.1086/300951. arXiv: astro-ph/9905016 [astro-ph].

Masci, F. J., et al. 2017. "The IPAC Image Subtraction and Discovery Pipeline for the Intermediate Palomar Transient Factory". *PASP* 129, no. 1 (): 014002. doi:10.1088/1538-3873/129/971/014002. arXiv: 1608.01733 [astro-ph.IM].

Masci, F. J., et al. 2019. "The Zwicky Transient Facility: Data Processing, Products, and Archive". *PASP* 131, no. 1 (): 018003. doi:10.1088/1538-3873/aae8ac. arXiv: 1902.01872 [astro-ph.IM].

Mathis, J. S., W. Rumpl, and K. H. Nordsieck. 1977. "The size distribution of interstellar grains". *ApJ* 217 (): 425–433. doi:10.1086/155591.

Mattila, S., and W. P. S. Meikle. 2001. "Supernovae in the nuclear regions of starburst galaxies". *MNRAS* 324 (): 325–342. doi:10.1046/j.1365-8711.2001.04255.x.

Mattila, S., W. P. S. Meikle, and R. Greimel. 2004. "Highly extinguished supernovae in the nuclear regions of starburst galaxies". *New A Rev.* 48, **numbers** 7-8 (): 595–600. doi:10.1016/j.newar.2003.12.033. arXiv: astro-ph/0310117 [astro-ph].

Mattila, S., L. A. G. Monard, and W. Li. 2005. "Supernovae 2005Q, 2005R, 2005S, 2005T, 2005U". *IAU Circ.* 8473 ().

Mattila, S., et al. 2007. "Adaptive Optics Discovery of Supernova 2004ip in the Nuclear Regions of the Luminous Infrared Galaxy IRAS 18293-3413". *ApJL* 659 (): L9–L12. doi:10.1086/516821. eprint: astro-ph/0702591.

Mattila, S., et al. 2012. "Core-collapse Supernovae Missed by Optical Surveys". *ApJ* 756, 111 (): 111. doi:10.1088/0004-637X/756/2/111. arXiv: 1206.1314 [astro-ph.CO].

Mattila, S., et al. 2008. "Massive stars exploding in a He-rich circumstellar medium - III. SN 2006jc: infrared echoes from new and old dust in the progenitor CSM". *MNRAS* 389 (): 141–155. doi:10.1111/j.1365-2966.2008.13516.x. arXiv: 0803.2145.

Mattila, S., et al. 2002. "Searching for Obscured Supernovae in Nearby Starburst Galaxies". *The Newsletter of the Isaac Newton Group of Telescopes* 6 (): 6–9. arXiv: astro-ph/0202087 [astro-ph].

Mattila, S., et al. 2005. "Supernova 2005V in NGC 2146". *IAU Circ.* 8474 ().

Mattila, S., et al. 2013. "Supernovae and radio transients in M82". *MNRAS* 431, no. 3 (): 2050–2062. doi:10.1093/mnras/stt202. arXiv: 1207.1889 [astro-ph.CO].

Matuszewski, M., et al. 2010. "The Cosmic Web Imager: an integral field spectrograph for the Hale Telescope at Palomar Observatory: instrument design and first results". In *Ground-based and Airborne Instrumentation for Astronomy III*, vol. 7735, 77350P. Proc. SPIE. doi:10.1117/12.856644.

Mauerhan, Jon, et al. 2013. "The Unprecedented Third Outburst of SN 2009ip: A Luminous Blue Variable Becomes a Supernova". In *American Astronomical Society Meeting Abstracts #221*, 221:233.03. American Astronomical Society Meeting Abstracts.

Maund, J. R., et al. 2004. "The massive binary companion star to the progenitor of supernova 1993J". *Nature* 427 (): 129–131. eprint: astro-ph/0401090.

Maund, J. R., et al. 2011. "The Yellow Supergiant Progenitor of the Type II Supernova 2011dh in M51". *ApJL* 739, L37 (): L37. doi:10.1088/2041-8205/739/2/L37. arXiv: 1106.2565 [astro-ph.SR].

Mazzali, P. A., et al. 2005. "An Asymmetric Energetic Type Ic Supernova Viewed Off-Axis, and a Link to Gamma Ray Bursts". *Science* 308 (): 1284–1287. doi:10.1126/science.1111384. eprint: astro-ph/0505199.

McCollum, B., et al. 2014. "The Optical and Infrared Photometric Evolution of the Recent Stellar Merger, V1309 Sco". *AJ* 147, 11 (): 11. doi:10.1088/0004-6256/147/1/11.

McCully, C., et al. 2018. "Real-time processing of the imaging data from the network of Las Cumbres Observatory Telescopes using BANZAI". In *Software and Cyberinfrastructure for Astronomy V*, vol. 10707, 107070K. Society of Photo-Optical Instrumentation Engineers (SPIE) Conference Series. doi:10.1117/12.2314340. arXiv: 1811.04163 [astro-ph.IM].

McLean, I. S., et al. 2012. "MOSFIRE, the multi-object spectrometer for infra-red exploration at the Keck Observatory". In *Ground-based and Airborne Instrumentation for Astronomy IV*, vol. 8446, 84460J. Proc. SPIE. doi:10.1117/12.924794.

McLean, Ian S., et al. 2010. "Design and development of MOSFIRE: the multi-object spectrometer for infrared exploration at the Keck Observatory". In *Proc. SPIE*, vol. 7735, 77351E. Society of Photo-Optical Instrumentation Engineers (SPIE) Conference Series. doi:10.1117/12.856715.

McQuinn, K. B. W., et al. 2017. "Accurate Distances to Important Spiral Galaxies: M63, M74, NGC 1291, NGC 4559, NGC 4625, and NGC 5398". *AJ* 154, 51 (): 51. doi:10.3847/1538-3881/aa7aad. arXiv: 1706.06586.

– . 2016. "The Distance to M51". *ApJ* 826, 21 (): 21. doi:10.3847/0004-637X/826/1/21. arXiv: 1606.04120.

Meikle, W. P. S., et al. 2006. "A Spitzer Space Telescope Study of SN 2002hh: An Infrared Echo from a Type IIP Supernova". *ApJ* 649, no. 1 (): 332–344. doi:10.1086/506143. arXiv: astro-ph/0605584 [astro-ph].

Meikle, W. P. S., et al. 2007. "A Spitzer Space Telescope Study of SN 2003gd: Still No Direct Evidence that Core-Collapse Supernovae are Major Dust Factories". *ApJ* 665, no. 1 (): 608–617. doi:10.1086/519733. arXiv: 0705.1439 [astro-ph].

Meikle, W. P. S., et al. 2011. "Dust and the Type II-plateau Supernova 2004dj". *ApJ* 732, 109 (): 109. doi:10.1088/0004-637X/732/2/109. arXiv: 1103.2885 [astro-ph.SR].

Meikle, W. P. S., et al. 1989. "Spectroscopy of supernova 1987A at 1-5 microns. I - The first year". *MNRAS* 238 (): 193–223. doi:10.1093/mnras/238.1.193.

Meikle, W. Peter, et al. 2005. *Infrared Study of Supernova Ejecta and Dust*. Spitzer Proposal.

Metzger, Brian D., and Ondřej Pejcha. 2017. "Shock-powered light curves of luminous red novae as signatures of pre-dynamical mass-loss in stellar mergers". *MNRAS* 471, no. 3 (): 3200–3211. doi:10.1093/mnras/stx1768. arXiv: 1705.03895 [astro-ph.HE].

Milisavljevic, D., et al. 2010. "Doublets and Double Peaks: Late-Time [O I] $\lambda\lambda$6300, 6364 Line Profiles of Stripped-Envelope, Core-Collapse Supernovae". *ApJ* 709 (): 1343–1355. doi:10.1088/0004-637X/709/2/1343. arXiv: 0904.4256 [astro-ph.CO].

Milisavljevic, D., et al. 2015. "Metamorphosis of SN 2014C: Delayed Interaction between a Hydrogen Poor Core-collapse Supernova and a Nearby Circumstellar Shell". *ApJ* 815, 120 (): 120. doi:10.1088/0004-637X/815/2/120. arXiv: 1511.01907 [astro-ph.HE].

Miluzio, M., et al. 2013. "HAWK-I infrared supernova search in starburst galaxies". *A&A* 554, A127 (): A127. doi:10.1051/0004-6361/201321192. arXiv: 1303.3803.

Modjaz, M., and W. D. Li. 1999. "Supernova 1999ec in NGC 2207". *IAU Circ.* 7268 ().

Modjaz, M., et al. 2008. "Double-Peaked Oxygen Lines Are Not Rare in Nebular Spectra of Core-Collapse Supernovae". *ApJL* 687, L9 (): L9. doi:10.1086/593135. arXiv: 0801.0221.

Modjaz, M., et al. 2005. "Supernova 2005cs in M51". *IAU Circ.* 8555 ().

Monard, L. A. G., et al. 2014. "Supernova 2014df in NGC 1448 = Psn J03442399-4440081". *Central Bureau Electronic Telegrams* 3977 ().

Moore, Anna M., et al. 2016. "Unveiling the dynamic infrared sky with Gattini-IR". In *Proc. SPIE*, 9906:99062C. Society of Photo-Optical Instrumentation Engineers (SPIE) Conference Series. doi:10.1117/12.2233694. arXiv: 1608.04510 [astro-ph.IM].

Morgan, C. W., et al. 2005. "RETROCAM: A Versatile Optical Imager for Synoptic Studies". *AJ* 129 (): 2504–2510. doi:10.1086/429594. eprint: astro-ph/0502274.

Muñoz-Mateos, J. C., et al. 2013. "The Impact of Bars on Disk Breaks as Probed by S^{4}G Imaging". *ApJ* 771, 59 (): 59. doi:10.1088/0004-637X/771/1/59. arXiv: 1304.6083.

Nakano, S., et al. 2014. "Supernova 2014dt in M61 = Psn J12215757+0428185". *Central Bureau Electronic Telegrams* 4011 ().

Nasonova, O. G., J. A. de Freitas Pacheco, and I. D. Karachentsev. 2011. "Hubble flow around Fornax cluster of galaxies". *A&A* 532, A104 (): A104. doi:10.1051/0004-6361/201016004. arXiv: 1106.1291.

Nordin, J., et al. 2019a. "Transient processing and analysis using AMPEL: Alert Management, Photometry and Evaluation of Lightcurves". *arXiv e-prints* (). arXiv: 1904.05922 [astro-ph.IM].

Nordin, J., et al. 2019b. "ZTF Transient Discovery Report for 2019-01-25". *Transient Name Server Discovery Report* 141 ().

Nousek, J. A. 2004. "Swift GRB mission". In *X-Ray and Gamma-Ray Instrumentation for Astronomy XIII*, ed. by K. A. Flanagan and O. H. W. Siegmund, 5165:169–174. Proc. SPIE. doi:10.1117/12.509880.

Ochner, P., et al. 2014. "Asiago spectroscopic classification of bright SNe in M61 and in PGC 024396". *The Astronomer's Telegram* 6648 ().

Oke, J. B., and J. E. Gunn. 1982. "An Efficient Low Resolution and Moderate Resolution Spectrograph for the Hale Telescope". *PASP* 94 (): 586. doi:10.1086/131027.

Oke, J. B., et al. 1995. "The Keck Low-Resolution Imaging Spectrometer". *PASP* 107 (): 375. doi:10.1086/133562.

Panagia, N., et al. 2006. "A Search for Radio Emission from Type Ia Supernovae". *ApJ* 646 (): 369–377. doi:10.1086/504710. eprint: astro-ph/0603808.

Pastorello, A., et al. 2007. "A giant outburst two years before the core-collapse of a massive star". *Nature* 447, no. 7146 (): 829–832. doi:10.1038/nature05825. arXiv: astro-ph/0703663 [astro-ph].

Pastorello, A., et al. 2013. "Interacting Supernovae and Supernova Impostors: SN 2009ip, is this the End?" *ApJ* 767, no. 1, 1 (): 1. doi:10.1088/0004-637X/767/1/1. arXiv: 1210.3568 [astro-ph.SR].

Pastorello, A., et al. 2004. "Low-luminosity Type II supernovae: spectroscopic and photometric evolution". *MNRAS* 347 (): 74–94. doi:10.1111/j.1365-2966.2004.07173.x. eprint: astro-ph/0309264.

Pastorello, A., et al. 2010. "Multiple major outbursts from a restless luminous blue variable in NGC 3432". *MNRAS* 408 (): 181–198. doi:10.1111/j.1365-2966.2010.17142.x. arXiv: 1006.0504 [astro-ph.SR].

Pastorello, A., et al. 2006. "SN 2005cs in M51 - I. The first month of evolution of a subluminous SN II plateau". *MNRAS* 370 (): 1752–1762. doi:10.1111/j.1365-2966.2006.10587.x. eprint: astro-ph/0605700.

Pastorello, A., et al. 2009. "SN 2005cs in M51 - II. Complete evolution in the optical and the near-infrared". *MNRAS* 394 (): 2266–2282. doi:10.1111/j.1365-2966.2009.14505.x. arXiv: 0901.2075 [astro-ph.GA].

Patat, F., et al. 2001. "The Metamorphosis of SN 1998bw". *ApJ* 555 (): 900–917. doi:10.1086/321526. eprint: astro-ph/0103111.

Patterson, M. T., et al. 2019. "The Zwicky Transient Facility Alert Distribution System". *PASP* 131, no. 1 (): 018001. doi:10.1088/1538-3873/aae904. arXiv: 1902.02227 [astro-ph.IM].

Pejcha, Ondřej, Brian D. Metzger, and Kengo Tomida. 2016a. "Binary stellar mergers with marginally bound ejecta: excretion discs, inflated envelopes, outflows, and their luminous transients". *MNRAS* 461, no. 3 (): 2527–2539. doi:10.1093/mnras/stw1481. arXiv: 1604.07414 [astro-ph.SR].

– . 2016b. “Cool and luminous transients from mass-losing binary stars”. *MNRAS* 455, no. 4 (): 4351–4372. doi:10.1093/mnras/stv2592. arXiv: 1509.02531 [astro-ph.SR].

Pérez-Torres, M. A., et al. 2009. “An extremely prolific supernova factory in the buried nucleus of the starburst galaxy IC 694”. *A&A* 507 (): L17–L20. doi:10.1051/0004-6361/200912964. arXiv: 0909.3959.

Perley, Daniel A. 2019. “Fully Automated Reduction of Longslit Spectroscopy with the Low Resolution Imaging Spectrometer at the Keck Observatory”. *PASP* 131, no. 1002 (): 084503. doi:10.1088/1538-3873/ab215d. arXiv: 1903.07629 [astro-ph.IM].

Perrott, Y. C., et al. 2013. “AMI Galactic Plane Survey at 16 GHz - I. Observing, mapping and source extraction”. *MNRAS* 429 (): 3330–3340. doi:10.1093/mnras/sts589. arXiv: 1208.5343.

Persson, S. E., et al. 2013. “FourStar: The Near-Infrared Imager for the 6.5 m Baade Telescope at Las Campanas Observatory”. *PASP* 125 (): 654. doi:10.1086/671164.

Pessev, P., et al. 2019. “Johnson-Cousins VRI Photometric Monitoring of AT2019abn”. *The Astronomer’s Telegram* 12506 ().

Podsiadlowski, P., et al. 1993. “The progenitor of supernova 1993J - A stripped supergiant in a binary system?” *Nature* 364 (): 509–511. doi:10.1038/364509a0.

Poznanski, D., et al. 2009. “Improved Standardization of Type II-P Supernovae: Application to an Expanded Sample”. *ApJ* 694 (): 1067–1079. doi:10.1088/0004-637X/694/2/1067. arXiv: 0810.4923.

Prieto, J. L. 2008. “Bright Infrared Progenitor of Luminous Transient in NGC300 implies Explosion of a Massive Star”. *The Astronomer’s Telegram* 1550 ().

Prieto, J. L., et al. 2008. “Discovery of the Dust-Enshrouded Progenitor of SN 2008S with Spitzer”. *ApJL* 681 (): L9–L12. doi:10.1086/589922. arXiv: 0803.0324.

Prieto, J. L., et al. 2014. “Light Echoes from η Carinae’s Great Eruption: Spectrophotometric Evolution and the Rapid Formation of Nitrogen-rich Molecules”. *ApJL* 787, L8 (): L8. doi:10.1088/2041-8205/787/1/L8. arXiv: 1403.7202 [astro-ph.SR].

Prieto, J. L., et al. 2012. “SN 2008jb: A “Lost” Core-collapse Supernova in a Star-forming Dwarf Galaxy at $\sim$10 Mpc”. *ApJ* 745, no. 1, 70 (): 70. doi:10.1088/0004-637X/745/1/70. arXiv: 1107.5043 [astro-ph.SR].

Querejeta, M., et al. 2015. “The Spitzer Survey of Stellar Structure in Galaxies (S^{4}G): Precise Stellar Mass Distributions from Automated Dust Correction at 3.6 μm”. *ApJS* 219, 5 (): 5. doi:10.1088/0067-0049/219/1/5. arXiv: 1410.0009.

Rau, A., et al. 2009. "Exploring the Optical Transient Sky with the Palomar Transient Factory". *PASP* 121 (): 1334. doi:10.1086/605911. arXiv: 0906.5355 [astro-ph.CO].

Rau, A., et al. 2007. "Spitzer Observations of the New Luminous Red Nova M85 OT2006-1". *ApJ* 659, no. 2 (): 1536–1540. doi:10.1086/512672. arXiv: astro-ph/0612161 [astro-ph].

Rayner, J. T., M. C. Cushing, and W. D. Vacca. 2009. "The Infrared Telescope Facility (IRTF) Spectral Library: Cool Stars". *ApJS* 185 (): 289–432. doi:10.1088/0067-0049/185/2/289. arXiv: 0909.0818 [astro-ph.SR].

Rest, A., et al. 2012. "Light echoes reveal an unexpectedly cool η Carinae during its nineteenth-century Great Eruption". *Nature* 482 (): 375–378. doi:10.1038/nature10775. arXiv: 1112.2210.

Rich, R. M., et al. 1989. "Luminous M giants in the bulge of M31". *ApJL* 341 (): L51–L54. doi:10.1086/185455.

Riess, A. G., et al. 2016. "A 2.4% Determination of the Local Value of the Hubble Constant". *ApJ* 826, 56 (): 56. doi:10.3847/0004-637X/826/1/56. arXiv: 1604.01424.

Rigault, M., et al. 2019. "Fully automated integral field spectrograph pipeline for the SEDMachine: pysedm". *A&A* 627, A115 (): A115. doi:10.1051/0004-6361/201935344. arXiv: 1902.08526 [astro-ph.IM].

Rizzi, L., et al. 2007. "Tip of the Red Giant Branch Distances. II. Zero-Point Calibration". *ApJ* 661 (): 815–829. doi:10.1086/516566. eprint: astro-ph/0701518.

Rodríguez, Ó., A. Clocchiatti, and M. Hamuy. 2014. "Photospheric Magnitude Diagrams for Type II Supernovae: A Promising Tool to Compute Distances". *AJ* 148, 107 (): 107. doi:10.1088/0004-6256/148/6/107. arXiv: 1409.3198.

Romero-Cañizales, C., et al. 2012. "e-MERLIN and VLBI observations of the luminous infrared galaxy IC 883: a nuclear starburst and an AGN candidate revealed". *A&A* 543, A72 (): A72. doi:10.1051/0004-6361/201218816. arXiv: 1205.2257 [astro-ph.CO].

Romero-Cañizales, C., et al. 2011. "The core-collapse supernova rate in Arp 299 revisited". *MNRAS* 415 (): 2688–2698. doi:10.1111/j.1365-2966.2011.18886.x. arXiv: 1104.1955.

Romero-Cañizales, C., et al. 2014. "The nature of supernovae 2010O and 2010P in Arp 299 - II. Radio emission". *MNRAS* 440 (): 1067–1079. doi:10.1093/mnras/stu430. arXiv: 1403.1036.

Roming, P. W. A., et al. 2005. "The Swift Ultra-Violet/Optical Telescope". *Space Sci. Rev.* 120 (): 95–142. doi:10.1007/s11214-005-5095-4. eprint: astro-ph/0507413.

Rubin, A., and A. Gal-Yam. 2016. "Unsupervised Clustering of Type II Supernova Light Curves". *ApJ* 828, 111 (): 111. doi:10.3847/0004-637X/828/2/111. arXiv: 1602.01446 [astro-ph.HE].

Sahu, D. K., et al. 2016. "Classification of AT 2016c in NGC 5247 as a type II supernova". *The Astronomer's Telegram* 8514 ().

Sanders, D. B., et al. 2003. "The IRAS Revised Bright Galaxy Sample". *AJ* 126, no. 4 (): 1607–1664. doi:10.1086/376841. arXiv: astro-ph/0306263 [astro-ph].

Sanders, N. E., et al. 2015. "Toward Characterization of the Type IIP Supernova Progenitor Population: A Statistical Sample of Light Curves from Pan-STARRS1". *ApJ* 799, 208 (): 208. doi:10.1088/0004-637X/799/2/208. arXiv: 1404.2004 [astro-ph.HE].

Sault, R. J., P. J. Teuben, and M. C. H. Wright. 1995. "A Retrospective View of MIRIAD". In *Astronomical Data Analysis Software and Systems IV*, ed. by R. A. Shaw, H. E. Payne, and J. J. E. Hayes, 77:433. Astronomical Society of the Pacific Conference Series. eprint: astro-ph/0612759.

Schlafly, E. F., and D. P. Finkbeiner. 2011. "Measuring Reddening with Sloan Digital Sky Survey Stellar Spectra and Recalibrating SFD". *ApJ* 737, 103 (): 103. doi:10.1088/0004-637X/737/2/103. arXiv: 1012.4804 [astro-ph.GA].

Schlegel, D. J., D. P. Finkbeiner, and M. Davis. 1998. "Maps of Dust Infrared Emission for Use in Estimation of Reddening and Cosmic Microwave Background Radiation Foregrounds". *ApJ* 500 (): 525–553. doi:10.1086/305772. eprint: astro-ph/9710327.

Schmidt, B., et al. 1994. "Supernova 1994I in NGC 5194". *IAU Circ.* 5962 ().

Shafter, A. W. 2017. "The Galactic Nova Rate Revisited". *ApJ* 834, no. 2, 196 (): 196. doi:10.3847/1538-4357/834/2/196. arXiv: 1606.02358 [astro-ph.SR].

Shappee, B. J., et al. 2016. "ASAS-SN Prediscovery Limits for SPIRITS16tn". *The Astronomer's Telegram* 9446 (): 1.

Sheth, K., et al. 2010. "The Spitzer Survey of Stellar Structure in Galaxies ()". *PASP* 122 (): 1397. doi:10.1086/657638. arXiv: 1010.1592.

Shigeyama, T., et al. 1994. "Theoretical light curves of Type IIb supernova 1993J". *ApJ* 420 (): 341–347. doi:10.1086/173564.

Shostak, G. S. 1975. "An H i Study of Scd Galaxies". *ApJ* 198 (): 527–536. doi:10.1086/153629.

Silverman, J. M., A. V. Filippenko, and S. B. Cenko. 2011. "PTF Discovery of a Type II Supernova in M51". *The Astronomer's Telegram* 3398 ().

Simcoe, R. A., et al. 2013. "FIRE: A Facility Class Near-Infrared Echelle Spectrometer for the Magellan Telescopes". *PASP* 125 (): 270–286. doi:10.1086/670241.

Simcoe, R. A., et al. 2008. “FIRE: a near-infrared cross-dispersed echellette spectrometer for the Magellan telescopes”. In *Ground-based and Airborne Instrumentation for Astronomy II*, vol. 7014, 70140U. Proc. SPIE. doi:10.1117/12.790414.

Skrutskie, M. F., et al. 2006. “The Two Micron All Sky Survey (2MASS)”. *AJ* 131 (): 1163–1183. doi:10.1086/498708.

Smartt, S. J., et al. 2014. “Supernova 2014bc in M106 = Psn J12185771+4718113”. *Central Bureau Electronic Telegrams* 3877 ().

Smith, N. 2014. “Mass Loss: Its Effect on the Evolution and Fate of High-Mass Stars”. *ARA&A* 52 (): 487–528. doi:10.1146/annurev-astro-081913-040025. arXiv: 1402.1237 [astro-ph.SR].

Smith, N., and S. P. Owocki. 2006. “On the Role of Continuum-driven Eruptions in the Evolution of Very Massive Stars and Population III Stars”. *ApJL* 645 (): L45–L48. doi:10.1086/506523. eprint: astro-ph/0606174.

Smith, N., et al. 2010. “Discovery of Precursor Luminous Blue Variable Outbursts in Two Recent Optical Transients: The Fitfully Variable Missing Links UGC 2773-OT and SN 2009ip”. *AJ* 139 (): 1451–1467. doi:10.1088/0004-6256/139/4/1451. arXiv: 0909.4792 [astro-ph.SR].

Smith, N., et al. 2011. “Luminous blue variable eruptions and related transients: diversity of progenitors and outburst properties”. *MNRAS* 415 (): 773–810. doi:10.1111/j.1365-2966.2011.18763.x. arXiv: 1010.3718 [astro-ph.SR].

Smith, N., et al. 2016. “Massive star mergers and the recent transient in NGC 4490: a more massive cousin of V838 Mon and V1309 Sco”. *MNRAS* 458 (): 950–962. doi:10.1093/mnras/stw219. arXiv: 1602.05203 [astro-ph.SR].

Smith, N., et al. 2009. “SN 2008S: A Cool Super-Eddington Wind in a Supernova Impostor”. *ApJL* 697 (): L49–L53. doi:10.1088/0004-637X/697/1/L49. arXiv: 0811.3929.

Smith, N., et al. 2012. “SN 2010jp (PTF10aaxi): a jet in a Type II supernova”. *MNRAS* 420 (): 1135–1144. doi:10.1111/j.1365-2966.2011.20104.x. arXiv: 1108.2868 [astro-ph.HE].

Soderberg, A. M., et al. 2012. “Panchromatic Observations of SN 2011dh Point to a Compact Progenitor Star”. *ApJ* 752, 78 (): 78. doi:10.1088/0004-637X/752/2/78. arXiv: 1107.1876 [astro-ph.HE].

Soderberg, A. M., et al. 2010. “Radio and X-ray Observations of the Type Ic SN 2007gr Reveal an Ordinary, Non-relativistic Explosion”. *ApJ* 725 (): 922–930. doi:10.1088/0004-637X/725/1/922. arXiv: 1005.1932.

Sorce, J. G., et al. 2014. “From Spitzer Galaxy photometry to Tully-Fisher distances”. *MNRAS* 444 (): 527–541. doi:10.1093/mnras/stu1450. arXiv: 1408.0729.

Sparks, W. B., et al. 2008. “V838 Monocerotis: A Geometric Distance from Hubble Space Telescope Polarimetric Imaging of its Light Echo”. *AJ* 135 (): 605–617. doi:10.1088/0004-6256/135/2/605. arXiv: 0711.1495.

Spyromilio, J., et al. 2004. “Optical and near infrared observations of SN 1998bu”. *A&A* 426 (): 547–553. doi:10.1051/0004-6361:20040570. eprint: astro-ph/0407177.

Stancliffe, R. J., and J. J. Eldridge. 2009. “Modelling the binary progenitor of Supernova 1993J”. *MNRAS* 396 (): 1699–1708. doi:10.1111/j.1365-2966.2009.14849.x. arXiv: 0904.0282 [astro-ph.SR].

Steele, T. N., et al. 2008. “Supernovae 2007GW, 2008S, 2008T, 2008AL, 2008AO, and 2008AP”. *Central Bureau Electronic Telegrams* 1275, no. 27 (): A1.

Stetson, P. B. 1987. “DAOPHOT - A computer program for crowded-field stellar photometry”. *PASP* 99 (): 191–222. doi:10.1086/131977.

Stritzinger, Maximilian, et al. 2012. “Multi-wavelength Observations of the Enduring Type IIn Supernovae 2005ip and 2006jd”. *ApJ* 756, no. 2, 173 (): 173. doi:10.1088/0004-637X/756/2/173. arXiv: 1206.5575 [astro-ph.CO].

Stritzinger, M., et al. 2016. “CSP Spectroscopic Classification of AT 2016adj in NGC 5128 (Centaurus A)”. *The Astronomer’s Telegram* 8657 ().

Szalai, T., and J. Vinkó. 2013. “Twelve type II-P supernovae seen with the eyes of Spitzer”. *A&A* 549, A79 (): A79. doi:10.1051/0004-6361/201220015. arXiv: 1211.0854 [astro-ph.SR].

Szalai, Tamás, et al. 2019a. “A Comprehensive Analysis of Spitzer Supernovae”. *ApJS* 241, no. 2, 38 (): 38. doi:10.3847/1538-4365/ab10df. arXiv: 1803.02571 [astro-ph.HE].

Szalai, T., et al. 2019b. “AT2019krl, new transient in M74, on pre-discovery Spitzer/IRAC images”. *The Astronomer’s Telegram* 12934 (): 1.

Szalai, T., et al. 2011. “Dust formation in the ejecta of the type II-P supernova 2004dj”. *A&A* 527, A61 (): A61. doi:10.1051/0004-6361/201015624. arXiv: 1012.2035 [astro-ph.SR].

Szczygieł, D. M., C. S. Kochanek, and X. Dai. 2012. “SN 2002bu—Another SN 2008S-like Transient”. *ApJ* 760, no. 1, 20 (): 20. doi:10.1088/0004-637X/760/1/20. arXiv: 1208.2688 [astro-ph.SR].

Szczygieł, D. M., et al. 2012. “Dust to Dust: Three Years in the Evolution of the Unusual SN 2008S”. *ApJ* 750, 77 (): 77. doi:10.1088/0004-637X/750/1/77. arXiv: 1202.0279 [astro-ph.SR].

Tachibana, Y., and A. A. Miller. 2018. “A Morphological Classification Model to Identify Unresolved PanSTARRS1 Sources: Application in the ZTF Real-time Pipeline”. *PASP* 130, no. 12 (): 128001. doi:10.1088/1538-3873/aae3d9. arXiv: 1902.01935 [astro-ph.IM].

Takáts, K., and J. Vinkó. 2006. "Distance estimate and progenitor characteristics of SN 2005cs in M51". *MNRAS* 372 (): 1735–1740. doi:10.1111/j.1365-2966.2006.10974.x. eprint: astro-ph/0608430.

Tartaglia, L., et al. 2018. "The Early Detection and Follow-up of the Highly Obscured Type II Supernova 2016ija/DLT16am". *ApJ* 853, 62 (): 62. doi:10.3847/1538-4357/aaa014. arXiv: 1711.03940 [astro-ph.HE].

Theureau, G., et al. 2007. "Kinematics of the Local Universe. XIII. 21-cm line measurements of 452 galaxies with the Nançay radiotelescope, JHK Tully-Fisher relation, and preliminary maps of the peculiar velocity field". *A&A* 465 (): 71–85. doi:10.1051/0004-6361:20066187. eprint: astro-ph/0611626.

Thompson, T. A., et al. 2009. "A New Class of Luminous Transients and a First Census of their Massive Stellar Progenitors". *ApJ* 705 (): 1364–1384. doi:10.1088/0004-637X/705/2/1364. arXiv: 0809.0510.

Tinyanont, S., et al. 2016. "A Systematic Study of Mid-infrared Emission from Core-collapse Supernovae with SPIRITS". *ApJ* 833, 231 (): 231. doi:10.3847/1538-4357/833/2/231. arXiv: 1601.03440 [astro-ph.SR].

Tinyanont, S., et al. 2019. "Supernova 2017eaw: molecule and dust formation from infrared observations". *arXiv e-prints* (). arXiv: 1901.01940 [astro-ph.HE].

Tonry, J. L., et al. 2018. "ATLAS: A High-cadence All-sky Survey System". *PASP* 130, no. 6 (): 064505. doi:10.1088/1538-3873/aabadf. arXiv: 1802.00879 [astro-ph.IM].

Torres, G. 2010. "On the Use of Empirical Bolometric Corrections for Stars". *AJ* 140 (): 1158–1162. doi:10.1088/0004-6256/140/5/1158. arXiv: 1008.3913 [astro-ph.SR].

Tsvetkov, D. Y., et al. 2009. "Photometric Observations and Modeling of Type IIb Supernova 2008ax". *Peremennye Zvezdy* 29 (). arXiv: 0910.4242 [astro-ph.SR].

Tully, R. B. 1988. *Nearby galaxies catalog*.

Tully, R. B., et al. 2013. "Cosmicflows-2: The Data". *AJ* 146, 86 (): 86. doi:10.1088/0004-6256/146/4/86. arXiv: 1307.7213.

Tylenda, R., et al. 2011. "V1309 Scorpii: merger of a contact binary". *A&A* 528, A114 (): A114. doi:10.1051/0004-6361/201016221. arXiv: 1012.0163 [astro-ph.SR].

Ulvestad, James S. 2009. "Radio Emission from Young Supernovae and Supernova Remnants in Arp 299". *AJ* 138, no. 5 (): 1529–1538. doi:10.1088/0004-6256/138/5/1529. arXiv: 0909.3534 [astro-ph.CO].

Vacca, W. D., M. C. Cushing, and J. T. Rayner. 2003. "A Method of Correcting Near-Infrared Spectra for Telluric Absorption". *PASP* 115 (): 389–409. doi:10.1086/346193. eprint: astro-ph/0211255.

Valenti, S., et al. 2016. "The diversity of Type II supernova versus the similarity in their progenitors". *MNRAS* 459 (): 3939–3962. doi:10.1093/mnras/stw870. arXiv: 1603.08953 [astro-ph.SR].

van Buren, D., et al. 1994. "Supernova 1992bu in NGC 3690". *IAU Circ.* 5960 ().

Van Dyk, S. D., et al. 2000. "SN 1997bs in M66: Another Extragalactic η Carinae Analog?" *PASP* 112 (): 1532–1541. doi:10.1086/317727. eprint: astro-ph/0009027.

Van Dyk, S. D., et al. 2013. "The Progenitor of Supernova 2011dh has Vanished". *ApJL* 772, L32 (): L32. doi:10.1088/2041-8205/772/2/L32. arXiv: 1305.3436 [astro-ph.SR].

Van Dyk, S. D., et al. 2011. "The Progenitor of Supernova 2011dh/PTF11eon in Messier 51". *ApJL* 741, L28 (): L28. doi:10.1088/2041-8205/741/2/L28. arXiv: 1106.2897.

Van Dyk, Schuyler D. 2013. "Late-time Dust Emission from the Type IIn Supernova 1995N". *AJ* 145, no. 5, 118 (): 118. doi:10.1088/0004-6256/145/5/118. arXiv: 1305.0028 [astro-ph.SR].

Van Dyk, Schuyler D., and Thomas Matheson. 2012. "The Supernova Impostors". In *Eta Carinae and the Supernova Impostors*, ed. by Kris Davidson and Roberta M. Humphreys, 384:249. Astrophysics and Space Science Library. doi:10.1007/978-1-4614-2275-4_11.

Varenius, E., et al. 2017. "The population of SNe/SNRs in the starburst galaxy Arp 220. A self-consistent analysis of 20 years of VLBI monitoring". *arXiv e-prints* (). arXiv: 1702.04772.

Velusamy, T., et al. 2008. "HiRes Deconvolution of Spitzer Infrared Images". *AJ* 136 (): 197–211. doi:10.1088/0004-6256/136/1/197.

Vincent, M. B., et al. 2003. "Near-infrared camera and Fabry-Perot spectrometer - NIC-FPS". In *Instrument Design and Performance for Optical/Infrared Ground-based Telescopes*, ed. by M. Iye and A. F. M. Moorwood, 4841:367–375. Proc. SPIE. doi:10.1117/12.459488.

Vink, Jorick S. 2012. "Eta Carinae and the Luminous Blue Variables". In *Eta Carinae and the Supernova Impostors*, ed. by Kris Davidson and Roberta M. Humphreys, 384:221. Astrophysics and Space Science Library. doi:10.1007/978-1-4614-2275-4_10. arXiv: 0905.3338 [astro-ph.SR].

Vinko, J., E. Varga-Verebelyi, and K. Sarneczky. 2016. "Non-detection of SPIRITS16tn in Sloan-i band". *The Astronomer's Telegram* 9451 (): 1.

Watson, A. M., et al. 2012. "Automation of the OAN/SPM 1.5-meter Johnson telescope for operations with RATIR". In *Ground-based and Airborne Telescopes IV*, 8444:84445L. Proc. SPIE. doi:10.1117/12.926927.

Werner, M. W., et al. 2004. "The Spitzer Space Telescope Mission". *ApJS* 154 (): 1–9. doi:10.1086/422992. eprint: astro-ph/0406223.

Wesson, R., et al. 2010. "The destruction and survival of dust in the shell around SN2008S". *MNRAS* 403, no. 1 (): 474–482. doi:10.1111/j.1365-2966.2009.15871.x. arXiv: 0907.0246 [astro-ph.GA].

Wiggins, P. 2017. "Psn J20344424+6011359 = Supernova 2017eaw in NGC 6946". *Central Bureau Electronic Telegrams* 4390 ().

Williams, R. 2012. "Origin of the "He/N" and "Fe II" Spectral Classes of Novae". *AJ* 144, 98 (): 98. doi:10.1088/0004-6256/144/4/98. arXiv: 1208.0380 [astro-ph.SR].

Wilson, J. C., et al. 2003. "A Wide-Field Infrared Camera for the Palomar 200-inch Telescope". In *Instrument Design and Performance for Optical/Infrared Ground-based Telescopes*, ed. by M. Iye and A. F. M. Moorwood, 4841:451–458. Proc. SPIE. doi:10.1117/12.460336.

Wooden, D. H., et al. 1993. "Airborne spectrophotometry of SN 1987A from 1.7 to 12.6 microns - Time history of the dust continuum and line emission". *ApJS* 88 (): 477–507. doi:10.1086/191830.

Woosley, S. E., et al. 1994. "SN 1993J: A Type IIb supernova". *ApJ* 429 (): 300–318. doi:10.1086/174319.

Woudt, P. A., et al. 2009. "The Expanding Bipolar Shell of the Helium Nova V445 Puppis". *ApJ* 706 (): 738–746. doi:10.1088/0004-637X/706/1/738. arXiv: 0910.1069 [astro-ph.SR].

Wright, E. L., et al. 2010. "The Wide-field Infrared Survey Explorer (WISE): Mission Description and Initial On-orbit Performance". *AJ* 140 (): 1868–1881. doi:10.1088/0004-6256/140/6/1868. arXiv: 1008.0031 [astro-ph.IM].

Xiao, L., and J. J. Eldridge. 2015. "Core-collapse supernova rate synthesis within 11 Mpc". *MNRAS* 452 (): 2597–2605. doi:10.1093/mnras/stv1425. arXiv: 1506.07908.

Yan, H., et al. 2018. "Revealing Dusty Supernovae in High-redshift (Ultra)Luminous Infrared Galaxies through Near-infrared Integrated Light Variability". *ApJ* 867, 21 (): 21. doi:10.3847/1538-4357/aadf38. arXiv: 1808.01780.

Yaron, O., and A. Gal-Yam. 2012. "WISeREP—An Interactive Supernova Data Repository". *PASP* 124 (): 668–681. doi:10.1086/666656. arXiv: 1204.1891 [astro-ph.IM].

Yin, Q. F., and D. S. Heeschen. 1991. "Two radio supernovae in the unusual galaxy Markarian 297". *Nature* 354 (): 130–132. doi:10.1038/354130a0.

Yuan, F., et al. 2016. "450 d of Type II SN 2013ej in optical and near-infrared". *MNRAS* 461 (): 2003–2018. doi:10.1093/mnras/stw1419. arXiv: 1605.06117 [astro-ph.SR].

Zackay, B., E. O. Ofek, and A. Gal-Yam. 2016. "Proper Image Subtraction—Optimal Transient Detection, Photometry, and Hypothesis Testing". *ApJ* 830, 27 (): 27. doi:10.3847/0004-637X/830/1/27. arXiv: 1601.02655 [astro-ph.IM].

Zhang, J., et al. 2016. "Spectroscopic Classification of ASASSN-16fq (=SN 2016cok) as a Type IIP Supernova". *The Astronomer's Telegram* 9093 ().

Zhang, T., et al. 2014. "Supernova 2014L in M99 = Psn J12184868+1424435". *Central Bureau Electronic Telegrams* 3795 ().

Appendix A

PHOTOMETRY OF SPIRITS TRANSIENTS

I describe our method for obtaining reliable photometry of transient candidates in our *Spitzer*/IRAC [3.6] and [4.5] difference images (described in Section 1.3) with robust estimates of the photometric uncertainties in Section A.1. I also describe our photometric constraints for SPIRITS transients obtained from coverage by wide-field, optical imaging surveys operating at Palomar Observatory in Section A.2.

A.1 Dealing with messy subtractions: photometry on *Spitzer*/IRAC difference images

Automated photometry is performed at the location of SPIRITS transients in the reference-subtracted images using a 4 mosaicked-pixel (2.″4) aperture and background annulus from 4–12 pixels (2.″4–7.″2). The extracted flux is multiplied by the aperture corrections of 1.215 for [3.6] and 1.233 for [4.5] as described in the IRAC instrument handbook[1], and converted to Vega system magnitudes using the handbook-defined zero magnitude fluxes of F_{ν_0} = 280.9 Jy for [3.6] and F_{ν_0} = 179.7 Jy for [4.5].

Our difference images are subject to a number of detector and processing artifacts, the most significant of which I briefly describe here. First, despite the stable and well-characterized point spread function (PSF) of the *Spitzer*/IRAC imaging system, our difference images are prone to subtraction artifacts from poor PSF-matching, in part due to the sparsely sampled PSF and in particular when there is a large rotation in the orientation of the spacecraft and imager FOV between the science and reference images. Second, we have found that the outlier rejection algorithms used to remove, e.g., cosmic ray hits, from individual "bcd" images during mosaicking may perform poorly in regions of high background flux and near the bright cores of galaxies, leading to "false positive" sources in our difference images. Third, very bright stars and the bright nuclei of galaxies cause changes in the intensity of the column where the signal is located (column pull-down/pull-up[2]), producing significant residuals in difference iamges that may contaminate flux measurements for transient candidates.

[1] `http://irsa.ipac.caltech.edu/data/SPITZER/docs/irac/iracinstrumenthandbook/`

[2] More information on these effects can be found in Chapter 7 of the IRAC instrument handbook.

Finally, we have found that the background variation in our difference images, even in cleanly subtracted regions free of contaminants, is typically non-Gaussian, and is as such a poor indicator of the uncertainty in flux measurements made on difference images.

To mitigate these issues we subsequently perform a conservative error estimation for our photometry on all available difference images of convincing, "by eye"-vetted candidates. We place a 5-by-5 grid of apertures spanning a 32″ box with 8″ spacing centered on the location of each candidate, excluding the central aperture, and perform aperture photometry on each with the same parameters as described above. We adopt a robust estimate of the rms in the distribution of flux measurements for the aperture grid ($0.5 \times [85^{\rm th} - 16^{\rm th}$ percentile]) as representative of the 1σ systematic uncertainties in our photometry, and employ a strict 5σ detection threshold. Our final *Spitzer*/IRAC difference-image photometry and uncertainty estimates for the full sample of SPIRITS transients is shown in Figure A.1.

A.2 Photometry from wide-field, optical surveys at Palomar Observatory

We obtained constraints on optical variability at the location of SPIRITS transients using the available coverage by the intermediate Palomar Transient Factory (iPTF; Cao, Nugent, and Kasliwal 2016), and the Zwicky Transient Facility (ZTF; Bellm et al. 2019a; Graham et al. 2019) on the 48-in. Telescope at Palomar Observatory (P48). For iPTF g- and Mould-R-band data taken between 2009 and 2016, we utilized forced PSF-fitting photometry at the transient location on the reference-subtracted difference images (Masci et al. 2017). ZTF g-, r-, and i-band images are reduced with the ZTF Science Data System pipelines (Masci et al. 2019), which perform image subtraction based on the Zackay, Ofek, and Gal-Yam (2016) algorithm and PSF photometry on the reference-subtracted images. For images taken as part of the ZTF Collaboration surveys and the Caltech surveys (Bellm et al. 2019b), and images taken prior to 2019 January 1 from the first ZTF Public Data Release[3] (ZTF-DR1), we also utilize forced PSF-fitting photomtery from the ZTF forced-photometry service. To obtain deeper limits, we stacked the iPTF and ZTF light curves within 10-day windows, and show the resulting differential optical light curves along with the IR measurements in Figure A.1.

[3] https://www.ztf.caltech.edu/page/dr1

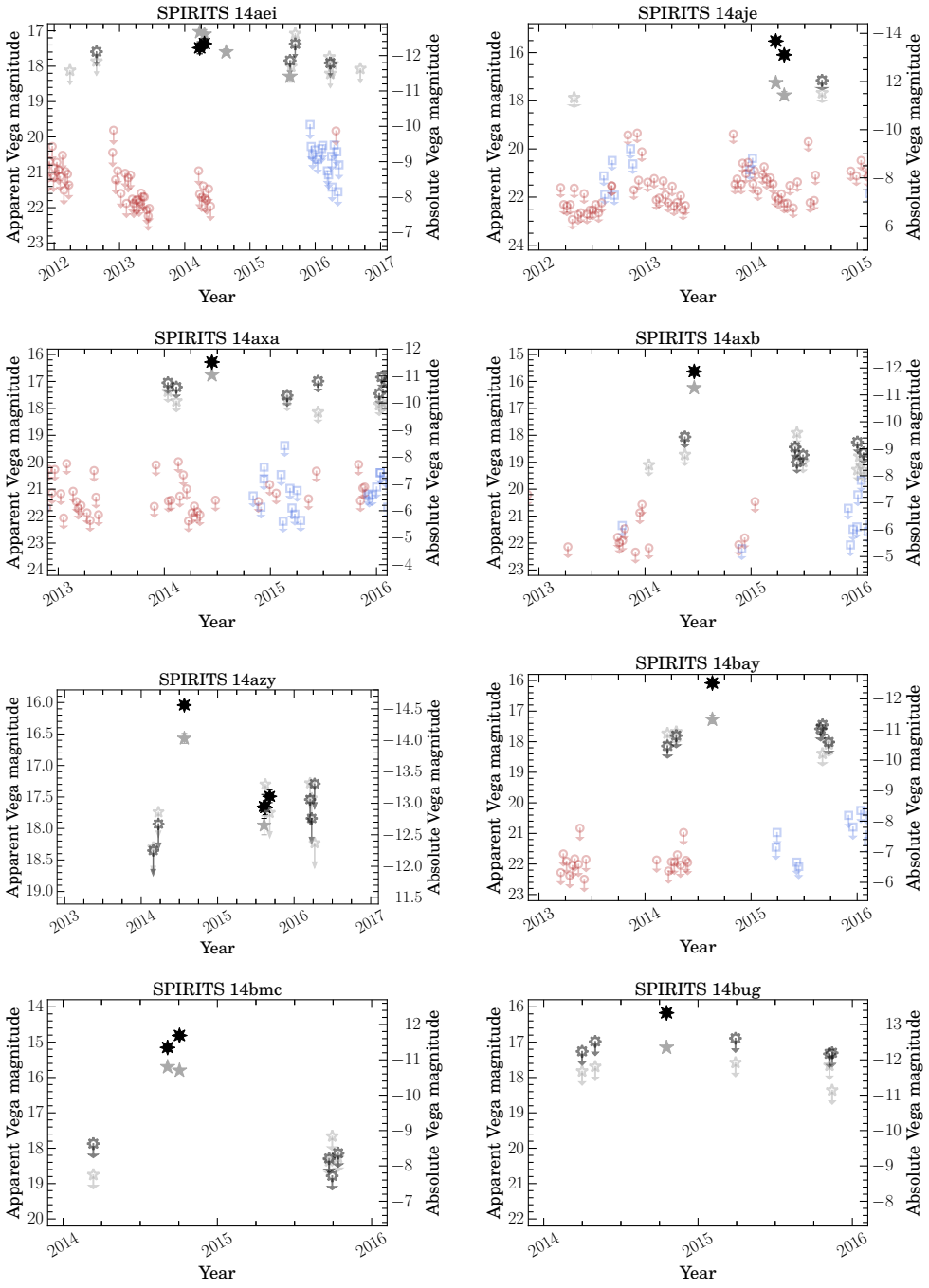

Figure A.1: Image subtraction light curves of all SPIRITS transients in the IR from *Spitzer*/IRAC at [3.6] (gray stars) and [4.5] (black eight-pointed stars), and the optical from iPTF and ZTF in g (blue squares), Mould R or r (red circles), and i (purple diamonds). Optical magnitudes on the AB system have been converted to the Vega system using the conversions of (Blanton and Roweis 2007). 5σ upper limits from nondetections are indicated as open symbols with downward-pointing arrows.

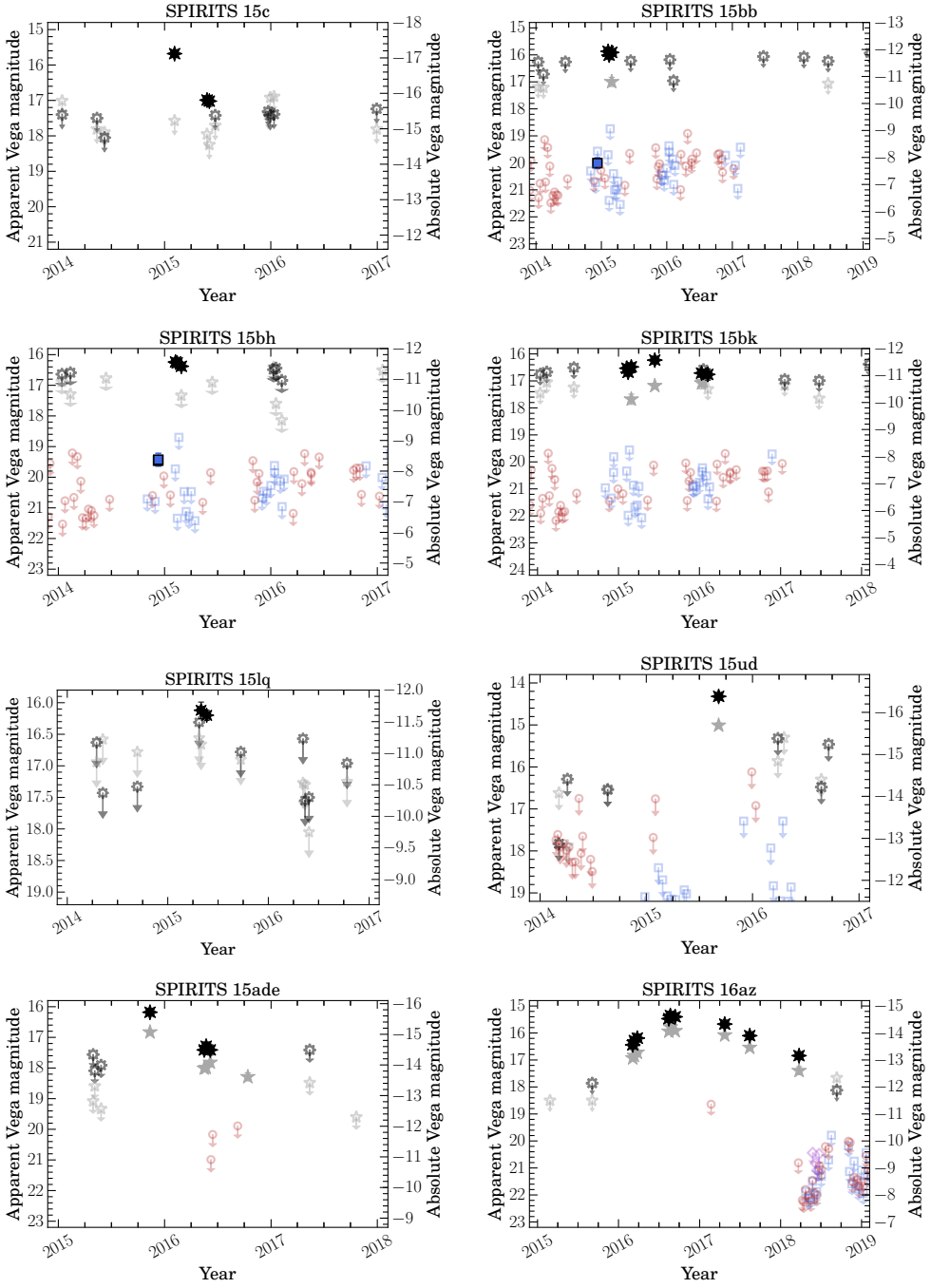

Figure A.1: Continued.

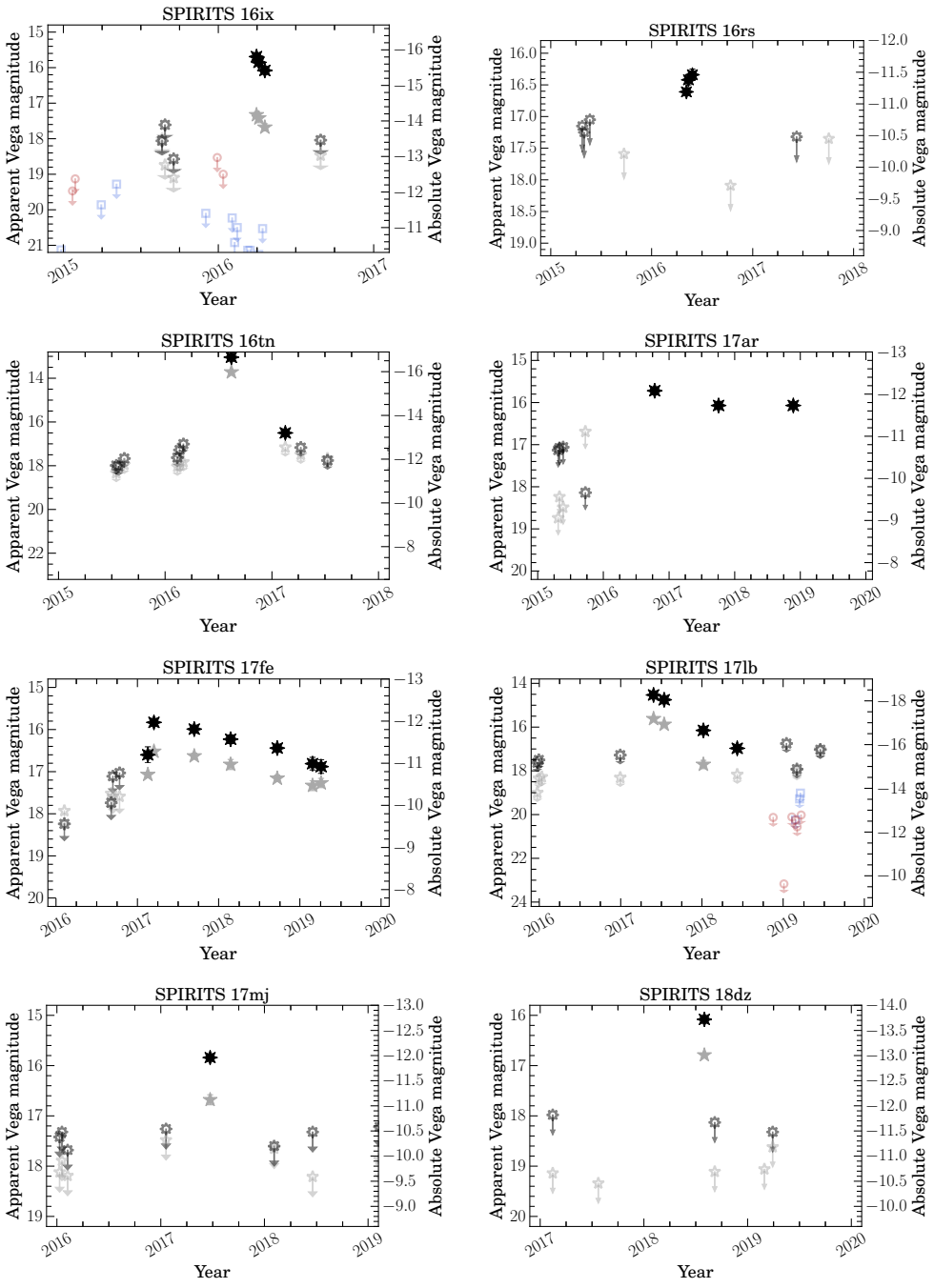

Figure A.1: Continued.

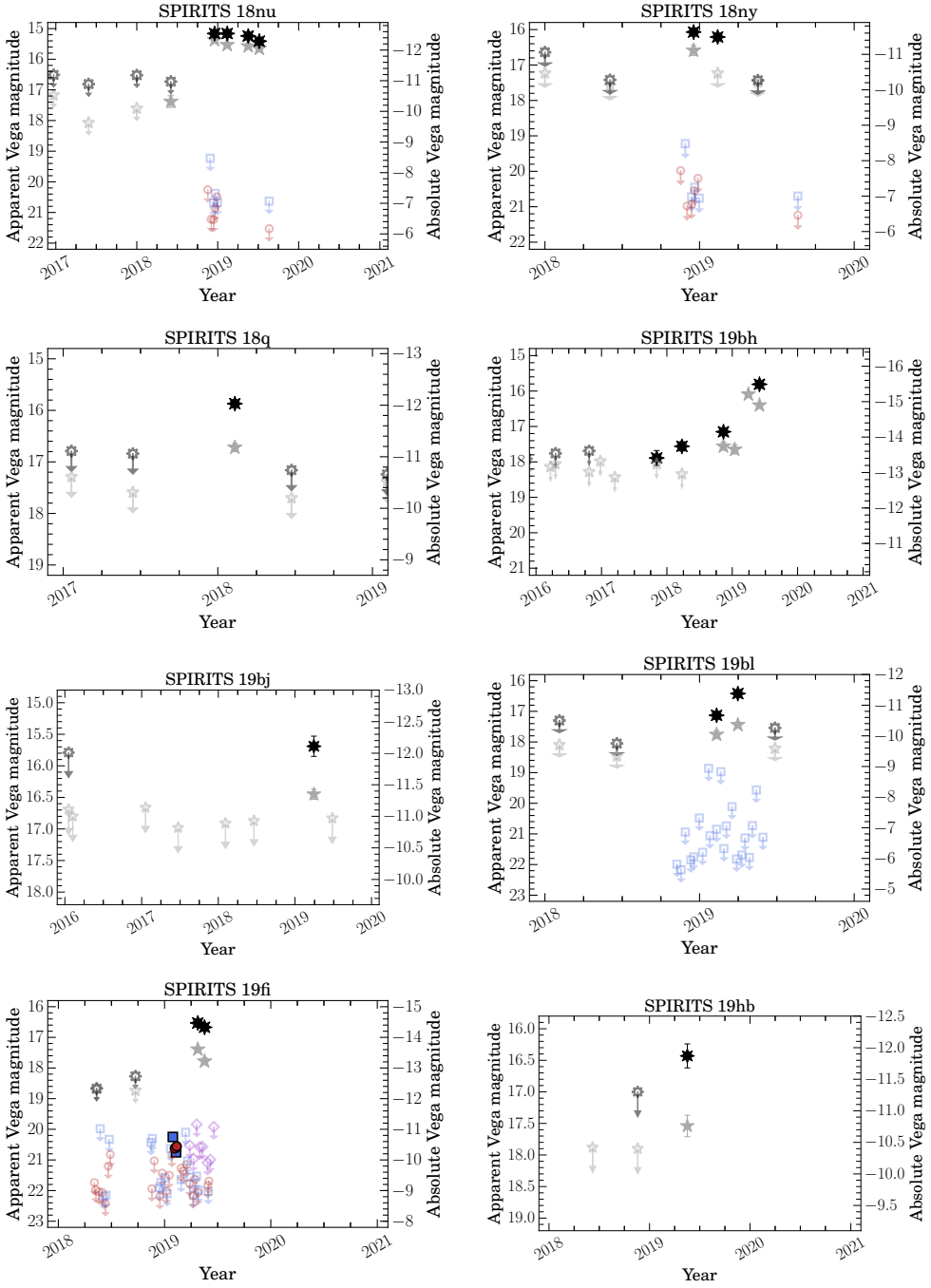

Figure A.1: Continued.